



HAL
open science

Thermodynamics and operational properties of nanoporous heterogeneous lyophobic systems for mechanical and thermal energy storage/dissipation

Yaroslav G. Grosu

► **To cite this version:**

Yaroslav G. Grosu. Thermodynamics and operational properties of nanoporous heterogeneous lyophobic systems for mechanical and thermal energy storage/dissipation. Other. Université Blaise Pascal - Clermont-Ferrand II, 2015. English. NNT : 2015CLF22579 . tel-01242111

HAL Id: tel-01242111

<https://theses.hal.science/tel-01242111>

Submitted on 11 Dec 2015

HAL is a multi-disciplinary open access archive for the deposit and dissemination of scientific research documents, whether they are published or not. The documents may come from teaching and research institutions in France or abroad, or from public or private research centers.

L'archive ouverte pluridisciplinaire **HAL**, est destinée au dépôt et à la diffusion de documents scientifiques de niveau recherche, publiés ou non, émanant des établissements d'enseignement et de recherche français ou étrangers, des laboratoires publics ou privés.

Numéro d'Ordre: D.U. 2579

UNIVERSITE BLAISE PASCAL
U.F.R. Sciences et Technologies
ECOLE DOCTORALE DES SCIENCES FONDAMENTALES

N°: 826

and

NATIONAL TECHNICAL UNIVERSITY OF UKRAINE
“KYIV POLYTECHNIC INSTITUTE”

COTUTELLE THESIS

In fulfillment of requirements for the Doctoral degree

by

Yaroslav G. GROSU

M.S. in Applied physics

THERMODYNAMICS AND OPERATIONAL PROPERTIES OF NANOPOROUS HETEROGENEOUS LYOPHOBIC SYSTEMS FOR MECHANICAL AND THERMAL ENERGY STORAGE/DISSIPATION

SPECIALITY:

Université Blaise Pascal: *Physical Chemistry*

National Technical University of Ukraine “Kyiv Polytechnic Institute”: *Engineering*

President:	J.-P. E. GROLIER	Université Blaise Pascal – Clermont-Ferrand 2
Reviewer:	E. CHARLAIX	Université Joseph Fourier – Grenoble 1
Supervisor:	V. EROSHENKO	National Technical University of Ukraine “Kyiv Polytechnic Institute”
Rewriter:	P. LLEWELLYN	CNRS, Marseille
Examiner:	V. STOUDENETS	National Technical University of Ukraine “Kyiv Polytechnic Institute”
Supervisor:	J.-M. NEDELEC	Ecole Nationale Supérieure de Chimie de Clermont-Ferrand

Defended on June 2nd 2015

ACKNOWLEDGEMENTS

I would like to express my deepest gratitude to Prof. Valentin Eroshenko for inspiring me for the preparation of this work and for his exemplary incentive to keep my motivation and productivity at high level from the first day of postgraduate work until the defense. I can't thank enough Prof. Jean-Pierre Grolier for always being open to help in any kind of problems, for being a bright example of successful scientist and kind person and for being unbelievably hard working with me all the time. I am very grateful to Prof. Jean-Marie Nedelec for his wide and strategic vision of the scientific problems and for being strong, but at the same time very positive boss.

I want to thanks to Dr. Victor Stoudenets and Nikolay Tsirin for their constant support and fruitful discussions during this work. I am much obliged to Prof. Stanislaw Randzio for his huge help on the handling and technical support of scanning transitiometer used as the main experimental equipment for this work.

I am very thankful to Dr. Leticia Carbajal for not only being a great friend, but also helping colleague especially for mercury porosimetry, gas sorption and DSC techniques. I want to thank to Dr. Geraldine Torin Ollarves for sharing her experience in scanning transitiomerty and for being a wonderful friend. Many thanks to Dr. Sandrine Renaudin for her help with XRD and FTIR experiments. I also want to express my thanks to principal constructor at Thermomolecular Energy (TME) laboratory Ivan Piatiletov for his useful advices on technical design and help with the graphics. I am glad I had an opportunity to work with great PhD-students of TME laboratory Oleksiy Ievtushenko, Artem Popik, Elisabeth Suzdalska and Tatiana Yarosh.

I want to thank Prof. Elizabeth Charlaix and Prof. Philip Llewellyn for their agreement to be reviewers of this work. I want to thanks to Prof. Valerii I. Deshko the head of Department of Thermal Engineering and Energy Saving of NTUU "KPI" for his support and positive attitude.

Special thanks to Prof. Helen Homonay for being an exceptionally inspiring professor and her great influence on my overall perception of our physical universe and the phenomenology to describe it.

I'm deeply indebted to the Grolier family for their warm welcoming me in France and their great help during my stay in this wonderful country. I want to thanks my good friends PhD-

students of UBP Alex Lowe and Barbara Liborio for their active participation in my after-work activities in Clermont-Ferrand.

I am very thankful to my family for their constant support and for always providing me with the freedom of my choices. My heartfelt and deepest thanks are expressed to my wife Maria for her strong support and understanding, for her profound and inspiring vision of our world and for her infinite beauty, which inspires me for newer and newer achievements.

I want to thanks to many people, who were not mentioned, but in different ways helped me in the preparation of this work.

I want to dedicate this collaborative work between France and Ukraine to so many Ukrainians currently struggling on the painful path to the new free future where their country is a part of Europe.

TABLE OF CONTENTS

LIST OF SYMBOLS AND ACRONYMS	7
INTRODUCTION	13
1. OPERATIONAL PRINCIPLES, TYPES AND MAIN CHARACTERISTICS OF POROUS HETEROGENEOUS LYOPHOBIC SYSTEMS (HLS)	17
2. EXPERIMENTAL TECHNIQUES AND MATERIALS	33
2.1. The main techniques	35
2.1.1. Scanning transitiometry	35
2.1.1.1. Transitiometer ST-7M	39
2.1.1.2. Experimental procedures and sample preparation	44
2.1.1.2.1. Calorimeter calibration	44
2.1.1.2.2. Bellows calibration	46
2.1.1.2.3. Sample preparation	47
2.1.1.2.4. Isothermal experiments	50
2.1.1.2.5. Isobaric experiments	50
2.1.1.2.6. Experiments under constant load	51
2.2. Additional techniques	52
2.2.1. X-ray Diffraction	52
2.2.2. Fourier Transform Infra-Red spectroscopy	52
2.2.3. Scanning Electron Microscopy	52
2.3. Materials	52
3. PROPERTIES OF HLSs	55
3.1. Describing HLS as complex thermodynamic system	58
3.1.1. Limitations of the usage of equilibrium thermodynamics	58
3.1.2. Thermal equation of state	59
3.1.3. Maxwell relations and thermal coefficients	67
3.1.4. Thermal effects of compression/decompression	75
3.1.5. Heat capacities and other properties of HLSs based on matrixes with complex pore size distribution functions	88
3.1.6. Effect of negative thermal expansion	105

3.2.	Temperature dependences of intrusion and extrusion pressures	125
3.3.	Stability of HLSs characteristics under operational conditions	137
CONCLUSIONS		157
REFERENCES		161
APPENDIXES		173
Appendix A. Maxwell relations		175
Appendix B. Thermal coefficients		178
Appendix C. Thermal effects of compression-decompression		181
Appendix D. Isochoric and isothermal heat capacity		182
Appendix E. Energetic characteristics of HLSs		183

LIST OF SYMBOLS AND ACRONYMS

C_i	Integration constant
$C_V^{int,ext}$	Heat capacity of HLS at constant volume, J/K
$C_P^{int,ext}$	Heat capacity of HLS at constant pressure, J/K
C_V^0	Heat capacity of liquid and matrix of HLS at constant volume, J/K
C_P^0	Heat capacity of liquid and matrix of HLS at constant pressure, J/K
$c_V^{int,ext}$	Specific heat capacity of HLS at constant volume, J/K
$c_P^{int,ext}$	Specific heat capacity of HLS at constant pressure, J/K
c_V^0	Specific heat capacity of liquid and matrix of HLS at constant volume, J/K
c_P^0	Specific heat capacity of liquid and matrix of HLS at constant pressure, J/K
$D_{int,ext}$	Dispersion of intrusion/extrusion pressure, Pa
F	Helmholtz energy, J
G	Gibbs potential, J
H	Enthalpy, J
I	Van der Waals integral, J·m/kg
\aleph	Calibration constant of calorimeter, W/V
k	Coefficient of geometry of pores
L	Calibration constant of LVDT, m ²
l	Values of LVDT, mm
P	Pressure, Pa
P_0	Pressure, Pa

Q	Heat, J
q	Heat flow, J
r	Pore radius, m
S	Entropy, J/K
T	Temperature, K
T_0	Temperature, K
t	Time, s
U	Internal energy, J
V	Volume, m ³
V_0	Volume of liquid and matrix of HLS, m ³
V_0^0	Initial volume of liquid and matrix of HLS, m ³
V_{pore}	Pore volume of the matrix, m ³
W	Work, J
$\alpha^{int,ext}$	Isobaric coefficient of thermal expansion of HLS, K ⁻¹
α^0	Isobaric coefficient of thermal expansion of liquid and matrix of HLS, K ⁻¹
$\beta^{int,ext}$	Isochoric coefficient of pressure of HLS, K ⁻¹
β^0	Isochoric coefficient of pressure of liquid and matrix of HLS, K ⁻¹
σ	surface tension of liquid, J/m ²
$\mu_T^{int,ext}$	coefficient of isothermal compressibility of HLS, Pa ⁻¹
μ_T^0	coefficient of isothermal compressibility of liquid and matrix of HLS, Pa ⁻¹
$\mu_S^{int,ext}$	coefficient of adiabatic compressibility of HLS, Pa ⁻¹
μ_S^0	coefficient of adiabatic compressibility of liquid and matrix of HLS, Pa ⁻¹
ρ	density, kg/m ³

τ	line tension, J/m
Ω	area of interface, m ²
K_i	polynomial coefficient
θ_A	advancing contact angle, rad
θ_R	receding contact angle, rad

Acronyms

CS	Calorimetric signal
NTE	Negative thermal expansion
HLS	Heterogeneous lyophobic system
RC	Repulsive clathrate
int	Intrusion
ext	Extrusion

INTRODUCTION

INTRODUCTION

The problem of rational energy consumption is one of the most important global problems of contemporary humanity, which greatly stimulates the scientific community to search for new sources of energy as well as methods for its efficient utilization and storage. In particular a problem of efficient thermal energy storage is one of unsolved challenges today.

The use of surface energy on ‘solid – liquid’ interface as a working body for mechanical and thermal energy storage and transformation was proposed as an alternative to conventional methods by Prof. Eroshenko in the 1980’s. It was shown that naturally such surface energy becomes dominant for systems with large specific surface (from 400 m²/g and higher) and reversible operational cycle (reversible interface area development-reduction) can be realized using highly porous Heterogeneous Lyophobic Systems (HLSs), that is an ensemble of a highly porous solid and a non-wetting liquid. Due to its nature such working bodies demonstrate distinguished properties and characteristics in comparison with conventional working bodies: high energy capacity, ability to simultaneously store (restore) both mechanical and thermal energy during compression (decompression), most frequently being in the form of a suspension an HLS has strongly nonlinear and orders of magnitude higher compressibility compared to simple liquid together with the ability to operate at very high frequencies without overheating. Apart from energy storage and transformation, HLSs with large stored-restored energy hysteresis were proposed to be used for efficient energy dissipation applications.

First publications on the properties and applications of HLS were in the form of classified patents by Eroshenko (Eroshenko 1981), (Eroshenko 1980, 1982, 1983, 1985a, 1985b, 1986, 1987a)¹. In the beginning of the 1990’s works in this area became unclassified (Eroshenko 1987b, 1990, 1996, 1997, 2000, 2003, 2007, Eroshenko and Fadeev 1995, Fadeev and Eroshenko 1997, Eroshenko et al. 2001, 2002, 2007, Eroshenko and Stoudenets 2002, Coiffard and Eroshenko 2006, Eroshenko and Lazarev 2012) and stimulated the development of mentioned above ideas in number of laboratories in different countries. Particularly a great number of porous materials coupled with water and aqueous solutions were investigated by Patarin and co-workers focusing on the energetic characteristics and operational stability of HLSs (Trzpit et al. 2007a, 2007b, 2008, 2009a, 2009b, Cailliez et al. 2008, Karbowski et al. 2010a, Saada et al. 2010a, 2010b, Tzanis et al. 2011, 2012a, 2012b, 2014, Ortiz et al. 2013, 2014a, 2014b, Khay et

¹ Multiple reference No. 30.

al. 2013, 2014). Impressive success in the development of devices for mechanical energy dissipation applications was achieved by Suciu, especially in the development of HLSs-based car shock-absorber (Suciu et al. 2000, 2003, 2004, 2005, 2010a, 2010b, 2010c, Iwatsubo et al. 2007, Suciu and Yaguchi 2009, Suciu 2008, 2010, Suciu and Tobiishi 2012, Suciu and Kimura 2012, Suciu and Buma 2013). Qiao and co-workers investigated a number of potential HLSs-based smart applications in the field of energy storage, dissipation and transformation and their characteristics (Han and Qiao 2006, 2007a, 2007b, 2007c, 2007d, Liu et al. 2008, 2009a, 2009b, Kong and Qiao 2005a, 2005b, Han et al. 2006, 2008a, 2008b, 2008c, 2008d, 2008e, 2009a, 2009b, Kong et al. 2005, Qiao et al. 2006, 2007, Surani et al. 2005, 2006, Surani and Qiao 2006a, 2006b, 2006c, Cao et al. 2008a, 2008b, Chen et al. 2006, 2008, Qiao and Han 2007, Xu et al. 2011a, 2011b). Several important insights into the physical mechanisms of HLSs operation can be found in the works supervised by Prof. E. Charlaix (Lefevre et al. 2004a, 2004b, Guillemot 2010, Guillemot et al. 2012a, 2012b, Michelin-Jamois et al. 2014). Highly valuable and still rare calorimetric measurements for HLSs were performed by Grolier and co-workers (Coiffard 2005) and Bellat and co-workers (Karbowiak 2009, 2010a, 2010b, 2013). The investigations focused on percolation effects during HLS operation can be found in the works of Borman et al. (Borman et al. 2000, 2001, 2004, 2005, 2009, 2011, 2012). Some important microscopic insights for HLS can be found in the works of Bushuev and Sastre (Bushuev and Sastre 2010, 2011, 2012).

Despite significant advances in the study of the properties of HLSs in recent years, the relevance of in-depth study of their thermodynamics properties is very high. Parameters of HLSs such as working (intrusion/extrusion) pressure, thermal effects, heat capacity, thermal conductivity and others are seldom studied in a wide temperature range, however, the investigation of the temperature dependence of the thermodynamic properties of HLSs is essential for expanding the class of devices based on them, as well as improving the efficiency of existing models, an in-depth thermodynamic description of HLSs is not yet proposed and operational mechanism of nano-HLSs is not fully understood.

Based on the above indicated problems the following tasks for this work were chosen.

1. Develop a mathematical description of HLSs by means of a thermodynamic of complex systems approach, including equation of state for real HLSs.

2. Making use of the results of the thermodynamic analysis, to implement an experimental and theoretical investigation of the properties and characteristics of HLSs, which are prominent in the processes of energy storage, dissipation and transformation, in a wide temperature range.

3. On the basis of the preceding tasks explore both experimentally and theoretically ways to improve, *i.e.* tune, the characteristics of HLSs for optimizing their use.

The thesis is organized in the following way. The Introduction is followed by Chapter 1 explaining the operational principles of the object of the study, which is porous Heterogeneous Lyophobic System (HLS), including the description of known types of HLSs and of their main characteristics. It also contains a short review of literature results, which is aimed at highlighting the evolution of the investigations of HLSs and topical problems still to be solved. In the following Chapter 2 the experimental techniques, equipment, materials and procedure of HLSs preparation are described. Next Chapter 3 presents an attempt to build the thermodynamic description of HLS by mean of equilibrium thermodynamics of complex systems by proposing an equation of state of an HLS, which includes pores size distribution function of the matrix (Paragraph 3.1). Special attention in Paragraph 3.2 is paid to experimental and theoretical investigation of the temperature dependence of the intrusion/extrusion pressure of HLSs as one of their most important characteristic. In Paragraph 3.3 the conditions (especially temperature ranges) which provide stability of characteristics of HLS are described. The last part of the thesis is Conclusions followed by the References. Appendixes providing additional information are placed at the end of the present document.

Most of the results presented in the Thesis were published in peer reviewed journals and are presented as reprints of corresponding papers (overall 10 papers). The citations are made in the (*author year*) form, which differs from the forms of citations used in reprints of the papers presented in here.

CHAPTER 1

OPERATIONAL PRINCIPLES, TYPES AND MAIN CHARACTERISTICS OF POROUS HETEROGENEOUS LYOPHOBIC SYSTEMS (HLSs)

**OPERATIONAL PRINCIPLES, TYPES AND MAIN
CHARACTERISTICS OF POROUS HETEROGENEOUS LYOPHOBIC
SYSTEMS (HLSs)**

The following reprint of the paper (Eroshenko and Grosu 2014a) published as proceedings of MMT-2014 conference (Ariel, Israel) is proposed. It describes essence and the physical model of HLSs and reports a brief review of characteristics of HLSs presented in the literature, underlining the desirable properties of HLSs in view of practical applications.

IMPORTANCE OF SYNTHESIS OF LYOPHOBIC POROUS MATERIALS AND CORRESPONDING LIQUIDS FOR DEVELOPMENT OF THERMOMOLECULAR ENERGY DEVICES OF NEW GENERATION

Eroshenko V.A. and Grosu Y.G.

National Technical University of Ukraine, Kyiv Polytechnic Institute, Laboratory of Thermomolecular Energetics, Prospect Peremogy 37, 03056 Kyiv, Ukraine.

E-mail: eroshenko@kpi.ua

Wetting phenomenon is of great importance in most of branches of natural science. Combined with confinement effect that takes place in microporous capillary systems, wetting is highly discussed topic today, with many fundamental questions to be answered. Thermomolecular energetics (TME) is a new area of non-traditional efficient energy transformation, accumulation and dissipation. The object of TME is repulsive clathrates (RC) – heterogeneous lyophobic system which consists of porous solid and non-wetting liquid. Further development of TME is closely linked with the progress in understanding of non-wetting phenomenon in capillary confinement as well as with success in synthesis of lyophobic porous materials and liquids with desirable characteristics. By means of technical thermodynamics the report reveals the essence of new working media (RC), which takes advantage of potential intermolecular forces at the solid-liquid interface. Fundamental questions of wetting which will give a powerful impetus for development and improvement of new energy devices are discussed. Examples of existing RC-based devices with efficiency and ecological indexes orders of magnitude higher in comparison with the conventional analogues are described.

Introduction

Solid – liquid interface can store and restore mechanical and thermal energy in the form of Gibbs surface energy W_{Ω} (1) and heat of interface development/reduction Q_{Ω} (2) [1]:

$$\delta W_{\Omega}^{int,ext} = -\sigma \cos\theta_{A,R} d\Omega \quad (1)$$

$$\delta Q_{\Omega}^{int,ext} = T \frac{d(\sigma \cos\theta_{A,R})}{dT} d\Omega \quad (2)$$

Where index “int” corresponds to the process of development of interface area Ω and index “ext” to its reduction; σ is surface tension of the liquid, θ_A and θ_R are advancing and receding contact angles, respectively; T is temperature.

To make the values of $W_{\Omega}^{int,ext}$ and $Q_{\Omega}^{int,ext}$ high enough to be attractive for engineering applications, it was proposed to use porous heterogeneous lyophobic systems (HLS) with high values of specific area (400 – 1800 m²/g) as new working media (fig. 1a) [2, 3].

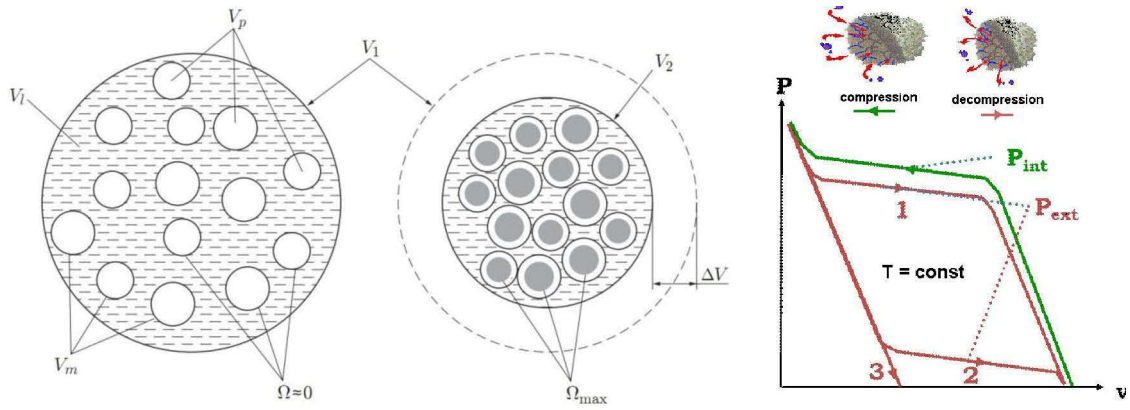


Fig. 1. a) Physical model of heterogeneous lyophobic system (HLS); b) HLS with different values of hysteresis in the compression-decompression cycle: curve 1 – minimum hysteresis, 2 – large hysteresis, 3 – 100% hysteresis.

HLS (or repulsive clathrate) [39] is presented by a porous matrix with open porosity and a liquid which does not wet the matrix. The system must be highly lyophobic: $120^\circ < \theta \leq 180^\circ$. The thermodynamic essence of energy conversion process is the following: during the HLS compression forced intrusion of the liquid into the pores takes place under external pressure P^{int} equal to or greater than the Laplace capillary pressure (3) [4]. This intrusion is followed by the development of a huge solid – liquid interface Ω and hence accumulation of a huge internal surface energy. By reducing the external pressure to some critical value P^{ext} , this energy can be released due to self-driven spontaneous extrusion of the liquid clusters from the pores (reduction of the interface).

$$P_{int,ext} = -\frac{\sigma \cos \theta_{A,R}}{kr}, \quad (3)$$

Where k is geometry coefficient of the pores ($k = 1/2$ for long cylinders, $k = 1/3$ for spheres) Depending on the nature of HLS the difference between P^{int} and P^{ext} can be small (curve 1 on the fig.1b), so system may be used for energy storage or conversion, or it can be large (curve 2 and 3 on the fig.1b), so system may be used for energy dissipation.

Taking into account that from thermodynamic point of view 2-dimensional interface acts as working body, HLS have number of interesting properties and characteristics, which were used to develop new class of energy applications in the field of thermomolecular energy, which will be briefly described below.

Development of new efficient energy equipment based on HLS is highly dependent on its key properties: porosity, specific area, lyophobicity, endurance of the porous matrix; crystallization and boiling temperatures, surface tension and its temperature dependence of the non-wetting liquid. This paper is dedicated to formulate priority problems in investigating properties of HLS based on review of available results and explain the perspectives it opens for development of new efficient energy equipment.

Examples of heterogeneous lyophobic systems

Below we provide information on investigated HLS based on different matrices and water. The names of the matrix in the table are similar to the ones used in original papers. Most of the microporous samples are zeolites and mesoporous are grafted silicas, the details of the synthesis and grafting procedure can be found in the original papers for which references are provided. The values of P^{int} and P^{ext} provided in the table are mean values on the intrusion and extrusion plateaus on the corresponding PV-diagrams. The values in the table are divided by the mass of the matrix. The values are presented under room temperature if other is not indicated. The values are presented for 1st cycle of intrusion and extrusion.

Table 1. Characteristics of HLSs based on water and different matrices

Porous matrix	e^{store} , J/g	$e^{restore}$, J/g	P_{intr} MPa	P_{extr} MPa	r, nm	Vpore, cm ³ /g	Ref.
MTS-4g	28,9	0	14,4	0	5,4	2,01	[5]
MTS-3g	23,8	1,7	35	2,5	2,0	0,68	[5]
MTS-1g	20,8	10,8	59,5	30,8	1,3	0,35	[5]
MTS-2g	19,5	2,7	44,4	6,2	1,6	0,44	[5]
ZSM-12	15,0	14,4	132	126	0,28-0,3	0,114	[6]
Ferrierite	15,0	14,5	147	142	0,175-0,24	0,102	[7]
HMS (50°C)	14,3	4,8	32,6	10,9	1,54	0,44	[8]
MCM-41 (50°C)	14,3	5,9	43,2	17,8	1,34	0,33	[8]
ZSM-22	14,0	12,7	186	172	0,23-0,285	0,075	[6]
Zif-8	13,3	11,2	27	22	0,19	0,5	[9]
Fluka 100 C ₈	12,9	0	23,5	0	7,8	0,55	[10]
Waters Symmetry Prep C8	9,8	1,0	18,5	1,9	4,2	0,53	[11]
Silicalite-1 (MFI-F)	9,3	8,4	88	83	0,3	0,14	[12]
EVA	9,2	1,1	21	3	4,0	0,51	[12]
ZSM-5	8,8	8,5	73	70,8	0,315	0,12	[13]
Silicalite-1 (MFI-F)	8,5	8,3	90	88	0,3	0,094	[14]
SBA-15 (50°C)	8,4	1,7	29,1	6,0	2,16	0,29	[8]
ITQ-12 (ITW)	8,1	8,1	172	172	(3.8×4.1Å) and (2.4 × 5.3 Å)	0,047	[15]
Silicalite-1 (MFI-F)	7,2	6,5	90	86,8	0,3	0,08	[16]
SSZ-23	7,0	5,6	40	33	0,12-0,175	0,13	[17]
DD3R	6,7	5,7	60	51	0,18-0,22	0,11	[17]
Silicalite-2	6,5	5,9	63	58	0,27	0,103	[17]
DGSBA-15	6,1	0	15	0	2,3	0,61	[18]
SSZ-24	5,8	5,6	58	55	0,365	0,102	[6]
ITQ-4	5,7	0	42	0	0,31-0,36	0,136	[19]
Silicalite-1 (MFI-OH)	5,6	5,5	80	76	0,3	0,12	[12]
Chabazite	5,5	4,6	37	31	0,19	0,15	[20]
CHA Zeosil	4,7	4,5	36	30	0,19	0,16	[21]
TGSBA-15	4,3	0	10	0	2,45	0,74	[18]

ITQ-7	4,3	0,5	30	0,3	0,325-0,305	0,21	[22]
TMS-PhSBA-1	1,8	0	25	0	2,0	0,144	[23]
RUB- 41	0,2	0,075	1,5	0,5	0,205-0,295	0,15	[24]

Desirable properties of porous materials

Energy capacity of HLS is proportional to the volume of the pores of the matrix V_{pore} and intrusion/extrusion pressure (3), as during the intrusion/extrusion of the liquid the work of compression/decompression is defined as:

$$W_{\Omega}^{int,ext} = P^{int,ext} \cdot V_{pore} \quad (4)$$

Although increasing of $P^{int,ext}$ values in principle increases $W_{\Omega}^{int,ext}$ engineering limitations should be taken into account. For example for number of zeolites (table 1) intrusion pressure exceeds 100 MPa, which greatly constricts the range of their applicability. While increasing specific volume of the pores V_{pore} (or the porosity) of the matrix does not bring such limitations and should be considered as priority method of increasing specific energy capacity of the HLS. Of course increasing the porosity affects the endurance of the matrix, which in most HLS-applications experiences rather high pressures during great number of cycles of compression-decompression. Synthesis of firm and stable materials with maximum possible porosity is most important challenge to develop highly efficient and compact energy equipment based on HLS.

Contrary to mechanical energy capacity of HLS (1), thermal one (2) may be only increased by increasing specific area of the matrix. Calorimetric measurements of compression-decompression cycle of some HLS [16, 21, 14, 12] shows rather high values of $\delta Q_{\Omega}^{int,ext}$ (5-7 J/g) under room temperature and expected to grow linearly with temperature (2). A good example of hydrophobic firm and stable porous material with highly developed area (1800 m²/g) and acceptable $P^{int,ext}$ pressures is metal organic framework Zif-8 tested recently with water [9].

The class of mesoporous silica gels are successfully used with water for HLS-based dissipators of energy (large intrusion-extrusion pressures hysteresis), but these porous materials must be grafted to achieve hydrophobicity. In principle the procedure of hydrophobization of materials is widely used and well known, but quite often as a result the pores of the grafted material became close (for example in case of polymeric hydrophobization). One of the methods to keep highly developed specific interface area and effective pore volume is to chemically bond hydrophobic molecules to the surface of the porous material. In this case the surface concentration of bonded molecules strongly affects wetting properties of grafted material such as dynamic and static contact angles, which are parameters of intrusion and extrusion pressures of HLS (3). Yet the dependence between level of hydrophobicity and concentration of bonded hydrophobic molecules may be rather complex and optimum conditions for specific application must be found. Figure 2 represents the dependence between advancing/receding contact angle on KSK-G silica gel ($r \sim 5\text{nm}$, $\Omega \sim 360\text{ m}^2/\text{g}$, $V_{pore} \sim 0,95\text{ cm}^3/\text{g}$) and surface concentration of bonded molecules of n-octyldimethylsilyl (the degree of the coverage of the surface).

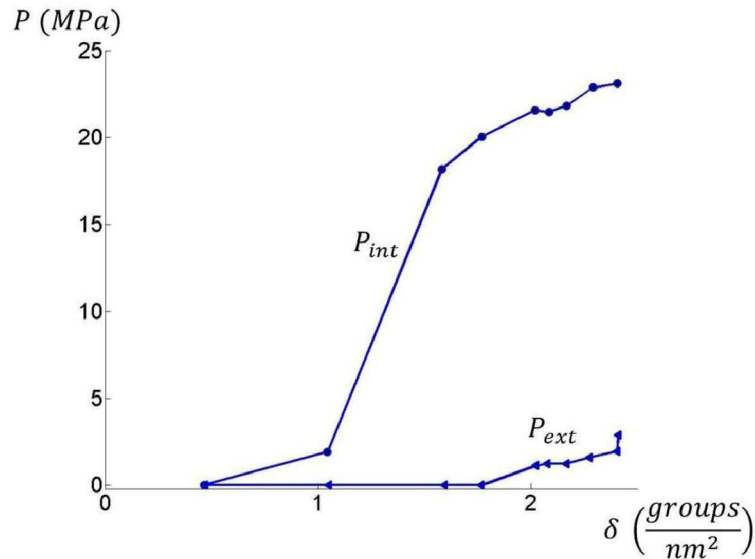


Fig. 2. The correlation between pressure of water intrusion–extrusion into KSK-G silica and bonding density of octyldimethylsilyl $\text{Si}(\text{CH}_3)_2\text{C}_8\text{H}_{17}$ groups.

It is important to note that contact angles inside mesoporous materials can not be measured directly and requires understanding of physical mechanism of intrusion/extrusion process. It seems that in most cases intrusion pressure is determined by capillary pressure (3) [12, 11, 14, 16], but for extrusion process most probably the conditions for bubble nucleation must be also satisfied [8, 5].

Desirable properties of liquids

The most important property of the non-wetting liquid for HLS is surface tension σ and its temperature dependence. Currently HLSs based on water and aqueous solutions, melted salts and metals, or low temperature eutectic alloys have been tested, which allows to vary the value of surface tension (and hence the value of $P_{int,ext}$ using the same matrix) in rather wide range (for example [25]).

Contrary the surface tension temperature dependence $\frac{d\sigma}{dT}$ is the parameter of HLS, which is much more difficult to vary as for most of the liquids $\frac{d\sigma}{dT}$ is of the same order as for example for water ($\sim 0,16$ mH/(m·K)) and greater values is rather rare case.

The variation of contact angles with temperature $\frac{d\theta_{A,R}}{dT}$ has attracted attention of the scientist for a quite a long time [26], yet there is no unified theory for this dependence today. Considering that for HLS mentioned dependence may be also affected by confined environment of pores, where size effects should be taken into account, determination of $\frac{d\theta_{A,R}}{dT}$ is one of the questions to be answered in the future. In ref. [27, 8, 5] the attempt to take into account the line tension of water for explaining the temperature dependence of intrusion/extrusion pressure was performed.

For engineering applications two extreme values of $\frac{d(\sigma \cos \theta_{A,R})}{dT}$ are of great interest:

1. $\frac{d(\sigma \cos \theta_{A,R})}{dT} \rightarrow 0$, which according to eq. (3) means stable values of working pressures under different temperatures of device and is desirable for such applications as HLS-based shock-absorbers, bumpers, anti-seismic systems, mechanical energy accumulators [28, 29, 30], etc.

2. $\frac{d(\sigma \cos \theta_{A,R})}{dT} \rightarrow \infty$, which according to eq. (2) means large values of thermal effects of intrusion/extrusion and is desirable for development of accumulators of thermal energy with large capacity, sensitive materials with negative thermal expansion, compact heat engines with high degree of carnotization [31, 30].

The values of temperature of liquid crystallization and temperature of boiling under working pressures directly determines the operation temperature range of HLS device, as for most of them liquid does not go through phase transition during HLS operation.

Perspectives of development of energy devices based on HLS with desirable properties

Described above properties of HLS directly determine their efficiency.

For HLS-based mechanical energy accumulators specific stored and restored energy may be defined as:

$$e^{store} = \frac{E^{int}}{V_{max}} = \frac{1}{\frac{1}{\varphi} + 1} P^{int} \quad (5)$$

$$e^{restore} = \frac{E^{ext}}{V_{max}} = \frac{1}{\frac{1}{\varphi} + 1} P^{ext} \quad (6)$$

Where $\varphi \left(\frac{cm^3}{cm^3} \right)$ is the porosity of the matrix.

For HLS-based thermal energy accumulators specific stored and restored energy may be defined as:

$$q^{store} = \frac{T}{kr \left(\frac{1}{\varphi} + 1 \right)} \frac{d\sigma \cos \theta_A}{dT} = \frac{T}{\frac{1}{\varphi} + 1} \frac{dP^{int}}{dT} \quad (7)$$

$$q^{restore} = \frac{T}{kr \left(\frac{1}{\varphi} + 1 \right)} \frac{d\sigma \cos \theta_R}{dT} = \frac{T}{\frac{1}{\varphi} + 1} \frac{dP^{ext}}{dT} \quad (8)$$

For HLS-based mechanical energy dissipaters specific energy of dissipation may be defined as:

$$e^{dis} = \frac{1}{\frac{1}{\varphi} + 1} (P^{int} - P^{ext}) \quad (9)$$

The carnotization of thermal cycle based on HLS with negligible hysteresis is defined as [31]:

$$\frac{\eta_{\Omega}}{\eta_c} = \frac{1}{1 - r \frac{k C_V^{\Sigma}}{\frac{d\sigma \cos\theta}{dT}} \eta_c} = \frac{1}{1 - \frac{C_V^{\Sigma}}{\frac{dP^{int}}{dT}} \eta_c} \quad (10)$$

Below we provide few examples of HLS-based devices and their characteristics.

Car shock absorber. As mentioned above HLS with large pressure hysteresis during compression-decompression cycle (Fig. 1b) may be used for mechanical energy dissipation. Shock absorbers based on the HLS have unique properties to operate under frequencies up to 22 Hz (inaccessible for classical analogues) for mechanical rods amplitude fluctuations of 0-80 mm [32 – 34, 38]. The stability of such devices has been proven experimentally in over 10 million cycles test of full compression/decompression, which agrees with the life of general machine elements [35]. The specific power of energy dissipation through the new shock absorber (20–50 W/cm³) is much higher compared to conventional (oil) analogue (0,10-0,15 W/cm³) [33], wherein ride-comfort of such shock absorber meets indices of traditional commercial analogues [36]. Traditional damper requires ~ 1500 cm³ of the technical oil, while HLS-based about 100 times less oil and about the same amount of {grafted silica gel + water} HLS, which increases ecological indexes of new device.

Autonomic actuator for space applications. An example of a successful constructive combination of accumulator and actuator is a device for deploying solar panels and operating optical instruments on satellites and spacecrafts [30]. The operational principle of device is very simple: after forced compression of device (intrusion, energy accumulation) device is being put on lock, which disables spontaneous extrusion of the liquid; next when required the lock is removed remotely, which is followed by discharge of device (extrusion, energy release). The design of its conventional analogue is based on the application of 13–15 "cleverly" connected Hooke type springs (in order to make the "force-displacement" characteristic more flat). While two times lighter device based on heterogeneous working medium has provided a 100 mm displacement with a constant force of 800 N (four as high as conventional analogue). The volume of the heterogeneous working medium was 16 cm³; the energy capacity $E = P \cdot \Delta V_{\Omega} \sim 6 \div 7 \text{ J/cm}^3$ under the pressure of $P \sim 20 \text{ MPa}$ and the porous volume of $\Delta V_{\Omega} \sim 0,5 \text{ cm}^3/\text{g}$.

Thermal lock. The essence of the smart autonomic compact device is the following. Under temperature higher than the temperature of the alloy crystallization T_{cry} , an alloy (or an eutectic) with a set down melting point is pumped through a pair of pistons and rods into the matrix pore space and under compressed state is cooled down to the environmental temperature. Under such conditions the alloy solidifies and remains in the matrix as long as its temperature is lower than T_{cry} . As soon as the room temperature rises to the melting point of the alloy, it will liquefy and under the capillary pressure will be thrown out from the matrix pore space. In such way the piston displacement may relieve the cooling agent (e.g. water or foam) to eliminate the source of overheating. Such "thermal lock" is fully autonomous and does not require any additional sensors. For example constructed sample with weight of only 600 g performed a constant force of 2000 N.

The above described system is successfully employed to create the thermal sensitivity of a trigger device to be used in the field of nuclear energy [37], namely for the emergency protection systems of the nuclear reactors from the overshooting of the

security temperature level. It also can be used to protect the chemical, technological and other energy equipment as regards their temperature level [37].

As can be seen from examples above, high energy capacity and other useful properties of HLS allows to develop efficient energy equipment with characteristics better in comparison with classical analogues. Any further development of parameters in eqs. (5) – (10) and described in previous paragraphs, open perspectives of expanding the range of applications of HLS as well as improve characteristics of existing ones.

Conclusions

Today properties and characteristics of many heterogeneous lyophobic systems have been investigated in order to use them in the processes of efficient energy storage, conversion or dissipation, which allowed to develop number of devices with attractive. Yet there is still great potential in the field of physical chemistry to improve characteristics of HLS, which opens perspectives of creating energy equipment of new generation.

The priority tasks are:

1. Synthesis of firm and stable lyophobic materials with maximum possible porosity.
2. Synthesis of liquids with extreme values of temperature coefficients of surface tension (zero or maximum).

A special case is synthesis of hydrophobic materials, as usage of water as non-wetting liquid not only makes such HLS environment friendly, but greatly lowers the price of such device.

Further success in the field of thermomolecular energetics is also highly dependent on success in solving fundamental problems of wetting theory, such as contact angle temperature dependence, the influence of confined environment on the properties of liquid inside meso- and micropores, the mechanism of liquid intrusion and extrusion.

References

1. Adamson A. W.: Physical chemistry of surfaces. New York: Wiley, 1997.
2. Eroshenko V. A.: Effect of heat exchange on filling of lyophobic pores and capillaries with liquid. Colloid J. USSR 1988 49(5).
3. Eroshenko V., Regis R. C., Soulard M., Patarin J.: 'Energetics: a new field of applications for hydrophobic zeolites'. Journal of the American Chemical Society 2001 123(33) 8129-8130.
4. Washburn E. W.: 'The dynamics of capillary flow'. Physical review 1921 17(3).
5. Lefevre B., Saugey A., Barrat J. L., Bocquet L., Charlaix E., Gobin P. F., Vigier G.: 'Intrusion and extrusion of water in hydrophobic mesopores'. Journal of chemical physics 2004 120 4927.
6. Tzanis L., Trzpit M., Soulard M., Patarin J.: 'High pressure water intrusion investigation of pure silica 1D channel AFI, MTW and TON-type zeolites'. Microporous and Mesoporous Materials 2011 146(1) 119-126.

7. Cailliez F., Trzpit M., Soulard M., Demachy I., Boutin A., Patarin J., Fuchs A. H.: 'Thermodynamics of water intrusion in nanoporous hydrophobic solids'. *Physical Chemistry Chemical Physics* 2008 10(32) 4817-4826.
8. Guillemot L., Biben T., Galarneau A., Vigier G., Charlaix É.: 'Activated drying in hydrophobic nanopores and the line tension of water' *Proceedings of the National Academy of Sciences of USA*. 2012 109(48) 19557-19562.
9. Ortiz G., Nouali H., Marichal C., Chaplais G., Patarin J.: 'Energetic Performances of the Metal-Organic Framework ZIF-8 by High Pressure Water Intrusion-Extrusion Experiments'. *Physical Chemistry Chemical Physics* 2013 15(14) 4888-4891.
10. Han A., Kong X., Qiao Y.: 'Pressure induced liquid infiltration in nanopores'. *Journal of applied physics* 2006 100(1) 014308.
11. Coiffard L., Eroshenko V.: 'Temperature effect on water intrusion/expulsion in grafted silica gels'. *Journal of colloid and interface science* 2006 300(1) 304-309.
12. Coiffard L., Eroshenko V. A., Grolier J. P. E.: 'Thermomechanics of the variation of interfaces in heterogeneous lyophobic systems'. *AIChE journal* 2005 51(4) 1246-1257.
13. Qiao Y., Punyamurtula V. K., Han A., Kong X., Surani F.: 'Temperature dependence of working pressure of a nanoporous liquid spring'. *Applied physics letters* 2006 89(25) 251905.
14. Karbowski et al.: 'New insights in the formation of silanol defects in silicalite-1 by water intrusion under high pressure'. *Physical Chemistry Chemical Physics* 2010 12(37) 11454-11466.
15. Khay I., Tzani L., Daou T. J., Nouali H., Ryzhikov A., Patarin J.: 'Energetic behavior of the pure silica ITQ-12 (ITW) zeolite under high pressure water intrusion'. *Physical Chemistry Chemical Physics* 2013 15(46) 20320-20325.
16. Ievtushenko O. V., Eroshenko V. A., Grosu Y. G., Nedelec J. M., & Grolier J. P. E.: 'Evolution of the energetic characteristics of {silicalite-1+ water} repulsive clathrates in a wide temperature range'. *Physical Chemistry Chemical Physics* 2013 15(12) 4451-4457.
17. Tzani L., Trzpit M., Soulard M., Patarin J.: 'Energetic Performances of Channel and Cage-Type Zeosils'. *The Journal of Physical Chemistry C* 2012 116(38) 20389-20395.
18. Gokulakrishnan N., Parmentier J., Trzpit M., Vonna L., Paillaud J. L., Soulard M.: 'Intrusion/Extrusion of Water Into Organic Grafted SBA-15 Silica Materials for Energy Storage'. *Journal of nanoscience and nanotechnology* 2013 13(4) 2847-2852.
19. Saada M. A., Rigolet S., Paillaud J. L., Bats N., Soulard M., Patarin J.: 'Investigation of the energetic performance of pure silica ITQ-4 (IFR) zeolite under high pressure water intrusion'. *The Journal of Physical Chemistry C* 2010 114(26) 11650-11658.
20. Trzpit M., et al.: 'The effect of local defects on water adsorption in silicalite-1 zeolite: A joint experimental and molecular simulation study'. *Langmuir* 2007 23(20) 10131-10139.
21. Karbowski T., Weber G., Bellat J. P.: 'Confinement of water in hydrophobic

- nanopores: effect of the geometry on the energy of intrusion'. *Langmuir* 2013 30 (1) 213–219.
22. Tzani L., Marler B., Gies H., Patarin J.: 'High-Pressure Water Intrusion Investigation of Pure Silica ITQ-7 Zeolite'. *The Journal of Physical Chemistry C* 2013 117(8) 4098-4103.
 23. Gokulakrishnan N., et al.: 'Improved hydrophobicity of inorganic–organic hybrid mesoporous silica with cage-like pores'. *Colloids and Surfaces A: Physicochemical and Engineering Aspects* 2013 421 34-43.
 24. Saada M. A., Soulard M., Marler B., Gies H., Patarin J.: 'High-Pressure Water Intrusion Investigation of Pure Silica RUB-41 and S-SOD Zeolite Materials'. *The Journal of Physical Chemistry C* 2010 155(2) 425-430.
 25. Tzani L., Nouali H., Daou T. J., Soulard M., Patarin J.: 'Influence of the aqueous medium on the energetic performances of Silicalite-1'. *Materials Letters* 2014 115 229-232.
 26. Sullivan D. E.: 'Surface tension and contact angle of a liquid–solid interface'. *The Journal of Chemical Physics* 1981 74 2604.
 27. Grosu Y., Ievtushenko O., Eroshenko V., Nedelec J. M., & Grolier J. P. E.: 'Water intrusion/extrusion in hydrophobized mesoporous silica gel in a wide temperature range: Capillarity, bubble nucleation and line tension effects'. *Colloids and Surfaces A: Physicochemical and Engineering Aspects* 2014 441 549-555.
 28. Eroshenko V. A.: 'Repulsive Clathrates. A New Operational Material for Efficient Seismic Isolation'. *Seismic Isolation, Passive Energy Dissipation and Active Control of Seismic Vibrations of Structure, Sicily, Italy, 1997*.
 29. V. A. Eroshenko, 'Damper with high dissipating power'. US Patent 20030010587 A1, 3 Aug 2003.
 30. Eroshenko V.A.: Heterogeneous structure for accumulation or dissipation of energy, process to use it and associated devices, Int. Patent WO 96/18040, 1996.
 31. Eroshenko V.A.: Heterogeneous Thermodynamic System. Eroshenko Cycle of Transformation of Thermal Energy into Mechanical Energy and Devices to Achieve It (in Russian), USSR-Russian Patent 1,254,811, 1981.
 32. Eroshenko V. A.: 'A new paradigm of mechanical energy dissipation. Part 1: theoretical aspects and practical solutions'. *Proceedings of the Institution of Mechanical Engineers, Part D: Journal of Automobile Engineering* 2007 221(3) 285-300.
 33. Eroshenko V. A., Piatiletov I., Coiffard L., Stoudenets V.: 'A new paradigm of mechanical energy dissipation. Part 2: experimental investigation and effectiveness of a novel car damper'. *Proceedings of the Institution of Mechanical Engineers, Part D: Journal of Automobile Engineering* 2007 221(3) 301-312.
 34. Guillemot L., Galarneau A., Vigier G., Abensur T., Charlaix É.: 'New device to measure dynamic intrusion/extrusion cycles of lyophobic heterogeneous systems'. *Review of Scientific Instruments* 2012 83(10) 105105.
 35. Suciú C. V., Yaguchi K.: 'Endurance tests on a colloidal damper destined to vehicle suspension'. *Experimental mechanics* 2009 49(3) 383-393.

36. Suciu C. V.: 'Ride-comfort of an automobile equipped with colloidal dampers at its frontal suspension'. In Proc. Int. Conf. on Noise and Vibration Eng 2010 4233-4245.
37. Egorov V.S., Portyanoy A.G., Sorokin A.P., Maltsev V.G., Voznesensky R.M. Ivchenko A.P.: Thermal sensitivity of the starting device, Russian patent No 2138086, 1996.
38. Eroshenko V. Virtually oil-free shock absorber having high dissipative capacity. U.S. Patent Application 13/820,977, 2011.
39. Eroshenko, V. A., and Yu F. Lazarev. Rheology and dynamics of repulsive clathrates. Journal of Applied Mechanics and Technical Physics. 53.1 (2012): 98-112.

CHAPTER 2

EXPERIMENTAL TECHNIQUES AND EQUIPMENT

EXPERIMENTAL TECHNIQUES AND EQUIPMENT

2.1. THE MAIN TECHNIQUES

Considering the goals of this investigation (see the Introduction) the technique of scanning transitiometry (<http://transitiometry.com/>) was chosen for experimental investigation of thermodynamic properties of HLSs. For HLSs based on mercury the classical technique of mercury porosimetry was preferable. Both techniques as well as experimental equipment and sample preparation are described below.

2.1.1. Scanning transitiometry

Scanning transitiometry is a relatively new method of thermodynamic study. It combines the use of both the fundamental thermodynamic principles and the newest technologies of controlling state variables (P , V , T) and measuring simultaneously the appropriate heat effects with extremely high sensitivity. From the heat effects and variations of the respective state variables both mechanical and thermal equations of state can be simultaneously determined (Randzio et al. 1994, Randzio et al. 1995, Randzio 1996, Randzio and Grolier 1998, Randzio et al. 2003).

A typical scanning transitiometer consists in the following parts: 1) the sensitive differential calorimeter (located in the solid state thermostat); 2) digital precise temperature and pressure controllers; 3) high-pressure pump driven by stepping motor; 4) a pair of identical thermopiles housing the measurement and reference cells.

Figure 2.1 shows a diagram of the thermodynamic relationships between selected independent variables of the system (P , V , T) and heat flux (q). The scheme shows that in

addition to the classical scanning calorimetry at a controlled temperature (differential scanning calorimetry), where the calorimetric signal (heat flux) that is recorded in proportion to heat generated, for scanning transitiometry two additional important regimes are available: 1) scanning calorimetry at a controlled pressure where calorimetric signal is proportional to coefficient of isobaric thermal expansion; 2) scanning calorimetry at a controlled volume where calorimetric signal is proportional to isochoric pressure coefficient.

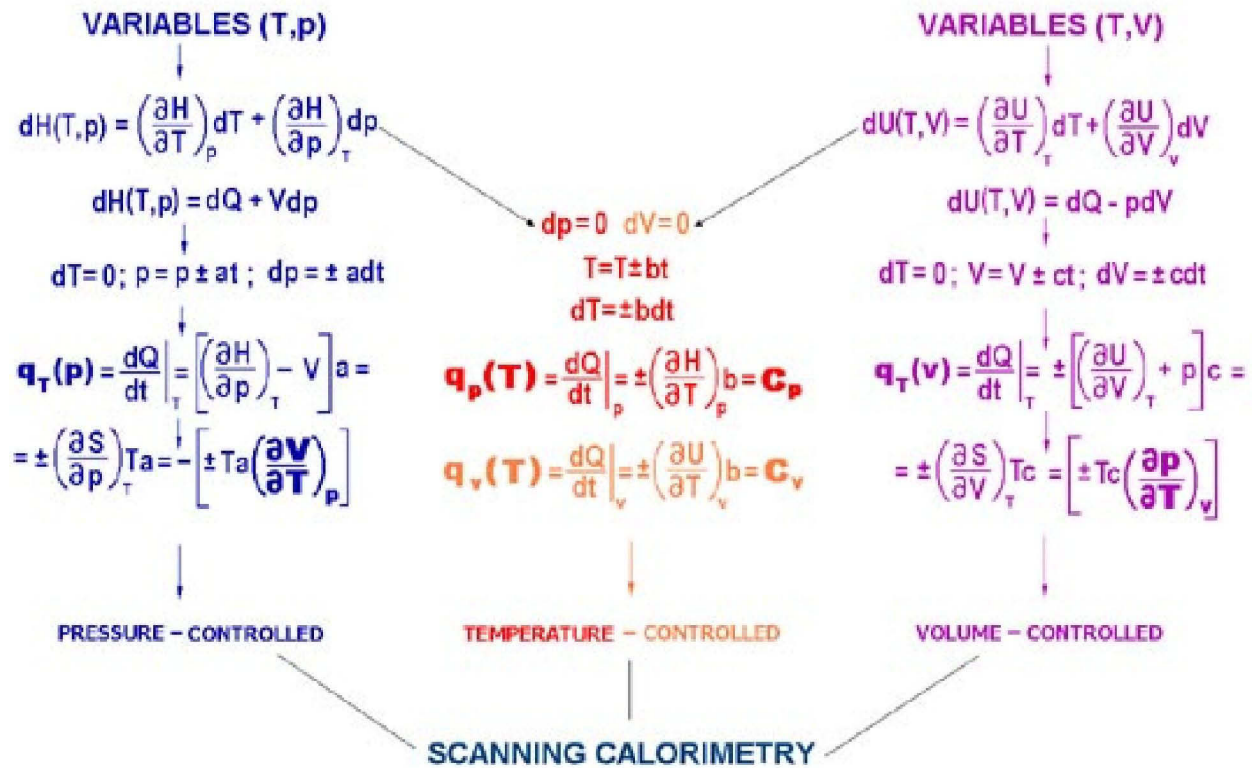


Fig. 2.1. A scheme of thermodynamic foundations for various types of PVT-controlled scanning calorimetry.

Simultaneous recording of calorimetric signal, allows using Maxwell relations, direct experimental measurement of thermodynamic derivatives fully describing a thermodynamic system. Below, the main derivatives are explained.

The enthalpy may be written as:

$$dH(T, P) = \left(\frac{\partial H}{\partial T}\right)_P dT + \left(\frac{\partial H}{\partial P}\right)_T dP = \delta Q + VdP. \quad (2.1)$$

It can be seen from eq. (2.1) that simultaneous recording of heat and PV -diagram with the scanning transitiometry technique allows obtaining the enthalpy of the system as a function of T and P .

Similarly, we can write for the internal energy:

$$dU(T, V) = \left(\frac{\partial U}{\partial T}\right)_V dT + \left(\frac{\partial U}{\partial V}\right)_T dV = \delta Q - PdV, \quad (2.2)$$

The calorimetric signal can be measured in four different modes depending on three variables (P, V, T) : $q_T(P)$ – heat flux provoked by compression-decompression of the sample by controlled pressure variation at isothermal conditions, $q_P(T)$ – heat flux provoked by heating-cooling of the sample by controlled temperature variation at isobaric conditions, $q_V(T)$ – heat flux provoked by heating-cooling of the sample by controlled temperature variation at isochoric conditions, $q_T(V)$ – heat flux provoked by compression-decompression of the sample by controlled volume variation at isothermal conditions.

Four indicated modes are presented in Fig. 2.2 and may be described as follows:

1) Recording the volume change of the investigated system as a result of a given change in pressure with time t at a constant controlled temperature:

$$T = const \Rightarrow dT = 0; P = P_0 + at \Rightarrow dP = a dt.$$

Next using classical thermodynamic transformation one may write:

$$\delta Q = \left(\left(\frac{\partial H}{\partial P}\right)_T - V\right) dP \Rightarrow \frac{\delta Q}{dt}\Big|_T = a \left(\left(\frac{\partial H}{\partial P}\right)_T - V\right).$$

On the other hand using Maxwell relations it can be written:

$$\frac{\delta Q}{dt}\Big|_T = q_T(P) = aT \left(\frac{\partial S}{\partial P}\right)_T = -aT \left(\frac{\partial V}{\partial T}\right)_P.$$

It can be seen that the heat flux measured under isothermal conditions $q_T(P)$ is proportional to the isobaric coefficient of thermal expansion $\left(\frac{\partial V}{\partial T}\right)_P$.

2) Recording the pressure change of the investigated system as a result of a given change in volume with time t at a constant controlled temperature:

$$T = const \Rightarrow dT = 0; V = V_0 + ct \Rightarrow dV = c dt.$$

Similarly to previous regime one may write:

$$\delta Q = \left(\left(\frac{\partial U}{\partial V} \right)_T + P \right) dV \Rightarrow \frac{\delta Q}{dt} \Big|_T = c \left(\left(\frac{\partial U}{\partial V} \right)_T + P \right),$$

and

$$\frac{\delta Q}{dt} \Big|_T = q_T(V) = cT \left(\frac{\partial S}{\partial V} \right)_T = cT \left(\frac{\partial P}{\partial T} \right)_V.$$

It can be seen that heat flux measured as a function of volume variation under isothermal conditions $q_T(V)$ is proportional to isochoric coefficient of pressure $\left(\frac{\partial P}{\partial T} \right)_V$.

3) Recording the volume change of the investigated system as a result of a given change in temperature with time t at a constant controlled pressure:

$$P = const \Rightarrow dP = 0; T = T_0 + bt \Rightarrow dT = bdt.$$

$$\frac{\delta Q}{dt} \Big|_P = q_P(T) = b \left(\frac{\partial H}{\partial T} \right)_P = bC_P.$$

The heat flux measured as a function of temperature variation under isobaric conditions $q_P(T)$ is proportional to isobaric the heat capacity C_P .

4) Registration of the pressure change of the system as a result of a given change in temperature with time t at a constant controlled volume:

$$V = const \Rightarrow dV = 0; T = T_0 + bt \Rightarrow dT = bdt.$$

$$\frac{\delta Q}{dt} \Big|_V = q_V(T) = b \left(\frac{\partial U}{\partial T} \right)_V = bC_V.$$

The heat flux measured as a function of temperature variation under isochoric conditions $q_V(T)$ is proportional to isochoric the heat capacity C_V .

block and solid state thermostat. All design is additionally thermoisolated and set into a stainless steel casing mounted on a stand that allows one to move the calorimeter up and down. In the lower position working chambers are inside the calorimetric block.

For the experiments with the temperatures below 273 K calorimeter is ventilated by dry air to prevent condensation.

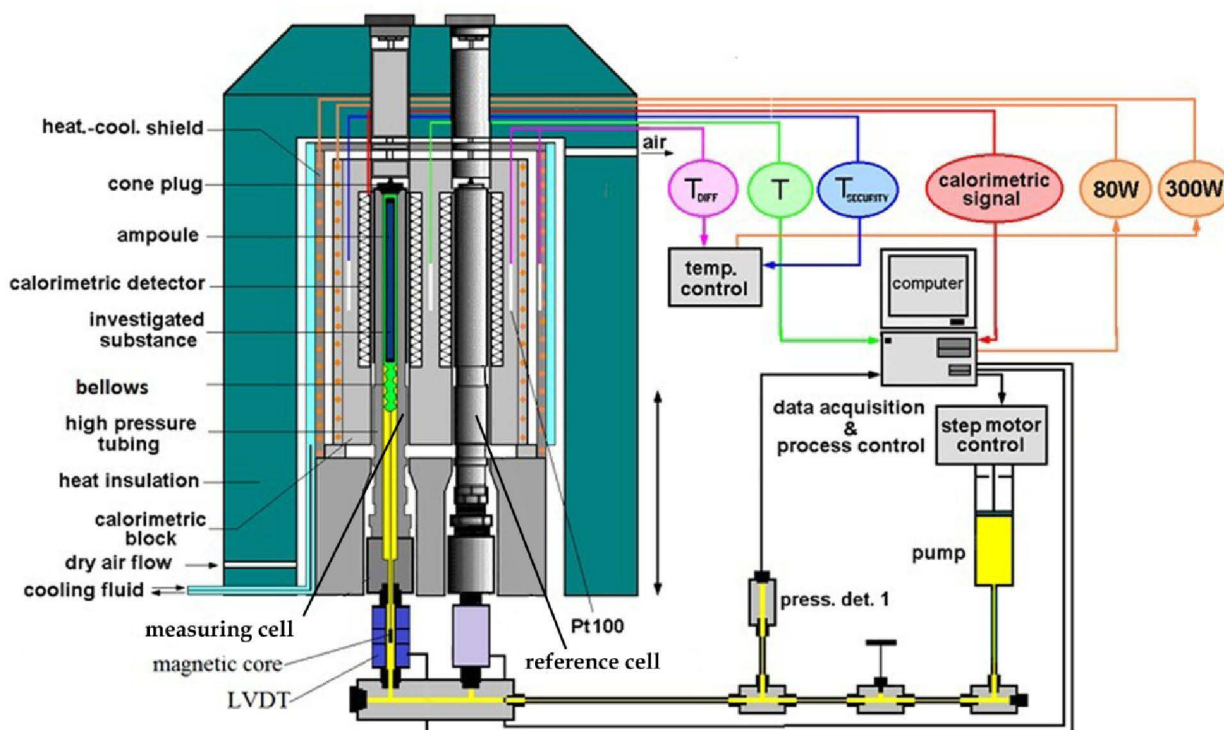


Fig. 2.3. Scheme of transitiometer ST-7M.



Fig. 2.4. Photo of transitiometer ST-7M.

The two calorimetric cells (measuring and reference) are made of stainless steel ss-439-6065 Fig.2.5a. During measurement the investigated sample is placed in the measuring cell. The inner diameter of the cells is 10 mm. Maximum operating pressure is 200 MPa.

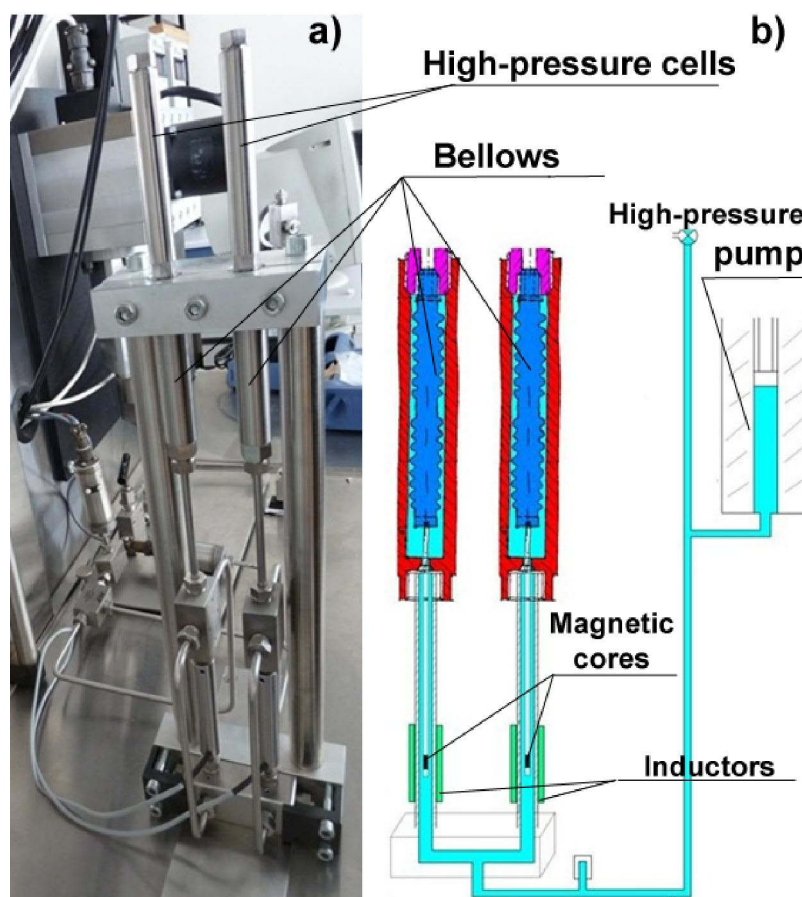


Fig. 2.5. Working chambers of transitiometer ST-7M: a) photo, b) scheme.

In contrast to the conventional ST-7 transitiometric standard model, metal bellows connected to high-precision induction volumeters were added to the high-pressure transitiometric cells of the ST-7M. As can be seen, from the experimental setup shown in Fig. 2.5. The opened upper ends of bellows are rigidly fixed to the bottoms of the cylindrical part of the transitiometric cells (the investigated sample is placed in the measuring cells while a reference sample is placed in the reference cell). The bottoms of bellows are connected through non-magnetic metal rods to the magnetic core of the induction sensors for the LVDT (linear variable differential transformer) detection (Fig. 2.5b). The active parts of induction sensors are located in chambers made of non-magnetic material, which are outside of the calorimeter detecting zone. Axial displacement of the bellows' bottoms (with a constant effective cross-section) represents the change in volume during the compression–decompression of the sample. The displacement is detected by LVDT (also simply called a differential transformer). The pressure in the measuring cell is generated by a high-pressure pump, driven by a stepping motor. In the ST-7 version,

changes in volume during compression – decompression were detected by the number of steps. In the improved version of the instrument (ST-7M), the unit “stepping motor + HP-pump” is still present, but is not used for volume variation registration. Changes in the system’s volume are recorded by the induction volumeters (LVDT), which noticeably improved the metrological characteristics of the instrument. Recording of pressure in the hydraulic system was made via a pressure sensor (press.det.1) built in the hydraulic line connecting the pump to the transiometric vessels (see Fig. 2.3.). Measurements are performed by controlling precisely the three thermodynamic variables, namely: pressure within ± 0.15 MPa, volume within $\pm 3.3 \cdot 10^{-4}$ cm³ and temperature within ± 0.01 K.

Hydraulic lines are made of thin capillaries of stainless steel. High pressure piston-pump is driven by a stepping motor in manual or automatic (via software) mode. Total capacity of transmission medium (which is oil in our case) that can be introduced in the hydraulic *PVT*-system is 9 cm³. Each step of a motor provides a pumping volume of $(5.24 \pm 0.04) \cdot 10^{-6}$ cm³. Pressure sensor – Vitaram BSS 245 – has a working range of 0-200 MPa and error of $\pm 0,15$ MPa, as declared by the manufacturer. The pressure sensor, the output of calorimeter amplifier and the stepping motor are connected to a multifunction NI PCI-MIO-16XE-50 board via a shielded connecting block NISCB-68. Recording the temperature and digital control of the calorimetric unit are made via a digital port. The software is realized through LabView V language and operates as a virtual instrument. Overall it consists of 90 sub-devices, each of which is responsible for its own function: measuring pressure, temperature, volume change, calorimetric signal, etc. Each of these devices is independent, but they form a hierarchical structure. In the main window (Fig. 2.6.) operator can observe all independent variables (P , V , T , CS) as a function of time (CS stands for calorimetric signal).

For the temperatures below room temperature additionally a cryostat Thermo Haake K20 was used (Fig. 2.7).

Cryostat Thermo Haake K20 has a wide operating temperature range (from -28 to 150 °C). The temperature stability is up to ± 0.04 °C according to the supplier. Cooling power is 320 W. Volume baths for refrigerant is 4.5 liters.

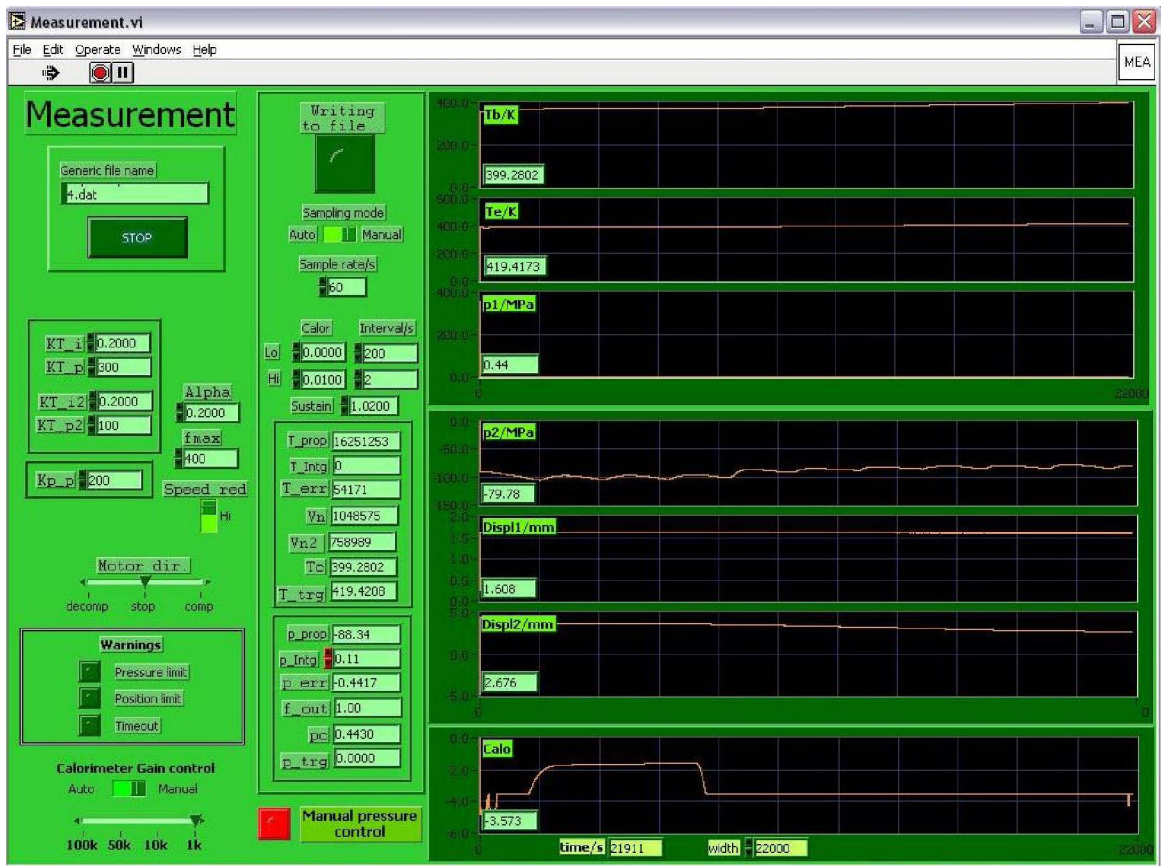


Fig. 2.6. Main window of transiometer ST-7M software.



Fig. 2.7. Cryostat Thermo Haake K20 connected to transiometer ST-7M.

2.1.1.2. Experimental procedures and sample preparation

2.1.1.2.1. Calorimeter calibration

Calibration of the calorimeter was carried out by recording the thermal effects of melting of reference samples. Comparison of calorimetric peak area corresponding to the phase transition of the reference samples (Fig. 2.8.) with the reference value of the enthalpy of fusion was used to calculate the conversion coefficient of calorimetric signal $CS \left(\frac{W}{\text{Volt}} \right)$. While comparison of recorded temperature of phase transition to reference one was used for calibration of temperature detectors. Reference samples used and their characteristics are presented in Table 2.1. Where m is mass, ΔH_F is enthalpy of fusion, T_F is melting point temperature, \aleph is obtained by the conversion coefficient of the calorimeter. All the samples were encapsulated in glass capsules that were previously degassed.

Table 2.1.

Characteristics of reference samples used for calibration of the calorimeter.

Reference sample	m , g	ΔH_F , J/g	T_F , K	\aleph , W/Volt
p-Bromochlorobenzene	0,24315	97,99	337,70	0.08790
p-di-Bromobenzene	0,23260	87,03	360,45	0.09287
Benzoic Acid	0.14670	147.9	395.55	0.10254
Indium	0.56205	28.59	429.75	0.01069

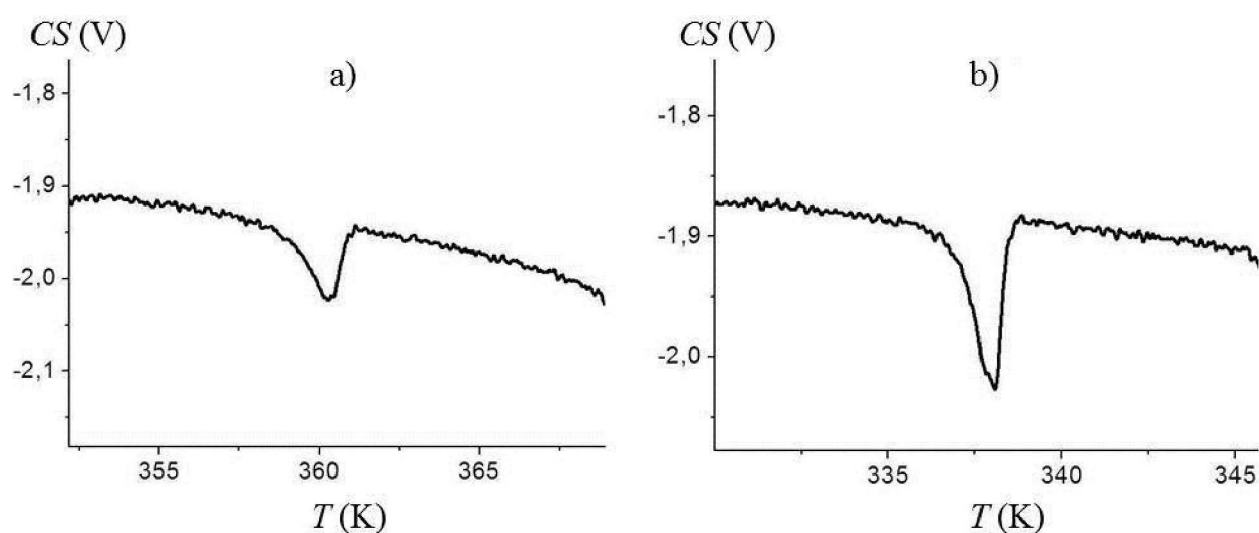


**Fig. 2.8. Peak of calorimetric signal obtained for the fusion of
a) p-di-Bromobenzene, b) p-Bromochlorobenzene.**

Account of inertia of calorimeter. Fig.2.9. represents the calorimetric signal and the pressure as a function of time in the experiment for the isothermal compression of {Zif-8 + Water} HLS. As can be seen during bulk phase compression calorimetric signal is close to constant. Upon reaching the intrusion pressure for which the development of "liquid - solid" interphase area occurs, endothermic effect takes place and that is accompanied by significant changes of calorimetric signal (calorimetric peak). Comparison of calorimetric signal time dependence and of the pressure time dependence clearly shows that at the end of the intrusion process (neat break in the pressure change) the calorimetric signal does not immediately return to the baseline value. This is due to the inertia of the calorimeter, which must be taken into account when processing calorimetric measurements.

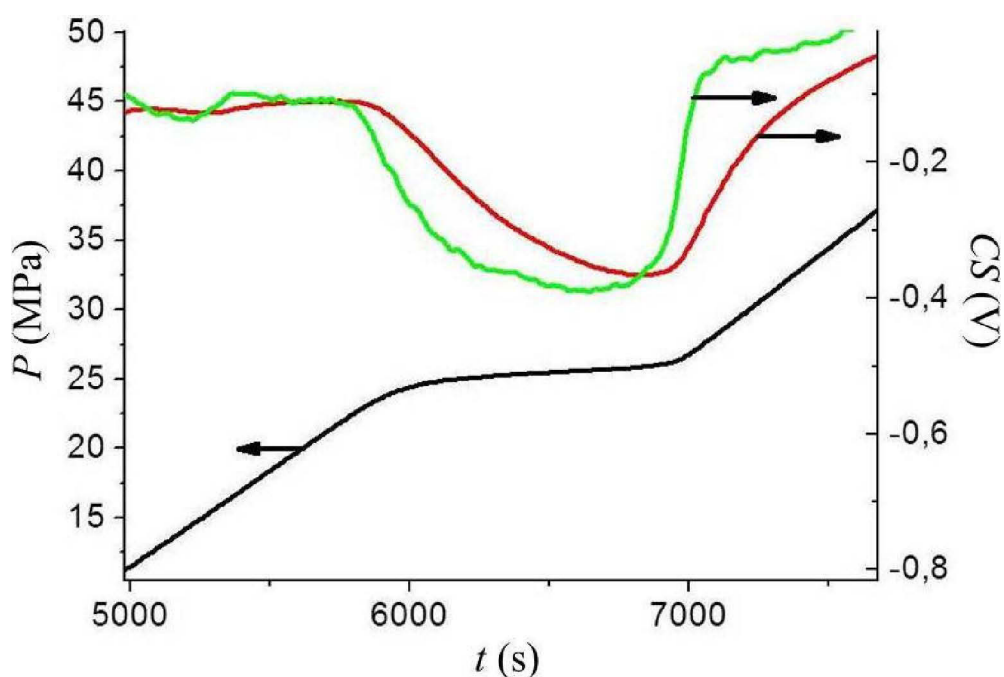


Fig. 2.9. Time dependence of the pressure (black line), original (red line) and corrected (green line) calorimetric signal during compression of system the {Zif8 + Water} HLS at isothermal conditions.

Unfortunately, most calorimeters do not directly measure the thermal energy (heat flux $q(t)$) generated or released by the sample, but they deliver the temperature difference in the form of thermogram. Heat generated, by endothermal or exothermal effects, exchanges with the environment (in the case of transitiometer with the calorimetric block). This means that the resulting thermogram depends not only on the energy processes occurring in the measuring cell, but also on the calorimetric system used. Having also some limited ability to respond to fluctuations in heat generated by the sample, the value of the heat flux will be distorted because

of the specific heat capacity of the calorimetric cell and the block. Consequently there is inertia of calorimetric system.

According to the theory of differential calorimetry relationship between the actual heat flow $q(t)$ and calorimetric signal ΔCS in the first approximation is given by:

$$q(t) = \kappa \left(\Delta s(t + \tau') + \tau \frac{d\Delta s(t + \tau')}{dt} \right), \quad (2.3)$$

where τ is the characteristic time of calorimeter inertia, τ' is the time delay in reaction of the calorimeter to the heat flow change.

As can be seen from Fig. 2.9 direct calorimetric signal delay is negligibly small. While inertia of calorimeter obviously requires consideration.

To find τ value equation (2.3) should be integrated from time t_0 , which is the initial time when $q(t_0) = 0$, and taking into account $\tau' = 0$, we obtain:

$$\ln(\Delta s(t)) = \ln(\Delta s(t_0)) - \frac{t - t_0}{\tau}. \quad (2.4)$$

For the example in Fig. 2.9 the inertia time is $\tau = 503,1$ s. Corrected due to the calorimeter inertia the calorimetric signal is presented by the green line in Fig. 2.9. It can be seen that indicated correction makes the calorimetric signal synchronized with pressure (and volume) signal, as required.

The inertia time was determined for each sample. In general, this value is between 400 – 550 s, which may depend on the sample, rate and direction of scan.

2.1.1.2.2. Bellows calibration

In order to find LVDT coefficient L (for conversion of values of LVDT (in millimeters) to unit of volume (cm^3)) experiments were performed on isothermal compression of reference samples of known volume and compressibility. Distilled water (working chamber is completely filled with water) and lead of a 99.96% purity (chamber filled with water and submerged in it lead) were used as reference samples.

Obtaining compressibilities of reference samples and knowing their reference values, the LVDT coefficient can be defined by the formula:

$$L = \frac{V_{Pb}(\mu_T^{H_2O} - \mu_T^{Pb})}{\left(\frac{dl_{H_2O}}{dP} - \frac{dl_{H_2O+Pb}}{dP}\right)}, \quad (2.5)$$

where V_{Pb} is the volume of lead, $\mu_T^{H_2O}$ is isothermal compressibility of water, μ_T^{Pb} is isothermal compressibility of lead, l_{H_2O} and l_{H_2O+Pb} are the values of LVDT in the experiment with water and lead + water respectively. Fig. 2.10 represents the Pl – isotherms of reference samples.

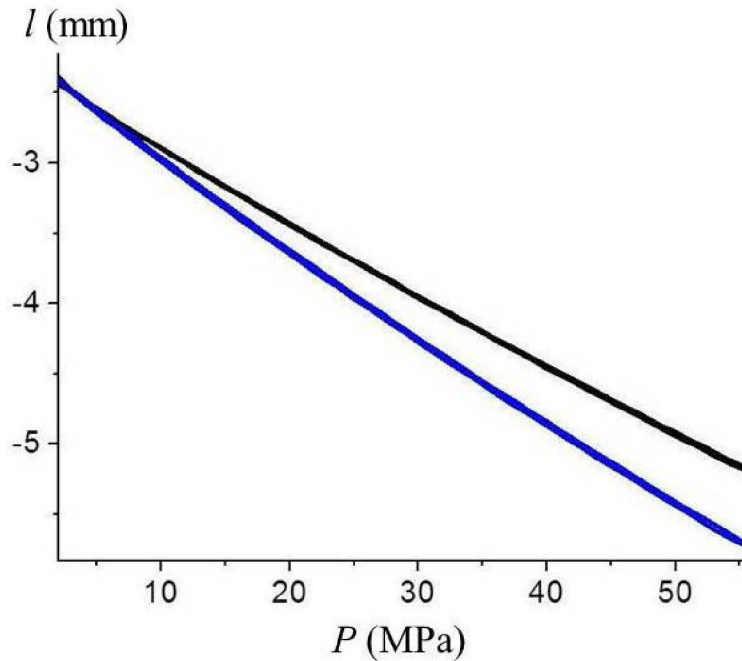


Fig. 2.10. Pl – isotherms of compression of water (blue line) and lead immersed in water (black line).

Using equation (2.5) and obtained Pl – dependences, the value of $L = 0,066 \text{ cm}^2$ is obtained.

The uncertainty of volume measurement is $\pm 3,3 \cdot 10^{-4} \text{ cm}^3$ according to supplier (Peltron Ltd., Poland) with maximum non-linearity of -0,555% for extreme value of LVDT which is 10.00 mm.

2.1.1.2.3. Sample preparation

The gas contained in the pores and in the interparticle space must be removed before preparing an HLS (mixing non-wetting liquid and porous matrix), since presence of gas may prevent the complete intrusion of liquid into the pores. This effect is known in practice of mercury porosimetry. Under considerable external pressure gas can be dissolved in water, but the presence of gas in the interparticle space leads to the presence of parasitic changes of the volume

of the system at low pressure, which negligibly increases the energy capacity of the HLS and largely increases its specific volume.

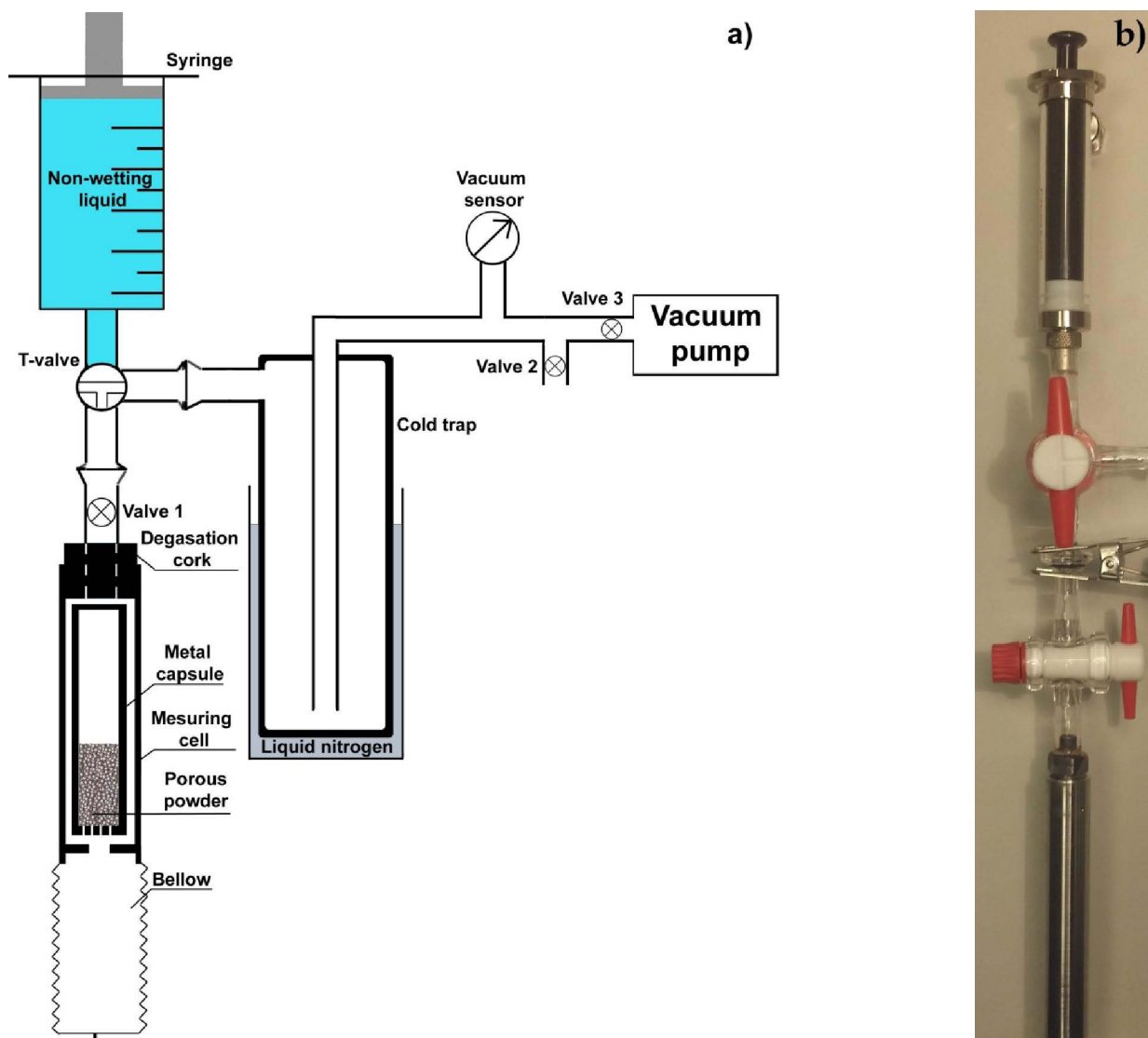


Fig. 2.11. Vacuum line for degasing the porous matrix of HLS a) scheme, b) photo

The vacuum line for an HLS preparation is shown in Figure 2.11. It consists of specially made degasation cork placed on the measuring cell instead of regular high-pressure cork and has a valve; a syringe which contains non-wetting liquid, which is connected directly to vacuum line and has a four position T-valve; a cold trap, which is cooled with liquid nitrogen and has two valves (valve 2 and valve 3); vacuum sensor (Edwards PRE 10K); vacuum pump (Edwards RV3).

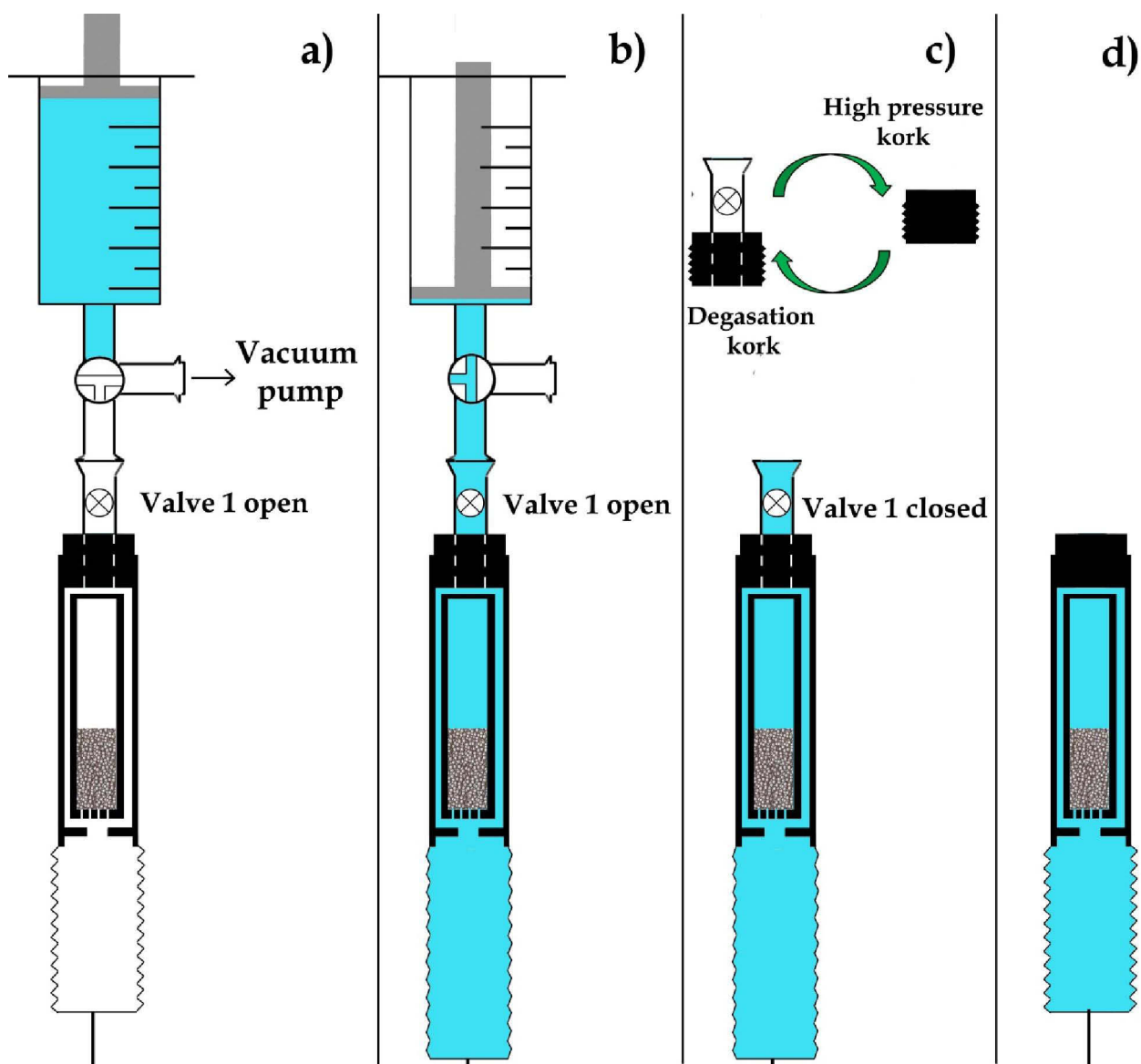


Fig. 2.12. Scheme of preparation of an HLS.

Figure 2.12 shows a simplified scheme of degasation of investigated porous heterogeneous lyophobic systems. Weighted porous matrix in the form of powder is placed in a metal capsule, which is then closed with a porous ceramic-metal bottom. Pore sizes of the bottom are in the range of a few micrometers, excluding elutriation of the particles of the porous powder. In the experiments performed the powder weight was within 0.3 - 1 g for different samples. Metal capsule with porous matrix is placed into the empty measuring cell. Next the cell is closed with the degasation cork through which the cell is connected to the vacuum line (Fig. 2.12a). The position of T-valve excludes non-wetting liquid to enter the vacuum line. The degasation is performed during 2 hours at $5 \cdot 10^{-2}$ mbar vacuum. After the degasation the T-valve is placed in the position shown in Fig. 2.12b which allows the non-wetting liquid to flow into measuring cell, while excluding its flow to the vacuum line. A small external force is applied to the piston of the

syringe to introduce even more liquid into the bellow by stretching it a little. Next keeping external force on the piston of the syringe the valve 1 is closed. This allows detaching the syringe from the cell (Fig. 2.12c). The valve 2 is used to equalize the pressure in the vacuum line to make the detachment possible. Next the degasation cork is removed, which is followed by excessive liquid expelled from the cell (bellow retracts itself to the equilibrium state) filling the volume which took the cork and forming a meniscus on the surface of the cell. The degasation cork is quickly (less than 1 second) replaced by the high-pressure cork (Fig. 2.12d). During closing the cell with the high-pressure cork liquid which was in contact with air is expelled from the cell through specially designed for that matter hole. The cell is now ready for the experiment.

An ultrasound degasation bath FB 15051 (Fisher Scientific) was used to degas water during 2 hours at temperature of 60 °C.

2.1.1.2.4. Isothermal experiments

In order to obtain PV -isotherms of studied porous Heterogeneous Lyophobic Systems (HLSs) prepared according to the above described procedure the investigated sample was subjected to compression with the rate pressure variation 1 MPa/min. After reaching the required pressure the system was maintained at a constant pressure for about 1 hour to achieve the equilibrium value of calorimetric signal. Next the pressure in the system was reduced with a similar rate to atmospheric value. Then the system again was kept under constant pressure to establish the equilibrium value of calorimetric signal. Next the compression-decompression cycle was repeated at least three times to check the good repeatability of registered results. Along with recording PV -diagram the calorimetric signal proportional to the thermal effect of compression/decompression is simultaneously recorded.

2.1.1.2.5. Isobaric experiments

The transitionmeter ST-7M was used to study the temperature dependence of heat-capacity and the thermal expansivity of HLSs under controlled constant pressure P_0 with accuracy of ± 0.15 MPa. The temperature scanning rate was $\left(\frac{\partial T}{\partial t}\right)_P = 5 \cdot 10^{-4}$ K/s. The value of heat-capacity was obtained as follows: $C_P \equiv \left(\frac{\partial q}{\partial T}\right)_P = \left(\frac{\partial q}{\partial t}\right)_P \left(\frac{\partial T}{\partial t}\right)_P^{-1}$, where heat flow $\left(\frac{\partial q}{\partial t}\right)_P$ was measured simultaneously with all thermodynamic parameters (P, V, T).

2.1.1.2.6. Experiments under constant load

The “constant load” operational mode of given HLS is a mode where the system experiences a constant external load (force), which creates the initial pressure in the system that exceeds atmospheric pressure. Hence, the pressure and the volume of the system changes due to the temperature variation. These conditions are close to those in which the HLS is used as a working body in the cycle of heat energy into mechanical transformation (Eroshenko 1981, Laouir et al. 2003). In principle these conditions are equivalent to the ones shown on Fig. 2.13: some constant force (in this representation – the gravitational force which affects the load) acts on the system and does not change during the temperature variation of the system, which provokes both pressure and volume change.

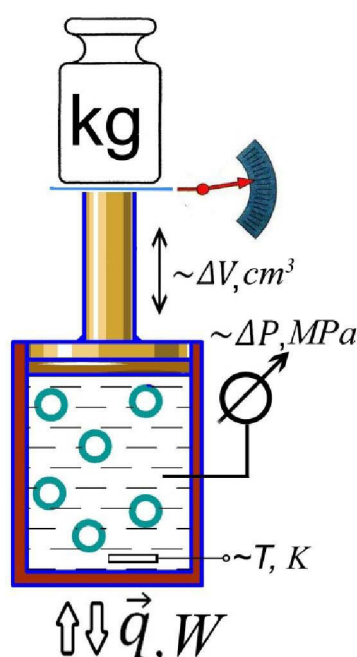


Fig. 2.13. Schematic representation of experiment with constant load.

In these experiments the initial pressure P_0 is manually reached. P_0 does not exceed intrusion pressure of HLS at the initial temperature T_0 . After reaching the required initial pressure the stepping motor is turned off and is not used during the experiment. Next heating-cooling cycle is performed in an automatic regime. After reaching the specified maximum temperature system is maintained at this temperature for at least an hour before cooling to a initial temperature T_0 . Thus, the heating-cooling cycle is performed, which provokes intrusion and extrusion of the fluid and, consequently, a significant reversible volume variation of the system.

2.2. ADDITIONAL TECHNIQUES

Some additional techniques were used to characterize porous materials before and after experiment with HLSs.

2.2.1. X-ray diffraction

X-ray Diffraction (XRD) patterns of pristine powders and of powders modified after intrusion/extrusion cycle were recorded on an X'Pert Pro PANalytical diffractometer θ - θ geometry, using Cu K α radiation ($\lambda = 1.54184 \text{ \AA}$). XRD patterns were recorded at room temperature in the interval of $3^\circ < 2\theta < 120^\circ$, with a step size of $\Delta 2\theta = 0.0167^\circ$ and a counting time of 119 s for each data value. A total counting time of about 200 min was used for each sample.

2.2.2. Fourier Transform Infra-Red spectroscopy

Fourier Transform Infra-Red spectroscopy (FTIR) spectra were recorded in transmission mode using the KBr pellet technique with a Nicolet 5700 spectrometer from Thermo Scientific.

2.2.3. Scanning Electron Microscopy

Scanning Electron Microscopy (SEM) micrographs were recorded on a Zeiss supra 55-VP microscope working at electron energy of 1.0 kV.

2.3. MATERIALS

The following porous materials were used to form the HLSs investigated in this work.

Waters Symmetry Prep C8 is a nanoporous grafted silica gel also known as SymmetryPrep C8, 7 μm supplied by Waters. The grafting was done with C8 chains octylsilanes with density 2.1 groups/ nm^2 according to the data provided by the supplier. The pore size distribution is very narrow for this type of material, formed by the aggregation of elementary particles. The average pore radius of the material before grafting is 4.6 nm, but the effective calculated pore radius is 3.8 nm (Coiffard and Eroshenko 2006), taking into consideration grafting thickness (Fadeev and Staroverov 1988, Eroshenko and Fadeev 1995). Nitrogen sorption measurements on the grafted

material at 77 K gives a porous volume of 0.53 cm³/g and an average pore radius of 4.2 nm, obtained from the desorption branch using the classical Barrett-Joyner-Halenda equation (Coiffard and Eroshenko 2006). Combined with water indicated porous matrix achieved considerable attention in the field of mechanical energy dissipation (Eroshenko 2007, Eroshenko et al. 2007, Suciu and Yaguchi 2009); primarily due to strong hysteresis and good resistance to mechanical stress.

Hypersil 5u HS C18 is a mesoporous silica grafted by linear chains of octylsilanes, but with greater length than the previous sample – C18 chains (C₁₈H₃₇). In previous studies it was found (Suciu 2003) that at room temperature {Hypersil 5u HS C18 + water} HLS demonstrates satisfactory performance for mechanical energy dissipation processes only for the first compression-decompression cycle. The lack of results for such HLS in a wide temperature range indicates the need to determine the optimal conditions for its use.

Silicalite-1 (prepared in fluoride medium) sample was bought from Sigma Aldrich. The pore space of Silicalite-1 has a simple topology (MFI) having almost ideal cylindrical pores with radius $r \sim 0.3$ nm and high hydrophobicity.

ZIF-8 (Zeolitic imidazolate framework). The structure of ZIF-8 consists of cage-like pores of ~ 11.6 Å diameter connected by 6-ring windows of only ~ 3.4 Å and is characterized by a huge specific surface area of c.a. 1800 m²/g. ZIFs is a subclass of metal-organic frameworks (MOFs). Analytical formula for ZIF-8 is C₈H₁₂N₄Zn; particle size is 4.9 μm.

Some of the characteristics of described above are summarized in table 2.2.

Table 2.2.

Characteristics of porous materials

	Waters SymmetryPrep C8	Hypersil 5u HS C18	Silicalite-1 (MFI-F)	Zif-8
Porosity (cm ³ /g)	0,51	0,40	0,14	0,38
Area (m ² /g)	221	138	400	1800
Average pore radius (nm)	4,0	3,9	0,3	0,17

As non-wetting liquid, distilled water was used. HLSs based on water present advantages of ecological safety, low price and availability.

CHAPTER 3

PROPERTIES OF HLSs

PROPERTIES OF HLSs

In this Chapter (particularly in Paragraph 3.1) an attempt to formulate the general thermodynamic description of a heterogeneous lyophobic system as a complex thermodynamic system (taking into account both bulk and interface phenomena) is presented. First of all we introduce a thermal equation of state which takes into account pore size distribution function of the porous matrix used for the HLS. Next using this equation in classical thermodynamics of complex systems some of important properties and transformations are highlighted. An important question is the possibility to realize an equilibrium quasi-static operational regime of the HLS; this point is discussed.

This thermodynamic analysis demonstrates that temperature dependence of intrusion and extrusion pressures is essential for nearly all potential and existing HLS applications. For that reason great attention was paid to experimental and theoretical investigation of such dependence, which is reported in Paragraph 3.2.

The stability of the characteristics of HLSs (which is associated with stability of porous matrix) during operational cycle is obviously important characteristic for practical applications. Investigation on stability of operational characteristics of HLSs is presented in Paragraph 3.3 focusing on HLSs based on Silicalite-1 and ZIF-8 metal-organic framework since for these systems (contrary to the ones based on grafted silica gels) under certain conditions the HLS operational cycles may cause irreversible changes in the porous matrix structure.

3.1. DESCRIBING HLS AS COMPLEX THERMODYNAMIC SYSTEM

3.1.1. Limitations of usage of equilibrium thermodynamics

Two limitations for using the concept of equilibrium thermodynamics were determined for HLS:

1. Pore size. The object of thermodynamics is a *macroscopic* system. Since some of the matrices used for HLS have pore size comparable to the size of a molecule of the liquid (Silicalite-1, ZIF-8 see. Table 2.2), it is important to determine the critical pore size in which the liquid can still be considered as a macroscopic substance. Based on literature data, the minimum diameter of 2-3 nm was considered. Hence only for mesoporous (not microporous) HLSs the thermodynamic description may be applied. It is important to note that a microporous HLS as a whole is still a macroscopic system allowing to use relations between macroscopic parameters (such as P , V , T , Q , W , etc.), but describing its parameters which are determined by the properties of the liquid confined in micropores obviously requires the microscopic comprehensive approach of phenomena, then macroscopic parameters (such as contact angle, surface tension, etc.) should not be used.

2. Speed of intrusion/extrusion of fluid during HLS operation. Within the framework of equilibrium thermodynamics only quasi-static processes can be described. The process of liquid intrusion (index «int») into the pores of the matrix occurs when pressure in the system reaches Laplace capillary pressure, which depends on the liquid surface tension σ , the advancing contact angle θ_A (for extrusion the index is «ext» and the contact angle is receding θ_R), the pore radii r , and the geometry of the pore space k ($k = 0,5$ cylinders, $k = 0,33$ for spheres)²:

$$P_{int,ext}^C = -\frac{\sigma \cos \theta_{A,R}}{kr}. \quad (3.1)$$

If the porous matrix of an HLS can be considered as uniporous (all the pores have the same radius) equation (3.1) under isothermal conditions can be written as

$$r = const \Rightarrow P_{int,ext} \Big|_{T=const} = const,$$

Which means that during the intrusion/extrusion process the volume change takes place at

² In the Paragraph 3.2 it is shown that additionally to equation (3.1) the bubble nucleation must occur for liquid to extrude from the pores of the matrix.

isobaric conditions:

$$\left. \frac{dV}{dP} \right|_{P=P_{int,ext}} \rightarrow \infty$$

This means that such process is non-controlled and is non-equilibrium.

On the other hand if pore sizes are described by some smooth (continuously differentiable) function f ($r = var \Rightarrow P_{int,ext}|_{T=const} = var$), the process of intrusion/extrusion becomes controlled, as infinitesimal variation of pressure under isothermal conditions leads to infinitesimal variation of the volume due to infinitesimal amount of pores being filled:

$$\left. \frac{dV}{dP} \right|_{P=P_{int,ext}} \neq \infty$$

Hence, some smooth pore size distribution can be considered as criterion of the possibility of realization of a quasi-static process for HLS and the possibility of applying the concept of equilibrium thermodynamics to describe it.

To account for such pore size distribution in thermodynamic description of HLS, a distribution function was introduced as part of the equation of state of HLS, which is described below.

3.1.2. Thermal equation of state

To take into account the pore size distribution function of the matrix the following general form of thermal equation of state of HLS was proposed:

$$f_{\Omega}(P, V_{\Omega}, T) + f_0(P, V_0, T) = 0 \quad (3.2)$$

where $f_{\Omega}(P, V_{\Omega}, T)$ is a function describing the relation between the pressure P , temperature T and the volume variation V_{Ω} due to the development/reduction of interface area Ω in the system during intrusion/extrusion process. And $f_0(P, V_0, T)$ is the equation of state of the whole bulk part of HLS (mainly the liquid and the porous matrix with no account for the interface phenomenon). The relation $f_0(P, V_0, T)$ may be defined by known thermal coefficients of the components of the HLS. The explicit form of $f_{\Omega}(P, V_{\Omega}, T)$ is determined by the type of the distribution function the porous matrix. For example if the pores are distributed according to a Cauchy function $\left(V = f_{int,ext}(P, T) = -\frac{V_{pore}}{\pi} \arctan g \left(\frac{P - P_{int,ext}(T)}{D_{int,ext}} \right) \right)$ the equation (3.2) may be rewritten as follows:

$$V + \frac{V_{pore}}{\pi} \arctan g \left(\frac{P - P_{int,ext}(T)}{D_{int,ext}} \right) + V_0^0 (\mu_T^0 P - \alpha^0 T) + C'_{int,ext} = 0 \quad (3.3)$$

where $C'_{int,ext} = -V_0^0 - \frac{V_{pore}}{\pi} \arctg\left(\frac{P_0 - P_{int,ext}(T_0)}{D_{int,ext}}\right) - V_0^0(\mu_T^0 P_0 - \alpha^0 T_0)$; V_{pore} is the pores volume of the matrix; P_0 and T_0 are initial pressure and temperature of the system, respectively; V_0 is the volume of the whole bulk phase (liquid and the matrix), which may change due to elastic compression/decompression or due to thermal expansion/contraction; $\mu_T^0 = -\frac{1}{V_0^0} \left(\frac{\partial V_0}{\partial P}\right)_{T,\Omega}$ is the isothermal compressibility of the liquid and the matrix; $\alpha^0 = \frac{1}{V_0^0} \left(\frac{\partial V_0}{\partial T}\right)_{P,\Omega}$ is the isobaric coefficient of thermal expansion; V_0^0 is the initial whole volume of the system (volume of the liquid plus the volume of the matrix); $D_{int,ext}$ is the dispersion of the values if intrusion and extrusion pressures, which can be determined from the dispersion of pore radii from their average value using equation (3.1).

In principle pores may be distributed according to any function or in case of a HLS based on several matrices may be described by superposition of known distribution functions.

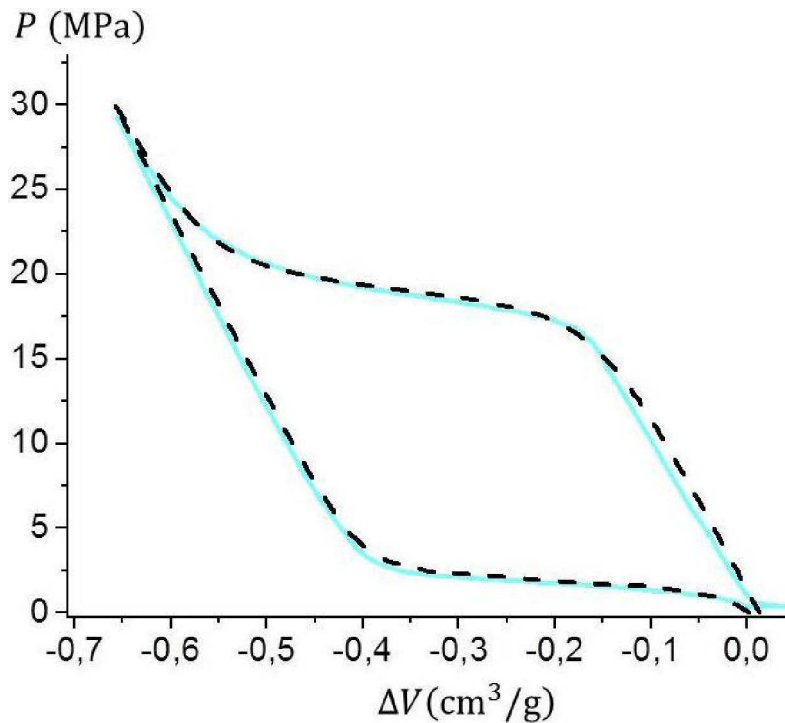


Fig. 3.1. PV – isotherm of the {Waters C8 + water} HLS. Solid line is experiment, dashed line – is the model according to equation (3.3).

Figure 3.1 represents the validation of equation (3.3) using the experimental PV – isotherm of the {Waters C8 + water} HLS. On this figure $\Delta V = V - V_0^0$. It can be seen that equation (3.3) describes quite well experimental dependence of PV –isotherm with the following parameters: $V_{pore} = 0,42 \text{ cm}^3/\text{g}$, $P_{int} = 19,11 \text{ MPa}$, $P_{ext} = 1,90 \text{ MPa}$, $D_{int,ext} = 0,19 \text{ MPa}$

and the isothermal compressibility of the bulk phase as taken from experiment (compression before and after intrusion).

Validation of equation (3.2) and (3.3) using different distribution functions is presented below to model the thermal coefficients, the thermal effects of compression/decompression and heat capacity of the HLS.

3.1.3. Maxwell relations and thermal coefficients

Differential Maxwell relations are extremely useful tools for the thermodynamic analysis that allows obtaining thermomechanical properties difficult to measure otherwise. These relations may be derived using Bernoulli- Euler's theorem on equality of the second mixed derivatives applied to thermodynamic characteristic functions (U, H, F, G).

For simple thermodynamic systems, each of the characteristic functions depends on two independent variables so there are only four macroscopic variables (P, V_0, T, S) determining the above characteristic functions; S being entropy. For HLS number of this variables is five: P, V_0, Ω, T, S . Using the classical definitions of the thermodynamic characteristic functions, the work of interface development ($PdV = \delta W = \delta W_0 + \delta W_{\Omega}^{int,ext} = PdV_0 - \sigma \cos\theta_{A,R} d\Omega$, see eq. (1) of Chapter 1) and the volume of HLS, which is

$$dV = dV_0 - kr d\Omega \equiv dV_0 + dV_{\Omega} \quad (3.4)$$

the characteristic functions for HLS may be written as follows.

Internal energy:

$$dU = TdS - PdV = TdS - PdV_0 - \sigma \cos\theta d\Omega \quad (3.5)$$

Enthalpy:

$$dH = TdS + VdP = TdS + (V_0 - kr\Omega)dP \quad (3.6)$$

Helmholtz free energy:

$$dF = -PdV - SdT = -PdV_0 - \sigma \cos\theta d\Omega - SdT \quad (3.7)$$

Gibbs energy:

$$dG = VdP - SdT = (V_0 - kr\Omega)dP - SdT \quad (3.8)$$

To obtain the Maxwell relations for complex thermodynamic system involves rotation of all parameters held constant for each characteristic function in order to use the Bernoulli-Euler's theorem. Thus the Maxwell relations for HLS can be written as follows (for mathematical details see Appendix A):

$$\left(\frac{\partial T}{\partial \Omega}\right)_{S, V_0} = -\left(\frac{\partial \sigma \cos \theta}{\partial S}\right)_{\Omega, V_0} \quad (3.9)$$

$$\left(\frac{\partial T}{\partial V_0}\right)_{S, \Omega} = -\left(\frac{\partial P}{\partial S}\right)_{V_0, \Omega} \quad (3.10)$$

$$\left(\frac{\partial \sigma \cos \theta}{\partial T}\right)_{\Omega, V_0} = \left(\frac{\partial S}{\partial \Omega}\right)_{T, V_0} \quad (3.11)$$

$$\left(\frac{\partial P}{\partial T}\right)_{V_0, \Omega} = \left(\frac{\partial S}{\partial V_0}\right)_{T, \Omega} \quad (3.12)$$

$$\left(\frac{\partial T}{\partial P}\right)_S = \left(\frac{\partial V_0}{\partial S}\right)_P - kr \left(\frac{\partial \Omega}{\partial S}\right)_P \quad (3.13)$$

$$-\left(\frac{\partial S}{\partial P}\right)_T = \left(\frac{\partial V_0}{\partial T}\right)_P - kr \left(\frac{\partial \Omega}{\partial T}\right)_P \quad (3.14)$$

As shown, relation (3.10) and (3.12) in which left-hand-side and right-hand-side derivatives are taken at constant surface Ω , coincide with the classical Maxwell relations for simple thermodynamic system, which is logical. While equations (3.13) and (3.14) becomes similar to corresponding relations if surface phenomena are negligible ($\Omega \approx \text{const}$). Which means that obtained relations are consistent with the correspondence principle.

Some of useful applications of obtained relations are presented below.

Relation (3.9) shows change of the temperature of the system during the interface development/reduction (compression/decompression of HLS) under adiabatic conditions neglecting the elastic compressibility of the liquid and the matrix.

The equation for entropy of HLS may be written:

$$\begin{aligned} dS(T, V_0, \Omega) &= \left(\frac{\partial S}{\partial T}\right)_{V_0, \Omega} dT + \left(\frac{\partial S}{\partial V_0}\right)_{T, \Omega} dV_0 + \left(\frac{\partial S}{\partial \Omega}\right)_{V_0, T} d\Omega \\ &= C_V^0 \frac{dT}{T} + \left(\frac{\partial P}{\partial T}\right)_{V_0, \Omega} dV_0 + \frac{d\sigma \cos \theta}{dT} d\Omega, \end{aligned} \quad (3.15)$$

where $C_V^0 = \left(\frac{\partial S}{\partial T}\right)_{V_0, \Omega}$ is the isochoric heat capacity of the liquid and the matrix.

Using relations (3.9) and (3.15) allows to obtain the following relation:

$$\left(\frac{\partial T}{\partial \Omega}\right)_{S,V_0} = -\frac{T}{C_V^0} \left(\frac{\partial \sigma \cos \theta}{\partial T}\right)_{\Omega,V_0}, \quad (3.16)$$

which shows that under adiabatic conditions the compression of HLS ($d\Omega > 0$) leads to the decrease of the temperature of the system, while the decompression ($d\Omega < 0$) induces temperature increase, in the case where $\left(\frac{\partial \sigma \cos \theta}{\partial T}\right)_{\Omega,V_0} > 0$, which is expected. A detail analysis of temperature dependences of surface tension and contact angle is discussed in Paragraph 3.2. The above property of HLSs is unusual for traditional working bodies (gas/vapor) and can be effectively used in engineering applications. For example it allows for an HLS-based shock absorber to operate at frequencies above 20 Hz (Eroshenko et al. 2007) (and theoretically even at much higher frequencies (Michelin-Jamois et al. 2013)) without overheating.

The relation (3.11), using well-known equation $\delta Q = TdS$, shows that thermal effect of the isothermal compression/decompression is determined by the temperature dependence of the surface tension and of the contact angle: $\left(\frac{\partial \sigma \cos \theta}{\partial T}\right)_{\Omega,V_0} = \frac{1}{T} \left(\frac{\partial Q}{\partial \Omega}\right)_{T,V_0}$.

The relation (3.13) allows finding a very important, but difficult to measure experimentally, pressure dependence of temperature of an HLS during an adiabatic compression/decompression. Using relation (3.15) the partial derivatives in the right-hand-side of equation (3.13) may be written as follows $\left(\frac{\partial S}{\partial V_0}\right)_P = \frac{C_V^0}{T} \left(\frac{\partial T}{\partial V_0}\right)_P + \left(\frac{\partial P}{\partial T}\right)_{V_0,\Omega} + \frac{d\sigma \cos \theta}{dT} \frac{1}{kr}$ and $\left(\frac{\partial S}{\partial \Omega}\right)_P = \frac{C_V^0}{T} \left(\frac{\partial T}{\partial \Omega}\right)_P + \left(\frac{\partial P}{\partial T}\right)_{V_0,\Omega} kr + \frac{d\sigma \cos \theta}{dT}$. Next using proposed earlier equation of state (3.2) one may write $\left(\frac{\partial T}{\partial \Omega}\right)_P = \frac{kr}{f'_{int,ext}} \left(\frac{dP_{int,ext}}{dT}\right)^{-1}$, where $f'_{int,ext} = \left(\frac{\partial V}{\partial P}\right)_{V_0} = -\frac{V_{pore}}{\pi D_{int,ext}} \frac{1}{\left(\frac{P-P_{int,ext}}{D_{int,ext}}\right)^2 + 1}$. On the other hand we may write $\left(\frac{\partial V}{\partial P}\right)_{T,V_0} = -\left(\frac{\partial V}{\partial r}\right)_T \frac{kr^2}{\sigma \cos \theta}$, where $\left(\frac{\partial V}{\partial r}\right)_T$ is pore size distribution function which normally is identification characteristics of the matrix or may be found from some of the characterization methods of mercury porosimetry or gas sorption.

Using previously proposed equation of state let us now define the thermal (thermophysical) coefficients of HLS (for mathematical details see Appendix B).

Isothermal coefficient of compressibility:

$$\mu_T^{int,ext} = -\frac{1}{V_0^0} \left(\frac{\partial V}{\partial P} \right)_T = -\frac{f'_{int,ext}}{V_0^0} + \mu_T^0, \quad (3.17)$$

where $f'_{int,ext} \equiv -\frac{V_{pore}}{\pi D_{int,ext}} \frac{1}{\left(\frac{P-P_{int,ext}}{D_{int,ext}} \right)^2 + 1}$ and indices “int” are used for intrusion process

and “ext” for extrusion process.

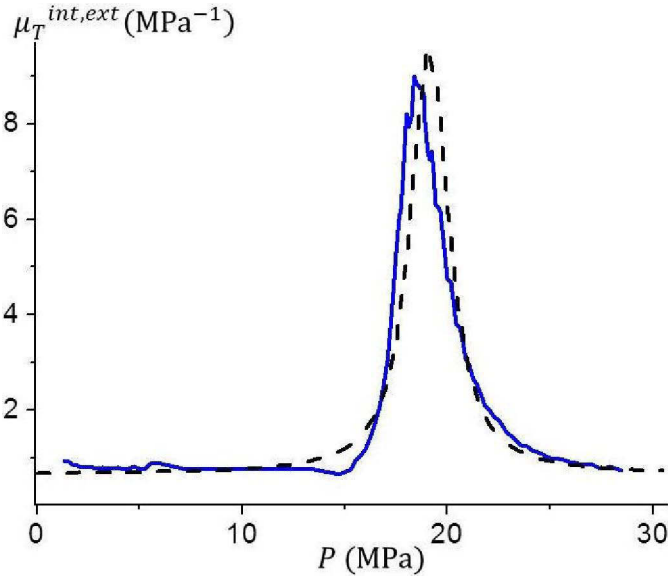


Fig. 3.2. Coefficient of isothermal compressibility of the {Waters C8 + water} HLS for the intrusion process. Solid line is experiment; dashed line is the model according to eq. (3.17).

The comparison of experimentally measured isothermal compressibility and calculated one according equation (3.17) for intrusion process (μ_T^{int}) is shown using values of parameters given in Paragraph 3.1.2.

Coefficient of adiabatic compressibility of an HLS was determined taking into account the temperature variation during adiabatic compression/decompression of an HLS:

$$\mu_S^{int,ext} = -\frac{1}{V_0^0} \left(\frac{\partial V_{int,ext}}{\partial P} \right)_S = -\frac{1 - P_0 \frac{dP_{int,ext}}{dT} \frac{T}{c_V} \beta^0 \mu_S^0}{\frac{1}{f'_{int,ext}} - \left(\frac{dP_{int,ext}}{dT} \right)^2 \frac{T}{c_V}} + \mu_S^0, \quad (3.18)$$

where $c_V = C_V/V_0^0$ is the specific heat capacity at constant volume, $\beta^0 = \frac{1}{P_0} \left(\frac{\partial P}{\partial T} \right)_{V,\Omega}$ is the isochoric coefficient of pressure, $\mu_S^0 = -\frac{1}{V_0^0} \left(\frac{\partial V_0}{\partial P} \right)_{S,\Omega}$ is the coefficient of adiabatic compressibility of the liquid and the matrix.

The isobaric coefficient of thermal expansion:

$$\alpha^{int,ext} = \frac{1}{V_0^0} \left(\frac{\partial V_{int,ext}}{\partial T} \right)_P = \alpha^0 - \frac{f'_{int,ext}}{V_0^0} \frac{dP_{int,ext}}{dT}, \quad (3.19)$$

where $\alpha^0 = \frac{1}{V_0^0} \left(\frac{\partial V_0}{\partial T} \right)_{P,\Omega}$ is the isobaric coefficient of thermal expansion of the liquid and the matrix. The temperature dependence of α for the process of intrusion (temperature increase) is shown on Fig. 3.3., compared to the literature temperature dependence of α^0 for water. From Fig. 3.3 it can be seen that after reaching the certain temperature for which the value of intrusion pressure P_{int} becomes equal to the value of the pressure in the system (in this case $P = 15$ MPa), α becomes negative, which means that the system reduces its volume while temperature is increasing. This phenomenon is known as Negative Thermal Expansion (NTE) and presents significant scientific interest in science and technology. The phenomenon of NTE for HLSs will be discussed in details in Paragraph 3.1.6.

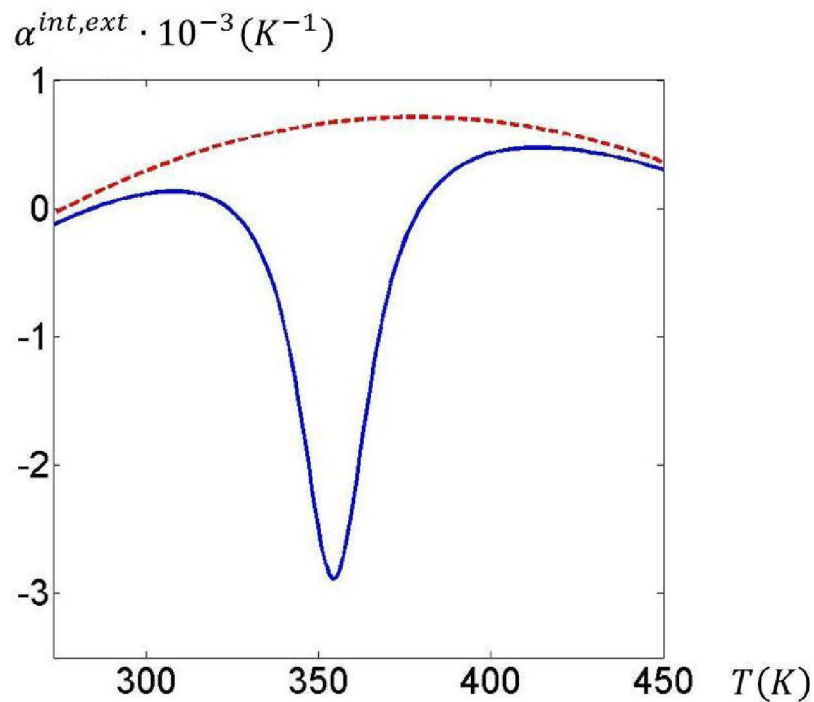


Fig. 3.2. Coefficient of isobaric thermal expansivity of the {Waters C8 + water} HLS for the intrusion process. Solid line is model according to equation (3.17), dashed line is coefficient of isobaric thermal expansivity of water according to available data (NIST Chemistry WebBook).

The isochoric coefficient of pressure:

$$\beta^{int,ext} = \frac{1}{P_0} \left(\frac{\partial P}{\partial T} \right)_V = \frac{\beta^0 - \frac{dP_{int,ext}}{dT} \frac{f'_{int,ext}}{P_0 V_0^0 \mu_T^0}}{1 - \frac{f'_{int,ext}}{V_0^0 \mu_T^0}} \quad (3.20)$$

It is important to note that if the interface effects are negligible for an HLS ($f'_{int,ext} \rightarrow 0$), correspondence principle is satisfied: that is the thermal coefficients of HLS become equal to the thermal coefficients of the liquid and the matrix of an HLS, and if dispersion of the pore radii is negligibly small (dispersion of intrusion/extrusion is also small ($D_{int,ext} \rightarrow 0$)) they become equal to the thermal coefficients of an HLS based on uniporous matrix.

It should be noted that obtained relations and thermal coefficients do not take into account the pore radii change during the compression/decompression process. An attempt to analyze such phenomena is presented here after in the reference (Eroshenko and Grosu 2013a), see the following reprint.

THEORETICAL
AND MATHEMATICAL PHYSICS

Maxwell's Relations and Thermal Coefficients for Repulsive Clathrates

V. A. Eroshenko* and Ya. G. Grosu

National Technical University of Ukraine "Kyiv Polytechnical Institute," pr. Pobedy 37, Kyiv, 03056 Ukraine

*e-mail: eroshenko@kpi.ua

Received April 8, 2012

Abstract—Prospects of nanotechnologies used for designing more effective thermomechanical devices and systems based on repulsive clathrates are outlined. Basic differences in thermodynamic properties of repulsive clathrates (that can be used for dissipation, accumulation, and transformation of large amount of energy in small volumes of working chambers) and traditional working bodies (gas/vapor) are demonstrated. Among unexpected characteristics of the systems being developed, the dependence of the adiabatic exponent on the parameters of the system is detected and negative values of the thermal elasticity coefficient are confirmed. The possibility of improving the accuracy of diagnostics of capillary–porous materials by taking into account additionally the thermal effects observed in repulsive clathrates is demonstrated.

DOI: 10.1134/S1063784213080124

INTRODUCTION

New working bodies [1, 2] that were initially called heterogeneous lyophobic systems (HLSs) (or briefly repulsive clathrates¹ [3, 4]), for which it was proposed for the first time that interface areas with molecular forces acting on them can be used for effective accumulation [5–7], dissipation [8–11], and transformation of energy [12, 13] in thermomechanical systems, has made it possible to employ them in power engineering also. On account of the fact that traditional power equipment with gas/vapor working bodies has almost attained the maximal technoeconomic indices [14–16], it is not surprising that the increasingly large number of researchers and designers are using repulsive clathrates (RCs) for solving fundamental [17–20] as well as applied [7, 11, 13, 21, 23] problems in engineering thermodynamics and power engineering.

It has been proved [1, 2, 12, 23–26] that new prospects for radical saving of fuel and structural materials can be associated with the use of RCs that possess better energy accumulating and transforming abilities owing to the use of “liquid–solid” interfaces in lyophobic condensed systems.

The thermodynamic features of HLSs (RCs) based on heteroporous matrices were described in [27]. Advances in basically new power engineering based on such HLSs (RCs) are impossible without the knowledge of Maxwell's relations and thermal coefficients

because these coefficients make it possible to calculate parameters and functions (such as volume and entropy) that are difficult for calculations from easily measurable parameters (such as pressure and temperature) and to determine optimal parameters of thermomechanical devices and systems being designed and constructed.

This study aims at further development of a thermodynamic and mathematical apparatus for describing peculiar operational properties and characteristics of repulsive clathrates and for specifying the field of their applications.

1. BRIEF DESCRIPTION OF A HETEROGENEOUS THERMODYNAMIC SYSTEM

Figure 1 shows schematically the working body, viz., HLS (RC) [1, 2] based on heteroporous matrix (pore radius $r = \text{var}$). The working body consists of capillary–porous matrix 1 (volume $V_M = \text{const}$) and liquid 2 ($V_L = \text{const}$) that does not wet the matrix. Hypothetical piston 3 can move in cylinder 4. The lyophobic nature of the matrix (contact angle $\theta > 90^\circ$) rules out spontaneous penetration of the working liquid into the pore space of the matrix ($V_p = \text{const}$). The decrease in the volume of the system as a result of its forced compression is associated with the development of interface area Ω (filling of the pore space of the matrix), while its increase is associated with spontaneous reduction of area Ω (emergence of the liquid from the lyophobic matrix) [1–13, 17–27]. This matrix in HLSs (RCs) can be in the form of a monolithic core (see Fig. 1) [27] or a powder [1–12, 17–24], which does not change the algorithm of the description of the

¹ In contrast to clathrates widely used in chemistry [6] ($A + B \rightarrow AB$, where A is the “host” molecule with a free internal space and B is the “guest” molecule), the process of combining the host and the guest is reversible ($A_{rc} + B_{rc} \leftrightarrow A_{rc}B_{rc}$) due to repulsive forces, which makes it possible to use them in nanotechnologies for constructing molecular springs [5].

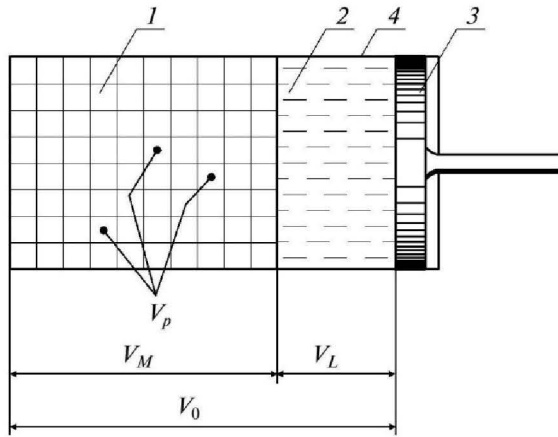


Fig. 1. Physical model of a repulsive clathrate.

HLS properties to within a numerical correction to the volume of the liquid used.

2. THERMODYNAMIC FUNCTIONS

It was shown in [23, 27] that the volume of the system and its variation are defined as

$$V = V_L + V_M - kr\Omega = V_0 - kr\Omega, \quad (1)$$

$$dV = -kr d\Omega, \quad (2)$$

where k is the coefficient taking into account the geometry of the pore space ($k = 0.5$ for long cylindrical capillaries and $k = 0.33$ for spheres).

Traditionally, the pressure in a HLS [23] is determined by the Laplace capillary pressure [28]

$$P = \sigma |\cos\theta| / (kr), \quad (3)$$

however, the change in pressure in the case considered here depends not only on the variation in temperature ($\sigma = \sigma(T)$), but also on $r = \text{var}$:

$$\begin{aligned} dP &= \left(\frac{d\sigma}{r} - \sigma \frac{dr}{r^2} \right) \frac{|\cos\theta|}{k} \\ &= \frac{1}{r} \left(d\sigma + k\sigma \frac{d\Omega}{\Gamma(r)} \right) \frac{|\cos\theta|}{k}, \end{aligned} \quad (4)$$

where

$$\Gamma(r) = \frac{dV}{dr} = -kr \frac{d\Omega}{dr} = \frac{b}{\sqrt{2\pi}a^2} \exp\left(-\frac{(r-r_0)^2}{2a^2}\right)$$

is the volume distribution for pores over their radii (which can be Gaussian) [29], b is the normalization factor, r_0 is a certain representative value of pore radii, and a is their dispersion.

It can be seen that the HLS state (in contrast to traditional gas/vapor) is determined unambiguously as before [23, 27] not by one but by two equations, (2)

and (4). However, in some cases, a single equation of state can be obtained for an HLS based on a heteroporous matrix using special functions.²

We assume that the surface tension coefficient depends on temperature linearly (which is observed for simple liquids [30]):

$$\sigma = \sigma_0(1 - T/T_{cr}) = \left. \frac{d\sigma}{dT} \right| (T_{cr} - T), \quad (5)$$

where T_{cr} is the critical temperature for the liquid and σ_0 is the hypothetical value of σ for $T = 0$. The HLS entropy is determined by the sum of its volume and interface components [23, 27],

$$dS = dS_V + dS_\Omega = \frac{C_V}{T} dT + \left. \frac{d\sigma}{dT} \right| |\cos\theta| d\Omega, \quad (6)$$

where C_V is the heat capacity of the bulk (volume) phase of the system for $V = \text{const}$.

It follows from Eq. (6) that the forced development of the interface under adiabatic conditions leads to a decrease in the temperature of the system as a whole (this was proved theoretically and demonstrated experimentally for the first time in [31]):

$$dS = 0 \Rightarrow dT = -\frac{T}{C_V} \left. \frac{d\sigma}{dT} \right| |\cos\theta| d\Omega. \quad (7)$$

Taking into account Eqs. (1)–(4), we can write the thermodynamic functions for the HLS at $r = \text{var}$ [27]:

$$dU = TdS - PdV = TdS + \sigma |\cos\theta| d\Omega, \quad (8)$$

$$dH = TdS - VdP$$

$$= TdS - \frac{(V_0 - kr\Omega)}{kr} \left[1 - \frac{k\sigma}{\Gamma(r)} \frac{d\Omega}{dT} \left. \frac{d\sigma}{dT} \right|^{-1} \right] |\cos\theta| d\sigma, \quad (9)$$

$$dF = -PdV - SdT = \sigma |\cos\theta| d\Omega - SdT, \quad (10)$$

$$dG = -VdP - SdT \quad (11)$$

$$= -\frac{(V_0 - kr\Omega)}{kr} \left[1 - \frac{k\sigma}{\Gamma(r)} \frac{d\Omega}{dT} \left. \frac{d\sigma}{dT} \right|^{-1} \right] |\cos\theta| d\sigma - SdT,$$

where U is the internal energy, H is the enthalpy, F is the Helmholtz free energy, and G is the Gibbs potential.

3. MAXWELL RELATIONS

Using the classical approach in thermodynamics and Eqs. (8)–(11), we obtain the system of Maxwell's relations

² In the case of a Gaussian distribution, we have $V = \int \Gamma(r) dr = b/2\text{erf}((r-r_0)/\sqrt{2}) + V(r_0)$, which gives $r = a\sqrt{2\text{erf}^{\text{inv}}(2(V-V(r_0))/b) + r_0}$; further, Eq. (3) leads to the equation of state $Pr(V) = \sigma(T)|\cos\theta|/k$, where erf is the error function and erf^{inv} is the inverse error function [29].

$$\left(\frac{\partial T}{\partial \Omega}\right)_s = \left(\frac{\partial \sigma}{\partial S}\right)_\Omega |\cos \theta|, \tag{12}$$

$$\left(\frac{\partial S}{\partial \Omega}\right)_p = \left(\frac{\partial P}{\partial \Omega}\right)_s \left|\frac{d\sigma}{dT}\right|^{-1} \frac{C_v k r}{R |\cos \theta|}, \tag{13}$$

$$\left(\frac{\partial S}{\partial \Omega}\right)_T = -\left(\frac{\partial \sigma}{\partial T}\right)_\Omega |\cos \theta|, \tag{14}$$

$$\left(\frac{\partial S}{\partial P}\right)_T = \left(\frac{\partial \Omega}{\partial r}\right)_p \frac{k r^2}{\sigma} \left|\frac{d\sigma}{dT}\right| |\cos \theta|. \tag{15}$$

These relations, which assume a nonstandard form (in view of the specific features of the lyophobic system under investigation), remain equally logical and helpful as their analogs for traditional thermodynamic gas/vapor systems. For example, Eqs. (12) and (13) make it possible to explain the favorable temperature regime of operation of a motorcar HLS shock absorber [9, 10] in which the rod experiences mechanical action with a frequency of up to 22 Hz (exerted by the road with a varying profile). At such a high frequency of perturbations (which cannot be suppressed in traditional hydraulic shock absorbers with their “transmission” frequency of 5–6 Hz), an HLS shock absorber successfully dissipated the energy of these perturbations without a noticeable increase in the temperature of the system. Such a peculiar phenomenon can be explained by the fact that in view of the endothermal nature of the processes of development of interface in HLS (7) under nearly adiabatic conditions (22 Hz), the heat of formation of this interface ($\delta Q = T dS_\Omega = T |d\sigma/dT| |\cos \theta| d\Omega$) is supplied not from external environment but from the heterogeneous system itself due to a decrease in the internal energy of its volume phase [9, 10, 31].

Comparative analysis of Eqs. (13) and (14) shows that the sign of variation of the interface area $d\Omega$ determines the sign of entropy variation dS (assuming that $\partial\sigma/\partial T < 0$ in Eq. (14)) and consequently the thermal effects of heat supply–removal. We observe the opposite effect of the temperature coefficient $d\sigma/dT$ of surface tension of the liquid on entropy variation dS in isobaric and isothermal processes.

Under isobaric conditions, the change in the HLS volume ($d\Omega \neq 0$) may be due only to the change in the surface tension of the liquid (see Eq. (4)), which in turn is determined by temperature T (5). Thus, the smaller the temperature derivative of surface tension of the liquid in the HLS, the larger the amount of heat that must be supplied to the system to change its volume, because for $d\sigma/dT \rightarrow 0$, we have $(\partial S/\partial \Omega)_p \rightarrow \infty$, which follows from Eq. (13).

Let us compare the heat expenditures in isothermal and isobaric processes for HLSs under investigation using Eqs. (4) and (6):

$$\begin{aligned} & \left(\frac{\partial S}{\partial \Omega}\right)_p / \left(\frac{\partial S}{\partial \Omega}\right)_T \\ &= 1 + \frac{C_v}{T} \frac{\sigma k}{\Gamma(r) |\cos \theta|} \left|\frac{d\sigma}{dT}\right|^2 \equiv 1 + i^*. \end{aligned} \tag{16}$$

Parameter i^* will be described in detail in Section 6.

Relation (16) shows that the heat ($\delta Q = T dS$) that must be supplied to the HLS for its compression under isobaric conditions exceeds the heat of formation of interface Ω , which must be supplied to the system for it to preserve its isothermal nature during forced compression. The limiting case is the equality of these quantities for an HLS based on uniporous matrix ($dr = 0 \Rightarrow \Gamma(r) = dV/dr \rightarrow \infty$); the equivalence of the isobaric and isothermal processes for such HLSs was noted earlier [23, 31]. Such features must be taken into account in designing effective devices based on repulsive clathrates [9–12].

4. ANALYSIS OF MAXWELL'S RELATIONS AND EXAMPLE OF THEIR POSSIBLE APPLICATION

It can be seen from Eqs. (13) and (15) that one of the macroscopic parameters for HLSs under investigation is radius r of the group of pores filled with/vacated from the liquid during compression/expansion of the system; parameters T and Ω play the role of independent variables as before [23, 27].

Relation (15) can be used for determining the distribution of pores and capillaries in the sample under investigation semiempirically. For example, using relations (2), (3), (15), and the classical expression $\delta Q = T dS$ for the amount of heat, we obtain

$$\Gamma(r) = \frac{kP}{T} \left|\frac{d\sigma}{dT}\right|^{-1} \left|\left(\frac{\partial Q}{\partial P}\right)_T\right|. \tag{17}$$

This relation shows that possible deviation from the isothermal behavior of the system in intrusion/extrusion processes in mercury [33] and water porosimetry [34] (the isothermality is only declared but not guaranteed by designers of porosimeters) may lead to inevitable distortion of the actual distribution of pores over their radii if partial derivative $\frac{\partial Q}{\partial P}$ (17) remains unchanged. This violation of isothermality may appear during the “gas–piston” regime of flow of elementary microjets in the capillary–pore space of the matrix, which in fact leads to quasi-adiabaticity of intrusion (decrease in temperature (7) [31] in the case of superfast development of the interface area ($\partial\Omega/\partial t$) because the heat flux $\partial Q_{ex}/\partial t$ from external medium becomes smaller than the heat flux required for the formation of interface ($\partial Q_\Omega/\partial t = T \partial S_\Omega/\partial t \sim \partial\Omega/dt$). This decrease in temperature leads to an increase in surface tension (5) and pressure (3) and, hence, to an unjustified decrease in the calculated pore radii in the

matrix (3) as compared to their actual values. It should be noted that it is impossible to avoid the gas–piston regime of matrix filling even when the rate of the increase in the external pressure is indefinitely small (as in operation of porosimeters) because the filling of each next group of pores with their own elementary radius occurs jumpwise when the corresponding intrusion pressure (3) is attained. Thus, the allowance for the actual thermal effects in porosimetry is expedient if it is necessary to improve the accuracy in diagnostics of porous materials. Relation (17) can also be used for solving the inverse problem: if the pore radial distribution function $\Gamma(r)$ of the sample is known, thermal effects [31] appearing during compression/expansion of the HLS used can be determined from expression (17).

5. THERMAL COEFFICIENTS

Taking into account the thermodynamic functions and Maxwell's relations derived above, we can write the expressions for thermal coefficients for repulsive clathrates ($r = \text{var}$).

With allowance for Eqs. (2), (4), and (5), the isothermal compressibility factor can be written as

$$\mu_T = -\frac{1}{V_0} \left(\frac{\partial V}{\partial P} \right)_T = \frac{\Gamma(r)r^2 k}{V_0 \sigma |\cos \theta|}. \quad (18)$$

It can be seen that this coefficient is determined by the nature of the liquid as well as the geometry and morphology of the porous space of the matrix used.

Using relations (2), (4), and (7), we obtain the adiabatic compressibility factor

$$\begin{aligned} \mu_S &= -\frac{1}{V_0} \left(\frac{\partial V}{\partial P} \right)_S \\ &= \frac{(kr)^2}{V_0 |\cos \theta|} \left(\left| \frac{d\sigma}{dT} \right|^2 \frac{T}{C_V} |\cos \theta| + \frac{k\sigma}{\Gamma(r)} \right)^{-1}. \end{aligned} \quad (19)$$

It should be noted that the compressibility of HLSs under adiabatic conditions considerably depends on the surface tension thermal coefficient $d\sigma/dT$ of the liquid. It can be seen from Eq. (4) that under a constant pressure, the change in the volume of the system (as well as a change in Ω) can be due only to a change in temperature; therefore, Eqs. (2) and (4) lead to the following expression for the isobaric expansion coefficient:

$$\begin{aligned} \alpha &= \frac{1}{V_0} \left(\frac{\partial V}{\partial T} \right)_P = -\frac{\Gamma(r)r}{V_0 \sigma} \left| \frac{d\sigma}{dT} \right| = -\frac{\Gamma(r)r}{V_0(T_{cr} - T)} \\ &\Rightarrow d\alpha = \frac{-\Gamma(r)r}{V_0(T_{cr} - T)^2} dT. \end{aligned} \quad (20)$$

This coefficient increases ($d\alpha > 0$) upon a decrease in temperature ($dT < 0$). This peculiar property of HLSs (a decrease in temperature induces an increase in the

volume) is not observed for simple thermodynamic systems ($d\alpha/dT > 0$).

The isochoric pressure coefficient depends on temperature like that for a gas; however, this dependence for HLSs assumes an unexpected form (the pressure in the system decreases upon an increase in temperature [24]):

$$\beta = \frac{1}{P_0} \left(\frac{\partial P}{\partial T} \right)_V = -\frac{1}{\sigma r} \left| \frac{d\sigma}{dT} \right| = -\frac{r_0}{r} \frac{1}{T_{cr} - T}, \quad (21)$$

where P_0 is the pressure under which pores with radius r_0 are filled in the matrix.

6. GENERATIZATION OF THE CONCEPTS CONCERNING PECULIAR THERMODYNAMIC PROPERTIES AND POTENTIALITIES OF APPLICATION OF REPULSIVE CLATHRATES

Let us compare the compressibility of HLSs in isothermal (18) and adiabatic (19) conditions. Taking into account equalities (5) and performing trivial transformations, we can write

$$\begin{aligned} \frac{\mu_T}{\mu_S} &= 1 + \frac{\Gamma(r)T |\cos \theta| \left| \frac{d\sigma}{dT} \right|^2}{\sigma k C_V} \\ &= 1 + \left(\frac{T_{cr}}{T} - 1 \right)^{-1} \left| \frac{d\sigma}{dT} \right| \frac{\Gamma(r) |\cos \theta|}{V_L k c_V \rho} \equiv 1 + \frac{2}{i^*}, \end{aligned} \quad (22)$$

where ρ is the density of the working liquid and c_V is its specific heat for $V = \text{const}$. It can be seen that during compression of HLS ($r = \text{var}$), its adiabatic exponent varies continuously and attains its maximal value for the maximal development of the interface area (i.e., for $r = r_0$ since $\Gamma_{\max}(r) = \Gamma(r_0)$).

It is interesting to compare equality (22) with its analog for an ideal gas [35]

$$\frac{\mu_T}{\mu_S} = \frac{C_P}{C_V} = 1 + \frac{2}{i}, \quad (23)$$

where i is the number of the degrees of freedom of molecules; for example, for $i = 5$ (diatomic gas), we obtain the well-known value of adiabatic exponent $C_P/C_V = 1.40$.

A distinguishing feature of HLSs based on heteroporous matrices is the possibility to “control” over the second terms in Eqs. (22) and (23) by changing parameters of the system. The adiabatic exponents for HLSs with various working liquids and capillary–pore matrices with mean pore radii $r_0 \sim 3.6$ nm and $r_0 \sim 0.3$ nm [8] are given in the table.

Comparing Eqs. (22) and (23), we can introduce the concept of the virtual degree of freedom i^* for HLSs, which is defined as

Variation of adiabatic exponent μ_T/μ_S depending on the nature of the liquid and pore radius of the matrix used

Working liquid	$d\sigma/dT$, mN/(m K)	c_V , J/(kg K)	ρ , kg/m ³	T_{cr} , K	T , K	k	$\Gamma(r_0)/V_L$, m ⁻¹	r_0 , m	μ_T/μ_S
Water	0.16	4183	1000	647	298	0.33	4.0×10^8	36×10^{-9}	1.03
							5.7×10^{10}	0.3×10^{-9}	4.67
Mercury	0.22	139	13546	1750	298	0.33	4.0×10^8	36×10^{-9}	1.02
							5.7×10^{10}	0.3×10^{-9}	3.69

$$i^* = \frac{C_V}{T} \frac{\sigma 2k}{\Gamma(r) |\cos\theta|} \left| \frac{d\sigma}{dT} \right|^{-2} \tag{24}$$

$$= \frac{V_L}{\Gamma(r)} \left(\frac{T_{cr}}{T} - 1 \right) \left| \frac{d\sigma}{dT} \right|^{-1} \frac{2kc_V\rho}{|\cos\theta|}$$

For example, for a uniporous matrix ($\Gamma(r) \rightarrow \infty$), we obtain $i^* = 0$, which indicates a strictly predetermined motion of molecules and clusters in narrow capillaries without the risk of intersection with other “elementary jets” (this is a criterion of a laminar flow in macrosystems). Conversely, in heteroporous matrices (with $i^* > 0$), their complex spatial structure determines the apparently random motion of liquid particles in the 3D space (i.e., the conditional turbulent nature of their flow in the capillary–pore space of the matrix), which is equivalent to an increase in the number of degrees of freedom of these particles.

Quantity i^* also appears in equality (16), which means that the surface entropy (in contrast to the traditional bulk entropy whose increase symbolizes the tendency of the system to equilibrium) in HLSs is the potential of the system (its driving force); indeed, an increase in the entropy characterizes accumulation of energy in an HLS and its decrease indicates active action of the HLS on the external medium. The larger the number of degrees of freedom (“premises of disorder”) in the system, the larger the amount of mechanical work or heat that must be imparted to the system for its ordering (filling of pores in the matrix) under isobaric conditions. The set of equalities (16) and (22) as well as (14) gives

$$\frac{\left(\frac{\partial V}{\partial P}\right)_s + \left(\frac{\partial S}{\partial \Omega}\right)_T}{\left(\frac{\partial V}{\partial P}\right)_T + \left(\frac{\partial S}{\partial \Omega}\right)_p} = \frac{\left(\frac{\partial V}{\partial P}\right)_s - \left(\frac{\partial \sigma}{\partial T}\right)_\Omega |\cos\theta|}{\left(\frac{\partial V}{\partial P}\right)_T - \left(\frac{\partial S}{\partial \Omega}\right)_p} \tag{25}$$

$$= \frac{\left(\frac{\partial V}{\partial P}\right)_s + \left|\frac{\partial \sigma}{\partial T}\right| |\cos\theta|}{\left(\frac{\partial V}{\partial P}\right)_T - \left(\frac{\partial S}{\partial \Omega}\right)_p} = 1.$$

This expression is a sort of thermodynamic junction characterizing tight interlacing of four processes in HLSs: iso-

thermal, isobaric, isochoric ($d\Omega = 0 \Rightarrow dV = 0$), and adiabatic. Apart from the obvious significance of this relation (analogous to Maxwell’s relations) for applications, equality (25) demonstrates the exceptional role of the surface tension thermal coefficient $d\sigma/dT$ in all processes in HLSs. It should be noted that when a sufficiently large body of experimental data is available, relation (25) can be useful in analysis of such parameter as contact angle θ , which remained enigmatic for a long time because the mechanisms of formation of this angle (which is obviously nonequilibrium) and the origin of its hysteresis in processes of forced intrusion/spontaneous extrusion (in the presence of the hydraulic degree of freedom, viz., sink) of the liquid into/from a rigid lyophobic microcavity (capillary, sphere, cone, etc.) have not been studied comprehensively as yet.

Using Eqs. (2) and (3), relation (25) can be written as

$$\frac{\left(\frac{\partial V}{\partial P}\right)_s}{\left(\frac{\partial V}{\partial P}\right)_T} + \frac{\left(\frac{\partial P}{\partial T}\right)_v}{\left(\frac{\partial S}{\partial V}\right)_p} = 1. \tag{26}$$

In such a form, the equality contains conventional macroscopic parameters characteristic of classical systems, which facilitates and extends experimental

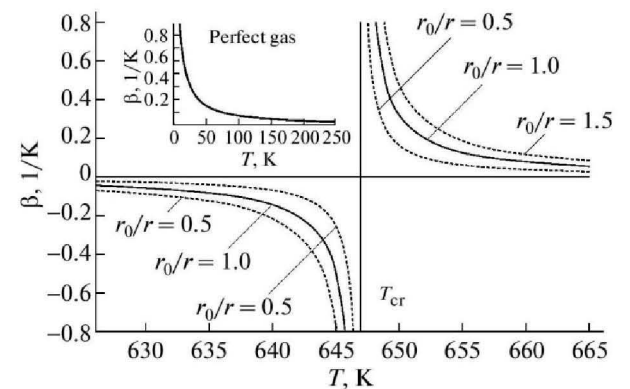


Fig. 2. Temperature dependence of the isochoric pressure coefficient for the HLS (RC) based on water. The inset shows the analogous dependence for a perfect gas.

investigation of thermodynamic properties of HLSs. Using Eq. (26) for an ideal gas, we can verify that it is also valid for this system, which indicates the universal nature of this relation. A transition from particular (25) to general relation (26) is the sound proof of the correctness of the above conclusions.

Figure 2 shows the temperature dependence of β for various values of r in comparison with the behavior of a perfect gas (inset to Fig. 2); it can be seen that the HLS and the gas/vapor systems as functions of temperature exhibit basically different behaviors. For example, at temperatures above T_{cr} , coefficient β for HLS varies analogously to that for the gas, which is not observed for the subcritical temperature range $T < T_{cr}$. At $T = 298^\circ\text{C}$, $\beta = +3.4 \times 10^{-3} \text{ K}^{-1}$ for the perfect gas, $\beta = -2.9 \times 10^{-3} \text{ K}^{-1}$ for a water-based HLS, and $\beta = -0.7 \times 10^{-3} \text{ K}^{-1}$ for a mercury-based HLS. It can be seen that the fact that β is negative for HLSs is nontrivial (an increase in temperature reduces the pressure!), which can effectively be used in engineering for designing nontraditional thermomechanical systems operating at $T < T_{cr}$.

It should be noted that Eqs. (8)–(15) and (18)–(21) can be reduced to corresponding equations derived for HLSs based on uniporous matrix [24, 31] for $r \rightarrow r_0 \Rightarrow \Gamma(r) = dV/dr \rightarrow \infty$ (i.e., the correspondence principle, which is fundamental in methodology, holds [36]).

CONCLUSIONS

The application of heteroporous matrices in HLSs (RCs) changes the form of Maxwell's relations and thermal coefficients and expands the range of practical applications of repulsive clathrates. Among other things, the following conclusions can be drawn.

1. The HLSs under investigation are characterized by a "controllable" adiabatic exponent (22) with the value determined by the parameters of the system.
2. One of the peculiar properties of the HLSs considered here is the negative value (in the subcritical temperature range) of the isochoric coefficient of pressure (see Fig. 2).
3. The Maxwell relations derived above combined with calorimetric data make it possible to determine the pore volume distribution functions over radii in the samples under investigation [17] more exactly as compared to widely used mercury [33] and water [34] porosimetry.
4. The ratio of partial derivatives observed in Eqs. (25) and (26) reflects in the single equation the close relation between parameters of the system in all four feasible conditions of the processes (isothermal, adiabatic, isochoric (surface), and isobaric).

5. Peculiar properties of the HLS considered here (including the concept of the virtual degree of freedom (24)) can be successfully used in nanotechnologies for designing basically new samples for electrical engineering [3–12, 21, 22, 37].

REFERENCES

1. V. A. Eroshenko, USSR Patent No. 1254811 (1981), Byull. Izobret. No. 3 (1996).
2. V. A. Eroshenko, Int. Patent No. WO 96/18040 (June 13, 1996).
3. V. A. Eroshenko and Yu. F. Lazarev, Prikl. Mekh. Tekh. Fiz. **53**, 114 (2012).
4. V. A. Eroshenko, in *Proceedings of the International Post-SMITR Conference on Seismic Isolation, Passive Energy Dissipation and Active Control of Seismic Vibrations of Structure, Taormina, Sicily, Italy, 1997*, pp. 783–794.
5. V. Eroshenko, R.-C. Regis, M. Soulard, and J. Patarin, J. Am. Chem. Soc. **123**, 8129 (2001).
6. V. Eroshenko, R.-C. Regis, M. Soulard, and J. Patarin, C.R. Physique **3**, 111 (2002).
7. Y. Qiao, V. K. Punyamurtula, and A. Han, Appl. Phys. Lett. **89**, 251905 (2006).
8. L. Coiffard, V. A. Eroshenko, and J.-P. E. Grolier, AIChE J. **51**, 1246 (2005).
9. V. A. Eroshenko, Proc. Inst. Mech. Eng., Part D (J. Automob. Eng.) **221**, 285 (2007).
10. V. A. Eroshenko, I. I. Piatiletov, L. Coiffard, and V. P. Stoudenets, Proc. Inst. Mech. Eng., Part D (J. Automob. Eng.) **221**, 301 (2007).
11. T. Iwatsubo, K. Washio, H. Yabo, and M. Miyazaki, J. Syst. Design Dyn. **2**, 1160 (2008).
12. V. A. Eroshenko, USSR Patent No. 943444 (1981); USSR Patent No. 1382078 (1982); USSR Patent No. 1380357 (1983); USSR Patent No. 1333870 (1985); USSR Patent No. 1434881 (1985); USSR Patent No. 1452262 (1986); USSR Patent No. 1508665 (1987).
13. A. Laouir, L. Luo, D. Tondeur, T. Cachot, and P. Le Goff, AIChE J. **49**, 764 (2003).
14. V. A. Eroshenko, Izv. Akad. Nauk SSSR, Energ. Transp., No. 2, 125 (1987).
15. *World Energy, Looking Ahead to 2020: Report* (IPC Science and Technology, New York, 1978).
16. V. A. Kirillin, *Energetics. General Problems: Questions and Answers* (Znanie, Moscow, 1997).
17. F. Cailliez, M. Trzpit, M. Soulard, I. Demachy, A. Boutin, J. Patarin, and A. H. Fuchs, Phys. Chem. Chem. Phys. **10**, 4817 (2008).
18. L. Liu, J. Zhao, P. J. Culligan, Y. Qiao, and X. Chen, Langmuir **25**, 11862 (2009).
19. R. Denoyel, I. Beurroies, and B. Lefevre, J. Petrol. Sci. Eng. **45**, 203 (2004).
20. D. Bougeard and K. S. Smirnov, Phys. Chem. Chem. Phys. **9**, 226 (2006).
21. A. Han and Y. Qiao, Appl. Phys. Lett. **91**, 173132 (2007).
22. T. Karbowiak, M.-A. Saada, S. Rigolet, A. Ballandras, G. Weber, I. Bezverkhyy, M. Soulard, J. Patarin, and

- Jean-Pierre Bellat, *Phys. Chem. Chem. Phys.* **12**, 11454 (2010).
23. V. A. Eroshenko, *Dokl. Akad. Nauk SSSR, Ser. A*, No. 10, 77 (1990).
24. V. A. Eroshenko, *Promyshl. Teplotekh.* **14** (1–3), 22 (1992).
25. V. A. Eroshenko, *Entropie*, No. 196, 17 (1996).
26. V. A. Eroshenko, *Entropie*, No. 202/203, 110 (1997).
27. V. A. Eroshenko and Ya. G. Grosu, *Promyshl. Teplotekh.* **33** (6), 73 (2011).
28. E. W. Washburn, *Phys. Rev.* **17**, 273 (1921).
29. M. Abramowitz and I. A. Stegun, *Handbook of Mathematical Functions with Formulas, Graphs, and Mathematical Tables* (Dover, New York, 1972).
30. T. Reis, *Introduction a la Chimie—Physique des Surfaces* (Dunod, Paris, 1952).
31. V. A. Eroshenko, *Koloidn. Zh.*, No. 5, 875 (1987).
32. V. V. Sychev, *Differential Equations of Thermodynamics* (Taylor and Francis, 1991).
33. T. G. Plachenov and S. D. Kolosentsev, *Porometry* (Khimiya, Leningrad, 1988).
34. V. A. Eroshenko and A. Yu. Fadeev, *Russ. Khim. Zh.* **40**, 92 (1996).
35. L. D. Landau and E. M. Lifshitz, *Course of Theoretical Physics, Vol. 5: Statistical Physics* (Pergamon, Oxford, 1980).
36. V. I. Moiseev, *Philosophy and Methodology of Science* (Tsentr. Chernozem. Knizhn. Izd., Voronezh, 2003).
37. V. A. Eroshenko, Int. Patent No. WO 01/55616 A1 (August 2, 2001).

Translated by N.V. Wadhwa

3.1.4. Thermal effects of compression/decompression

In the previous paragraph it was shown that using the Maxwell relations thermal effects of compression/decompression (due to interface development(intrusion)/reduction(extrusion)) may be calculated using parameters of the matrix and the liquid used for HLS. In the reference (Eroshenko and Grosu 2013b) analysis of such thermal effects as well as some operational properties are presented. The reprint of this publication is given hereafter. The prediction of such thermal effects, but while taking into account bulk thermal coefficients is also discussed in the next paragraph.

Thermodynamic and Operational Properties of Heterogeneous Lyophobic Systems

V. A. Eroshenko^{1*}, Y.G. Grosu²

National Technical University of Ukraine "KPI", Department of Energy Saving and Energy Management, Laboratory of Thermomolecular Energetics, Peremogu pr. 37, Kiev, Ukraine.

E-mail: ¹eroshenko@kpi.ua, ²grosu.y@ukr.net

Abstract: The grounds for further fundamental study of heterogeneous lyophobic systems (HLS) under technical thermodynamics in order to create nontraditional high-performance thermo-mechanical devices (dampers, accumulators and energy converters) are presented. A number of unusual HLS properties have been analyzed in view of their practical use: nontypical for conventional working bodies (gas, vapor) compression/decompression endo-/exothermal effects; operational features under adiabatic and cycling conditions. Thermodynamic model describing HLS behavior under conditions that are useful for operational requirements of technical devices and systems is proposed.

Key words: Adiabatic; capillary; energy transformation; lyophobic; surface tension; thermodynamics.

1. Introduction

"Lyophobic porous solid – liquid" interfaces utilization in order to transform, dissipate and store mechanical energy provides new opportunities for nontraditional energetics (Eroshenko 1992, 1987b). The new working bodies – heterogeneous lyophobic systems¹ (HLS) – generate interest among scientists due to many unusual and useful properties and characteristics (Bougard and Smirnov 2006; Cailliez et al. 2008; Coiffard, Eroshenko, Grolier 2005; Denoyel, Beurroies, Lefevre 2004; Eroshenko and Aistov 1990; Eroshenko and Lazarev 2012; Han and Qiao 2007; Iwatsubo, Washio, Yano, Miyazaki 2008; Karbowski, Paulin, Bellat 2010; Laouir, Luo, Tondeur, Cachot, Le Goff 2003; Liu, Zhao, Culligan, Qiao, Chen 2009; Martin et al. 2002; Qiao, Punyamurtula, Han 2006).

New features of HLS are caused by new mechanism of energy transformation: contrary to conventional working bodies (gas and vapor which are successfully used over two centuries) where molecular kinetic energy is dominant, HLS takes advantage of potential energy of molecular interactions. Among the distinctive and promising characteristics of HLS extremely high energy density per unit volume should be mentioned (Laouir et al. 2003), which is similar to thermodynamic compactness (TC) of thermal machine (Eroshenko 1981, 1996):

$$TC = \frac{\Delta W}{\Delta V \Delta T} \left(\frac{J}{m^3 K} \right), \text{ where } \Delta W \text{ is the net work output}$$

during the cycle, ΔV and ΔT are the volume and temperature change during the "heat – work" transformation in this cycle. Obviously TC is proportionally correlated with thermal efficiency of the cycle. Best modern thermal machines (working body is gas) have the following TC values² (next: the name of cycle inventor – TC value (J/m³K)): Stirling – 375, Joule-Brayton – 210, Otto-Beau de

Rochas – 490, Diesel – 520, Trinkler – 420. In spite of great variety of approaches and design solutions, TC of modern thermal machines has almost reached their ceiling values. It is possible to reach TC value about 600-700 (J/m³K) using conventional working bodies, but it requires new constructive materials which are able to stay under much higher gas temperature and pressure. These kinds of materials with acceptable cost are so far unavailable. While new HLS-based cycle³ gives opportunity to build thermal machine with TC value much higher (1-2 order of magnitude) compared to conventional ones. This promotes radical fuel economy, constructive materials amount reduction and environment safety level increase, as explosion stroke in HLS-thermal machine takes place under ambient temperature. So HLS utilization brings up the new paradigm in energy transformation process: utilization of surface free energy in heterogeneous lyophobic nanosystems ("liquid and porous matrix, which is not wetted by this liquid"), where liquid surface tension is intensive parameter of the system and huge (200-1000 m² per 1 gram of the matrix) "solid – liquid" interface is extensive one.

The detailed expertise of HLS-based thermal machines is presented in (Laouir et al. 2003), dissipation devices characteristics and design solutions are described in (Eroshenko 2007; Eroshenko 2001a; Eroshenko, Piatiletov, Coiffard, Stoudenets 2007; Iwatsubo et al. 2008; Suci, Iwatsubo, Deki 2003) and HLS-accumulation process features are given in (Eroshenko, Regis, Soulard, Patarin 2002; Qiao et al. 2006).

The purpose of this article is further and deeper analysis of HLS thermal and mechanical properties and development of specific mathematical methods to describe them. Presented models are tested using experimental data previously obtained (Coiffard et al. 2005, Karbowski et al. 2009, 2010). Note that developing model which allows to predict adiabatic properties of the system according to its isothermal ones is rather important issue, because most

¹ These systems were also called "repulsive clathrates" (Eroshenko 1997; Eroshenko and Lazarev 2012)

² Detailed calculation and analysis of TC for existing cycles according to available construction materials and temperature ranges are available elsewhere (Eroshenko 1987b).

³ Initially new cycle has been described in (Eroshenko 1981a, 1982) and detailed expertise is given in (Laouir et al. 2003)

theoretical and experimental investigations of thermodynamic and thermophysical properties of HLS are carried out on the basis of scientific equipment, that allows to register only isothermal (slow) compression – decompression processes, and power equipment operation typically requires understanding and predicting working media behavior in adiabatic (fast) conditions. We also focus on defining the thermodynamic characteristics of HLS based on matrices with an arbitrary pore size distribution function.

2. Heterogeneous lyophobic systems principles

Figure 1 represents principle scheme of new working body – HLS based on a matrix with different size pores (pore radius $r = \text{var}$). The system consists of a capillary-porous matrix 1 (volume $V_M = \text{const}$) and liquid 2 ($V_L = \text{const}$) which does not wet this matrix. Hypothetical piston 3 can be displaced in the cylinder 4. As matrix is lyophobic (contact angle $\theta > 90^\circ$) it eliminates the spontaneous penetration of fluid in the pore space. Volume reduction of the system during its forced decompression is due to interface area development (liquid intrusion into the porous matrix space), and not due to HLS components deformation (in this work we consider that matrix and liquid are incompressible).

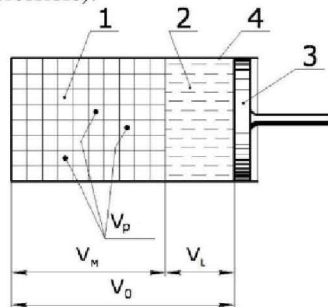


Figure 1. Heterogeneous lyophobic system physical model.

The HLS matrix can be presented as monolithic solid or as powder which porous particles are surrounded by fluid and have the same total volume of pore space as a monolithic solid. In the case of powder, the fluid volume should be increased according to interparticle volume, which must be filled during system compression. The following methodology is not affected by matrix nature (monolithic solid or powder).

3. Approaches and assumptions for the correct HLS experimental results interpretation

As system volume variation is only due to liquid penetration into the porous matrix space (interphase area development), it is usually defined as (Eroshenko 1990, 2007; Eroshenko and Grosu 2011):

$$dV = -kr d\Omega \quad (1)$$

where k is the pore space geometry coefficient ($k = 0.50$ for long cylindrical capillary, $k = 0.33$ for spheres).

Traditionally we express liquid intrusion pressure by the Laplace – Washburn equation (Washburn 1921), but in slightly modified form (with correcting factor B):

$$P_{\text{int}} = \frac{\sigma \cos \theta}{B_{\text{int}} kr} \quad (2)$$

where σ is the “liquid – gas/vapor” surface tension (bulk phase). Here and below the $\cos \theta$ module is used and the value of contact angle θ is assumed to be taken for the planer “liquid – solid” interface.

Correcting factor B is used in equation (2) to preserve its original phenomenological structure despite the fact that microscopic properties of the liquid confined in the capillary, with diameter comparable with the size of the molecules of the liquid (Coiffard et al. 2005; Eroshenko 2000, 2001b; Karbowski et al. 2009, 2010), may not coincide with its macroscopic properties, which are usually given for a massive phase in the references (Vargaftik 1972). Particularly, due to the molecular bonds number decrease (molecules were “wrested” from the bulk liquid phase and placed in a microcapillary), the liquid surface tension in such capillary is lower than in the bulk phase (Rusanov 1981, Kirkwood and Buff 1949), which is confirmed by molecular dynamic simulations according to which a single- or double-chain of liquid molecules is formed (Mann and Halls 2003; Moravsky and Loutfy 2004). Whereas, in water intrusion experiments on superhydrophobic silicalites (Coiffard et al. 2005; Eroshenko 2000, 2001b; Karbowski et al. 2009, 2010) with the pore radius $r \sim 0,25\text{nm}$ measured Laplace capillary pressure was about 5-7 times lower than calculated on the basis that confined and bulk water surface tensions are equal (Eroshenko 2002). Correction factor B may be useful for more accurate calculation of non-standard processes in heterogeneous nanosystems, like HLS thermal effects of compression (intrusion) and decompression (extrusion).

In view of the above, the pressure of spontaneous extrusion of fluid from the pore space of the matrix will be determined by equation similar to Eq.(2):

$$P_{\text{ext}} = \frac{\sigma \cos \theta}{B_{\text{ext}} kr} \quad (3)$$

The difference between the values of B_{int} and B_{ext} reflexes experimentally observed hysteresis in HLS forced compression – spontaneous decompression cycle (Figure 2a, 2b: intruded water volume – pressure dependence. Dots represent experimental results obtained by Coiffard et al. 2005). Currently, the nature of this hysteresis is not fully understood, but there are a number of alleged reasons for this: the contact angle hysteresis (Coiffard and Eroshenko 2006), the presence of metastable states (Woo and Monson 2003), etc. Correcting factor B is determined from experimental intrusion/extrusion pressure $P_{\text{int,ext}}^*$ and the one calculated according to original Laplace – Washburn equation ratio:

$$B_{\text{int,ext}} = \frac{\sigma \cos \theta}{P_{\text{int,ext}}^* kr} \quad (4)$$

Numerous experimental results (Coiffard and Eroshenko 2006; Kong and Qiao 2005; Liu et al. 2009; Qiao et al. 2006) show that in most cases, the HLS pressure temperature dependence is nearly linear, which in view of Eqs. (2) and (3) allows to write it in the general form:

$$\sigma \cos \theta = A(T - T_0) + P_0^{\text{int,ext}} k r_0 B_{\text{int,ext}}, \text{ where } A = \frac{\partial(\sigma \cos \theta)}{\partial T},$$

$P_0^{\text{int,ext}}$ is the intrusion/extrusion pressure at $T = T_0$ (initial temperature) under which pores with radius r_0 are filled.

The entropy of a heterogeneous system is the sum of its bulk and surface components (Guggenheim 1965), so that its variation can be expressed as:

$$dS_{\text{int,ext}} = dS_v + dS_\Omega = \frac{c_v m}{T} dT + \frac{A}{B_{\text{int,ext}}} d\Omega \quad (5)$$

where c_v is the HLS total specific thermal capacity at constant volume and m is its mass.

We can see from Eq. (5) that for lyophobic systems ($A > 0$) surface development ($d\Omega > 0$, B_{int}) is accompanied by system temperature decrease (experimentally verified (Eroshenko 1987a)):

$$dS = 0 \Rightarrow dT_{\text{int,ext}} = -\frac{TA}{B_{\text{int,ext}} mc_v} d\Omega \quad (6)$$

One of the key characteristic of the $r = \text{var}$ porous matrix is its pore size distribution function – system volume variation as a function of radius of pores that are filled $\Gamma(r) = dV/dr$. Due to Eqs. (2)/(3) this function defines PV-compression/decompression isothermal dependence. At the engineering stage this characteristic of the matrix is rather important and is always known, so it is appropriate to use it as input information for the model. In this paper, we use slightly modified Gaussian function as approximation for $\Gamma(r)$ (Abramowitz and Stegun 1972):

$$\Gamma(r) = \frac{dV}{dr} = \frac{rb}{a\sqrt{2\pi}} \exp\left(-\frac{(r-r_0)^2}{2a^2}\right), \quad (7)$$

where a is the radius value deviation parameter and b is the normalization factor. They are determined from the PV-compression isotherms of HLS (Figure 2).

4. Specificity of HLS thermomechanical processes under isothermal and adiabatic conditions

Isothermal conditions. We define the heat of isothermal interphase area development based on the classical thermodynamic concepts, but in view of the above-described HLS specific: using traditional heat definition $\delta Q = TdS$ and Eq. (5) and considering the isothermal process ($T = T_0 = \text{const}$), we obtain:

$$\delta Q_{\text{int,ext}} = B_{\text{int,ext}}^{-1} T_0 A d\Omega \quad (8)$$

The sign of the heat effect in Eq. (8) is determined according to the sign of the surface differential. Similarly, the expression for the work, defined as $\delta W = -PdV$, can be obtained by using Eq. (1) and (2):

$$\delta W_{\text{int,ext}} = B_{\text{int,ext}}^{-1} \sigma \cos \theta d\Omega \quad (9)$$

Note, since in real systems, there is a nonzero compressibility of the matrix and the liquid, initial conditions for Eqs. (8) and (9) will be $Q(\Omega=0) = Q_0$ and $W(\Omega=0) = W_0$ (Q_0 and W_0 are respectively heat and work produced during the system compression before reaching the intrusion pressure (Eq.(2)).

Since the aim of this paper is to study the processes of intrusion – extrusion of the liquid in the pore space of the matrix, the model does not include well-known compression – decompression processes of quasi condense components of the system (liquid + matrix), which with no harm for the problems discussed simplifies the mathematical expressions and specifies practical recommendations.

It is convenient to express interphase surface value during the compression – decompression in terms of easily controllable parameter of the system – its pressure. Thus, using Eqs. (1), (2) and (7), we obtain:

$$\Omega = -\frac{1}{k} \int \frac{\Gamma(r)}{r} dr = \frac{1}{k} \int \frac{\Gamma(P)}{P} dP \quad (10)$$

As indicated below, the solution of Eq. (10), in most cases can be solved using special functions (Abramowitz and Stegun 1972) and thus the amount of heat and work under isothermal conditions as a function of the pressure in the system and, consequently, as the degree of its compression can be obtained.

Adiabatic conditions. Under adiabatic conditions, the calculation of the work required to compress the system would be complicated due to the temperature decrease during interface Ω development (see Eq. (6)). This decrease is due to the fact that in isolated system interphase area development heat (8) is compensated not by environment heat supply (as it is under isothermal conditions), but by reducing internal energy of the system (its bulk phase) (Eroshenko 1987a). Solving the differential equation (6) and taking into account that initial temperature of the system is T_0 , we obtain:

$$T_{\text{int}} = T_0 \exp\left(-\frac{\Omega A}{B_{\text{int}} mc_v}\right) \quad (11)$$

Initial conditions for the spontaneous decompression of the system are: $T_0 \rightarrow \min(T_{\text{int}}) \equiv T_{\text{int}}^{\text{min}}$ – temperature reached after full HLS compression ($\Omega = \Omega^{\text{max}}$). Therefore, we get:

$$T_{\text{ext}} = T_{\text{int}}^{\text{min}} \exp\left(\frac{(\Omega^{\text{max}} - \Omega) A}{B_{\text{ext}} mc_v}\right) \quad (12)$$

To calculate HLS compression/decompression work under adiabatic conditions first we use its classical P-V coordinates definition and then take into account Eqs. (11), (12), (1) – (4), and, $\sigma \cos \theta$ linear temperature dependence:

$$W_{\text{int}}^S = -\int PdV = B_{\text{int}}^{-1} \int \sigma \cos \theta d\Omega = \left(\frac{AT_0}{B_{\text{int}}} + P_0^{\text{int}} k r_0\right) \Omega + T_0 mc_v \left(\exp\left\{-\frac{\Omega A}{B_{\text{int}} mc_v}\right\} - 1\right) \quad (13)$$

$$W_{\text{ext}}^S = - \left(\frac{AT_0}{B_{\text{ext}}} + P_0^{\text{ext}} k r_0 \right) (\Omega_{\text{max}} - \Omega) + T_{\text{int}}^{\text{min}} m c v \left(\exp \left\{ \frac{(\Omega_{\text{max}} - \Omega) A}{B_{\text{ext}} m c v} \right\} - 1 \right) \quad (14)$$

Taking into account the pressure–temperature dependence under adiabatic conditions in Eq. (10), equations (10) – (14) allow us to calculate system work and its temperature at any stage of HLS compression and decompression.

5. Proposed model validation

Verification of proposed model adequacy was performed using calorimetric and volumetric data (experiment procedure described in (Coiffard et al. 2005; Karbowski et al. 2009, 2010)). Experiments were obtained on three heterogeneous lyophobic systems based on superhydrophobic silicalites with quasi-cylindrical pores (average radius $r_0 \sim 0,25\text{nm}$).

In all systems, the working fluid is distilled water, and the difference between systems comes from matrix synthesis mode: for MFI-OH matrix reaction medium contained OH⁻ ions (Coiffard et al. 2005), while for MFI-F1 (Coiffard et al. 2005) and MFI-F2 (Karbowski et al. 2009, 2010) matrices F⁻ ions. These features led to a different hydrophobicity of the matrices. Thus, the use of fluoride anions instead of hydroxide, apparently, leads to a number of lattice defects decrease and hence a smaller number of hydrophilic silanol groups. This leads to a greater hydrophobicity of the MFI-F1 and MFI-F2 matrices and, consequently, according to Eq. (2) to the increasing intrusion/extrusion pressure, which is reflected on the experimental compression/decompression PV-isotherms (see Figure 2).

Using Eqs. (2), (7) and compression PV–isotherms (Figure 2), we obtain $\Gamma(r)$ function for the matrices (Figure 2 frame). The approach we used to calculate thermal effects and work as an experimental input information requires PV–compression/decompression isotherms, as they allow to obtain $\Gamma(r)$ function (7), which gives us developed "liquid - solid" interface value at every stage of the system compression/decompression and hence its heat and work.

Approximating the experimental dV/dr dependence (Figure 2, frame), calculated from the PV-compression isotherms, we obtain for the MFI-F1:

$$b_{\text{MFI-F1}} = 397,5, a_{\text{MFI-F1}} = 2 \cdot 10^{-3} (\text{nm}); \text{MFI-F2: } b_{\text{MFI-F2}} = 370, a_{\text{MFI-F2}} = 3 \cdot 10^{-3} (\text{nm}); \text{MFI-OH: } b_{\text{MFI-OH}} = 215, a_{\text{MFI-OH}} = 4 \cdot 10^{-3} (\text{nm}).$$

Despite the fact that described matrices are defined as mono-porous ($r = \text{const}$), a small pressure dispersion during the intrusion process is experimentally observed for all the samples (Figure 2), which under the proposed approach is reflected as non-zero $a_{\text{MFI-F1}}$, $a_{\text{MFI-F2}}$ and $a_{\text{MFI-OH}}$ values. Such small variations in the pressure of the intrusion can hardly be caused by the presence of different pore radii in the matrices. However, as it is shown below, this phenomenon account is necessary, and the use of non-zero radius value deviation parameter for this matter is acceptable.

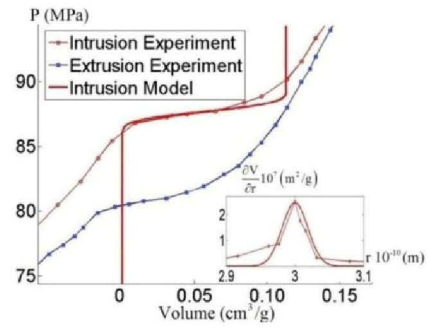


Figure 2a. Isothermal (303K) PV diagram during a cycle for MFI-F1 + water and its $\Gamma(r)$ function in the frame

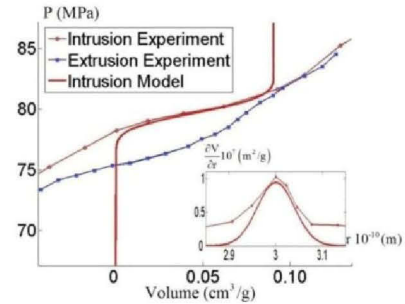


Figure 2b. Isothermal (303K) PV diagram during a cycle for MFI-OH + water and its $\Gamma(r)$ function in the frame

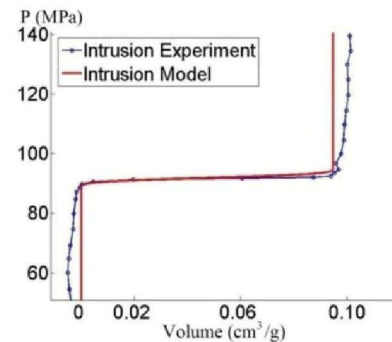


Figure 2c. Isothermal (298K) PV diagram during intrusion for MFI-F2 + water

Also note, that it is possible to avoid minor discrepancies of experimental and theoretical curves (Figure 2), using a more complex distribution function than Eq.(7), but that unnecessarily increases calculations cumbersome.

Nevertheless, the use of the approximate function (7) still gives a quite satisfactory outcome prediction of thermal effects: in worst case scenario of MFI-OH based system the experimental intrusion heat effect is 5.7 ± 0.2 (J/g) versus calculated value of 6.14 (J/g), which gives a relative error not exceeding $\sim 10\%$.

Using Eq. (1), (7) and (10), interface value may be expressed as:

$$\Omega = - \frac{b}{2k} \left(\operatorname{erf} \left(\frac{r - r_0}{\sqrt{2}a} \right) - \operatorname{erf} \left(\frac{r_{\text{max}} - r_0}{\sqrt{2}a} \right) \right) \quad (15)$$

where $\text{erf}(x) = \frac{2}{\sqrt{\pi}} \int_0^x \exp(-t^2) dt$ is the error function (Abramowitz and Stegun 1972), and r_{max} is conditional maximum pore radius of the matrix, at which intrusion begins ($\Omega \approx 0$).

In the following calculations we use the assumption " $\theta \approx \text{const}$ ", which is correct for a number of HLS (Naidich 1972), while for others HLS, the contact angle might be slightly dependent on the temperature (Coiffard and Eroshenko 2006). In view of MFI matrices superhydrophobicity (Coiffard et al. 2005; Karbowski et al. 2009, 2010) consider $\cos\theta \approx 1$. Keeping in mind that experimental PV-compression /decompression dependence is input parameter of the model, coefficient $B_{\text{int,ext}}$ approximation compensates inaccuracies associated with contact angle value. Using Eq. (2) – (4) we obtain for system based on a MFI-F1 matrix ($T_0 = 303\text{K}$, $d\sigma/dT = -0,16 \cdot 10^{-3} (\text{Hm}^{-1} \text{K}^{-1})$): $B_{\text{int}} \approx 5,41$, $B_{\text{ext}} \approx 5,93$; for MFI-F2: $B_{\text{int}} \approx 5,68$, $B_{\text{ext}} \approx 6,48$; for MFI-OH: $B_{\text{int}} \approx 5,88$, $B_{\text{ext}} \approx 6,25$. Next, using Eqs. (1) – (4), (7) and (8), heat flow per pressure variation Φ_p can be expressed as:

$$\Phi_p^{\text{int,ext}} = \frac{dQ}{dP} = \pm \Gamma(r) r \frac{T_0 B_{\text{int,ext}}}{\sigma} \frac{d\sigma}{dT} = \pm \frac{\Gamma(P) T_0}{P_{\text{int,ext}} k} \frac{d\sigma}{dT} \quad (16)$$

here "plus" sign refers to the process of intrusion, and "minus" – to extrusion.

The compressibility of the system (volume variation per pressure variation) can be written as:

$$\varepsilon_{\text{int,ext}} = \frac{dV}{dP} = - \frac{kr^2 \Gamma(r)}{\sigma B_{\text{int,ext}}} \quad (17)$$

Figure 3 represents theoretical and experimental (Coiffard et al. 2005; Karbowski et al. 2009, 2010) results comparison of Φ_p pressure dependence. To put in correspondence thermal and mechanical processes of HLS, both theoretical and experimental compressibility of the system ε_{int} , as a function of pressure, is shown in the same Figure (bottom frame).

As might be seen, there is a reasonable agreement between theoretical and experimental curves for the liquid intrusion and extrusion processes followed by respectively endo- and exothermal effects. For the compression processes it is shown that maximum end thermal effect variation coincides with the maximum system compressibility (Figure 3 bottom frame). Figure 3a top frame also shows experimental and theoretical (Eq. (8) and (15)) heat of interphase area development as a function of pressure for "MFI-F1 + water" system. Experimental and model compressibility curves correlation (Figure 3, bottom frame) shows that this parameter can also be predicted within approach proposed. Φ_p and ε curves comparison confirms the fact that the greatest system heat demand appears at the maximum interface development trends $d\Omega/dP$.

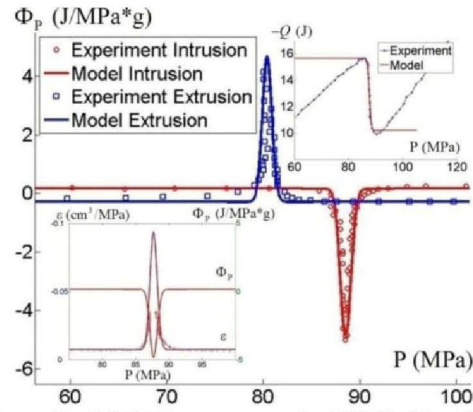


Figure 3a. MFI-F1 + water cycle (303K): Heat flow Φ_p vs. pressure. Φ_p and compressibility ε comparison (bottom frame). Thermal energy $-Q$ during compression (top frame)

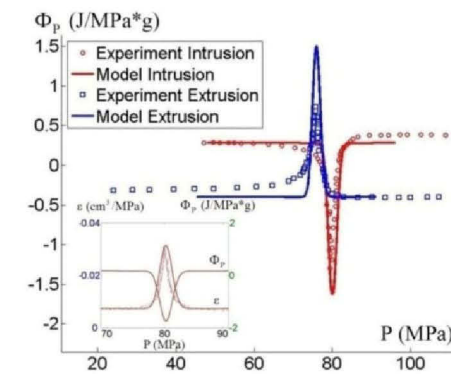


Figure 3b. MFI-OH + water cycle (303K): Heat flow Φ_p vs. pressure. Φ_p and compressibility ε comparison (frame)

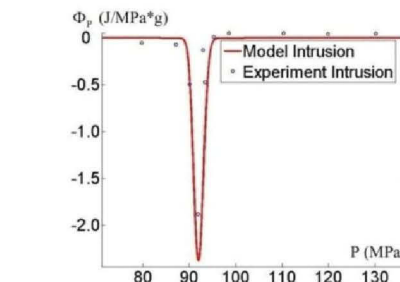


Figure 3c. MFI-F1 + water cycle (298K): Heat flow Φ_p vs. pressure.

As mentioned above, described approach allows predicting behavior of the system under adiabatic conditions. Figure 4 shows intrusion work – pressure dependence comparison in a heterogeneous system «MFI-F1 + Water» (Coiffard et al. 2005) under isothermal conditions (experiment and model ((9), (15)) based on the incompressible component of the system) and under adiabatic conditions after 150 and 300 successive intrusion/extrusion cycles (HLS successive cycling is described below).

As might be seen from Figure 4, there is good agreement between simulated and experimental curves under isothermal conditions, which confirms the adequacy of the thermodynamic description of the HLS based on porous matrix with pore radius in angstrom range.

According to Eq. (11) temperature decrease, due to full HLS compression ($\Omega = \Omega_{\max}$) under adiabatic conditions, reaches $\Delta T_{\text{int}} \approx 1,5$ (K), which increases the work expended in system compression on the value of $\Delta W \approx 20$ (mJ). Although, this increase is rather small in comparison with the work of compression under isothermal conditions $W \approx 10^4$ (mJ), its contribution begins to play a significant role in high-cycle system loading. The explanation of this effect should be given: experiments designed to study the temperature dependence of HLS pressure, show this dependence is different for intrusion and extrusion processes (Kong and Qiao 2005; Liu et al. 2009; Qiao et al. 2006): $\frac{dP_{\text{int}}}{dT} > \frac{dP_{\text{ext}}}{dT}$ (which is reflected in described approach as $B_{\text{int}} < B_{\text{ext}}$), and as it follows from Eqs. (11), (12) and (2), (3) leads to a consistent decrease in temperature of the system after each cycle of the "forced compression – spontaneous decompression" under adiabatic conditions: $\max(T_{\text{ext}}) < T_0$.

As might be seen from Figure 4, this temperature reduction leads to an increase of intrusion-extrusion pressure (according to Eqs. (2) - (3)) and, consequently, to an increase of the work expended for system compression. The same Figure (frame) displays W^S (system compression work) and T (temperature) at the end of each next successive intrusion/extrusion cycle, as a function of the number of the cycles N .

As might be seen, there are linear relationships: W^S growth and T decline as number of cycles N increase. So, after 100 adiabatic cycles growth is $\Delta W \sim 330$ (mJ), and the temperature drop is ~ 15 (K).

6. Discussion

Presented in Figure 3 data suggest that thermal effects, due to the compression-decompression of heterogeneous lyophobic systems based on capillary-porous matrices with radii in the nanometer range, are associated with significant energy cost/release during the development/reduction of the huge interface (breaking of intermolecular bonds during intrusion of the liquid is accompanied by endothermal effect, and their recovery – by exothermal effect).

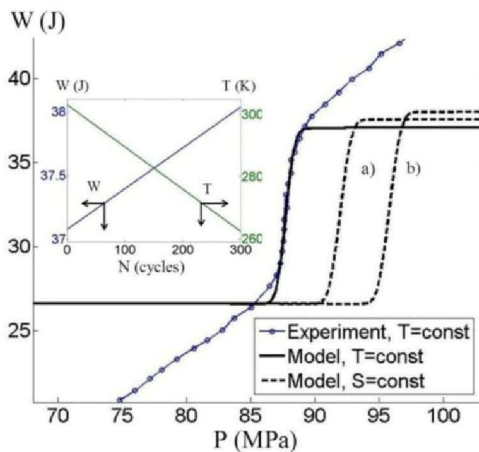


Figure 4. Mechanical energy vs. pressure during the compression of MFI-F1 + water under isothermal (303K) and adiabatic conditions after a) 150 and b) 300 cycles

As might be seen from Figure 3, the peak of the system heat flow is observed during isothermal filling of pores with radii close to r_0 , the value that indicates the maximum heat demand must be satisfied at the moment of maximum interface development Ω to meet the isothermal conditions. This property, in the present model and experiments carried out by (Coiffard et al. 2005 and Karbowski et al. 2009, 2010), suggests that compression mechanical work is greater under adiabatic conditions, due to system temperature drop (6). This phenomenon has been observed experimentally (Eroshenko 1987a); abnormally high intrusion pressure rise, due to velocity of the HLS compression increase, was apparently because of the fact that under quasiadiabatic conditions (stroke!) the interface development heat was taken only from that part of the system, which is directly adjacent to the mouth of the pore (channel), apparently due to the thermal resistance of the medium. Occurring local anomalous temperature drop near the pore mouth led to a substantial liquid surface tension increase in that area, and therefore, to local capillary Laplace pressure increase (2), (pressure of the intrusion), and hence to a whole heterogeneous system pressure increase (Pascal's hydraulic law).

In view of Eq. (9) and linear $\sigma \cos\theta$ temperature dependence, the difference between the values of work under adiabatic and isothermal conditions can be displayed as:

$$\delta W_{\text{int}}^S = \delta W_{\text{int}}|_{T=T_0} + B_{\text{int}}^{-1}(T_0 - T_{\text{int}}) \text{Ad}\Omega \quad (18)$$

$$\delta W_{\text{ext}}^S = \delta W_{\text{ext}}|_{T=T_{\text{int}}^{\min}} + B_{\text{ext}}^{-1}(T_{\text{int}}^{\min} - T_{\text{ext}}) \text{Ad}\Omega \quad (19)$$

Since during intrusion $\delta W_{\text{int}} > 0$ (work is done on the system), $T_0 - T_{\text{int}} > 0$ (according to (11), temperature decreases during intrusion), and $d\Omega > 0$ (development of the interface), adiabatic compression work is greater than isothermal one on the value of $\Delta W_{\text{int}} = B_{\text{int}}^{-1}(T_0 - T_{\text{int}}^{\min}) \text{Ad}\Omega_{\max}$. Using the same logic for extrusion process ($d\Omega < 0$, $\delta W_{\text{ext}} < 0$, $(T_{\text{int}}^{\min} - T_{\text{ext}}) < 0$) it is obtained $\Delta W_{\text{ext}} = B_{\text{ext}}^{-1}(T_{\text{int}}^{\min} - T_{\text{ext}}^{\max}) \text{Ad}\Omega_{\max}$. Due to the temperature irreversibility during intrusion-extrusion cycle under adiabatic conditions inequation $T_0 > T_{\text{ext}}^{\max}$ can be obtained, and taking into account the fact that $B_{\text{ext}} > B_{\text{int}}$, it could be shown that $\Delta W_{\text{ext}} < \Delta W_{\text{int}}$. Such system reaction on cycling leads to continuous growth of the difference between the compression and decompression work, with each successive adiabatic cycle. In other words dissipative power of the system will increase (intrusion-extrusion pressure hysteresis increase).

Note that using Eqs. (8) and (9), equations (13) and (14) might be rewritten as

$$W_{\text{int}}^S = W_{\text{int}} + |Q_{\text{int}}| - mc_v(T_0 - T_{\text{int}}), \quad (20)$$

$$W_{\text{ext}}^S = W_{\text{ext}} - |Q_{\text{ext}}| + mc_v(T_{\text{ext}} - T_{\text{int}}^{\min}). \quad (21)$$

According to Eq. (18) the difference $Q_{\text{int}} - mc_v(T_0 - T_{\text{int}}) > 0$, so the work of intrusion in adiabatic process will always be greater than in isothermal

one. For the process of spontaneous adiabatic extrusion of the system (21) this effect is converse (adiabatic operation will be less than isothermal one) according to the inequality: $-|Q_{\text{ext}}| + mc_V(T_{\text{ext}} - T_{\text{int}}^{\text{min}}) < 0$ (see Eq. (19)).

Equations (20) and (21) show that work under adiabatic conditions can be expressed as an algebraic sum: conditional work of the interphase area development/reduction under isothermal conditions $W_{\text{int,ext}}$ at $T = T_0$ (9) plus a conditional heat of the interface development/reduction under isothermal conditions $Q_{\text{int,ext}}$ at $T = T_0$ (8), which is compensated by reducing the internal energy of the system, (its temperature) – third term. Note, that on the basis of equations (13) and (14), adiabatic work of compression/decompression is structurally identical to the same work obtained previously for lyophilic systems (Laouir and Tondeur 2008), which indicates the absence of contradictions of proposed approach with the energy balance equations and correct supplement of practically useful Equations (13) and (14).

A nontrivial property of the system to reduce its temperature after each subsequent adiabatic cycle of compression / decompression (Figure 4b), can be effectively used to create a fundamentally new class of refrigerators. High-pressure cold generating process based on matrices with $r < 1$ (nm) provides an extremely high thermodynamic compactness (Eroshenko 1981a, 1996) ($\delta W_C / (\Delta V \Delta T)$) of thermomolecular coolers (cooling capacity W_C per volume unit of the working chamber and per one degree of working temperature range).

Taking into account HLS temperature reduction, due to its adiabatic cycling, is no less important in case of dissipating systems creating, because this effect will lead to an increase of intrusion pressure (2) and the work of compression (13), which increases the resistance of the HLS to external mechanical disturbances.

An additional advantage of this approach is its applicability for the description of the systems based on matrices with varying complexity pores radii distribution function $\Gamma(r)$ (including composites based on several different matrices). In this case $\Gamma(r) = \sum_i \Gamma_i(r)$, where

$\Gamma_i(r)$ is the pore radii distribution function of i -th porous matrix, and the description logic remains unchanged. It is important to note, that a purely thermodynamic approach to describing the behavior of these systems is justified only for samples that are based on matrices with ultra-low pore radius ($r \sim 1$ nm and lower), since when $r > 1$ nm the system shows a more complex nature of dependencies studied in this work (Coiffard et al. 2005; Karbowski et al. 2009, 2010) and for an adequate description consideration of complex mechanics of the process seems to require. In-depth understanding of these processes with the further extension of the studied systems class is the subject of future studies.

7. Conclusions

1. Theoretical and experimental analysis of heterogeneous lyophobic systems (HLS) thermodynamic and operational properties allows, using as an input experimentally easy determinant P-V isotherm, to understand

the nature of some HLS phenomena and to predict practically useful effects and properties on every compression/decompression stage:

- Nontraditional thermal responses due to system mechanical perturbation and relaxation.
- Temperature variations due to adiabatic compression / decompression.
- Compression / decompression work under isothermal and adiabatic conditions and a comparison of these works.
- Compressibility reduction of the system as it becomes compressed in adiabatic process (Eroshenko 1987a, 2007; Eroshenko et al. 2007).

2. Theoretically confirmed the experimentally observed (Eroshenko 1987a) temperature drop of the system after intrusion/extrusion cycle under adiabatic conditions.

3. Theoretically predicted and experimentally observed properties of heterogeneous lyophobic systems based on different types of matrices ($r = \text{const}$ or $r = \text{var}$) (Coiffard et al. 2005; Eroshenko 1987b, 2007; Eroshenko et al. 2007; Karbowski et al. 2009, 2010), offer the prospect of creating a fundamentally new working mediums for nanotechnology (Eroshenko 1981a, 1996), cost-saving and ecological friendly systems and equipment in modern energetics (Eroshenko 1996, 1997, 2001a, 2007; Eroshenko et al. 2007; Han and Qiao 2007; Iwatsubo et al. 2008; Martin et al. 2002; Qiao et al. 2006).

Nomenclature

a	pore radii dispersion parameter	m
b	distribution function coefficient	m ²
B	pressure correction coefficient	-
C	heat capacity	JK ⁻¹
c	specific heat capacity	JK ⁻¹ kg ⁻¹
HLS	heterogeneous lyophobic system	
k	pore geometry coefficient	-
m	mass	kg
N	cycle number	-
P	pressure	Pa
Q	heat	J
RC	repulsive clathrate	
r	pore radius	m
S	entropy	JK ⁻¹
T	temperature	K
V	volume	m ³
W	work	J
Γ	pore radii distribution function	m ²
ϵ	volume variation per pressure variation	cm ³ Pa ⁻¹
θ	contact angle	-
σ	surface tension	Jm ⁻²
Φ	heat flow per pressure variation	JPa ⁻¹
Ω	surface area	m ²

Subscripts

P	pressure
MFI-F1	system based on MFI-F1 type matrix
MFI-F2	system based on MFI-F2 type matrix
MFI-OH	system based on MFI-OH type matrix
int	intrusion
ext	extrusion
*	experiment

V	volume
Ω	surface area
S	adiabatic

Superscript

min	minimum
max	maximum

References

- Abramowitz, M., and Stegun, I. A. (1972). Handbook of Mathematical Functions with Formulas, Graphs, and Mathematical Tables. New York: Dover.
- Bougeard, D. and Smirnov, K., S. (2006) Modelling studies of water in crystalline nanoporous aluminosilicates. *Physical Chemistry Chemical Physics*, 9(2), 226–245.
- Cailliez, F., Trzpit, M., Soulard, M., Demachy, I., Boutin, A., Patarin, J., and Fuchs, A., H. (2008). Thermodynamics of water intrusion in nanoporous hydrophobic solids. *Physical Chemistry Chemical Physics*, 10(32), 4817–4826.
- Coiffard, L., Eroshenko, V. (2006). Temperature effect on water intrusion/expulsion on grafted silica gels. *J. of Colloid and Interface Science*, 300(1), 304–309.
- Coiffard, L., Eroshenko, V., A., Grolier, J.-P., E. (2005). Thermomechanics of the Variation of Interfaces in Heterogeneous Lyophobic Systems. *AIChE J*, 51(4), 1246–1257.
- Denoyel, R., Beurroies, I., Lefevre, B. (2004). Thermodynamics of wetting: information brought by microcalorimetry. *J. of Petroleum Science & Engineering*, 45(3-4), 203–212.
- Eroshenko V. A. and Lazarev Yu. F. (2012). Rheology and dynamics of repulsive clathrates. *J. Of Applied Mechanics And Technical Physics*, 53(1), 98–112.
- Eroshenko, V. A. (1981a). Heterogeneous Thermodynamic System, Eroshenko Cycle of Transformation of Thermal Energy into Mechanical Energy and Devices to Achieve It (in Russian). Soviet-Russian Patent No. 1,254,811.
- Eroshenko, V. A. (1987a). Effect of Heat Exchange on Filling of Lyophobic Pores and Capillaries with Liquid. *Colloid J. USSR*, 49, 769-773.
- Eroshenko, V. A. (1987b). Limiting efficiency or maximum thermodynamic compactness of Heat Engines (in Russian). *USSR Academy of Science J., Energy and Transport*, 2, 125–133.
- Eroshenko, V. A. (1990) Unusual Properties of One complex Thermodynamic System (in Russian). *C. R. Acad. Sci. Ukraine, Ser. A*, 10, 79.
- Eroshenko, V. A. (1992). Thermomolecular energetics (in Russian). *Industrial Heat Engineering*, 14(1-3), 22-25.
- Eroshenko, V. A. Heat Engines and Different Energy devices. Soviet-Russian Patents: No943,444 (1981b); No1,382,078 (1982); No1,380,357 (1983); No1,333,870 (1985); No1,434,881 (1985); No1,452,262 (1986); No1,508,665 (1987c).
- Eroshenko, V. A., and Aistov, V. I. (1990). Heat Engine Cycles Optimization According to Thermodynamic Compactness (in Russian). *Industrial Heat Engineering*, 12(3), 60–64.
- Eroshenko, V. A., Grosu, Y. G. (2011). Properties of Heterogeneous Lyophobic Systems Based on Matrixes With Different Pore Size (in Russian). *Industrial Heat Engineering*, 33(6), 73-79.
- Eroshenko, V., A. (1996). Heterogeneous structure for accumulation or dissipation of energy, process to use it and associated devices. *Int. Patent WO 96/18040*.
- Eroshenko, V., A. (1997). Repulsive clathrates. New operational material for efficient seismic isolation. *Proceedings of International Post-SMITR Conference «Seismic Isolation, passive Energy Dissipation and active Control of Seismic Vibrations of Structure»*, Taormina, Sicily, Italy, August 25 to 27, 783–794.
- Eroshenko, V., A. (2001a). Damper with high dissipating power. *Int. Pat. WO 01/55616 A1*, 1–33.
- Eroshenko, V., A. (2007). A New Paradigm of Mechanical Energy Dissipation. Part 1: Theoretical Aspects and practical Solutions. *Journal Proceedings of Mechanical Engineers, Part D: Journal of Automobile Engineering*, 221(3), 285–300.
- Eroshenko, V., A., Piatiletov, I., I., Coiffard, L., and Stoudenets, V., P. (2007). A New Paradigm of mechanical Energy Dissipation. Part 2: Experimental Investigation and effectiveness of a novel Damper. *Journal Proceedings of Mechanical Engineers, Part D: Journal of Automobile Engineering*, 221(3), 301–312.
- Eroshenko, V., Regis, R.-C., Soulard, M., and Patarin, J. (2001b). Energetics: A New Field of Applications for Hydrophobic Zeolites. *J. of American Chemical Society*, 123(33), 8129–8130.
- Eroshenko, V., Regis, R.-C., Soulard, M., and Patarin, J. (2002). The heterogeneous systems 'water–hydrophobic zeolites': new molecular springs. *C.R.PHYSIQUE*, 3(1), 111–119.
- Guggenheim, E., A. (1965). *Thermodynamique*. Paris: «Dunod».
- Han, A., and Qiao, Y. (2007). A volume-memory liquid. *Applied Physics Letters*, 91(17), 173132.
- Iwatsubo, T., Washio, K., Yano, H., and Miyazaki, M. (2008). Experimental Study of a Colloidal Damper to Practical Application. *J. of System Design and Dynamics*, 2(5), 1160 – 1169.
- Karbowiak, T., Paulin, C., Ballandras, A., Weber, G., and Bellat, J.-P. (2009). Thermal Effects of Water Intrusion in Hydrophobic Nanoporous Materials. *J. of American Chemical Society Communications*, 131(29), 9898 – 9899.
- Karbowiak, T., Paulin, C., Bellat, J.-P. (2010). Determination of water intrusion heat in hydrophobic microporous materials by high pressure calorimetry. *Microporous and Mesoporous Materials*, 134(1-3), 8–15.

- Kirkwood, J., G., Buff, F., P. (1949) The Statistical Mechanical Theory of Surface Tension. *J. of Chemical Physics*. 17(3), 338–343.
- Kong, X., Qiao, Y. (2005). Thermal effects on pressure-induced infiltration of a nanoporous system. *Philosophical Magazine Letters*, 85(7), 331 – 337.
- Laouir, A., Luo, L., Tondeur, D., Cachot, T., Le Goff, P. (2003). Thermal Machines Based on Surface Energy of Wetting: Thermodynamic Analysis. *AIChE Journal*, 49(3), 764–781.
- Laouir, A., Tondeur, D. (2008). Some New Results From Applying Thermodynamics to Wetting Phenomena. *Int. J. of Thermodynamics*, 11(2), 61-69.
- Liu, L., Zhao, J., Culligan, P., J., Qiao, Y., and Chen, X. (2009). Thermally Responsive Fluid Behaviors in Hydrophobic Nanopores. *Langmuir*, 25(19), 11862 – 11868.
- Martin, T., Lefevre, B., Brunel, D., Galarneau, A., Di Renzo, F., Fajula, F., Gobin, P., et al. (2002). Dissipative water intrusion in hydrophobic MCM-41 type materials. *Chemical Communications*, No1, 24–25.
- Naidich, Y. V. (1972). Contact phenomena in metallic melts (in Russian). Kiev: Naukova dumka.
- Qiao, Y., Punyamurtula, V., K., and Han, A. (2006). Temperature dependence of working pressure of a nanoporous liquid spring. *Applied Physics Letters*, 89(25), 251905.
- Rusanov, A., I. (1981). The connection between the heat of evaporation and surface energy (in Russian). *Reports of the USSR Academy of Sciences*. 261(3), 700–703.
- Suciu, C.,V., Iwatsubo, T. and Deki, Sh. (2003) Investigation of a colloidal damper. *J. of Colloid and Interface Science*, 259(1), 62–80.
- Wargaftik, N. B. (1972). Handbook of thermophysical properties of gases and liquids (in Russian). Moscow: Nauka.
- Washburn, E., W. (1921). The Dynamics of Capillary Flow. *The Physical Review*, 17(3), 273–283.
- Woo, H.-J., Monson, P., A. (2003). Phase behavior and dynamics of fluids in mesoporous glasses. *The Physical Review E*, 67(4), 041207.

Temperature dependence of thermal effects of compression/decompression was investigated for the {Hypersil C18 + water} HLS (Fig. 3.3 and Fig. 3.4).

For intrusion as expected from the thermodynamic analysis the thermal effect is endothermic (interface development) and for extrusion it is exothermic (interface reduction), see Fig. 3.3. Such behavior is consistent with calorimetric studies for other HLSs available in the literature (Coiffard et al. 2005, Karbowski et al. 2010a).

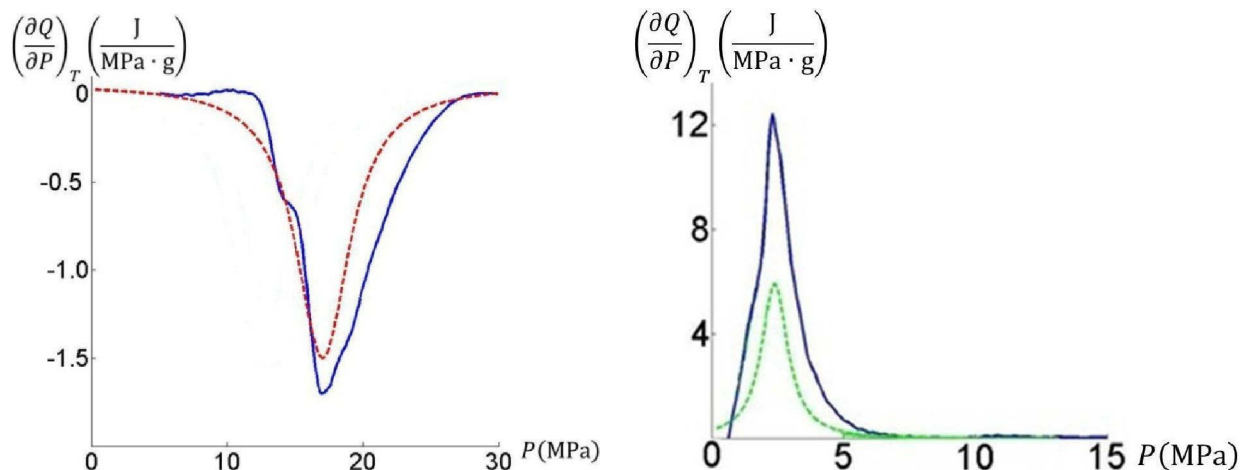


Fig. 3.3 Thermal effects of a) intrusion and b) extrusion of the {Hypersil C18 + water} HLS: solid line is experiment; dashed line is the model according to eq. (3.21)

Evolution of the amount of heat generated during intrusion and extrusion at different temperatures is shown in the Fig. 3.4.

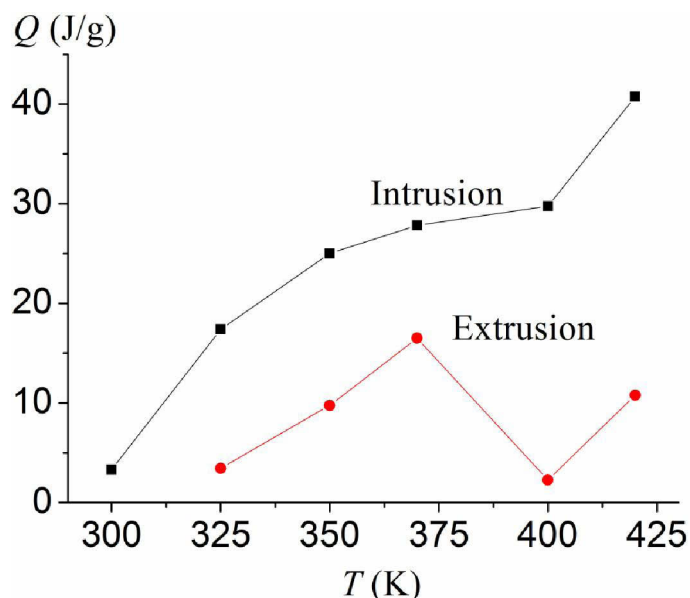


Fig. 3.4. Heat of intrusion (squares) and extrusion (circles) for the {Hypersil C18 + water} HLS.

Using equation (3.15) and equation of state (3.2) one may write the thermal effect of intrusion/extrusion as follows (for mathematical details see Appendix C):

$$\left(\frac{\partial Q_{int,ext}}{\partial P}\right)_T = T \left(\frac{\partial S_{int,ext}}{\partial P}\right)_T = -TP_0V_0\mu_T^0\beta^0 - T \left(\frac{d\sigma}{dT} - \frac{d\Delta\rho}{dT} I_{int,ext}\right) \frac{f'_{int,ext}}{kr} \quad (3.21)$$

Where $\Delta\rho$ is the density difference between water and its vapor and $I_{int,ext}$ is Wan der Waals integral for intrusion and extrusion process.

To obtain this equation temperature dependence of contact angles was used calculated by means of ‘‘Sharp-kink’’ approximation, which is in details described in reference (Grosu et al. 2014c). Reprint of this publication is presented in paragraph 3.2.

Equation (3.21) allows calculating the thermal effect with at least 15% error, which may be considered satisfactory (Fig. 3.4).

Investigation of temperature dependences of thermal effects of other HLSs is also presented in the Paragraphs 3.3 and 4.1.

3.1.5. Heat capacity and HLS based on matrixes with complex pore size distribution functions

Using classical definition of heat capacity $C_x = \left(\frac{\partial Q}{\partial T}\right)_x$, where x can be volume or pressure and proposed equation of state (3.2) it can be written (for mathematical detail see Appendix D):

$$C_V^{int,ext} = C_V^0 - T \left(P_0\beta^0 - \frac{dP_{int,ext}}{dT}\right)^2 f'_{int,ext} \quad (3.22)$$

$$C_P^{int,ext} = C_P^0 - T \left(\frac{dP_{int,ext}}{dT}\right)^2 f'_{int,ext} \quad (3.23)$$

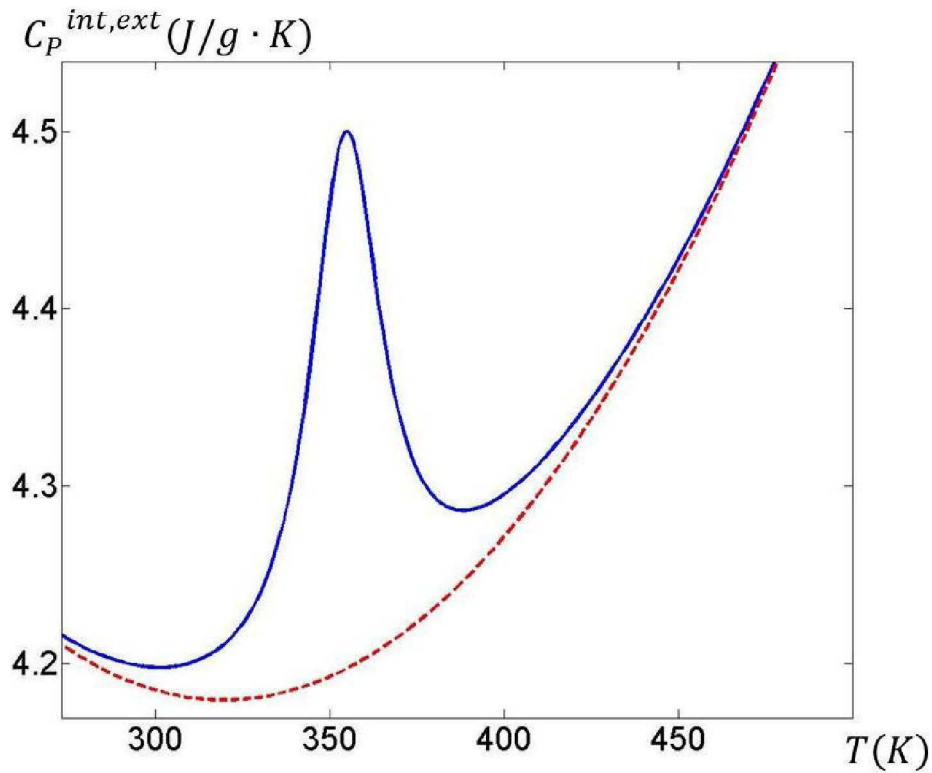


Fig. 3.5. Isobaric heat capacity of the {Waters C8 + water} HLS at $P = 15$ (MPa) calculated according eq. (3.23) for intrusion provoked by temperature increase. Solid line is for HLS; dashed line is for water.

It was determined that although the process of intrusion/extrusion for HLS based on the porous matrix with smooth distribution function is controlled and may be presented as quasi-equilibrium, the peak of heat capacity ($\Delta C_p = C_p^{int,ext} - C_p^0$) which is associated with the additional heat of interface development/reduction, which must be supplied to the HLS during intrusion/extrusion, is described by Ehrenfest equation $\Delta C_p = -T \left(\frac{dP}{dT} \right)^2 \Delta \left(\frac{\partial V}{\partial P} \right)_T$. This equation is used for second order phase transition. Parameters of this heat capacity peak (such as mean value and dispersion) are determined by the pore size distribution function. Detailed analysis of such dependence including the case when HLS is formed by several porous materials with different pore size distribution functions is described in the reference (Eroshenko and Grosu 2013c). Experimental investigation of heat capacity of the {ZIF-8 + water} HLS is presented in reference (Grosu et al. 2015a), where it is shown that non-standard temperature dependence of intrusion/extrusion pressure leads to a novel working mode and has strong effect on its heat capacity. Reprints of both publications are presented hereafter.

THERMOMECHANICAL AND THERMOPHYSICAL PROPERTIES OF REPULSIVE CLATHRATES

V. A. Eroshenko and Ya. G. Grosu

UDC 532.6: 536.7: 539.6: 620.22: 621.1: 62-567

Abstract: The range of the characteristic properties of repulsive clathrates (RCs), which are new working media used for efficient energy conversion in thermomechanical systems, has been extended. The dissipation, storage, and conversion of energy by means of RCs is based on the use of the intermolecular forces acting on the interface of the system of a liquid and a nonwetting solid capillary-porous matrix and leading to ejection of the liquid from the pores of the matrix. It has been shown that it is possible to control characteristics of RCs such as compressibility, amount of the dissipated (accumulated) mechanical energy, specific heat, and thermal parameters of the compression–expansion process. The properties of RCs providing unique operation modes of power systems that are not realizable with conventional working media (gas, steam).

Keywords: porous solids, liquids, interfacial surface, lyophobic property, hysteresis, capillary pressure, compression–expansion isotherm, specific heat, adiabatic exponent.

DOI: 10.1134/S0021894413050131

INTRODUCTION

The use of interfaces between nonwetting liquids and porous solids for efficient energy conversion is a new promising area of technical thermodynamics. Theoretical studies of heterogeneous lyophobic systems (HLS) [1–3] and their application as new working media for dissipation [4–6], accumulation [7–9], and conversion [10–12] of energy in thermomechanical systems has made it possible to solve theoretical [13–19], and applied [20–25] problems within the framework of a new scientific and technological direction — thermomolecular energetics [3, 26].

In contrast to conventional working media (gas, steam), which use the kinetic energy of random thermal motion of molecules (the potential energy of intermolecular interaction is not taken into account), HLSs use the potential energy and forces of intermolecular interaction at large-area interfaces in condensed nanosystems consisting of a liquid and a capillary-porous matrix which is not wettable by this liquid (the contact angle at the solid–liquid is $\theta \gg 90^\circ$). In HLSs in which the pore and capillary sizes (and, hence, the sizes of clusters of the intruded liquid) are a few nanometers and fractions of a nanometer (commensurate with the size of molecules) the kinetic energy of the molecules plays a less important role. The use of matrices with open porosity and specific surface areas of about 200–1000 m²/g provides large solid–liquid systems interfaces acted upon by molecular forces seeking to repulse the liquid from the pores of the matrix. For this reason, HLSs are also called repulsive clathrates (RCs) [19, 27].

All thermodynamic transformations using RCs are based on the forced production of large interfacial surfaces Ω (liquid intrusion into the pore space of matrices at external pressures equal to or greater than the capillary Laplace pressure) and spontaneous reduction of these surfaces (ejection of liquid clusters from the pore space at low external pressure). Studies have shown that for nanoscale capillaries in a closed space under high pressure, the capillary evaporation process changes significantly [43, 44] and its contribution to the basic processes occurring

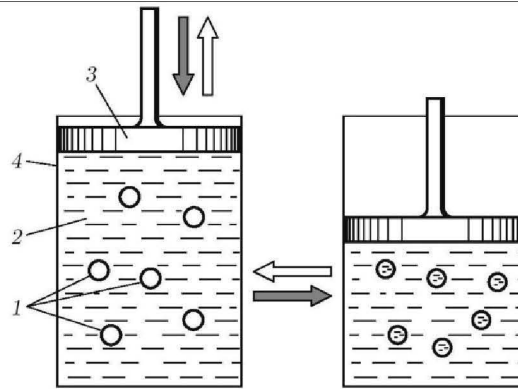


Fig. 1. Physical model of a repulsive clathrate: (1) capillary-porous matrix; (2) working liquid; (3) hypothetical piston; (4) cylinder; dark arrows show forced compression (pore filling) light arrows show spontaneous expansion.

in RCs reduces. Negligible contribution of the dissolved gas (air) and liquid–vapor phase transition in quasicondensed lyophobic systems over the entire range of their operation temperature is responsible for the high efficiency of energy conversion using RCs [6, 17, 19] (one to two orders of magnitude greater than that using gas and vapor). The Gibbs potential surface energy [1, 2], which depends on the process temperature [28, 29], was first used for energy conversion systems in thermo-mechanical systems.

Results of experiments [30] indicate that for the storage of mechanical energy using RCs, optimal capillary-porous matrices are hydrophobic zeolites [8]. Using water as a working fluid, the amount of energy accumulated by such RCs reaches 15 J/g (per 1 g of zeolite), and this system can use 97% of this amount to perform useful work [30].

In studies of mechanical energy dissipation [4–6, 19, 20, 31], the most widely used capillary-porous matrix is silica gel. In this case, the typical dissipated energy is about 12 J/g (based on 1 g of the porous matrix). An automobile shock absorber based on RCs is able to function by effectively dissipating mechanical energy at frequencies above 20 Hz.

Despite the large number of studies of RCs, not all of their properties have been well investigated. In particular, no studies have been made of the full range of performance capabilities of RCs, the evolution of their entropy, specific heat of heterogeneous systems, etc.. This is due not only to the complexity of the investigated RCs, but also to the choice of approaches to solving important theoretical and practical problems. For example, the conditions of applicability of equilibrium thermodynamics to the description of the investigated working media have not been determined although, in most cases, it is required to predict the behavior of heterogeneous system with acceptable accuracy by using relatively simple mathematical and thermodynamic approaches.

The present paper considers available technological and mathematical approaches to analyzing existing RCs or designing RCs with new mechanical and thermal properties providing unique operation modes of power systems that cannot be achieved using conventional systems (gas, pairs).

PHYSICAL MODEL AND MATHEMATICAL DESCRIPTION OF REPULSIVE CLATHRATES

Typically, a repulsive clathrate (Fig. 1) is a capillary-porous matrix *1* placed in a cylinder *4* with a working liquid *2* which does not wet this matrix ($\theta \gg 90^\circ$) [2, 32]. Because the matrix is lyophobic, the liquid cannot spontaneously penetrate into its pore space. For this, it is necessary to apply external pressure to the hypothetical piston *3*. Compression of the system leads to filling of the pores of the matrix with the liquid, i.e., to a forced increase in the interfacial surface area Ω of the liquid–solid system and, as a consequence, to a reduction in the volume of the system. Spontaneous release of the liquid from the pore space is accompanied by a decrease in the

interfacial surface area Ω and an increase in the total volume of the heterogeneous system with decreasing external pressure.

The pressure leading to forced intrusion of a liquid (quantities with the subscript “int”) into the pore space of the matrix and its spontaneous extrusion (quantities with the subscript “ext”) are usually determined by the Laplace–Washburn equation [33]

$$P_{\text{int,ext}} = \sigma |\cos \theta_{\text{int,ext}}| / (kr), \quad (1)$$

where r is the radius of the pores and capillaries in the matrix, k is a coefficient that depends on the geometry of the pore space of the matrix ($k = 0.5$ for long capillaries and $k = 0.33$ for spheres), and σ is the surface tension of the liquid on the boundary with the gas (vacuum). For small pore radii r in the matrix, the value of σ should be corrected for the curvature of the surface, using, e.g., the Gibbs–Tolman–Konniġ–Buff equation [34]

$$\sigma = \sigma_{\infty} (1 + 2\delta/r)^{-1} \equiv \sigma_{\infty} b,$$

where σ_{∞} is the surface tension of the flat surface and δ is Tolman constant. Note that, since in the approach proposed here, the (P – V) compression–expansion isotherm of the RC is assumed to be known (basic characteristic of RCs), the quantity $P_{\text{int,ext}}$ is also assumed to be known. Equation (1) is used to calculate the temperature dependence of the intrusion (extrusion) pressure taking into account that the Tolman correction is independent of temperature [$b \neq b(T)$]:

$$\frac{dP_{\text{int,ext}}}{dT} = \frac{d(\sigma_{\infty} \cos \theta)}{dT} \frac{b}{kr} = \frac{d(\sigma_{\infty} \cos \theta)}{dT} \frac{P_{\text{int,ext}}}{\sigma_{\infty} \cos \theta}.$$

This relation is used in the further analysis of the properties of RC.

According to Eq. (1), the difference between the intrusion pressure P_{int} and the extrusion pressure P_{ext} observed in experiments [3, 17, 35] is expressed in terms of the difference of the respective contact angles

$$P_{\text{int}} - P_{\text{ext}} = \frac{\sigma |\cos \theta_{\text{int}} - \cos \theta_{\text{ext}}|}{kr}, \quad \theta_{\text{int}} > \theta_{\text{ext}}.$$

The hysteresis value $H = P_{\text{int}} - P_{\text{ext}}$ determines the scope of applicability of the new working media: RCs with large H are used for effective dissipation of mechanical energy in mechanical engineering (car shock absorber, damper [5, 6, 20]), anti-seismic systems [27, 36], and RCs with small H ($P_{\text{int}} \approx P_{\text{ext}}$) [17, 24] are used for storage and conversion of mechanical and thermal energies, in particular, in space technology [37], as well as for the creation of molecular springs [8]. The presence of hysteresis allows the use of RCs as memory cells [38] in intelligent systems (an analog of shape memory materials [39]).

Note that in real materials, the large number of capillaries and pores even in uniporous matrices [in Eq. (1), $r = \text{const} \Rightarrow P_{\text{int,ext}} = \text{const}$] leads to the fact that the radii of the microvoids are always characterized by at least small variance (this is confirmed by a large number of experiments [8, 17, 24]); therefore, the value of the derivative $dV/dP_{\text{int,ext}}$ is finite [in Eq. (1), it is assumed that the radius r is a variable]. This allows us to consider the compression–expansion of a RC as a quasistatic process (a finite change in the external pressure always leads to a finite change in the volume of the system) and to use the foundations of equilibrium thermodynamics to study such systems.

It should be noted that equilibrium thermodynamics is only applicable to quasistatic processes, whereas the operation of RCs obviously involves speed response (nonequilibrium processes). Nevertheless, models for slow quasistatic processes based equilibrium thermodynamics can be used to study the kinetics of these systems. To test the model, we performed experiments under nearly quasistatic conditions (the compression–expansion process was carried out at a rate of 10^{-4} cm³/s [17]), which allowed us to estimate the adequacy of the proposed equations.

As noted above, a change in the RC volume is determined by the increase in the interfacial area Ω ($dV_{\Omega} = -kr d\Omega$ [2, 40]) and by the change in the volume of the liquid (V_L) and matrix (V_M) during dynamic or thermal deformation:

$$dV = dV_L + dV_M + dV_{\Omega} = dV_0 - kr d\Omega \quad (2)$$

(V_0 is the initial volume of the system). Thus, being a complex thermodynamic system, a RC has an additional macroscopic parameter (interfacial surface area Ω) which influences the entropy of the RC:

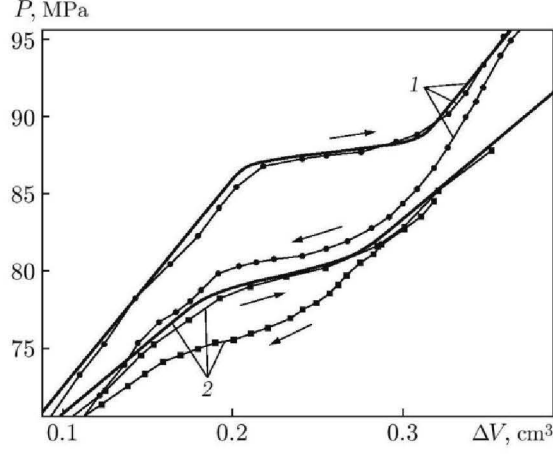


Fig. 2. $(P-V)$ isotherms ($T = 303$ K) of compression–expansion of repulsive clathrates based on MFI-F matrix (1) and MFI-OH matrix (2) and water: solid curves correspond to the calculation results in the case of intrusion and points to the results of experiments.

$$\begin{aligned}
 dS_{\text{int,ext}}(T, V_0, \Omega) &= \left(\frac{\partial S}{\partial T} \right)_{\Omega, V_0} dT + \left(\frac{\partial S}{\partial V_0} \right)_{T, \Omega} dV_0 + \left(\frac{\partial S}{\partial \Omega} \right)_{T, V_0} d\Omega \\
 &= C_V^0 \frac{dT}{T} + \left(\frac{\partial P}{\partial T} \right)_{V_0, \Omega} dV_0 + \left| \frac{\partial (\sigma \cos \theta_{\text{int,ext}})}{\partial T} \right|_{V_0, \Omega} d\Omega = C_V^0 \frac{dT}{T} + \beta P_0 dV_0 + \left| \frac{\partial (\sigma \cos \theta_{\text{int,ext}})}{\partial T} \right|_{V_0, \Omega} d\Omega. \quad (3)
 \end{aligned}$$

The presence of the temperature coefficient of surface tension implies that in (3) and below, the inverse temperature dependence of the surface tension σ is taken into account [29]. In (3), $\beta = P_0^{-1}(\partial P/\partial T)_{V_0, \Omega}$ is the isochoric pressure coefficient of the liquid–matrix system for $d\Omega = 0$, P_0 is the initial pressure in the system, $C_V^0 = T(\partial S/\partial T)_{\Omega, V_0}$ is the isochoric specific heat of the liquid–matrix system for $d\Omega = 0$. In Eq. (3), the replacement of $(\partial S/\partial V_0)_{T, \Omega}$ by $(\partial P/\partial T)_{V_0, \Omega}$ and $(\partial S/\partial \Omega)_{T, V_0}$ by $|\partial (\sigma \cos \theta_{\text{int,ext}})/\partial T|_{V_0, \Omega}$ follow from Maxwell’s equations for the Helmholtz free energy of the complex thermodynamic system [28]. Below we show that the value of C_V^0 is not equal to the isochoric specific heat C_V of the repulsive clathrate: Eq. (2) implies that at constant volume of the RC, the interfacial surface area Ω can increase due to the temperature deformation of the liquid and matrix [$dV = 0 \Rightarrow d\Omega = dV_0/(kr)$]. The above evolution of the interfacial surface Ω is accompanied by thermal effects [17, 24], resulting in a change in the specific heat of the RC.

Note that Eq. (3) contains not only the volume entropy components of the heterogeneous system (the first and second terms) but also the surface entropy (third term) [32, 40]. The second term defines the entropy change due to the change in the spatial arrangement of the molecules of the matrix and liquid due to their deformation at $d\Omega = 0$. A feature of the investigated heterogeneous working body is a spontaneous reduction in the surface entropy in an isothermal process, which is due to the motion of the system in the direction of decreasing excess surface energy (attainment of equilibrium) by reducing the interfacial surface area: $d\Omega < 0$ [28, 29]. Since in this case, an exoeffect [17, 24] is observed, in an adiabatically isolated lyophobic system, a reduction in the surface area Ω leads to an increase in temperature, i.e., to the conversion of the surface entropy to volume entropy.

Figure 2 shows $(P-V)$ compression isotherms of RCs based on MFI-F and MFI-OH hydrophobic silicalites with an average pore radius $r_0 \approx 0.3$ nm. In both systems, the working liquid is water, and the difference in the performance is caused by the difference in the methods of synthesis of the matrices (for more details, see [17]). The $(P-V)$ compression isotherms of the RCs has three regions (typical of all known RCs): the pre-intrusion region ($d\Omega = 0$ and $dV = dV_0$), the main intrusion region ($d\Omega \neq 0$), and the post-intrusion region ($d\Omega = 0$ and $dV = dV_0$). A similar arrangement of the regions of the $(P-V)$ isotherm is observed for the extrusion process. In the pre-intrusion and post-intrusion (pre-extrusion and post-extrusion) region, the pressure changes in the respective ranges $P \in (0; P_{\text{int,ext}})$ and $P \in (P_{\text{int,ext}}; \infty)$, and the volume change of the RCs is determined by the deformation of the condensed components ($dV = dV_0$ and $d\Omega = 0$). In the intrusion (extrusion) region, the pressure corresponds to the capillary Laplace pressure (1) and changes in the range $P \in [\min(P_{\text{int,ext}}); \max(P_{\text{int,ext}})]$, where $\min(P_{\text{int,ext}}) =$

Parameters of real and hypothetical capillary-porous matrices for repulsive clathrates

Matrix	$P_{r_0}^{\text{int}}$, MPa	D , MPa	V^{pore} , cm ³ /g
EVA	21.00	3.84	0.54
MTS	35.50	20.00	0.39
M1	14.00	5.00	0.46
M2	24.00	5.00	0.46
M3	34.00	5.00	0.46
M4	44.00	5.00	0.46
M5	54.00	5.00	0.46
MFI-F	87.70	0.50	0.09
MFI-OH	79.70	0.87	0.06
M6	82.23	1.00	0.09
M7	85.20	1.00	0.09

$\sigma \cos \theta_{\text{int,ext}}/(k \max(r))$ and $\max(P_{\text{int,ext}}) = \sigma \cos \theta_{\text{int,ext}}/(k \min(r))$. During intrusion (extrusion), the significant change in the volume of the RC (see Fig. 2) is due to the reversible (as the pressure decreased, the liquid entirely exited the pore space) increase in the interfacial surface area Ω according to Eq. (2).

Generally speaking, relations (1) and (2) characterize the state of the RC i.e., the relationship between the volume of the system with the pressure applied to it at some temperature T ; the latter unambiguously determines the surface tension $\sigma(T)$. In accordance with the present approach, approximating an experimental (P - V) dependence, one can obtain an analytical expression describing the state of the system. This expression, and the expression for the entropy of (3) allow one to study and predict the new properties of the RC within classical thermodynamics.

As shown below, the (P - V) isotherm is conveniently modeled using the error function used in probability

theory $\text{erf}(x) = \frac{2}{\sqrt{\pi}} \int_0^x \exp(-t^2) dt$ [41]:

$$\Delta V^{\text{int,ext}} = V_0 - V = \frac{V^{\text{pore}}}{2} \text{erf}\left(\frac{P - P_{r_0}^{\text{int,ext}}}{\sqrt{2}D}\right) + V_0\mu P + C; \quad (4)$$

$$\left(\frac{dV}{dP}\right)^{\text{int,ext}} = -\frac{V^{\text{pore}}}{\sqrt{2\pi}D} \exp\left(-\frac{(P - P_{r_0}^{\text{int,ext}})^2}{2D^2}\right) - V_0\mu. \quad (5)$$

Here V^{pore} is the volume of the pore space [defines the change in the volume of the system in the intrusion (extrusion) region] and D is the variance of the Laplace pressures in the intrusion (extrusion) processes at the pressure $P_{r_0} = \sigma |\cos \theta_{\text{int,ext}}|/(kr_0)$ that leads to filling of the pores of radius r_0 , prevailing in the matrix, $\mu = -V_0^{-1}(\partial V/\partial P)_{T,\Omega}$ is the isothermal compressibility of the working liquid-matrix system for $d\Omega = 0$, C is the constant of integration determined from the condition $\Delta V|_{P=P_0} = 0$. Although the error function is written in quadrature, it is convenient to use this function because it is built in most modern mathematical packages. The results of comparison of Eqs. (2) and (5) show the physical meaning of each term in Eq. (5):

$$kr\left(\frac{d\Omega}{dP}\right)^{\text{int,ext}} = \frac{V^{\text{pore}}}{\sqrt{2\pi}D} \exp\left(-\frac{(P - P_{r_0}^{\text{int,ext}})^2}{2D^2}\right) \equiv \Gamma^{\text{int,ext}}(P), \quad \frac{dV_0}{dP} = -V_0\mu. \quad (6)$$

In Fig. 2, the solid curves show the calculated curves constructed using the equation of state of RCs (4) for the compression process. It can be seen that the function used adequately describes the (P - V) relations. The values of the model parameters are given in the table. A similar relation for the case of spontaneous expansion of RCs is obtained using an experimental (P - V) diagram of expansion (extrusion).

REPULSIVE CLATHRATES BASED ON AN ENSEMBLE OF MATRICES

The form of the (P - V) compression-expansion isotherm of any working medium determines the functional capabilities of power systems based on this working medium. In particular, using the same working liquid, the (P - V) compression-expansion isotherm of a RC can be controlled by applying several different matrices in one

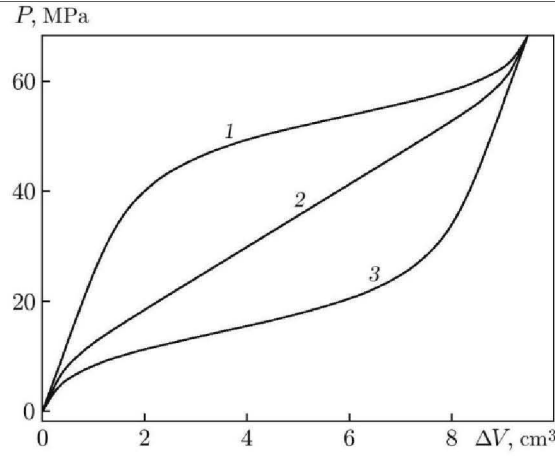


Fig. 3. (P – V) compression isotherms of RCs based on water and three different ensembles of matrices: (1) M3, M4, and M5 matrices with a mass ratio of 1 : 5 : 25; (2) M1, M2, M3, M4, and M5 matrices with a mass ratio of 1 : 1 : 1 : 1 : 1; (3) M1, M2, and M3 matrices with a mass ratio of 25 : 5 : 1.

heterogeneous system. In this case, the pressure–volume relationship is determined by the sequence of the processes of filling and emptying the pore space of the individual matrices, each of which has a particular distribution of pores in size and shape (along the radius r and the coefficient k) and in partial volume (in the parameters D and V^{pore}), i.e., $\Delta V = \sum_i \Delta V_i$, where ΔV_i is the change in volume of the RC caused by the filling of the i -th matrix. As before, the pressure in the intrusion (extrusion) processes also depends on the value of $\cos \theta_{\text{int,ext}}$ (1) and the change in the volume depends on the degree of filling of the pore space and the elastic strain of the condensed components of the system (liquid and matrix).

Figure 3 shows the (P – V) compression isotherm of RCs based on water and five M1–M5 hypothetical capillary-porous matrices (see the table), which differ only in the values of the pore radii P_{r_0} . In Fig. 3, it is evident that by varying the volume fraction of the matrix used, it is possible to obtain an (P – V) compression isotherm of the required form that satisfies the condition $|dV/dP| \geq |dV_0/dP|$. Thus, if the system has an increased volume fraction of matrices with a small pore radius, the most significant volume change occurs at high pressure (curve 1); in a RC with an increased volume fraction of matrices with large pore radii, the most significant volume change occurs at lower pressures, (curve 3); at equal volume fractions of matrices with large and small pore radii, the P – V dependence is almost linear (curve 2 in Fig. 3). Note that the curves in Fig. 3 can be displaced along the ordinate [the displacement of the range of operating pressure (1)] due to a change in the working liquid (changeTs in the surface tension and contact angle $\sigma \cos \theta_{\text{int,ext}}$).

The characteristics of the hypothetical matrices used in the calculation are similar to those of EVA [17] and MTS real matrices [35] (see the table). Since a large number of different matrices have been studied [20–25], it is possible to create the required ensemble of matrices.

HEAT EFFECTS IN REPULSIVE CLATHRATES

As noted above, the compression–expansion of RCs involve unusual thermal effects. Thus, along with heat release by the compressed system in the pre-intrusion and post-intrusion regions (Figs. 4 and 5), there is heat absorption by the system (untypical of classical systems) caused by a forced increase in the interfacial surface area Ω [17–24].

Using the classical definition of entropy $\delta Q = T dS$ and Eqs. (1), (3), and (6), we obtain the heat of isothermal compression–expansion of a RC:

$$\left(\frac{dQ_{\text{int,ext}}}{dP} \right)_T = T \left(-\alpha V_0 + \frac{\Gamma^{\text{int,ext}}(P)P}{\sigma |\cos \theta_{\text{int,ext}}|} \left| \frac{\partial (\sigma \cos \theta_{\text{int,ext}})}{\partial T} \right| \right). \quad (7)$$

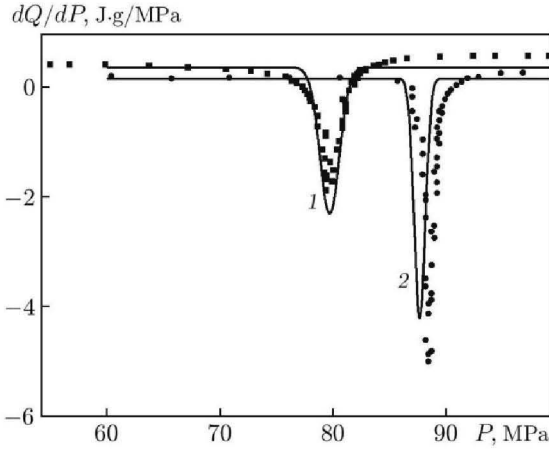


Fig. 4.

Fig. 4. Derivative dQ/dP versus pressure in RCs based on water and MFI-OH matrix (1) and MFI-F matrix (2) during their compression: curves correspond to calculation results, and points to the experimental results.

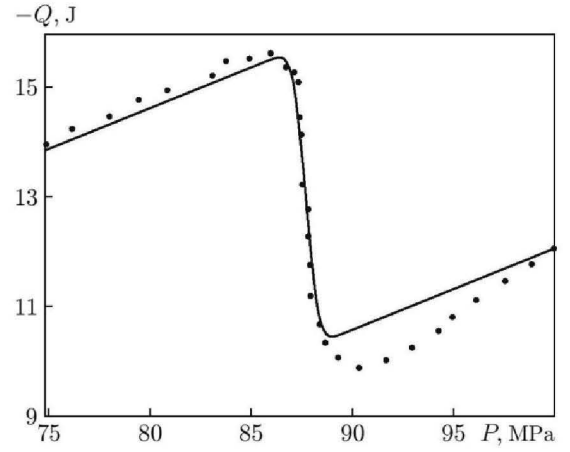


Fig. 5.

Fig. 5. Amount of heat absorbed during compression of a RC based on MFI-F matrix versus pressure: curves correspond to calculation results, and points to the experimental results.

Here $\alpha = V_0^{-1}(\partial V_0/\partial T)_{P,\Omega}$ is the volume expansion coefficient of the massive phase (liquid and matrix) of the RC at constant pressure. In the derivation of (7), we used the relationship between the temperature coefficients $\alpha = \mu\beta P_0$ known for homogeneous systems [28].

Comparison of the model relation (7) with the results of calorimetric measurements (see Figs. 4 and 5) for RCs based on water and two different matrices (MFI-F and MFI-OH) [17] shows that they are in satisfactory agreement. The calculated amount of heat released prior to the start of intrusion is equal to the amount of heat released during the compression of the volume components of the RC. The amount of heat absorbed during intrusion of the working liquid due to an increase in the interfacial area Ω is about 5 J/g (per 1 g of the matrix); the calculation error does not exceed 10%.

Equation (7) contains the pressure derivative $\Gamma^{\text{int,ext}}(P)$, which is determined in terms of the distribution of the pore radii of the matrix used. This makes it possible to define (determine) heat effects for an ensemble of RCs based on different matrices in the same way as was done in programming the required form of (P - V) isotherms (see Fig. 3).

Knowledge of the laws of release and absorption of heat in lyophobic working bodies makes it possible to clarify their specific heat and its dependence on temperature. Using the definition of the specific heat $C_x = (\partial Q/\partial T)_x$ at the constant parameter x , the relationship between the specific heats of the bulk phase of a RC at constant volume and pressure $C_P^{\text{L-M}} = C_V^{\text{L-M}} + TP_0V_0\beta\alpha$ [28], and Eqs. (2), (3), and (6), we write

$$C_P^{\text{int,ext}} = C_P^{\text{L-M}} + \frac{TP_0\Gamma(P_0)}{\sigma|\cos\theta_{\text{int,ext}}|kr_0} \left(\frac{\partial(\sigma\cos\theta_{\text{int,ext}})}{\partial T} \right)^2; \quad (8)$$

$$C_V^{\text{int,ext}} = C_V^{\text{L-M}} + TT(P) \left(\left| \frac{\partial(\sigma\cos\theta_{\text{int,ext}})}{\partial T} \right| \frac{P}{\sigma|\cos\theta_{\text{int,ext}}|} - \frac{\beta}{P_0} \right) \left(\left| \frac{\partial(\sigma\cos\theta_{\text{int,ext}})}{\partial T} \right| \frac{P(r_0)}{\sigma\cos\theta_{\text{int,ext}}} + \frac{\beta}{P_0} \right), \quad (9)$$

where $P(r_0)$ is the pressure corresponding to the maximum degree of compression of RC (filling of pores with radius r_0).

Note that in Eqs. (8) and (9), the pressure P in the system and the characteristic intrusion (extrusion) pressure $P_{r_0}^{\text{int,ext}}$ are functions of temperature. The value of P can be determined using the pressure coefficient β at constant volume, and the value of $P_{r_0}^{\text{int,ext}}$ is uniquely defined by the temperature dependence of the surface tension and the contact angle $\sigma\cos\theta$ (1). Thus, in the case of constant pressure at a certain critical intrusion

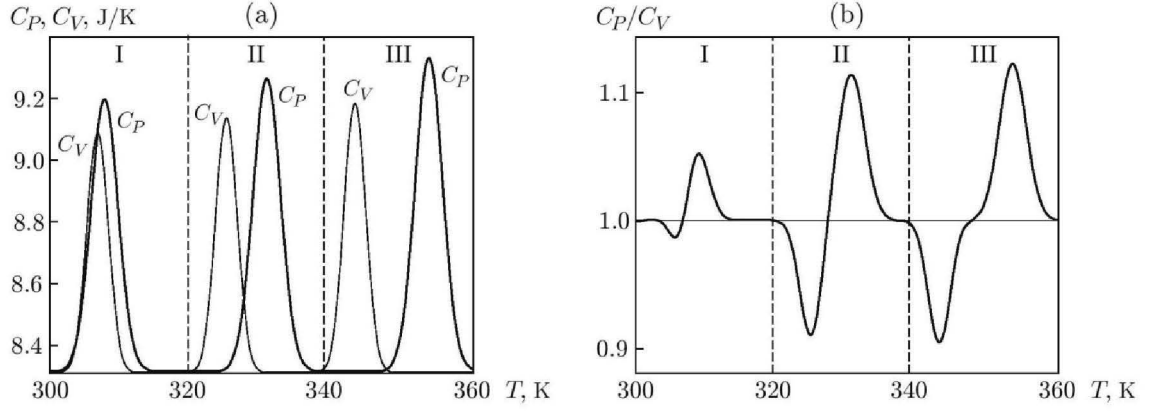


Fig. 6. Specific heats C_V and C_P of RCs based on water and MFI-F matrix (a) and the adiabatic exponent C_P/C_V (b) versus temperature for $P_0 = 86$ (I), 80 (II), and 74 MPa (III).

temperature T_{int} [for $P_{r_0}(T) \approx P_0$], the liquid penetrates into the pore spaces of the matrix, which is accompanied by additional heat consumption for increasing the interfacial surface area Ω , i.e., by an increase in the specific heat C_P . In the case of constant volume [the integral volume of the RC remains the same: $dV = 0(2)$], heating of the system leads to further intrusion of the liquid. The reasons for this are, on the one hand, an increase in the pressure P in the system due to the predominantly thermal expansion of the liquid relative to the pressure in the crystalline matrix and, on the other hand, a decrease in the surface tension of the working liquid and, hence, the capillary counter-pressure $P_{r_0}(T)$, facilitating the penetration of the liquid in the pore space.

Thus, the attainment of the intrusion pressure during heating a RC based on a matrix with a small variance of pore radii leads not only to an increase in the specific heat but also to pressure stabilization in the system. That is, the thermal expansion of the liquid and the matrix is compensated by the filling of the pore space with the liquid, and further increase in the temperature does not lead to an increase in the pressure in the system up to the moment of complete filling of the pores and capillaries.

These thermomechanical and thermophysical characteristics of the compression–expansion of RCs are responsible for the nonstandard form of the temperature dependence of the adiabatic exponent of the investigated heterogeneous lyophobic system.

Using Eqs. (8) and (9) and assuming that the temperature dependence of surface tension is linear (which is valid for simple and most other liquids [42]), we construct curves of the specific heats C_V and C_P (Fig. 6a) and the adiabatic exponent RC C_P/C_V on temperature (Fig. 6b). It is evident that for the RC based one matrix (close to a uniporous matrix), this curve is similar to a phase-transition curve, i.e., the specific heat undergoes a jump ΔC_P , which in the case of constant pressure can be described by the Ehrenfest equation [28]

$$\Delta C_P = -T \left(\frac{dP}{dT} \right)^2 \Delta \left(\frac{\partial V}{\partial P} \right)_T,$$

where the function $\Delta(\partial V/\partial P)_T$ for classical systems is stepwise, and for RCs, it is continuous and dependent on the pressure in the system. Thus, another feature of RC is that the characteristics of this jump of the specific heat can be controlled by varying the value of $\Delta(\partial V/\partial P)_T$, just as it was done in the creation of a RC with a given form of the (P – V) compression isotherm (see Fig. 3).

Figure 7 shows the temperature dependence of the jump of the specific heat $\Delta C_V = C_V - C_V^0$ at constant volume for a RC based on an ensemble of matrices. The heterogeneous system consists of two real matrices MFI-F and MFI-OH [17] and two hypothetical matrices M6 and M7 with characteristics similar to those of the two real matrices (see the table). The intrusion temperatures of these matrices are different due to the difference in pore radius between these matrices.

Thus, the specific heat of RCs can be changed by varying the ratios of the volumes and masses of the matrices. This makes it possible to control the specific heat in the required temperature range.

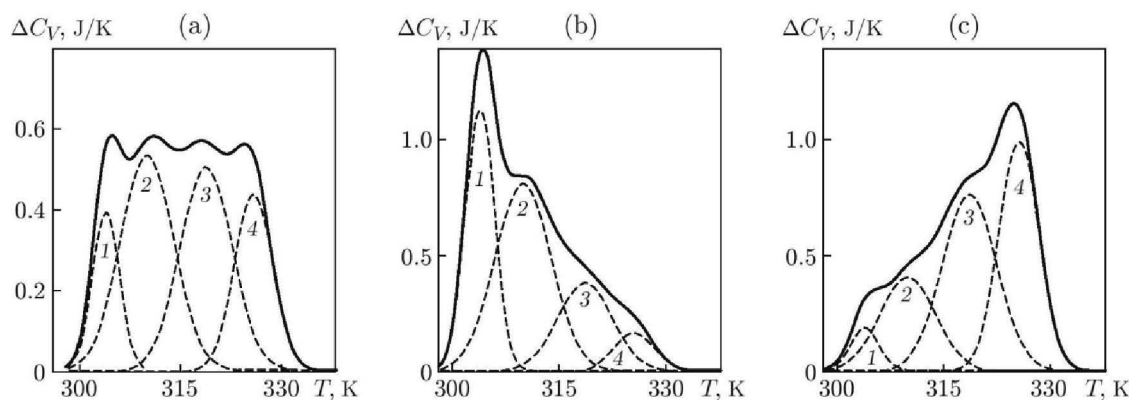


Fig. 7. Temperature dependence of the jump of the specific heat at constant volume of a RC (solid curve) based on water and an ensemble of two real matrices MFI-OH (1) and MFI-F (4) and two hypothetical matrices M6 (3) and M7 (2) with different masses of the matrices in the ensemble: (a) $m_1 = 1.0$ g, $m_2 = 1.6$ g, $m_3 = 1.8$ g, and $m_4 = 1.0$ g; (b) $m_1 = 2.9$ g, $m_2 = 2.7$ g, $m_3 = 1.2$ g, and $m_4 = 0.4$ g; (c) $m_1 = 0.5$ g, $m_2 = 1.3$ g, $m_3 = 2.4$ g, and $m_4 = 2.3$ g.

CONCLUSIONS

The properties and characteristics of new working media (repulsive clathrates) have been studied. Consideration of these properties and characteristics makes it possible to specify the optimal form of the (P - V) compression–expansion isotherms for each technical solution and the pressure hysteresis of RCs; to obtain the required temperature dependences of the specific heats C_P and C_V , to calculate the amount of heat absorbed or released during compression–expansion and control these processes; to obtain the necessary adiabatic exponent of the system in the required temperature range.

Mathematical and thermodynamic apparatus and some specific physic-technological approaches that can be used to design new high-performance working bodies and calculate their parameters based on equilibrium thermodynamics were presented.

REFERENCES

1. V. A. Eroshenko, "Thermodynamics of Intrusion of Liquid Metals in Porous Solid Matrices," in *Capillary Properties and Adhesion of Alloys* (Naukova Dumka, Kiev, 1987), pp. 100–109 [in Russian].
2. V. A. Eroshenko, "Unusual Properties of One Complex Thermodynamic System," *Dokl. Ukr. Akad. Nauk*, No. 10, 79–82 (1990).
3. V. A. Eroshenko, "Thermomolecular Energetics," *Prom. Teplotekh.* **14** (1–3), 22–25 (1992).
4. V. A. Eroshenko, "Damper with High Dissipating Power," France Patent No. WO 01/55616 A1, F 16 F 9/00, Publ. 08.02.01.
5. V. A. Eroshenko, "A New Paradigm of Mechanical Energy Dissipation. Part 1. Theoretical Aspects and Practical Solutions," *Proc. Mech. Eng., Pt DJ Automobile Eng.* **221** (3), 285–300 (2007).
6. V. A. Eroshenko, I. I. Piatiletov, L. Coiffard, and V. P. Stoudenets, "A New Paradigm of Mechanical Energy Dissipation. Part 2. Experimental Investigation and Effectiveness of a Novel Damper," *Proc. Mech. Eng., Pt DJ Automobile Eng.* **221** (3), 301–312 (2007).
7. V. A. Eroshenko, "Hydrocapillary Battery," USSR Patent No. 943444, 1980 (RF Patent, 1993), F 15 B 1/04, Appl. 04.28.1980, Publ. 07.15.1982, Byul. No. 26.
8. V. Eroshenko, R.-C. Regis, M. Soulard, and J. Patarin, "Energetics: A New Field of Applications for Hydrophobic Zeolites," *J. Amer. Chem. Soc.* **123** (33), 8129–8130 (2001).
9. V. Eroshenko, R.-C. Regis, M. Soulard, and J. Patarin, "The Heterogeneous Systems "Water–Hydrophobic Zeolites:" *New Molecular Springs, C. R. Phys.* **3** (1), 111–119 (2002).

10. V. A. Eroshenko, "Eroshenko Method of Converting Thermal Energy into Mechanical Energy," USSR Patent No. 1380357 A2, 1983 (RF Patent, 1993), F 03 G 7/00, Appl. 11.30.1983, Publ. 09.30.1996, Byul. No. 3.
11. V. A. Eroshenko, "Eroshenko Rotary Heat Engine," USSR Patent No. 1452262, 1986 (RF Patent, 1993), A1 F03 G 7/00, Appl. 06.16.1986, Publ. 09.30.1996, Byul. No. 3.
12. A. Laouir, L. Luo, D. Tondeur, et al., "Thermal Machines Based on Surface Energy of Wetting: Thermodynamic Analysis," *AIChE. J.* **49** (3), 764–781 (2003).
13. F. Cailliez, M. Trzpit, M. Soulard, et al., "Thermodynamics of Water Intrusion in Nanoporous Hydrophobic Solids," *Phys. Chem. Chem. Phys.* **10** (32), 4817–4826 (2008).
14. L. Liu, J. Zhao, P. J. Culligan, et al., "Thermally Responsive Fluid Behaviors in Hydrophobic Nanopores," *Langmuir* **25** (19), 11862–11868 (2009).
15. R. Denoyel, I. Beurroies, and B. Lefevre, "Thermodynamics of Wetting: Information Brought by Microcalorimetry," *J. Petrol. Sci. Eng.* **45** (3/4), 203–212 (2004).
16. D. Bougeard and K. S. Smirnov, "Modelling Studies of Water in Crystalline Nanoporous Aluminosilicates," *Phys. Chem. Chem. Phys.* **9** (2), 226–245 (2007).
17. L. Coiffard, V. A. Eroshenko, J.-P. E. Grolier, "Thermomechanics of the Variation of Interfaces in Heterogeneous Lyophobic Systems," *AIChE J.* **51** (4), 1246–1257 (2005).
18. L. Coiffard and V. Eroshenko, "Temperature Effect on Water Intrusion/Expulsion on Grafted Silica Gels," *J. Colloid Interface Sci.* **300** (1), 304–309 (2006).
19. V. A. Eroshenko and Yu. F. Lazarev, "Rheology and Dynamics of Repulsive Clathrates," *Prikl. Mekh. Tekh. Fiz.* **53** (1), 114–131 (2012) [*J. Appl. Mech. Tech. Phys.* **53** (1), 98–112 (2012)].
20. C. V. Suciu, T. Iwatsubo, and Sh. Deki, "Investigation of a Colloidal Damper," *J. Colloid Interface Sci.* **259** (1), 62–80 (2003).
21. A. Galaitis, "Heterogeneous Lyophobic System for Accumulation, Retrieval and Dissipation of Energy," Patent No. 7,767,301 US B 2. Publ. 08.03.10.
22. T. W. Ku, S. B. Jeon, V. H. Bui, and W. J. Song, "Numerical and Experimental Approach on Energy Dissipation in Nano Colloidal Damper," *J. Mech. Sci. Technol.* **21** (10), 1464–1470 (2007).
23. T. Iwatsubo, K. Washio, H. Yano, and M. Miyazaki, "Experimental Study of a Colloidal Damper to Practical Application," *J. System Design Dyn.* **2** (5), 1160–1169 (2008).
24. T. Karbowski, M.-A. Saada, S. Rigolet, et al., "New Insights in the Formation of Silanol Defects in Silicalite-1 by Water Intrusion under High Pressure," *Phys. Chem. Chem. Phys.* **12** (37), 11454–11466 (2010).
25. E. N. Serdun', A. G. Portyanoi, A. P. Sorokin, and G. A. Portyanoi, "On the Possibility of Developing Power systems Based on Lyophobic Capillary-Porous Systems," *Teploenergetika*, No. 12, 64–68 (2000).
26. V. B. Tsomaya, "Thermomolecular Energy and the Prospects for Its Use," *Mikrosist. Tekh.*, No. 3, 15–18 (2000).
27. V. A. Eroshenko, "Repulsive Clathrates. New Operational Material for Efficient Seismic Isolation," in *Seismic Isolation, Passive Energy Dissipation and Active Control of Seismic Vibrations of Structure, Proc. of the Int. Post-SMITR Conf., Taormina (Sicily, Italy), Aug. 25–27, 1997* (GLIS-IAEA, Roma, 1997), pp. 783–794.
28. V. V. Sychev, *Differential Equations of Thermodynamics* (Vysshaya Shkola, Moscow, 1991) [in Russian].
29. E. A. Guggenheim, *Thermodynamique* (Dunod, Paris, 1965).
30. L. Tzanis, M. Trzpit, M. Soulard, and J. Patarin, "Energetic Performances of Channel and Cage-Type Zeolites," *J. Phys. Chem.* **116** (38), 20389–20395 (2012).
31. C. V. Suciu, S. Tani, and K. Miyoshi, "Experimental Study on Thermal Characteristics of a Colloidal Damper," *J. System Design Dyn.* **4** (6), 899–913 (2010).
32. V. A. Eroshenko, "Adiabatic Non-compressibility and Non-dilatibility in a Complex Thermodynamic System," *Entropie*, No. 196, 17–23 (1996).
33. E. W. Washburn, "The Dynamics of Capillary Flow," *Phys. Rev.* **17** (3), 273–283 (1921).
34. R. C. Tolman, "The Effect of Droplet Size on Surface Tension," *J. Chem. Phys.* **17** (3), 333–337 (1949).
35. B. Lefevre, A. Saugey, J. L. Barrat, et al., "Intrusion and Extrusion of Water in Hydrophobic Mesopores," *J. Chem. Phys.* **120** (10), 4927–4938 (2004).
36. V. A. Eroshenko, V. P. Studenets, I. I. Pyatiletov, and V. Yu. Shchuchenko, "Using Repulsive Clathrates in Devices and Systems Providing the Earthquake Resistance of Structures," *Stroit. Tekhnogen. Bezopas.*, No. 35, 127–132 (2011).
37. V. A. Eroshenko, "Heterogeneous Structure for Accumulation or Dissipation of Energy, Process to Use It and Associated Devices," France Patent No. WO 9 6/18040, F 15 B 1/04, F 16 F 9/00, 5/00, F 15 B 21/06. Publ. 06.13.1996.

38. A. Han and Y. Qiao, "A Volume-Memory Liquid," *Appl. Phys. Lett.* **91** (17), 173132 (2007).
39. A. S. Tikhonov, A. P. Gerasimov, and I. I. Prokhorova, *Using the Shape Memory Effect in Modern Engineering* (Mashinostroenie, Moscow, 1981) [in Russian].
40. V. A. Eroshenko and Ya. G. Grosu, "Properties of Lyophobic Heterogeneous Systems Based on Matrices with Varying Pore Size," *Prom. Teplotekh.* **33** (6), 73–79 (2011).
41. M. Abramowitz and I. A. Stegun, *Handbook of Mathematical Functions with Formulas, Graphs, and Mathematical Tables* (Dover, New York, 1972).
42. T. Reis, *Introduction à la Chimie-Physique des Surfaces* (Dunod, Paris, 1952).
43. O. Beckstein and M. Sansom, "Liquid–Vapor Oscillations of Water in Hydrophobic Nanopores," *Proc. Nat. Acad. Sci. USA* **100** (12), 7063–7068 (2003).
44. N. Giovambattista, P. J. Rossky, P. G. Debenedetti, "Effect of Pressure on the Phase Behavior and Structure of Water Confined between Nanoscale Hydrophobic and Hydrophilic Plates," *Phys. Rev. E* **73** (4), 041604 (2006).



PCCP

COMMUNICATION



Cite this: *Phys. Chem. Chem. Phys.*, 2015, 17, 1572

Received 2nd September 2014,
Accepted 18th November 2014

DOI: 10.1039/c4cp03944k

www.rsc.org/pccp

A new working mode for molecular springs: water intrusion induced by cooling and associated isobaric heat capacity change of a {ZIF-8 + water} system†

Ya. Grosu,^{abc} V. Eroshenko,^{*c} J. M. Nedelec^{ab} and J. P. E. Grolier^{ab}

Hydrophobic microporous metal–organic framework ZIF-8 combined with water forms a molecular spring (MS), which by the forced intrusion of water into the pores and its spontaneous extrusion can store and restore large amounts of mechanical and thermal energy. Using scanning transitiometry technique, we demonstrate that the simultaneous effect of temperature and pressure on the porosity of ZIF-8 leads to a non-standard temperature dependence of intrusion and extrusion pressures of MS, which allows to provoke water intrusion into the hydrophobic pores of ZIF-8 by decreasing the temperature of the system under constant pressure. A remarkably strong effect of intrusion on the isobaric heat-capacity of {ZIF-8 + water} MS is discovered.

A system consisting of a lyophobic porous matrix and a non-wetting liquid can accumulate mechanical and thermal energy by the forced intrusion of liquid into pores and its spontaneous extrusion.^{1,2} During the intrusion process ($d\Omega > 0$) the system stores mechanical energy in the form of Gibbs work ($\delta W^{\Omega} = \sigma \cos \theta d\Omega$) and thermal energy in the form of heat of interface Ω development ($\delta Q^{\Omega} = T \frac{d\sigma \cos \theta}{dT} d\Omega$). The system restores the indicated energies due to reduction of interface during the extrusion process ($d\Omega < 0$); where $\theta > 90^\circ$ is the contact angle, σ is the surface tension of the liquid, and T is the temperature. If this process is close to reversible process, the system acts as a molecular spring (MS),^{2–6} if not it behaves as a shock-absorber or bumper.^{7–10} Strong interest in the investigation of MSs (such heterogeneous lyophobic systems also called repulsive clathrates¹¹)

is due to their energy capacity, which is orders of magnitude higher in comparison with conventional working bodies^{2,6,12,13} that are obtained using lyophobic porous materials with large values of specific surface area. Recently, the range of porous matrices for MSs has been extended to the metal–organic framework (MOF) ZIF-8.¹² MOFs are of great interest due to their exceptional stability and large porosity, which are well applicable in many fields of science and technology.^{14,15} Particularly, the hydrophobic microporous (orifice of the pores ~ 0.34 nm) ZIF-8 with its large surface area (~ 1800 m² g⁻¹) has received attention as a component of a MS.¹⁶

Investigation of the thermodynamic properties of a MS is crucial for their efficiency improvement, as well as to understand their operational principles. To date, investigations under conditions other than at room temperature are still very rare in the literature.

In this study, thermodynamic properties of a MS were investigated for the first time under isobaric conditions over an extended temperature range using scanning transitiometry:¹⁷ transitiometer ST-7M (high-pressure scanning calorimeter, which can work under isothermal, isochoric or isobaric conditions) described in our previous work¹¹ (also see Fig. S1 in the ESI†) was used to study the temperature dependence of the heat-capacity and thermal expansion under controlled constant pressure $P_0 = 23.80 \pm 0.15$ MPa. The temperature scanning rate was $\left(\frac{\partial T}{\partial t}\right)_P = 5 \times 10^{-4}$ K s⁻¹. The value of the heat-capacity was obtained as follows: $C_P \equiv \left(\frac{\partial Q}{\partial T}\right)_P = \left(\frac{\partial Q}{\partial t}\right)_P \left(\frac{\partial T}{\partial t}\right)_P^{-1}$, where heat flow $\left(\frac{\partial Q}{\partial t}\right)_P$ was simultaneously measured with all the thermodynamic parameters (P, V, T). For the {ZIF-8 + water} MS, isothermal compression–decompression cycles were recorded at two different temperatures other than room temperature: namely 275 K and 330 K. The MS investigated consisted of about 1 g of microporous ZIF-8 (purchased from Sigma Aldrich as Basolite Z1200) and distilled water.

The obtained isothermal PV -diagrams (Fig. 1) are typical for all MSs:^{2–6} the initial pressure increase was followed by the

^a Clermont University ENSCCF, Institute of Chemistry of Clermont-Ferrand, BP 10448, 63000 Clermont-Ferrand, France

^b CNRS, UMR 6296, ICCF, 24 av. des Landais, 63171 Aubière, France

^c Laboratory of Thermomolecular Energetics, National Technical University of Ukraine “Kyiv Polytechnic Institute”, Prospect Peremogy 37, 03056 Kyiv, Ukraine. E-mail: eroshenko@kpi.ua

† Electronic supplementary information (ESI) available: Description of the procedure for sample preparation and the pressure dependence of the compressibility of the {ZIF-8 + water} MS during a compression–decompression cycle. See DOI: 10.1039/c4cp03944k

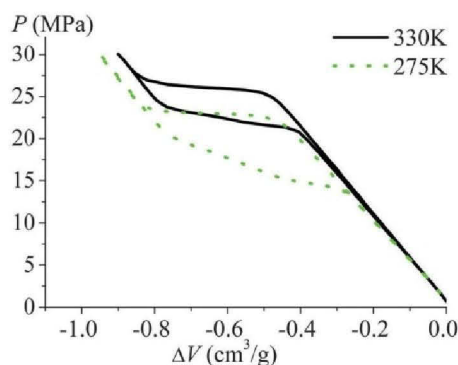


Fig. 1 Isothermal compression–decompression cycle of the (ZIF-8 + water) system at 275 K (dotted line) and 330 K.

elastic compression of the components of the MS (porous matrix and liquid), and then after reaching a certain critical pressure P_{int} , intrusion of liquid into the pores of the matrix takes place, which is followed by a rapid decrease in volume (a plateau on the PV -diagram is formed). Next, when the pores are completely filled, further increase in the pressure produces only elastic compression of the components of the MS. After the pressure was decreased, the liquid is expelled from the pores at the extrusion pressure P_{ext} . The values of the stored and restored mechanical energy calculated excluding the effect of elastic compressibility are presented in Table 1.

$$H = \frac{W_{\text{stored}} - W_{\text{restored}}}{W_{\text{stored}}} \times 100\%$$

One observes that both P_{int} and P_{ext} increase as T increases. P_{ext} appears to follow a two-step extrusion (Fig. 1). This unusual and previously non-observed behaviour of P_{int} for water-based MSs was most likely due to the temperature dependent compressibility of ZIF-8 (Fig. 1): higher compressibility leads to smaller sized pores under pressure, which leads to higher intrusion pressure, according to the Laplace–Washburn equation $P_{\text{int}} = -\frac{2\sigma \cos \theta}{r}$. Of course for microporous materials like ZIF-8 with pore opening radii $r \sim 0.17$ nm, the applicability of this macroscopic equation is questionable, to date the assumption that the value of P_{int} must be inversely proportional to the pore size is quite obvious. The same effect can explain the similar temperature dependence of P_{ext} . Previously, a positive temperature dependence of P_{int} was only reported for MSs based on electrolytes^{4,5} as a result of the temperature dependent solubility of the electrolyte in an aqueous solution, which increases its surface tension. A positive temperature dependence of P_{ext} is only typical for mesoporous heterogeneous lyophobic systems.^{8–10} Higher compressibility also leads to a smaller volume of intruded

Table 1 Energetic characteristics of the “ZIF-8 + water” molecular spring

T (K)	W_{stored} (J g ⁻¹)	W_{restored} (J g ⁻¹)	V_{int} (cm ³ g ⁻¹)	H (%)
275	8.03 ± 0.08	5.74 ± 0.07	0.35	28.5
330	8.83 ± 0.08	7.36 ± 0.07	0.33	16.7

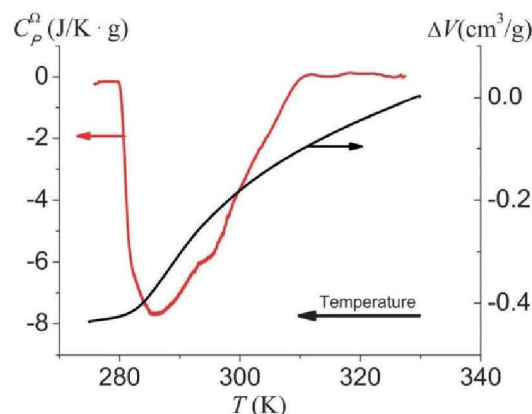


Fig. 2 Heat-capacity and volume of the (ZIF-8 + water) system under isobaric cooling ($P_0 = 23.8$ MPa). The values are specific to one gram of ZIF-8.

water V_{int} at higher temperatures (Table 1 and Fig. 1). All the changes in the PV -diagram at 330 K are reversible: after cooling the system the PV -diagram was similar to the one obtained prior to the higher temperature experiments. We see from Fig. 1 and Table 1 that the investigated MS was more efficient at higher temperatures and the difference between the stored and restored energy is smaller.

The unusual temperature dependence of intrusion pressure obtained allows the realization of a new regime for operation of a MS when intrusion of the liquid is provoked by cooling the system; we can see from Fig. 2 that the decrease in temperature under a controlled constant pressure P_0 from 330 K ($P_0 < P_{\text{int}|T=330\text{K}}$) to 275 K ($P_0 > P_{\text{int}|T=275\text{K}}$) was followed by a pronounced step indicating water intrusion into the pores of ZIF-8. In addition, the simultaneously measured calorimetric signal indicates that the intrusion process induces a large decrease in the isobaric heat capacity (maximum value of $C_p^{\Omega} = -7.6 \pm 0.4$ J K⁻¹ g⁻¹) – an effect of the negative heat-capacity. The quantity of total heat-capacity of MS $C_p = C_p^{\Omega} + C_p^V$ is the sum of the additional negative heat-capacity (which is a result of the interface development Ω during intrusion) C_p^{Ω} and the isobaric heat-capacity of the bulk phase of the MS (ZIF-8 and water) C_p^V . A negative value for C_p^{Ω} is expected as for most MSs intrusion process induces endothermal effect^{3,6,11,18} due to forced breaking of the intermolecular bonds of the liquid. Recently, the observed exothermal effect of intrusion is rather rare for microporous MSs.¹⁸ Heat capacity is defined as the amount of heat supplied to (or taken from) the system to increase (or decrease) its temperature by one degree. Hence, the endothermal effect of intrusion will (partially or completely) compensate the heat that should be taken from the system to decrease its temperature (*i.e.* the decrease in heat-capacity).

Using a macroscopic approach to qualitatively understand this phenomenon, we can write from the heat of interface development $\left(\delta Q^{\Omega} = T \frac{d\sigma \cos \theta}{dT} d\Omega\right)$: $C_p^{\Omega} = \left(\frac{\partial Q^{\Omega}}{\partial T}\right)_P \approx T \frac{d\sigma}{dT} \cos \theta \left(\frac{\partial \Omega}{\partial T}\right)_P$. For the {Zif-8 + water} MS $\left(\frac{\partial \Omega}{\partial T}\right)_P < 0$ (Fig. 2), $\frac{d\sigma}{dT} < 0$ (for water) and $\cos \theta < 0$ (non-wetting conditions); hence, $C_p^{\Omega} < 0$, which is

experimentally confirmed (Fig. 2). We note that the value of C_p^{Ω} depends on the surface of the porous material Ω (its value), while the value of C_p^V mostly depends on the quantity of liquid, which indicates that if a porous material with a large specific surface forms a MS with a minimal amount of liquid (just sufficient to fill its pores), the overall heat-capacity of such a MS $C_p = C_p^{\Omega} + C_p^V$ can actually become negative. This infers that if the temperature of the system is decreased to a value at which the process of intrusion starts, the corresponding endothermal effect would generate a further decrease in temperature and result in a non-controlled (non-equilibrium) filling of the pores of the matrix. Hence, to perform controlled cooling of the system (as carried out in this work) additional heat must be supplied to the system (*i.e.* an effect of negative heat-capacity).

We also note that the temperature dependence of heat-capacity C_p^{Ω} has two peaks (Fig. 2): the main peak at ~ 285 K and a weakly marked secondary peak at ~ 295 K. This observation is consistent with the two-step extrusion curve under isothermal conditions at 275 K (Fig. 1 and Fig. S2 in the ESI†). However, it is not true with a one-step intrusion under isothermal conditions (Fig. 1 and Fig. S2, ESI†). Similar differences in the intrusion and extrusion curves can be seen in the PV -diagrams at room temperature obtained by Patarin and co-workers.¹²

The properties and characteristics determined for the investigated {ZIF-8 + water} molecular spring may be extended to numerous applications in the field of mechanical and thermal energy storage, as well as for thermal to mechanical energy transformation.^{1,2,19} Previously, non-observed simultaneous and reversible effects of temperature and pressure on the porosity of ZIF-8 (Fig. 1) are important for MOF applications.¹⁴

Conclusions

The temperature dependence of compressibility for ZIF-8 leads to an unusual positive temperature dependence for the intrusion pressure of the {ZIF-8 + water} molecular spring (MS), which is not observed for other water-based MSs. This property allowed the realization of a new mode of MS operation such as the intrusion of water into the hydrophobic pores of ZIF-8 upon decreasing the temperature of the system under isobaric conditions. This process induces a large endothermic effect (~ 1800 m² g⁻¹ interface development) and as a result decreases the isobaric heat capacity of the MS. The obtained properties of the {ZIF-8 + water} molecular spring are exceptional among other MSs and are useful for the improvement of applications of molecular springs in the field of energy storage and transformation.

Acknowledgements

One of us (G. Ya.) gratefully acknowledges the financial support from the French Ministry of Foreign Affairs (Embassy of

France in Ukraine) for his stay at the Institute of Chemistry of Clermont-Ferrand, where all experimental measurements have been carried out. Useful advice and technical support on transitiometry technique from Prof. Randzio S.L. are highly appreciated.

Notes and references

- 1 V. Eroshenko, *Int. Pat. WO* 96/18040, 1996.
- 2 V. Eroshenko, R. C. Regis, M. Souldard and J. Patarin, *J. Am. Chem. Soc.*, 2001, **123**(33), 8129–8130.
- 3 T. Karbowski, M. A. Saada, S. Rigolet, A. Ballandras, G. Weber, I. Bezverkhyy, M. Souldard, J. Patarin and J. P. Bellat, *Phys. Chem. Chem. Phys.*, 2010, **12**(37), 11454–11466.
- 4 Y. Qiao and A. Han, *Philos. Mag. Lett.*, 2007, **87**(1), 25–31.
- 5 A. Han, W. Lu, T. Kim, X. Chen and Y. Qiao, *Phys. Rev. E: Stat., Nonlinear, Soft Matter Phys.*, 2008, **78**(3), 031408.
- 6 L. Coiffard, V. A. Eroshenko and J. P. E. Grolier, *AIChE J.*, 2005, **51**(4), 1246–1257.
- 7 V. A. Eroshenko, *Proc. Inst. Mech. Eng., Part D*, 2007, **221**(3), 285–300; G. Ortiz, H. Nouali, C. Marichal, G. Chaplais and J. Patarin, *J. Phys. Chem. C*, 2014, **118**(37), 21316–21322.
- 8 C. V. Suci, S. Tani and K. Miyoshi, *Journal of System Design and Dynamics*, 2010, **4**(6), 899–913.
- 9 L. Guillemot, T. Biben, A. Galarneau, G. Vigier and É. Charlaix, *Proc. Natl. Acad. Sci. U. S. A.*, 2012, **109**(48), 19557–19562.
- 10 Y. Grosu, O. Ievtushenko, V. Eroshenko, J. M. Nedelec and J. P. E. Grolier, *Colloids Surf., A*, 2014, **441**, 1549–1555.
- 11 O. V. Ievtushenko, V. A. Eroshenko, Y. G. Grosu, J. M. Nedelec and J. P. E. Grolier, *Phys. Chem. Chem. Phys.*, 2013, **15**(12), 4451–4457.
- 12 G. Ortiz, H. Nouali, C. Marichal, G. Chaplais and J. Patarin, *Phys. Chem. Chem. Phys.*, 2013, **15**(14), 4888–4891.
- 13 L. Tzani, M. Trzpit, M. Souldard and J. Patarin, *J. Phys. Chem. C*, 2012, **116**(38), 20389–20395.
- 14 J. Canivet, A. Fateeva, Y. Guo, B. Coasne and D. Farrusseng, *Chem. Soc. Rev.*, 2014, **43**, 5594–5617.
- 15 U. Mueller, M. Schubert, F. Teich, H. Puetter, K. Schierle-Armdt and J. Pastre, *J. Mater. Chem.*, 2006, **16**(7), 626–636.
- 16 G. Ortiz, H. Nouali, C. Marichal, G. Chaplais and J. Patarin, *J. Phys. Chem. C*, 2014, **118**(14), 7321–7328; M. Michelin-Jamois, C. Picard, E. Charlaix and G. Vigier, 2014, arXiv preprint arXiv:1404.5318.
- 17 S. L. Randzio, *Chem. Soc. Rev.*, 1996, **25**(6), 383–392; S. L. Randzio, J. P. E. Grolier, J. Zaslona and J. R. Quint, *French Pat.*, 9109227, 1994.
- 18 T. Karbowski, G. Weber and J. P. Bellat, *Langmuir*, 2014, **30**(1), 213–219.
- 19 B. Xu, Y. Qiao, T. Park, M. Tak, Q. Zhou and X. Chen, *Energy Environ. Sci.*, 2011, **4**(9), 3632–3639.

3.1.6. Effect of negative thermal expansion

As was demonstrated in Paragraph 3.1.3 thermal expansivity may become negative for some HLS under certain conditions. Such effect is called effect of Negative Thermal Expansion (NTE) and attracts great attention due to its wide range of practical applications. Detailed experimental and theoretical investigation is presented in references (Grosu et al. 2014b) and (Eroshenko et al. 2015), reprints of which are presented hereafter.

YA.G. GROSU,¹ V.A. EROSHENKO,¹ O.V. IEVTUSHENKO,^{1,2,3} J.-M. NEDELEC,^{2,3} J.-P.E. GROLIER^{2,3}

¹ National Technical University of Ukraine "Kyiv Polytechnical Institute".
Laboratory of Thermo-molecular Energetics

(37, Peremoga Ave., Kyiv 03056, Ukraine; e-mail: eroshenko@kpi.ua)

² Clermont University, ENSCCF, Institute of Chemistry of Clermont-Ferrand
(63000 Clermont-Ferrand, France)

³ CNRS, UMR 6296, ICCF
(24, Landais Av., 63171 Aubière, France)

ANOMALOUS NEGATIVE THERMAL EXPANSION IN A CONDENSED HETEROGENEOUS LYOPHOBIC SYSTEM

PACS 62.10.+s, 65.20.+w

A reduction in the volume of a heterogeneous lyophobic system (HLS) at the temperature growth (the so-called negative thermal expansion, NTE) is experimentally observed. For the investigated HLS "silicalite-1 + water", the NTE effect is shown to exceed the corresponding values observed for other known materials by more than an order of magnitude. The physical principles of this phenomenon are explained, and a mathematical model for its description is proposed.

Keywords: phase interface, porous body, PV-isotherm, intrusion/extrusion, simulation, experiment.

1. Introduction

The phenomenon of negative thermal expansion is a process, in which the volume of a body diminishes, as its temperature increases [1–7]. This phenomenon can be classified as abnormal, because the overwhelming majority of substances and systems are characterized by positive thermal expansion coefficients (TECs) [6, 7]. Only such rare representatives as the family of cubic zirconium tungstate ZrW_2O_8 [5], the family of AM_2O_7 compounds, where $A = U, Th, Zr, Hf, Sn$ and $M = P, V$ [3], and some zeolite and zeolite-like compounds [4] reduce their volume when the temperature increases in a certain interval. This phenomenon is used for the solution of some technical problems [7] in such domains as materials science, electronics, medicine, photonics, and others. The most important of those problems is the creation of composite materials with a required (given) TEC. This task is solved by combining materials with positive and negative TECs. An illustrative partial case of the problem concerned is the creation of a material with the zero TEC: the practical importance of

a substance, whose dimensions remain insensitive to the temperature, is evident.

Bearing the practical applicability of indicated materials in mind, their major characteristics are the degree of material volume, V , reduction as the temperature, T , changes, i.e. the quantity $\frac{dV}{dT}$, and its temperature dependence. A negative value of TEC is one of the unusual properties of heterogeneous lyophobic systems (HLSs) [2]. In this article, we continue to develop ideas concerning the negative thermal expansion in a wide class of HLS by attracting new experimental data and theoretical viewpoints. Physical mechanisms, which this phenomenon is based on, are explained. They allow the value of derivative $\frac{dV}{dT}$ to be considerably increased and the character of its temperature dependence to be changed in comparison with those for known materials with the negative TEC.

2. Theoretical Foundations

The heterogeneous lyophobic system or the repulsive clathrate (RC) [2, 8–10] is a condensed system consisting of a capillary-porous solid and a liquid that does not wet the former (the contact wetting angle $\theta \gg 90^\circ$). Such thermomechanical systems have a number of physical properties, which allows them

© YA.G. GROSU, V.A. EROSHENKO,
O.V. IEVTUSHENKO, J.-M. NEDELEC,
J.-P.E. GROLIER, 2013

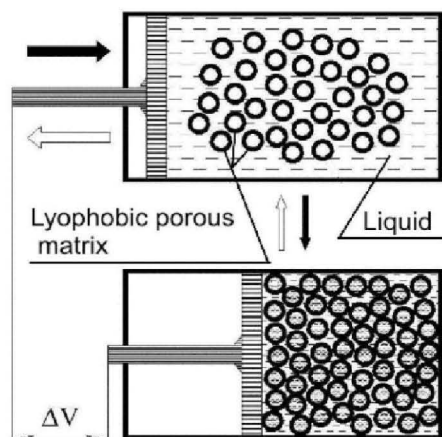


Fig. 1. Example of the physical model of repulsive clathrate

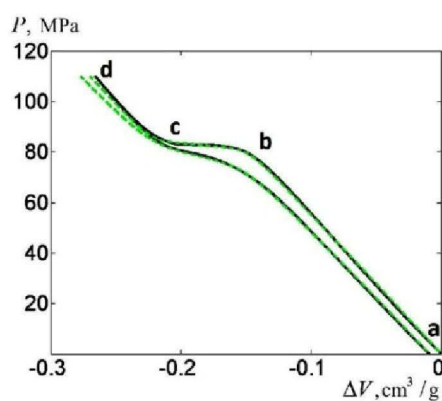


Fig. 2. PV -isotherm (at 323 K) of the “mechanical” compression/expansion of repulsive clathrate on the basis of silicalite-1 and water. The solid and dashed curves demonstrate, respectively, the experimental data and the results of model calculations according to Eq. (6)

to be used – although nonconventionally, but effectively – for the accumulation of thermal and mechanical energy [11–13], for the dissipation of the latter [10, 14–18], and for the transformation of thermal energy into mechanical one and *vice versa* [19, 20]. The physical model of the HLS/RC system is explained in Fig. 1. A capillary-porous body (a matrix, which is usually a powder of porous particles [11–13, 16–18] or, more seldom, a monolithic framework [21]) and a liquid that does not wet this body ((the contact wetting angle $\theta \gg 90^\circ$) are placed into a working chamber of the “cylinder–piston” type. The lyophobic character of the system prohibits the liquid from an un-

lowed penetration into the energy unprofitable space of the porous matrix. For the liquid to penetrate into the pores/capillaries (the process of forced intrusion), it must overcome a potential barrier, which is determined by the Laplace capillary pressure written down in the Washburn form as follows [22]:

$$P^{\text{int,ext}} = \frac{\sigma |\cos \theta^{\text{int,ext}}|}{kr}. \quad (1)$$

Formula (1) testifies that the coefficient of liquid surface tension σ , the intrusion contact angle $\theta^{\text{int}} \gg 90^\circ$, the pore radius r , and the geometry of the matrix pore space (the factor $0.33 < k < 0.5$) influences the magnitude of pressure P^{int} that should be applied to the system for the intrusion (the subscript “int”) of the liquid into matrix pores to take place. Of course, for Eq. (1) to be able to describe nano-capillary HLSs, corrections related to a considerable curvature of the tension surface must be introduced into it.

The intrusion process is accompanied by a reduction in the volume of heterogeneous system by the volume of matrix pores ($\Delta V = V_{\text{pore}}$) and a development of the interphase surface Ω at the solid–liquid interface, with the accumulation of the Gibbs free energy in the system, $G = \sigma \Omega \cos \theta$. Afterward, this energy can be released, partially or almost completely, for executing a useful mechanical work. We adopt that the hysteresis of the wetting contact angle, $\Delta\theta$ (the difference between the intrusion, θ^{int} , and extrusion, θ^{ext} , contact angles), governs the magnitude of pressure hysteresis, $H = P^{\text{int}} - P^{\text{ext}}$; the quantity P^{ext} is the pressure of a free liquid outflow from the matrix pore space. The hysteresis H defines the functional capability of RC; namely, if H is small ($P^{\text{int}} \approx P^{\text{ext}}$), the system is expedient to be used for the accumulation or transformation of energy in thermomechanical systems, and, at large H ($P^{\text{int}} \gg P^{\text{ext}}$), for its dissipation.

A typical PV -isotherm of HLS (the dependence of the system volume V on the pressure P applied to the system) is shown in Fig. 2. It has three characteristic sections. At a preliminary compression stage (section a–b), the increase of the pressure in the system ($P < P^{\text{int}}$) changes the system volume slightly (here, we have the elastic deformation of the liquid and the empty porous matrix). In the section b–c (at $P = P^{\text{int}}$), the intrusion of the liquid into the matrix pores takes place, which is accompanied by a substantial reduction in the HLS/RC volume. For

real matrices, there always exists a certain deviation of pore dimensions from the average value r , i.e. the pore size dispersion D_r , which induces the dispersion of values for the intrusion and extrusion pressures. A further growth of the pressure ($P > P^{\text{int}}$, section c-d) results in an insignificant change of the condensed system volume (the elastic deformation of the liquid and the filled porous matrix, which is somewhat smaller in comparison with that in the first section). The inverse process (section d-a) takes place for the process of free extrusion (Fig. 2). The compression/expansion PV -isotherm is a key characteristic of repulsive clathrate, being determined by the properties of the liquid, geometry of the pore space (including the size distribution of pore radii), and the phobicity of the system.

The application of HLS/RC with a large hysteresis H allows the mechanical energy with a power of 40–50 W/cm³ to be effectively dissipated at frequencies higher than 20 Hz [15, 23], which are inaccessible for ordinary hydraulic shock-absorbers. A high stability of the operation characteristics for such HLS/RCs after 10⁶–10⁷ cycles of complete compression/decompression was demonstrated [17]. A typical value of dissipated energy in a cyclic process amounts to about 12 J per gram of the matrix mass [16]; the corresponding values for the irreversible regime (e.g., for a special bumper) acquire magnitudes up to 41 J/g [18]. Accumulation of mechanical energy with the help of the system “super-hydrophobic zeolite + water” is characterized by values up to 15 J/g, and 97% of this energy can be released to execute a useful work [13]. The phenomenon of abnormal dilatometry for one class of HLSs [24] found its application in the nuclear power engineering [25].

3. Experimental Part

3.1. Materials

In this work, we used repulsive clathrates “super-hydrophobic silicalite-1 + water”. Silicalite-1 is a zeolite with the MFI-structure. It is naturally super-hydrophobic. The average radius of its pores $r \approx 3$ nm, the specific interphase surface $\Omega \approx 400$ m²/g, and the specific pore volume $V_{\text{pore}} \approx 0.12$ cm³/g. By its energy parameters – a high accumulated specific energy at a small hysteresis $H = P^{\text{int}} - P^{\text{ext}}$ – the used RC (silicalite-1 + water) is not a “champion” among the available and studied materials [11–

13]. However, owing to its simple topology (the pore space in silicalite-1 is composed of independent parallel cylinders), this material is a good example of super-hydrophobic capillary-porous matrices for the creation of repulsive clathrates. It makes the research of main clathrate characteristics and the phenomena occurring in clathrates simpler, including the verification of HLS/RC mathematical models. In this work, we used a commercial variant of silicalite-1 (Aldrich) synthesized following the standard procedure in the presence of fluorine ions.

3.2. Experimental equipment and the procedure of specimen fabrication

To obtain the diagram of the temperature-, $V(T)$, or pressure-induced, $V(P)$, volume change in the course of the RC heating/cooling or compression/expansion, respectively, cycle, we used a scanning transitiometer ST-7M, a highly baric ergo-calorimeter developed and modernized by Prof. S.L Randzio at the design department and the plant of scientific equipment of the Institute of Physical Chemistry (the Polish Academy of Sciences) according to the idea and technical documentation of Prof. V.A. Eroshenko (the NTUU “Kyiv Polytechnical Institute”). Unlike the basic ST-7 unit [26–28], high-precision induction volumeters on the basis of metal sylphon bellows were mounted in the high-pressure measuring chambers (up to 200 MPa) of the ST-7M unit.

The scheme of the experimental installation is depicted in Fig. 3, *a*. One can see that the open ends of sylphon bellows are rigidly attached to the cylindrical section of measuring chambers (the test sample is placed into one of them and the reference sample into another one); their other ends are connected to metal non-magnetic rods with crimped magnetic cores (armatures) of induction sensors. The windings of the latter are located beyond the hydraulic chamber manufactured of a non-magnetic material. The axial shift of sylphon bellows (with a constant effective cross-section) characterizes the volume variation during the processes of RC compression/expansion or heating/cooling. This shift is registered by linear variable differential transformers (LVDT-sensors) [29]. The readout of the signal from the LVDT-sensors calibrated in volume units can be done in the ST-7M unit both in parallel and differentially.

The pressure in the measuring chambers is provided with the help of a high-pressure pump driven

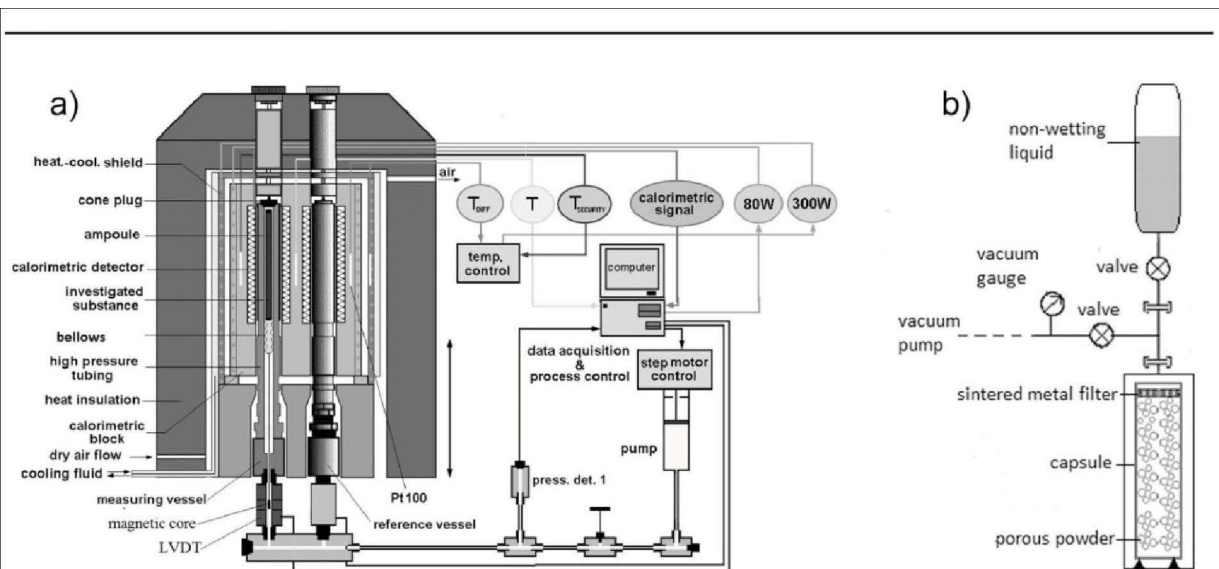


Fig. 3. Experimental installation for measuring $V(P)$ - and $V(T)$ -diagrams with the simultaneous registration of thermal effects (a); Schematic diagram of a stand for the specimen fabrication (b)

by a step motor. In the case of the basic ST-7 unit version, the number of steps (the number of separate doses) was used to evaluate the volume change during the processes of compression/expansion or heating/cooling of the system. Possible failures in the course of operation of a step motor and a counter device gave rise to considerable errors in the determination of volume change, while measuring the $V(P)$ -isotherms. In the modified construction (the ST-7M unit), the assembly “step motor–pump” was retained, but it played a second-order role. Real volume changes in the studied system were evaluated according to the readings of an induction volumeter, which made the metrological characteristics of the ST-7M unit much better. A high determination accuracy of thermal effects and reading out the PV -isotherms were achieved owing to the application of an automatic temperature control system on the basis of a proportional-integral-derivative (PID) controller. The readout of a pressure signal in the hydrosystem was carried out with the help of a pressure transducer built into the hydraulic pipe connecting the pump and the measuring chambers.

The ST-7M unit can operate in various regimes [26–28]. In this work, we simultaneously registered a variation of the specimen volume as a result of the compression/expansion, heating/cooling, or pressure growth in the chambers. As a rule, the rate of compression/expansion in the experiments of

the type “forced mechanical intrusion–free extrusion” amounted to 10^{-3} MPa/s. In the experiments with the “thermal” intrusion/extrusion, the rates of heating and cooling were 4×10^{-3} K/s. In both cases, the low rate was needed to ensure the quasistatic character of the processes of “mechanical” and “thermal” intrusion of the liquid into matrix pores. The accuracy of measurements in both experiments was checked with respect to three thermodynamic parameters: ± 0.15 MPa for the pressure, $\pm 3.3 \times 10^{-4}$ cm³ for the volume, and ± 0.01 K for the temperature.

In Fig. 3, b, a simplified scheme of the specimen preparation is shown. The weighed amount of silicalite-1 was inserted into a metallic capsule and closed by a ceramic-metal porous cover. The porous matrix mass in a capsule was approximately equal to 2 g. The capsule with the matrix was carefully degassed for 2 to 4 h until a pressure of about 10^{-2} mbar was attained. After degassing, the capsule with the matrix was filled with distilled preliminarily degassed water through the porous cover. The capsule was filled with water under vacuum to ensure the effective filling of the space between porous particles of the hydrophobic matrix with water (the procedure of RC fabrication). When the calorimeter body was in the extreme upper position (Fig. 3, a), the capsule with RC and the capsule with water were put into the measuring and compensation, respectively, high-pressure chambers, which were preliminary filled with

degassed distillate. When embedding the capsules, excess water was freely displaced from the chambers through their input holes, which excluded the ingress of air into the chamber. Afterward, the chambers were tightly closed using special screw covers, and the calorimeter body with two reception channels acting on the thermal detectors was carefully put down on both measuring chambers. The sliding fit of chambers in the calorimeter channels provided an effective heat exchange between the measuring chambers and the thermal detectors.

3.3. Experimental procedure

The compression/expansion $P(V)$ -isotherms were registered automatically. A specimen (repulsive clathrate) prepared as was described above and arranged in the working chamber was undergone an external pressure that grew linearly in time at the rate $\frac{dP}{dt} = 10^{-3}$ MPa/s from the initial value to $P_{\max} \approx 110$ MPa. Then the pressure was lowered down at the same rate to the initial value. During the whole experiment, the temperature was maintained constant by an automated system on the basis of a PID-controller.

While registering the $V(T)$ -dependences, the initial pressure $P = 80.5$ MPa was created in the working chamber. Then the cycle of heating/cooling was executed in the interval from $T_{\min} = 283$ K to $T_{\max} = 313$ K at the rate $\frac{dT}{dt} = 4 \times 10^{-3}$ K/s.

3.4. Experimental results and their discussion

In Fig. 4, the temperature dependence of the volume of RC created on the basis of “silicalite-1 + water”, which was measured provided a constant loading on the system (the initial pressure in the system amounted to $P = 80.5$ MPa), is depicted (the solid curve). The plot of the thermal cycle testifies that the increase of the temperature from its initial value $T = 283$ K to the temperature $T \approx 303$ K does give rise to substantial variations in the system volume. If the temperature grows further, $T > 303$ K, a linear reduction of the specific volume of the system is observed, which is associated with the water intrusion into the pores of silicalite-1. In particular, in the course of intrusion, the coefficient of negative thermal expansion for the investigated system at the stage of the matrix filling was equal to $\beta = \frac{1}{V_0} \left(\frac{\partial V}{\partial T} \right)_{P_{\text{int}}} = -5.7 \times 10^{-3} \text{ K}^{-1}$.

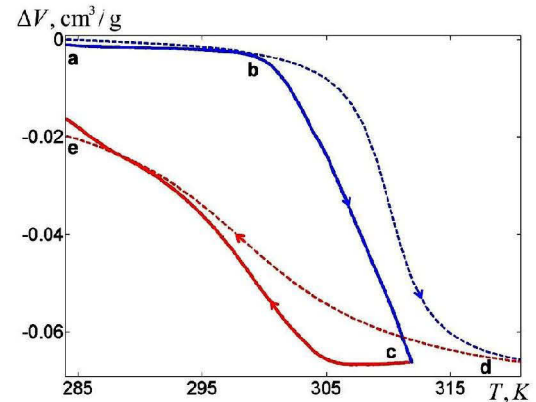


Fig. 4. Cycle of “thermal” intrusion/extrusion for RC on the basis of silicalite-1 and water at the initial pressure $P_0 = 80.5$ MPa. The solid curve corresponds to experimental data, the dashed one to the results of model calculations

Let us compare the result obtained with the corresponding data for known materials with a negative TEC. In most cases, the relevant magnitudes are of the order of -10^{-5} K^{-1} [3–7]. For instance, the phenomenon of negative thermal expansion recently described for cubic ScF_3 is characterized by $\beta = -1 \times 10^{-5} \text{ K}^{-1}$ [30], and the value $\beta = -9 \times 10^{-5} \text{ K}^{-1}$ was obtained for a $\text{Ca}_{0.8}\text{La}_{0.2}\text{Fe}_2\text{As}_2$ specimen [31]. Those parameters were considered to be anomalously high and attracted a substantial theoretical interest in the scientific community [32, 33].

Hence, the value of TEC for the HLS on the basis of “silicalite-1 + water” is considerably larger than the corresponding values for known materials. Namely, the actual record results are exceeded by more than an order of magnitude. It should be noted that the result obtained for the examined HLS was observed in a rather narrow temperature interval, which is not true for $\text{Ca}_{0.8}\text{La}_{0.2}\text{Fe}_2\text{As}_2$ and ScF_3 materials. However, as will be shown below, the temperature range, in which TEC is negative, can be considerably extended by combining various capillary-porous matrices into a single HLS.

As the temperature decreases, the volume of the system “silicalite-1 + water” increases. This process has a hysteresis in the temperature interval of “thermal” intrusion and extrusion (Fig. 4): when the system is cooled down to the initial temperature, its volume is somewhat smaller (point *e*) than the initial value (point *a*). In view of the existence of a hysteresis in the isothermal process of compression/expansion

sion/expansion of RC with the intrusion/extrusion with respect to the pressure (Fig. 2), this result seems quite expectable. Of course, a hysteresis in the cycle of HLS heating/cooling can be regarded as an undesirable phenomena in this case. However, as was mentioned above, the system “silicalite-1 + water” is a good model example, whereas HLSs with the minimal hysteresis are more expedient to be used for practical purposes. A number of zeolites, which were studied experimentally with respect to their interaction with water [11–13], satisfy this condition; namely, they have a small hysteresis magnitude with respect to the parameter “pressure” (less than 3%) and a high stability of their properties. The difference between the inflow and outflow behaviors of the liquid in the course of the isothermal “mechanical” cycle (Fig. 2) and the origins of its emergence were studied in work [34]. In particular, it was demonstrated that this difference is a result of silanol defects on the internal matrix surfaces and can be eliminated by synthesizing the high-quality matrices.

4. Theoretical Analysis

The reported experiments were carried out in a regime that can be characterized as quasistatic. Therefore, it is expedient to apply the apparatus of equilibrium thermodynamics to the interpretation of the results. In work [34], it was shown that the equation

$$\Delta V^{\text{int,ext}} = V_0 - V = f^{\text{int,ext}}(P) + \kappa_T^{V_0} P + C \quad (2)$$

can be used for simulating the compression/expansion PV -isotherms. Here, ΔV is a change of the RC volume (the superscript “int” stands for intrusion, and “ext” for extrusion); V_0 is the initial volume of a working substance consisting of the initial liquid volume V_p and the empty matrix V_m ($V_0 = V_p + V_m$); the term with the coefficient $\kappa_T^{V_0} = \left(\frac{\partial V_0}{\partial P}\right)_T$ determines the isothermal elastic deformation of bulk RC components under the pressure P ; C is the integration constant determined from the initial condition $[\Delta V^{\text{int,ext}}]_{P_0} = 0$, where P_0 is the initial pressure in the system; and the function $f^{\text{int,ext}}(P)$ describes a change of the RC volume owing to the intrusion/extrusion of the liquid into the pore space of the matrix. Since the dependence of the degree of filling of the pore space on the pressure applied to the system is governed by the distribution of matrix

pore radii (the relation between the pressure and the radius of filled pores is determined by Eq. (1)), it is convenient to use the distribution functions from probability theory for the functions $f^{\text{int,ext}}(P)$. For example, if the matrix pores are characterized by a certain dominating average radius, and symmetric deviations from this average value are insignificant, it is expedient to use the Cauchy distribution function [35],

$$f^{\text{int,ext}}(P) = \frac{V_{\text{pore}}}{\pi} \arctan\left(\frac{P - P^{\text{int,ext}}}{D^{\text{int,ext}}}\right) \quad (3)$$

or the Gauss distribution [35],

$$f^{\text{int,ext}}(P) = \frac{V_{\text{pore}}}{2} \operatorname{erf}\left(\frac{P - P^{\text{int,ext}}}{\sqrt{2}D^{\text{int,ext}}}\right), \quad (4)$$

where the error function is defined by the formula

$$\operatorname{erf}(x) = \frac{2}{\sqrt{\pi}} \int_0^x e^{-t^2} dt. \quad (5)$$

The volume of the pore space V_{pore} , the average pressures $P^{\text{int,ext}}$ inducing the intrusion/extrusion, and their dispersions $D^{\text{int,ext}}$ can be determined from the passport characteristic of the matrix. For this purpose, the distribution functions of pore volumes over pore radii and Eq. (1) are used. This is a procedure that is inverse to what is applied in the practice of mercury [36] and water [37] porosimetries. If the distribution of pore radii is more complicated—for example, it is asymmetric—the corresponding functions from probability theory, such as Weibull, log-normal, and others [35], or their combination (if that or another RC is synthesized on the basis of several matrices combined into a single RC) can be used. For instance, let us use the values $P^{\text{int}} = 82.85$ MPa, $P^{\text{ext}} = 78.63$ MPa, $D^{\text{int}} = 0.9$ MPa, $D^{\text{ext}} = 3.5$ MPa, $V_{\text{pore}}^{\text{int}} = 0.073$ cm³/g, $V_{\text{pore}}^{\text{ext}} = 0.068$ cm³/g (the inequality $V_{\text{pore}}^{\text{ext}} < V_{\text{pore}}^{\text{int}}$ means that not all the liquid left the matrix), and $\kappa_T^{V_0} = -1.8 \times 10^{-3}$ cm³/MPa/g, and the Cauchy distribution function [35] to plot the model curves for the compression/expansion PV -isotherms according to Eq. (3) and compare them with the experimental result (Fig. 2),

$$\begin{aligned} \Delta V^{\text{int,ext}} &= V_0 - V = \\ &= \frac{V_{\text{pore}}^{\text{int,ext}}}{\pi} \arctan\left(\frac{P - P^{\text{int,ext}}}{D^{\text{int,ext}}}\right) + \kappa_T^{V_0} P + C. \end{aligned} \quad (6)$$

ISSN 2071-0186. Ukr. J. Phys. 2014. Vol. 59, No. 1

The applicability of Eq. (6) to the description of isothermal processes and the simulation of “unordinary” thermal effects (the endothermic effect of RC compression and the exothermic effect of RC expansion) [34] allows us to suppose that an equation of type (2) can be proposed as an equation of the HLS state, because it describes a relation of the basic macroscopic parameters in the thermodynamic system: the pressure P , the volume V , and the temperature T (through the unambiguous relation of the temperature to the liquid surface tension σ and, therefore, to the intrusion/extrusion pressures by means of Eq. (1)). However, the equation of state must be verified not only for the isothermal process, but for other processes—isochoric, isobaric, adiabatic, and so on—as well. In this work, the equation is verified with the use of a non-standard process, which is more complicated in comparison with the processes mentioned above, but is more adequate to the practical application of HLS; this is the process with a constant constraint.

In this process, RC undergoes the action of a constant force, which is not enough for the liquid to penetrate into the matrix pores at the initial temperature. The temperature growth with respect to the initial one (which is given beforehand) gives rise to two effects. First, the pressure in the system increases owing to the thermal expansion of its bulk components (the liquid and the matrix). Second, the coefficient of liquid surface tension decreases. Both those effects result in that, at a certain characteristic temperature, the pressure in the system becomes equal to the Laplace capillary pressure at the specified temperature. As a result, the liquid fills the matrix capillaries, and the RC volume diminishes (Fig. 4).

To describe this process, Eq. (3) must make allowance for the temperature dependence of the intrusion/extrusion pressures $P^{\text{int,ext}}$ and a change of the pressure in the system $P(T)$ occurring due to the thermally induced deformation of the liquid and the matrix. As a rule, the both dependences are linear [38, 39]. According to Eq. (1), the quantities $P^{\text{int,ext}}$ are determined by the temperature dependences of the surface tension coefficient σ and the wetting contact angle θ . For some systems—in particular, for the system “silicalite-1 + water” [38]—the temperature dependence of the contact angle can be neglected (of course, this is a certain approximation). Using

Eq. (1), the following equation can be written down:

$$P^{\text{int,ext}}(T) = \frac{d\sigma}{dT} \frac{P(T_0)}{\sigma(T_0)} (T - T_0) + P(T_0). \quad (7)$$

It is well-known that the liquid surface tension considerably changes if the liquid surface becomes substantially curved, and this phenomenon undoubtedly does take place in nano-sized capillaries. This variation is usually taken into account by using the Gibbs–Tolman–Koenig–Buff (GTKB) equation [40],

$$\sigma = \sigma_\infty \left(1 + 2\frac{\delta}{r}\right)^{-1}, \quad (8)$$

where σ_∞ is the surface tension of a flat surface, and δ is the Tolman length. In his work [40], R. Tolman derived the GTKB equation, by using the approximation $\delta = \text{const}$, which enables us to use the transformation

$$\frac{d\sigma}{dT} \frac{1}{\sigma(T_0)} = \frac{d\sigma_\infty}{dT} \frac{1}{\sigma_\infty(T_0)} \quad (9)$$

in Eq. (4) and, hence, to avoid the determination of the Tolman length in the analysis to follow.

The pressure change in the system, $P(T)$, is determined by means of the isochoric coefficient for the pressure in the liquid and the matrix, $\left(\frac{\partial P}{\partial T}\right)_V$. Using Eq. (7) and the classical relation between the thermal coefficients for simple systems [39]

$$\left(\frac{\partial V}{\partial T}\right)_P = - \left(\frac{\partial V}{\partial P}\right)_T \left(\frac{\partial P}{\partial T}\right)_V, \quad (10)$$

let us rewrite Eq. (6) in the form

$$\Delta V^{\text{int,ext}} = V_0 - V = \frac{V_{\text{pore}}^{\text{int,ext}}}{\pi} \times \arctan \left(\frac{P(T) - P^{\text{int,ext}}(T)}{D^{\text{int,ext}}} \right) + \left(\frac{\partial V}{\partial T}\right)_P T + C_2. \quad (11)$$

Here, the constant C is determined from the condition $[\Delta V^{\text{int,ext}}]_{T_0} = 0$, and the term $\left(\frac{\partial V}{\partial T}\right)_P T$ is responsible for the temperature dependence of variations of the volume (the expansion and the reduction of system’s bulk components, the liquid and the matrix). In view of the conditions, under which the experiment dealing with “thermal” intrusion/extrusion was carried out, this effect could not bring about the volume change, because the system undergone the action of a

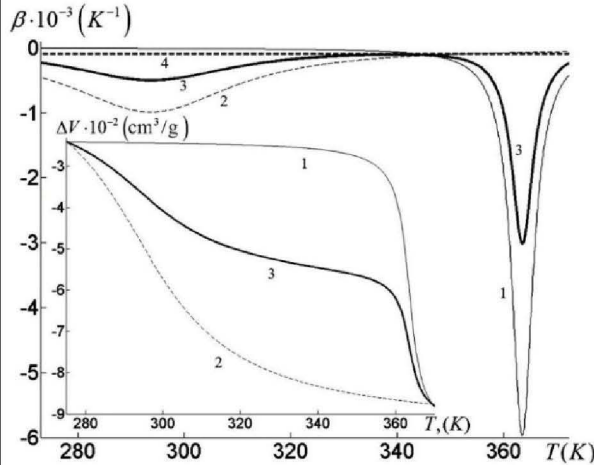


Fig. 5. Thermal expansion coefficient for HLSs on the basis of water + silicalite-1 (1), water + zeolite SSZ (2), their combination “water + 2 matrices”(3), and for a $\text{Ca}_{0.8}\text{La}_{0.2}\text{Fe}_2\text{As}_2$ specimen (4) (work [31]). The inset demonstrates the behavior of variations of the volume, as the temperature grows

constant loading (the initial pressure P_0). Nevertheless, those conditions gave rise to the pressure growth in the system at its heating (and to the pressure drop at cooling) owing to the isochoric heating/cooling of the system to the intrusion/extrusion temperature. Hence, while comparing the model curve plotted in accordance with Eq. (11) and the experimental one, the terms $(\frac{\partial V}{\partial T})_P T$ can be neglected, and the pressure growth can be taken into consideration in the form

$$P(T) = \left(\frac{\partial P}{\partial T}\right)_V (T - T_0) + P(T_0). \quad (12)$$

Using the values [39] $T_0 = 283 \text{ K}$, $P_0 = 80.5 \text{ MPa}$, $\frac{d\sigma_\infty}{dT} = -1.6 \times 10^{-4} \text{ J/m}^2/\text{K}$, $\sigma_\infty(T_0) = 74.31 \times 10^{-3} \text{ J/m}^2$, $\frac{1}{V_0} (\frac{\partial V}{\partial T})_P = 3 \times 10^{-4} \text{ K}^{-1}$, and $\frac{1}{P_0} (\frac{\partial P}{\partial T})_V = 2.2 \times 10^{-3} \text{ K}^{-1}$ and making allowance for the remarks made above, let us compare the theoretical curve of “thermal” intrusion/extrusion plotted in accordance with Eq. (11) and the corresponding experimental dependence (Fig. 4). One can see that Eq. (11) satisfactorily approximates experimental results (the theoretical curve is shifted with respect to the experimental one by about 4 K). A difference between the behavior of the liquid inflow/outflow during the heating/cooling of the system is also observed: the dispersion of the theoretical curve is smaller than that of the experimental

one. This difference is expectable, because the dependence $P(T)$, which is used in Eq. (11), does not consider the change in the volume owing to the gradual penetration/exit of the liquid into/from the pore matrix space. This means that, within the intrusion/extrusion interval, the temperature dependence of the pressure, $P(T)$, is less considerable. Nevertheless, the application of basic thermodynamic analysis gave satisfactory theoretical results, which can be improved by considering the features of a real thermomechanic system.

Note that, if an HLS/RC system combined of n different matrices is used, the first term in Eq. (2) reads

$$f(P) = \sum_i^n f_i(P), \quad (13)$$

where the function f_i demonstrates the dependence of the pressure on the pore distribution in the i -th matrix. Let us illustrate this trick by plotting the theoretical temperature dependence of TEC β in Fig. 5 (the derivative of Eq. (2) with respect to the temperature) and the “thermal” intrusion/extrusions $V(T)$ (Eq. (11)) for a heterogeneous system on the basis of water and silicalite-1 (this system is studied experimentally in this work) and for zeolite of the SST type with the use of the experimental PV -isotherm for the latter [13]. Let us also compare the same dependences of TEC β for the $\text{Ca}_{0.8}\text{La}_{0.2}\text{Fe}_2\text{As}_2$ specimen taken from work [31].

One can see from Fig. 5 that the required temperature dependence of the thermal expansion coefficient for HLS/RC can be obtained by varying the number and the kinds of capillary-porous matrices in the course of synthesis of a required heterogeneous system. There is a logic dependence between the TEC value and the temperature interval length, where this dependence holds: the smaller the dispersion of pore radii in the matrix, the larger is the TEC value and the narrower is the working temperature range (and *vice versa*). The maximum obtained TEC values were $\beta = -10^{-3} \text{ K}^{-1}$ for HLS/RC on the basis of water and zeolite of the SSZ type and $\beta = -5.7 \times 10^{-3} \text{ K}^{-1}$ for the HLS on the basis of silicalite-1. Those values exceed the TEC values for known materials by more than an order of magnitude [3–7, 30, 31]. While fabricating HLSs by combining the matrices specified above and taking them in the equal volume ratio, the

temperature interval where the TEC had considerable negative values was extended to about 100 K.

The adequacy of Eq. (2) for the description of isothermal processes [34] and the processes running at a constant loading, which are considered in this work, is a sound argument for its application as the equation of state for heterogeneous lyophobic systems. This is an extremely important factor for the possibility of a comprehensive thermodynamic analysis of the system. Equation (2) must also be verified, using the experimental results obtained under isobaric, isochoric, adiabatic, and other conditions. This verification, as well as experiments where the HLS/RCs with the minimal hysteresis H are used, will be the subject of following publications.

5. Conclusions

To summarize, the phenomenon of negative thermal expansion and the origins of its anomalous value for heterogeneous lyophobic systems, repulsive clathrates, has been studied experimentally and theoretically. The following main results were obtained.

1. It was experimentally shown for the first time that the coefficient of negative thermal expansion for the HLS/RC system can be larger by more than an order of magnitude than the corresponding values for known materials [3–7, 30, 31].

2. A physico-mathematical model of HLS/RC was proposed which takes into account the phenomenon of negative TEC and allows its value to be obtained proceeding from the parameters of the liquid and the matrix (or the combination of matrices). The theoretical approximation correlates well with the results calculated from experimentally obtained compression/expansion PV -isotherms of examined HLS/RCs.

3. On the basis of experimental data concerning the “thermal” intrusion/extrusion of the liquid in HLS/RC at a constant hydrostatic loading on the system, the equation of its state (Eq. (2)) was substantiated and verified.

4. A possibility of creating HLS/RCs with required negative TECs by combining several matrices into a single HLS/RC is indicated. Such systems can be prepared in the form of suspensions or colloid solutions.

The authors express their sincere gratitude to the Ministry of Education and Science, Youth and Sport of Ukraine for sponsoring the visit of O.V. Ievtushenko to the Institute of Chemistry of Clermont–

Ferrand at the Blaise Pascal University (France), where all the experiments and the preparation of HLS/RC specimens were carried out.

1. C.V. Raman and T.M.K. Nedungadi, *Nature* **145**, 147 (1940).
2. V.A. Eroshenko, *Dokl. Akad. Nauk Ukr. SSR Ser. A*, No. 10, 79 (1990).
3. V. Korhuis, N. Khosrovani, A.W. Sleight, N. Roberts, R. Dupree, and W.W. Warren, *Chem. Mater.* **7**, 412 (1995).
4. P. Tschaufeser and S.C. Parker, *J. Phys. Chem.* **99**, 10609 (1995).
5. J.S.O. Evans, T.A. Mary, T. Vogt, M.A. Subramanian, and A.W. Sleight, *Chem. Mater.* **8**, 2809 (1996).
6. J.S.O. Evans, *J. Chem. Soc. Dalton Trans.* **19**, 3317 (1999).
7. G.D. Barrera, J.A.O. Bruno, T.H.K. Barron, and N.L. Allan, *J. Phys. Condens. Matter* **17**, 217 (2005).
8. V.A. Eroshenko, in *Capillary Properties and Adhesion of Alloys* (Naukova Dumka, Kyiv, 1987), p. 100 (in Russian).
9. V.A. Eroshenko, *Promyshl. Teplotekhn.* **14**, 22 (1992).
10. V.A. Eroshenko and Yu.F. Lazarev, *Prikl. Mech. Tekhn. Fiz.* **53**, 98 (2012).
11. V. Eroshenko, R.-C. Regis, M. Soulard, and J. Patarin, *J. Amer. Chem. Soc.* **123**, 8129 (2001).
12. V. Eroshenko, R.-C. Regis, M. Soulard, and J. Patarin, *C.R. Acad. Sci. Ser. B* **3**, 111 (2002).
13. L. Tzanis, M. Trzpit, M. Soulard, and J. Patarin, *J. Phys. Chem. C* **116**, 20389 (2012).
14. V.A. Eroshenko, Patent France WO 01/55616 A1, F 16 F 9/00.
15. V.A. Eroshenko, I.I. Piatiletov, L. Coiffard, and V.P. Stoudenets, *Proc. Mech. Eng. D* **221**, 301 (2007).
16. C.V. Suci, S. Tani, and K. Miyoshi, *J. Syst. Design Dynam.* **4**, 899 (2010).
17. C.V. Suci and K. Yaguchi, *Exper. Mech. Int. J.* **49**, 383 (2009).
18. F.B. Surani, X. Kong, D.B. Panchal, and Y. Qiao, *Appl. Phys. Lett.* **87**, 163111 (2005).
19. V.A. Eroshenko, Patent USSR 1380357 A2, F 03 G, Bull. Izobr. N 3 (1996).
20. A. Laouir, L. Luo, D. Tondeur, T. Cachot, and P. Le Goff, *Am. Inst. Chem. Eng.* **49**, 764 (2003).
21. V.A. Eroshenko and Ya.G. Grosu, *Promyshl. Teplotekhn.* **33**, 73 (2011).
22. E.W. Washburn, *Phys. Rev.* **17**, 273 (1921).
23. L. Guillemot, *Ph.D. thesis* (Institut National des Sciences Appliquees de Lyon, 2010).
24. V.A. Eroshenko and S.G. Tkachenko, *Ukr. Fiz. Zh.* **38**, 1789 (1993).
25. V.S. Egorov, A.G. Portyanoi, A.P. Sorokin, V.G. Mal'tsev, and R.M. Voznesenskii, Patent Russia RU (11) 2138086 (13) C1 (<http://www.findpatent.ru/patent/213/2138086.html>).

26. S.L. Randzio, Chem. Soc. Rev. **25**, 383 (1996).
27. S.L. Randzio and J.-P.E. Grolier, Anal. Chem. **70**, 2327 (1998).
28. S.L. Randzio, Ch. Stachowiak, and J.-P.E. Grolier, J. Chem. Thermodyn. **35**, 639 (2003).
29. D.S. Nyce, *Linear Position Sensors: Theory and Application* (Wiley-Interscience, Hoboken, NJ, 2004).
30. B.K. Greve, K.L. Martin, P.L. Lee, P.J. Chupas, K.W. Chapman, and A.P. Wilkinson, J. Am. Chem. Soc. **132**, 15496 (2010).
31. A. Rebello, J.J. Neumeier, Z. Gao, Y. Qi, and Y. Ma, Phys. Rev. B **86**, 104303 (2012).
32. C.W. Li, T. Xiaoli, J.A. Munoz, J.B. Keith, S.J. Tracy, D.L. Abernathy, and B. Fultz, Phys. Rev. Lett. **107**, 195504 (2011).
33. J.P. Attfield, Nature **480**, 465 (2011).
34. O.V. Ievtushenko, V.A. Eroshenko, Y.G. Grosu, J.-M. Nedelec, and J.-P. E. Grolier, Phys. Chem. Chem. Phys. **15**, 4451 (2013).
35. N.L. Johnson, S. Kotz, and N. Balakrishnan, *Continuous Univariate Distributions, Vol. 1* (Wiley, New York, 1994).
36. T.G. Plachenov and S.D. Kolosentsev, *Porosimetry* (Khimiya, Leningrad, 1988) (in Russian).
37. V.A. Eroshenko and A.Yu. Fadeev, Ross. Khim. Zh. **40**, 92 (1996).
38. L. Coiffard, and V. Eroshenko, J. Colloid Interface Sci. **300**, 92 (2006).
39. *NIST Chemistry Web Book* <http://webbook.nist.gov/chemistry/>.
40. R.C. Tolman, J. Chem. Phys. **17**, 333 (1949).

Received 11.03.2013.

Translated from Ukrainian by O.I. Voitenko

Я.Г. Гросу, В.А. Єрошенко,
О.В. Євтушенко, Ж.-М. Неделек, Ж.-П.Е. Грол'є

ЯВИЩЕ АНОМАЛЬНОГО ВІД'ЄМНОГО
ТЕРМІЧНОГО РОЗШИРЕННЯ У КОНДЕНСОВАНІЙ
ГЕТЕРОГЕННІЙ ЛІОФОБНІЙ СИСТЕМІ

Резюме

У роботі експериментально підтверджено явище зменшення об'єму гетерогенної ліофобної системи (ГЛС) при збільшенні її температури, так зване явище від'ємного термічного розширення (ВТР). Показано, що для дослідженої ГЛС "сілікаліт-1 + вода" величина ВТР більш ніж на порядок перевищує показники ВТР для відомих матеріалів. Пояснено фізичні принципи, що лежать в основі отриманого явища та запропоновано математичну модель для його опису.

Exceptionally Large and Controlled Effect of Negative Thermal Expansion in Porous Heterogeneous Lyophobic Systems

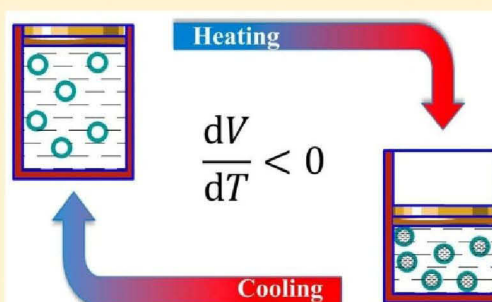
Valentin Eroshenko,^{*,†} Yaroslav Grosu,^{†,‡,§} Nikolay Tsyryn,[†] Victor Stoudenets,[†] Jean-Marie Nedelec,^{‡,§} and Jean-Pierre E. Grolier^{‡,§}

[†]Laboratory of Thermomolecular Energetics, National Technical University of Ukraine "Kyiv Polytechnic Institute", Prospect Peremogy 37, 03056 Kyiv, Ukraine

[‡]Institute of Chemistry of Clermont-Ferrand, BP 10448, Clermont University ENSCCF, 63000 Clermont-Ferrand, France

[§]CNRS, UMR 6296, ICCF, 24 av. des Landais, 63171 Aubière, France

ABSTRACT: Negative thermal expansion (NTE) is the process in which a system decreases its size upon heating and increases it upon cooling. NTE effect is unusual and useful for a great number of practical applications in the fields of electronics, medicine, mechanics, etc. In this work, NTE effect is experimentally investigated for three porous Heterogeneous Lyophobic Systems (HLS), associating water and two grafted mesoporous silicas or the microporous metal–organic framework ZIF-8. Considerable NTE effect, more than 1 order of magnitude higher than best-known materials, is observed for these systems. Additionally, it is demonstrated that for HLS, the temperature range in which NTE takes place is easily controlled by basic characteristics of the porous solid such as pore size distribution.



INTRODUCTION

Most materials and systems expand upon temperature increase and shrink when decreasing their temperature.¹ Reverse effect (when the size of the system is inversely proportional to its temperature) is called negative thermal expansion (NTE) and is rarely observed.^{1–4} Associating NTE materials with regular positive thermal expansion materials opens the possibility of creating systems with controlled (for example zero) expansivity. Such opportunity is attractive in a wide range of practical applications in the fields of electronics, medicine, photonics,⁴ high-precision optics, mechanics,^{5,6} etc.

Range of materials with NTE includes the ZrW₂O₈ (cubic zirconium tungstate) family,³ some zeolites and zeolite-like materials,⁷ the family of AM₂O₇ compounds (where A = U, Th, Zr, Hf, Sn and M = P and V),⁸ Cd(CN)₂, ReO₃,^{9,10} and NaZn₁₃-type La(Fe, Si, Co)₁₃ compounds.¹¹

The value of NTE $\{\alpha = (1/V)[(\partial V/\partial T)]_p\}$ and the temperature range (the possibility to set it) where NTE is observed are naturally considered as the most important parameters of this phenomenon. For most known materials, the value of NTE is about $\alpha \approx -10^{-6} \text{ K}^{-1}$. Yet for some materials, higher values were obtained and were fairly considered as huge: $\alpha = -1 \times 10^{-5} \text{ K}^{-1}$ for ScF₃¹² and $\alpha = -9 \times 10^{-5} \text{ K}^{-1}$ for crystals of Ca_{0.8}La_{0.2}Fe₂As₂.¹³ The colossal value of $\alpha = -1 \times 10^{-2} \text{ K}^{-1}$ registered for fluorine metal organic framework (FMOF-1) should be noted, even though it was obtained due to sorption of N₂ molecules during the cooling process of the porous FMOF-1 and was claimed by the authors as "apparent NTE".¹⁴

Large negative coefficient of linear thermal expansion $\{\alpha_i = (1/L)[(\partial L/\partial T)]_{p,i} = a,b,c\}$ along the *c*-orientation of about $\alpha_c \approx -10^{-5} \text{ K}^{-1}$ was reported for NaZn₁₃-type La(Fe, Si, Co)₁₃ compounds¹¹ and for porous polyacrylamide polymer film with $\alpha_c \approx -1.2 \times 10^{-3} \text{ K}^{-1}$.¹⁵ One of the highest values of *c*-axial linear negative thermal expansion were also registered for pentamorphic organometallic martensite reaching values of $\alpha_c \approx -7.9 \times 10^{-5} \text{ K}^{-1}$,¹⁶ for Ag₃[Co(CN)₆] with $\alpha_c \approx -1.3 \times 10^{-4} \text{ K}^{-1}$,^{17,18} for FMOF-1 with $\alpha_c \approx -1.7 \times 10^{-4} \text{ K}^{-1}$ under vacuum,¹⁴ for (S,S)-octa-3,5-diyne-2,7-diol with maximum value of $\alpha_c \approx -1.0 \times 10^{-4} \text{ K}^{-1}$,¹⁹ but due to exceptionally large values of positive thermal expansion along the *a* and *b* axes, overall (volumetric) thermal expansion of indicated materials is positive and is very large.

In this paper, we experimentally demonstrate that the orders of magnitude larger effect of negative volumetric thermal expansion (values of α) may be achieved for porous heterogeneous lyophobic systems (HLS) in a temperature range which can be easily controlled by basic characteristics of HLS. A sound thermodynamic analysis is also provided to explain the observed results.

OPERATIONAL PRINCIPLES

Porous heterogeneous lyophobic system (HLS) is an ensemble of porous solid with large specific surface area (400–2000 m²/

Received: March 4, 2015

Revised: April 20, 2015

g) and corresponding nonwetting liquid,^{20,21} which under certain conditions may have negative values of thermal expansion.^{22,23} The condition of lyophobicity (contact angle between solid material and corresponding liquid $\theta > 90^\circ$) does not allow for the liquid to spontaneously penetrate into the pores of the solid under ambient conditions (pressure and temperature). Forced intrusion of the liquid into the pores (say due to the increase of the pressure to some critical value P_{int}) decreases the volume of the HLS by the value of the pores volume of the lyophobic solid $\Delta V_{\text{int}} = -V_{\text{pores}}$. So the work that the system stores upon the intrusion process may be written as

$$W_{\text{int}} = -P_{\text{int}} \Delta V_{\text{int}} = P_{\text{int}} V_{\text{pores}} \quad (1)$$

The presence of nonwetting liquid inside the lyophobic pores is energetically unfavorable (capillary forces tend to expulse it), so the process of liquid extrusion from the pores is spontaneous and occurs when the pressure is decreased to some critical value P_{ext} . If liquid is fully expelled from the pores, the HLS returns to its initial state $\Delta V_{\text{ext}} = V_{\text{pores}}$. The work associated with the extrusion process which the system restores may be written as

$$W_{\text{ext}} = -P_{\text{ext}} \Delta V_{\text{ext}} = -P_{\text{ext}} V_{\text{pores}} \quad (2)$$

From eqs 1 and 2, it can be seen that specific mechanical energy which the HLS stores ($w_{\text{int}} = W_{\text{int}}/V_0^0$) and restores ($w_{\text{ext}} = W_{\text{ext}}/V_0^0$) is proportional to the porosity of the matrix $\varphi = [V_{\text{pores}}/(V_0^0)]$ and to the intrusion/extrusion pressures $P_{\text{int,ext}}$. Although extreme values of this parameter have obvious technical limitations. Here V_0^0 is initial volume of HLS.

In many cases, P_{int} and P_{ext} can be identified with Laplace capillary pressures:

$$P_{\text{int,ext}} = -\frac{\sigma \cos \theta_{A,R}}{kr_0} \quad (3)$$

where the advancing contact angle θ_A is used for the intrusion pressure P_{int} and the receding contact angle θ_R is used for the extrusion pressure P_{ext} ; σ is the surface tension of the liquid and k is a geometry parameter ($k = 0.5$ for cylinders and $k = 0.33$ for spheres), r_0 is an average pore radius. Due to the nonwetting condition ($\theta_{A,R} > 90^\circ$) $\cos \theta_{A,R} < 0$. Although it should be noted that direct application of eq 3 is often questionable for a HLS due to the small size of its pores: for microporous materials, where the diameter of the pore is only of few molecular layers,^{21,24–27} such macroscopic parameter as the contact angle θ does not exist. On the other hand for a mesoporous HLS, the extrusion pressure is additionally determined by the condition of critical bubble nucleation inside the pores^{28,29} and for both intrusion and extrusion pressures the effect of the line tension on the values of $\theta_{A,R}$ should be taken into account.^{29,30}

Reversible intrusion/extrusion process is followed by the development/reduction of a large “solid–liquid” interface Ω development as

$$\Delta V_{\text{int,ext}} = -kr \Delta \Omega \quad (4)$$

Hence if eq 3 is applicable, the mechanical energy that HLS stores/restores during the intrusion/extrusion process is determined by the Gibbs work of interface development/reduction:

$$\delta W_{\text{int,ext}} = -\sigma \cos \theta_{A,R} d\Omega \quad (5)$$

Such development/reduction of the interface Ω is followed by an endothermal/exothermal effect (breakage/recovery of intermolecular bonds of the liquid), so during compression/

decompression a HLS also stores/restores thermal energy in the form of Gibbs heat of interface development/reduction:

$$\delta Q_{\text{int,ext}} T \frac{d(\sigma \cos \theta_{A,R})}{dT} d\Omega \quad (6)$$

For a real HLS, as described above, the surface effects (which are dominant for a HLS) are always accompanied by classical bulk effects of the liquid and of the porous matrix. So the overall work and heat for HLS is defined as

$$\delta W_{c,d} = \delta W_{\text{int,ext}} + \delta W_0 = -\sigma \cos \theta_{A,R} d\Omega + P dV_0 \quad (7)$$

$$\delta Q_{c,d} = \delta Q_{\text{int,ext}} + \delta Q_0 = T \frac{d(\sigma \cos \theta_{A,R})}{dT} d\Omega + \delta Q_0 \quad (8)$$

Where indexes “c” and “d” stand for compression and decompression, respectively, “0” indicates the bulk phase (liquid and matrix), $dV_0 = dV_L + dV_M$ determines change of the volume of the liquid V_L and of the matrix V_M due to pressure or temperature change.

Total volume change for HLS may be written as

$$dV_{c,d} = dV_{\text{int,ext}} + dV_0 \quad (9)$$

In the general case, the volume of HLS is a function of pressure P and temperature T , hence the total differential of $V_{c,d}$ may be written:

$$dV_{c,d}(P, T) = \left(\frac{\partial V_{\text{int,ext}}}{\partial P} \right)_T dP + \left(\frac{\partial V_{\text{int,ext}}}{\partial T} \right)_P dT - V_0^0 \mu_T^0 dP + V_0^0 \alpha^0 dT \quad (10)$$

where $\mu_T^0 = -(1/V_0^0)[(\partial V_0/\partial P)]_{T,\Omega}$ is the isothermal compressibility and $\alpha^0 = -(1/V_0^0)[(\partial V_0/\partial T)]_{P,\Omega}$ is the isobaric coefficient of thermal expansion of components of the HLS (liquid and matrix) when interface effects do not take place (i.e., $\Omega = \text{const}$).

NEGATIVE THERMAL EXPANSION OF POROUS HETEROGENEOUS LYOPHOBIC SYSTEMS

The form of the first term of eq 10 is determined by the pore size distribution function of the matrix: $(\partial V_{\text{pores}}/\partial r)_T \sim (\partial V_{\text{int,ext}}/\partial P)_T \equiv f[P, P_{\text{int,ext}}(T)]$, considering that during the intrusion/extrusion process, the pressure is determined by the Laplace pressure, eq 3. This function may be obtained by one of the known techniques of porous materials characterization (mercury or water porosimetry, gas sorption, etc.). Particularly for a HLS, the pressure–volume diagram (Figure 2), which represents its mechanical energy performances, also provides information on pore size distribution function (isothermal porosimetry experiment). For example, if pore sizes are normally distributed, f may be considered as a Gaussian function normalized of the volume of the pores of the matrix V_{pores} :

$$f[P, P_{\text{int,ext}}(T)] \equiv \left(\frac{\partial V_{\text{int,ext}}}{\partial P} \right)_T = -\frac{V_{\text{pores}}}{\sqrt{2\pi}D} e^{-[P-P_{\text{int,ext}}(T)]^2/2D} \quad (11)$$

where $D = (P - P_{\text{int,ext}})^2$ is a dispersion of intrusion/extrusion pressures (caused by dispersion of pore radii—deviation from average value r_0).

By using the known thermodynamic identity $(\partial V/\partial T)_P = -(\partial P/\partial T)_V (\partial V/\partial P)_T$ and considering that during the intrusion/extrusion process the pressure in the HLS corresponds to the Laplace pressure (eq 3), one may write

$$\left(\frac{\partial V_{\text{int,ext}}}{\partial T}\right)_P = \frac{1}{kr_0} \left(\frac{\partial \sigma \cos \theta}{\partial T}\right)_V \left(\frac{\partial V_{\text{int,ext}}}{\partial P}\right)_T \equiv \frac{1}{kr_0} \left(\frac{\partial \sigma \cos \theta}{\partial T}\right)_V f[P, P_{\text{int,ext}}(T)] \quad (12)$$

Taking into account eqs 11 and 12, eq 10 may be rewritten as follows:

$$\begin{aligned} dV_{c,d}(P, T) = & \{f[P, P_{\text{int,ext}}(T)] - V_0^0 \mu_T^0\} dP \\ & + \left(\frac{1}{kr_0} \left(\frac{\partial \sigma \cos \theta}{\partial T}\right)_V f[P, P_{\text{int,ext}}(T)] \right. \\ & \left. + V_0^0 \alpha^0\right) dT \end{aligned} \quad (13)$$

Basically, eq 13 is a thermal equation of state of the HLS in the differential form, which takes into account the pore size distribution of the HLS matrix. Using this equation, we may determine isobaric coefficient of thermal expansion of HLS:

$$\alpha_{\text{int,ext}} \equiv \frac{1}{V_0^0} \left(\frac{\partial V_{c,d}}{\partial T}\right)_P = \alpha^0 + \frac{1}{kr_0 V_0^0} \left(\frac{\partial \sigma \cos \theta}{\partial T}\right)_V f[P, P_{\text{int,ext}}(T)] \quad (14)$$

Since $f_T < 0$, in the case of positive value of the derivative $(\partial \sigma \cos \theta / \partial T)_V$ (in general it may be either positive or negative), $\alpha_{\text{int,ext}}$ may become negative (effect of negative thermal expansion).

In Figure 1, the temperature dependence of α_{int} at $P = P_0 = 15$ MPa for the {WC8 + water} HLS obtained using eq 14 is

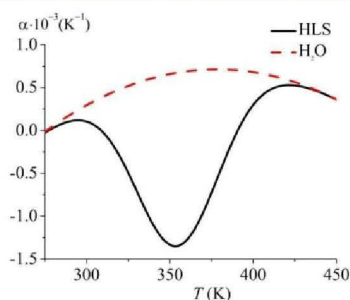


Figure 1. Isobaric coefficients of thermal expansion of the {WC8 + water} HLS and of water at 15 MPa.

presented (description of the system is provided in the Materials section). The values of $D = 2$ MPa and $P_{\text{int}}^0 = 19.11$ MPa for eq 11 was obtained experimentally from an isothermal ($T_0 = 303$ K) compression experiment (Figure 2). Temperature dependence of intrusion pressure for eq 11 was calculated as follows:

$$P_{\text{int}}(T) = \frac{\cos \theta}{kr} \frac{d\sigma}{dT} (T - T_0) + P_{\text{int}}^0 \quad (15)$$

where for simplicity, $\cos \theta$ was considered independent from temperature. The values of α^0 and $(d\sigma/dT)$ are well-known for

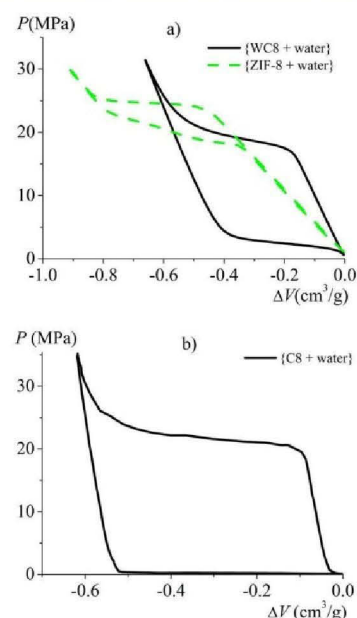


Figure 2. Isothermal (303 K) compression–decompression cycles of (a) {WC8 silica + water}, {ZIF-8 + water}, and (b) {C8 + water} systems.

water.³¹ Such simplifications are made only for demonstrative reasons. In fact, prediction of intrusion/extrusion temperature dependence is more complicated and requires consideration of size effects and temperature dependence of the contact angle.^{28–30}

As can be seen from Figure 1 the values of α for HLS may become negative in a certain temperature range, which indicates a negative thermal expansion. This effect takes place when the value of $P_{\text{int}}(T)$ gets closer to value of $P = P_0$ so that the intrusion provoked by the temperature increase occurs, which leads to the interface Ω development and the decrease of the volume of the HLS according to eq 4. The calculated value of α reaches a maximum value of almost $-1.5 \times 10^{-3} \text{ K}^{-1}$, which is more than an order of magnitude higher compared to best reported results.¹³ Additionally there is a simple method for determining the temperature range in which NTE occurs for the HLS: by choosing the matrix with the right values of the average pore radius r_0 and its dispersion $D_r = (r - r_0)^2$, the values of $P_{\text{int}}^0 = -[\sigma(T_0) \cos \theta_{A,R}(T_0)/kr_0]$ for eq 15 and D for eq 11 may be determined, respectively. The higher the value of D , the wider the temperature range the NTE. Higher values of P_{int}^0 shifts the temperature dependence of α (Figure 1) to a higher temperature and vice versa. If a more complicated temperature dependence of α is required, HLSs based on several (n) matrices may be used. In this case, eq 11 should be written as

$$f = \sum_n^{i=1} f_i \quad (16)$$

where f_i is determined by the characteristics of the i th matrix (for example as in eq 11).

Apart from the matrix properties, obviously the initial pressure P_0 and the properties of the liquid (such as $\sigma \cos \theta$) must be used for the NTE control. Particularly if heating/cooling of the system takes place at nonisobaric (say

polytropic) conditions, a temperature increase would not only cause the decrease of $P_{\text{int}}(T)$ value but also the increase of pressure P in the system. Which means that a slower temperature change is required for the values of the intrusion pressure and of the pressure in the system to obtain ($P \approx P$) and the NTE to occur. In what follows experimental investigation of three HLSs under such conditions is presented.

The above-described effect of Negative Thermal Expansion (NTE) is due to the intrusion/extrusion of guest molecules of a nonwetting liquid into the nanopores of the lyophobic solid, which under ambient conditions represents energetically unfavorable environment for these molecules. Meanwhile, the structure of the solid is preserved. Hence, the NTE effect of an HLS may also be considered as “apparent” by analogy with the effect described in ref 14. In both cases, it is interesting to note that NTE effect originates from a structuration of the solid beyond the atomic scale typically at the nanoscopic level. The important advantage in the case of HLSs is that such effect is reversible, so basically from the thermodynamic point of view, an HLS presents the working body in the form of a suspension possessing effect of negative thermal expansion.

EXPERIMENTAL SECTION

Materials. In the present work, 3 porous heterogeneous lyophobic systems HLSs based on water were used. Hydrophobic porous materials are as follows: (1) Commercial mesoporous silica gel SymmetryPrep C8, in the shape of 7 μm granules grafted with octylsilanes with density of 2.1 groups/ nm^2 according to the data provided by the supplier (WATERS). The average pore radius is 4.2 nm; the pore volume is 0.53 cm^3/g ; the HLS based on this matrix is referred to as {WC8 + water}. (2) KSK-G silica gel (GOZ VNII NP, Russia) grafted with octylsilanes with a density of 2.0 groups/ nm^2 according to the procedure described elsewhere.³² The average pore radius is 5.3 nm, the pore volume is 0.54 cm^3/g . The HLS based on this matrix is referred to as {C8 + water}. (3) Hydrophobic microporous Zeolitic imidazolate frameworks ZIF-8 purchased from Sigma-Aldrich as Basolite Z1200, with orifice of the pores of 0.34 nm and a huge surface area of 1800 m^2/g ; the HLS based on this matrix is referred to as {ZIF-8 + water}.

Equipment. A modified ST-7 M transiometer of the ST-7 model instrument (BGR-Tech)^{33–35} was used to obtain compression–decompression as well as heating–cooling cycles of the HLS. Detailed description of experimental setup is given elsewhere.²⁴ In this study, ST-7 M was used as PVT-stand with the possibility to perform measurements by controlling precisely the pressure within ± 0.15 MPa, volume within $\pm 3.3 \times 10^{-4}$ cm^3 and the temperature within ± 0.01 K.

For each experiment at isothermal conditions, 3 compression–decompression cycles were realized at a low rate of 1 MPa/min to ensure the good reproducibility of measurements.

Typical compression–decompression cycles are presented in Figure 2.

For experiments with variable temperature, heating and cooling were performed at 4×10^{-3} K/s rate. During the controlled temperature change, both volume (Figure 3) and pressure (Figure 4) of the system were recorded.

Additionally, PVT-stand developed in NTUU “KPI” described elsewhere^{32,36–38} was used in order to ensure the repeatability of obtained effects and to perform preliminary experiments on different HLSs (as this machine allows much faster regimes, compared to ST-7M, of both compression–

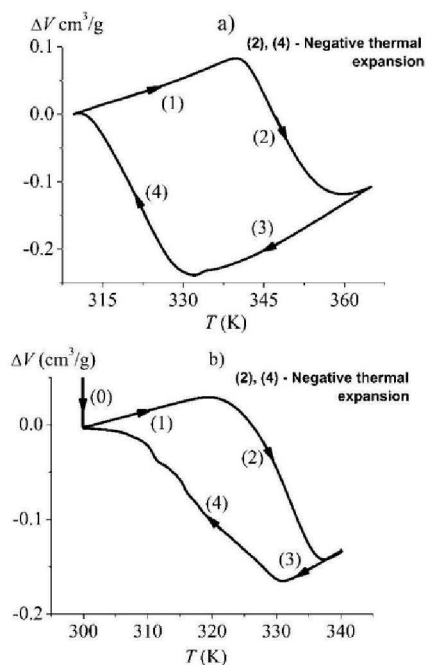


Figure 3. Heating–cooling cycles of (a) {WC8 silica + water} ($P_0 = 0.1$ MPa) and (b) {ZIF-8 + water} ($P_0 = 15$ MPa) systems.

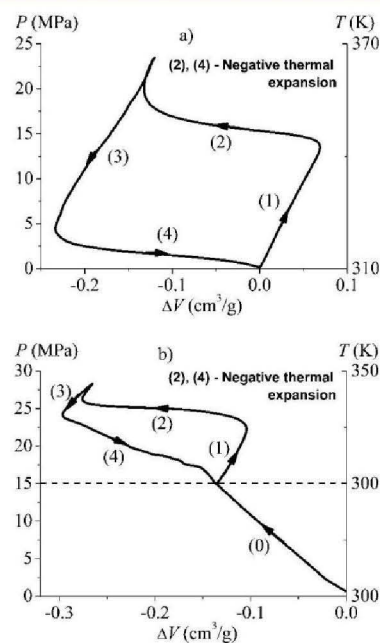


Figure 4. PV-diagrams during heating–cooling cycles of (a) {WC8 + water} ($P_0 = 0.1$ MPa) and (b) {ZIF-8 + water} ($P_0 = 15.0$ MPa) HLSs.

decompression and heating–cooling cycles) following the procedure described above.

EXPERIMENTAL RESULTS AND DISCUSSION

Compression–decompression cycles at constant controlled temperature were performed for all three porous heterogeneous lyophobic systems HLSs under investigation (Figure 2). The

D

DOI: 10.1021/acs.jpcc.5b02112
J. Phys. Chem. C XXXX, XXX, XXX–XXX

obtained PV -diagrams are well-reproducible and reversible with the presence of hysteresis for intrusion–extrusion pressure. All HLSs have typical plateau on PV -diagrams, which is due to intrusion of the liquid into the pores (for compression) and its extrusion (for decompression). Characteristics of the indicated cycles are presented in Table 1. The results are consistent with

Table 1. Characteristics of Isothermal Compression–Decompression Cycles of HLSs

HLS	P_{int} (MPa)	P_{ext} (MPa)	$\Delta V_{\text{int,ext}}$ (cm^3/g)
{ZIF-8 + water}	24.6	20.4	0.40
{WC8 + water}	19.5	2.3	0.39
{C8 + water}	21.5	0.15	0.47

previously published ones.^{25,27,29} The average value of the intrusion/extrusion pressure was taken as the middle point of the intrusion plateau on the PV -diagrams of HLSs. Although it may be seen that extrusion for {ZIF-8 + water} HLS occurs in two steps. Such behavior was discussed previously.³⁹

Next, heating–cooling cycles of HLSs were performed as follows (Figure 3 and Figure 4): under isothermal conditions ($T = T_0$), a certain initial pressure P_0 was set for each HLS, which corresponds to sequence (0) in Figures 3 and 4. Then the temperature of the system was increased linearly, yielding both volume (Figure 3) and pressure (Figure 4) variations in the system [see sequences (1) and (2) in Figures 3 and 4]. After reaching a certain maximum temperature, the system was cooled down to the initial temperature T_0 with the same rate, which corresponds to sequences (3) and (4) in Figures 3 and 4.

The corresponding temperature dependences of VT -diagrams are shown in Figure 3. For all HLSs, a similar dependence is observed. In a first sequence (1), an increase of temperature leads to an increase of the volume of the HLS due to the thermal expansion of its components (liquid and empty matrix). In a second sequence (2), at a certain temperature (when pressure in the system becomes equal to intrusion pressure at actual temperature), water penetrates inside the pores and is followed by a volume decrease (effect of negative thermal expansion (NTE) (i.e., HLS decreases its volume due to temperature increase). After pores of the matrix are completely filled with water, further increase of the temperature again leads to the increase of the volume of the HLS due to thermal expansion of water and filled matrix. During the consecutive cooling of the system, that is in sequences (3) and (4), opposite effects take place and the HLS return to initial conditions. The presence of a hysteresis loop on the VT -dependence (Figure 3) is expected due to its presence on PV -isotherms (Figure 2). Interestingly, for the {ZIF-8 + water} HLS, the positive temperature dependence of the intrusion pressure P_{int} was observed and it was shown that intrusion of the water into the pores of ZIF-8 can be provoked by cooling.²⁵ Which means that the intrusion due to the temperature increase observed in this work (Figure 2) was due to the pressure increase in the system. Whereas for the {WC8 + water} HLS, the P_{int} temperature dependence is negative,²⁹ which means that both the pressure increase and the intrusion pressure decrease contribute to intrusion during heating of this system.

For most applications, the hysteresis loop observed in Figure 2 is a undesirable effect for NTE, then the use of HLSs with minimum hysteresis would be preferable.

The maximum values of the negative thermal expansion coefficient $\epsilon = (1/V)(dV/dT)$ calculated from experimental data are listed in Table 2; they are more than 1 order of

Table 2. Coefficients of Negative Thermal Expansion of Different Systems/Materials

system/material	ϵ (K^{-1})	ref
{ZIF-8 + water}	-9×10^{-3}	this work
{WC8 + water}	-8×10^{-3}	this work
ScF_3	-1×10^{-5}	12
crystals of $\text{Ca}_{0.8}\text{La}_{0.2}\text{Fe}_2\text{As}_2$	-9×10^{-5}	13

magnitude higher than the known materials with the largest ϵ values.^{12,13} Here we use symbol ϵ (instead of α) to indicate that the NTE effect is not necessarily observed under isobaric conditions. While α is used to indicate isobaric coefficient of thermal expansion.

Corresponding PV -diagrams of the investigated HLSs during heating–cooling cycles are presented in Figure 4. It can be seen in sequence (1) that the initial temperature increase, which is followed by the expansion of the system (Figure 3), leads to a rapid pressure increase in the HLS. While in sequence (2), during the intrusion process, the pressure is much less sensitive to temperature [since at this stage the HLS decreases its volume in response to the temperature increase (Figure 3)]. Cooling of the system during sequences (3) and (4) brings it back to the initial state (volume and pressure wise). Naturally, the hysteresis loop is observed on the PV -diagram during the heating–cooling cycle.

It is important to note that the reversible heating–cooling cycle of the HLS may only occur if the initial pressure P_0 in the system does not exceed the minimum extrusion pressure of HLS at the initial temperature T_0 . Otherwise, cooling of the system down to T_0 does not provoke the extrusion of the liquid and hence the consecutive heating–cooling cycle would not be accompanied by the negative thermal expansion effect. Such a case is shown in Figure 5 for the {C8 + water} HLS for which

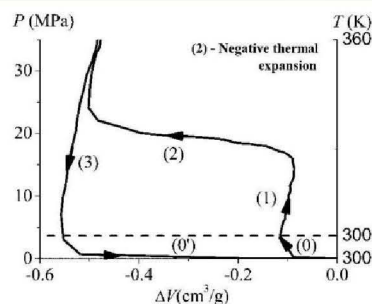


Figure 5. PV -diagram during heating–cooling cycle of {C8 + water} HLS ($P_0 = 3.5$ MPa).

the initial pressure $P_0 = 3.5$ MPa exceeds $P_{\text{ext}} = 0.5$ MPa at the initial temperature of 300 K (Figure 2). It can be seen that although heating of the system provokes the water intrusion [and NTE is observed in the sequence (2)], cooling the system to initial temperature [sequence (3)] does not bring the system to its initial volume as extrusion does not occur. Extrusion of the liquid from the pores of silica gel may be achieved only by a decrease of the pressure to atmospheric value [sequence (0')] in

E

DOI: 10.1021/acs.jpcc.5b02112
J. Phys. Chem. C XXXX, XXX, XXX–XXX

Figure 5]. After such action, the system may be used again to obtain the NTE effect.

CONCLUSION

In this paper, effect of negative thermal expansion (NTE) of three porous heterogeneous lyophobic systems (HLSs) is investigated experimentally and by detailed thermodynamic analysis. It is demonstrated that the coefficient of NTE is orders of magnitude higher for studied HLSs compared to the best-known materials and can be obtained in a temperature range, which may be easily controlled by basic characteristics of HLSs' matrices (mean pore size and associated pore size distribution). Unlike most materials and systems, which are in the solid form, HLSs are in the liquid suspension form; this opens new perspectives for practical applications where compensation of large positive thermal expansion is required.

AUTHOR INFORMATION

Corresponding Author

*Address: Valentin Eroshenko Laboratory of Thermomolecular Energetics, National Technical University of Ukraine "Kyiv Polytechnic Institute", Prospect Peremogy 37, 03056 Kyiv, Ukraine. E-mail: eroshenko@kpi.ua.

Author Contributions

The manuscript was written through contributions of all authors. All authors have given approval to the final version of the manuscript. All authors contributed equally.

Notes

The authors declare no competing financial interest.

REFERENCES

- Evans, J. Negative Thermal Expansion Materials. *Dalton Trans.* **1999**, *19*, 3317–3326.
- Raman, C. V.; Nedungadi, T. M. K. The α - β Transformation of Quartz. *Nature* **1940**, *145*, 147–147.
- Evans, J. S. O.; Mary, T. A.; Vogt, T.; Subramanian, M. A.; Sleight, A. W. Negative Thermal Expansion in ZrW_2O_8 and HfW_2O_8 . *Chem. Mater.* **1996**, *8*, 2809–2823.
- Barrera, G. D.; Bruno, J. A. O.; Barron, T. H. K.; Allan, N. L. Negative Thermal Expansion. *J. Phys.: Condens. Matter* **2005**, *17*, R217–R252.
- Evans, J. S.; Hu, Z.; Jorgensen, J. D.; Argyriou, D. N.; Short, S.; Sleight, A. W. Compressibility, Phase Transitions, and Oxygen Migration in Zirconium Tungstate, ZrW_2O_8 . *Science* **1997**, *275*, 61–65.
- Hao, Y.; Gao, Y.; Wang, B.; Qu, J.; Li, Y.; Hu, J.; Deng, J. Negative Thermal Expansion and Magnetic Properties of $Y_2Al_3Fe_{14-x}Mn_x$ Compounds. *Appl. Phys. Lett.* **2011**, *78*, 3277–3279.
- Tschaufeser, P.; Parker, S. C. Thermal Expansion Behavior of Zeolites and AlPO₄s. *J. Phys. Chem.* **1995**, *99*, 10609–10615.
- Korthuis, V.; Khosrovani, N.; Sleight, A. W.; Roberts, N.; Dupree, R.; Warren, W. J. Negative Thermal Expansion and Phase Transitions in the ZrV_2-xPxO_7 Series. *Chem. Mater.* **1955**, *7*, 412–417.
- Takenaka, K. Negative Thermal Expansion Materials: Technological Key for Control of Thermal Expansion. *Sci. Technol. Adv. Mater.* **2012**, *13*, 013001-1–013001-11.
- Chatterji, T.; Hansen, T. C.; Brunelli, M.; Henry, P. F. Negative Thermal Expansion of ReO_3 in the Extended Temperature Range. *Appl. Phys. Lett.* **2009**, *94*, 241902–241902.
- Huang, R.; Liu, Y.; Fan, W.; Tan, J.; Xiao, F.; Qian, L.; Li, L. Giant Negative Thermal Expansion in $NaZn_{13}$ -type La (Fe, Si, Co) 13 Compounds. *J. Am. Chem. Soc.* **2013**, *135*, 11469–11472.
- Greve, B. K.; Martin, K. L.; Lee, P. L.; Chupas, P. J.; Chapman, K. W.; Wilkinson, A. P. Pronounced Negative Thermal Expansion from a Simple Structure: Cubic ScF_3 . *J. Am. Chem. Soc.* **2010**, *132*, 15496–15498.
- Rebello, A.; Neumeier, J. J.; Gao, Z.; Qi, Y.; Ma, Y. Giant Negative Thermal Expansion in La-doped $CaFe_2As_2$. *Phys. Rev. B* **2012**, *86*, 104303–1–104303–6.
- Yang, C.; Wang, X.; Omary, M. A. Crystallographic Observation of Dynamic Gas Adsorption Sites and Thermal Expansion in a Breathable Fluorous Metal–Organic Framework. *Angew. Chem., Int. Ed.* **2009**, *121*, 2538–2543.
- Shen, X.; Viney, C.; Johnson, E. R.; Wang, C.; Lu, J. Q. Large Negative Thermal Expansion of a Polymer Driven by a Submolecular Conformational Change. *Nat. Chem.* **2013**, *12*, 1035–1041.
- Panda, M. K.; Runčevski, T.; Sahoo, S. C.; Belik, A. A.; Nath, N. K.; Dinnebier, R. E.; Naumov, P. Colossal Positive and Negative Thermal Expansion and Thermosalient Effect in a Pentamorphic Organometallic Martensite. *Nat. Commun.* **2014**, *5*, 1–8.
- Goodwin, A. L.; Kepert, C. J. Negative Thermal Expansion and Low-Frequency Modes in Cyanide-Bridged Framework Materials. *Phys. Rev. B* **2005**, *71*, 140301–1–140301–4.
- Goodwin, A. L.; Calleja, M.; Conterio, M. J.; Dove, M. T.; Evans, J. S.; Keen, D. A.; Peters, L.; Tucker, M. G. Colossal Positive and Negative Thermal Expansion in the Framework Material Ag₃[Co(CN)₆]. *Science* **2008**, *319*, 794–797.
- Das, D.; Jacobs, T.; Barbour, L. J. Exceptionally Large Positive and Negative Anisotropic Thermal Expansion of an Organic Crystalline Material. *Nat. Mater.* **2009**, *9*, 36–39.
- Eroshenko, V. A. Heterogeneous Thermodynamic System. Eroshenko Cycle of Transformation of Thermal Energy into Mechanical Energy and Devices to Achieve It (in Russian). USSR-Russian Patent 1,254,811, 1981.
- Eroshenko, V.; Regis, R. C.; Soulard, M.; Patarin, J. Energetics: A New Field of Applications for Hydrophobic Zeolites. *J. Am. Chem. Soc.* **2001**, *123*, 8129–8130.
- Eroshenko, V. A. Thermomolecular Energy (in Russian). *Ind. Heat Eng.* **1992**, *1–3*, 22–25.
- Grosu, Y.; Eroshenko, V.; Ievtushenko, O.; Nedelec, J. M.; Grolier, J. P. E. Anomalous Negative Thermal Expansion in a Condensed Heterogeneous Lyophobic System. *Ukr. J. Phys.* **2014**, *59*, 69–78.
- Ievtushenko, O. V.; Eroshenko, V. A.; Grosu, Y. G.; Nedelec, J. M.; Grolier, J. P. E. Evolution of the Energetic Characteristics of {Silicalite-1+ Water} Repulsive Clathrates in a Wide Temperature Range. *Phys. Chem. Chem. Phys.* **2013**, *15*, 4451–4457.
- Grosu, Y.; Eroshenko, V.; Nedelec, J.-M.; Grolier, J.-P. E. A New Working Mode for Molecular Springs: Water Intrusion Induced by Cooling and Associated Isobaric Heat Capacity Change of {ZIF-8 + Water} System. *Phys. Chem. Chem. Phys.* **2014**, *17*, 1572–1574.
- Tzani, L.; Trzpit, M.; Soulard, M.; Patarin, J. Energetic Performances of Channel and Cage-Type Zeolites. *J. Phys. Chem. C* **2012**, *116*, 20389–20395.
- Ortiz, G.; Nouali, H.; Marichal, C.; Chaplais, G.; Patarin, J. Energetic Performances of the Metal-Organic Framework ZIF-8 by High Pressure Water Intrusion-Extrusion Experiments. *Phys. Chem. Chem. Phys.* **2013**, *15*, 4888–4891.
- Lefevre, B.; Saugey, A.; Barrat, J. L.; Bocquet, L.; Charlaix, E.; Gobin, P. F.; Vigier, G. Intrusion and Extrusion of Water in Hydrophobic Mesopores. *J. Chem. Phys.* **2004**, *120*, 4927–4938.
- Grosu, Y.; Ievtushenko, O.; Eroshenko, V.; Nedelec, J. M.; Grolier, J. P. E. Water Intrusion/Extrusion in Hydrophobized Mesoporous Silica Gel in a Wide Temperature Range: Capillarity, Bubble Nucleation and Line Tension Effects. *Colloids Surf., A* **2014**, *441*, 549–555.
- Guillemot, L.; Biben, T.; Galarneau, A.; Vigier, G.; Charlaix, É. Activated Drying in Hydrophobic Nanopores and the Line Tension of Water. *Proc. Natl. Acad. Sci. U.S.A.* **2012**, *109*, 19557–19562.
- NIST Chemistry WebBook. webbook.nist.gov/chemistry.
- Fadeev, A. Y.; Eroshenko, V. A. Study of Penetration of Water into Hydrophobized Porous Silicas. *J. Colloid Interface Sci.* **1997**, *187*, 275–282.

(33) Randzio, S. L.; Grolier, J. P. E.; Zaslona, J.; Quint, J. R. Procédé et dispositif pour l'étude de transitions physicochimiques et leurs applications (In French). French patent 9109227, 1994.

(34) Randzio S. L., Grolier J. P. E., Zaslona J., Quint J. R. Sposób i urządzenie do badania przemian fizykochemicznych (In Polish). Polish Patent 295285, 1995.

(35) Randzio, S. L. Scanning transmittometry. *Chem. Soc. Rev.* **1996**, *25*, 383–392.

(36) Eroshenko, V.; Regis, R. C.; Soulard, M.; Patarin, J. Les Systèmes Hétérogènes «Eau–Zéolithe Hydrophobe»: de Nouveaux Ressorts Moléculaires. *C. R. Acad. Sci.* **2002**, *3*, 111–119.

(37) Eroshenko, V. A.; Fadeev, A. Y. Water Porosimetry Technique in Studying of Hydrophobic Porous Solids. *Mendeleev Chem. J.* **1996**, *40*, 116–125.

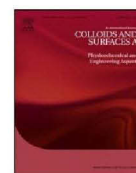
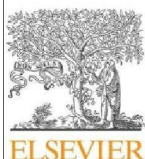
(38) Eroshenko, V. A.; Fadeev, A. Intrusion and Extrusion of Water in Hydrophobized Porous Silica. *Colloid J.* **1995**, *57*, 446–449.

(39) Grosu, Y.; Renaudin, G.; Eroshenko, V.; Nedelec, J.-M.; Grolier, J.-P. E. Synergetic Effect of Temperature and Pressure on Energetic and Structural Characteristics of {ZIF-8 + Water} Molecular Spring. *Nanoscale* **2015**, accepted. DOI: 10.1039/C5NR01340B.

3.2. TEMPERATURE DEPENDENCES OF INTRUSION AND EXTRUSION PRESSURES

As shown by the thermodynamic analysis provided in previous paragraphs the temperature dependence of intrusion/extrusion pressure $\frac{dP_{int,ext}}{dT}$ can be considered as one of the most important characteristics of HLSs, which appear in the equations of all thermal coefficients and heat capacities.

Detailed analysis of temperature dependences of intrusion and extrusion pressures for several HLSs was performed. Investigation of the mesoporous {Waters C8 + water} HLS is presented in the reference (Grosu et al. 2014c). After reprint of this publication presented, which is give here after, the results of the same investigation are presented for the mesoporous {Hypersil C18 + water} HLS. Investigation of intrusion/extrusion pressure temperature dependences of microporous {ZIF-8 + water} and {Silicalite-1 + water} HLSs are presented in references (Grosu et al. 2015b) and (Ievtushenko et al. 2013), respectively. Reprints of these publications are given in the Paragrap 3.3.



Water intrusion/extrusion in hydrophobized mesoporous silica gel in a wide temperature range: Capillarity, bubble nucleation and line tension effects



Ya. Grosu^a, O. Ievtushenko^{a,b,c}, V. Eroshenko^{a,*}, J.M. Nedelec^{b,c}, J.P.E. Grolier^{b,c,*}

^a National Technical University of Ukraine, Kyiv Polytechnic Institute, Laboratory of Thermomolecular Energetics, Prospect Peremogy 37, 03056 Kyiv, Ukraine

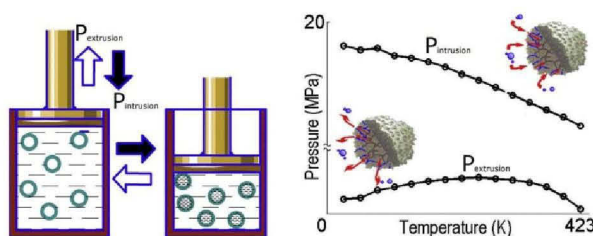
^b Clermont Université, ENSCCF, Institute of Chemistry of Clermont-Ferrand, BP 10448, 63000 Clermont-Ferrand, France

^c CNRS, UMR 6296, ICCF, 24 Av. des Landais, 63171 Aubière, France

HIGHLIGHTS

- Intrusion and extrusion pressures of {silica gel C8+water} system were investigated in the 10–150 °C temperature range.
- Unexpected non-linear temperature dependence for extrusion pressure is observed.
- Results are treated by means of capillary and nucleation theories.
- Temperature dependence of contact angles is calculated under the “Sharp-kink” approximation.
- Line tension effect is taken into account.

GRAPHICAL ABSTRACT



ARTICLE INFO

Article history:

Received 20 August 2013

Received in revised form 2 October 2013

Accepted 3 October 2013

Available online xxx

Keywords:

Interface

Porous media

PV-isotherm

Heterogeneous lyophobic system

Contact angle

ABSTRACT

The pressure under which forced intrusion of non-wetting liquid into capillary takes place (intrusion pressure) is a very important parameter for a number of devices using intrusion/extrusion characteristics of porous materials. For molecular springs, dumpers and shock-absorbers based on heterogeneous lyophobic systems (HLS) their efficiency is determined by the pressure of both intrusion and extrusion, the latter being the pressure under which intruded liquid extrudes from the capillary. In this paper the temperature dependence of intrusion and extrusion pressures of a {grafted silica gel+water} HLS is investigated in the 10–150 °C temperature range. An unexpected non-linear temperature dependence of extrusion pressure is obtained. The interpretation of these results is provided with the help of capillary and bubble nucleation theories. The calculations include the line tension effect and contact angles temperature dependence.

© 2013 Elsevier B.V. All rights reserved.

1. Introduction

Methods of forced intrusion of non-wetting liquid (such as mercury or water porosimetry) are widely used for porous materials characterization in such fields as catalysis, chromatography, adsorption, pharmaceutical and petroleum science [1,2] and are still under improvement [3]. The process of reversible intrusion of water into hydrophobic porous media (with contact angle $\theta \gg 90^\circ$)

* Corresponding author at: Clermont Université, ENSCCF, Institute of Chemistry of Clermont-Ferrand, BP 10448, 63000 Clermont-Ferrand, France.

E-mail addresses: eroshenko@kpi.ua, vae29@i.com.ua (V. Eroshenko), j-pierre.grolier@univ-bpclermont.fr (J.P.E. Grolier).

forms the basis for molecular springs (repulsive clathrate) operation [4–9]; while novel high efficient shock-absorbers based on heterogeneous lyophobic systems (HLS) take advantage of liquid intrusion irreversibility [10–18]: the pressure under which forced intrusion takes place (intrusion pressure) is much higher than the pressure under which intruded water extrudes from the lyophobic pores (extrusion pressure). Naturally, these processes are temperature dependent. But when it comes to wetting, temperature dependence still remains one of the problems to be solved, especially if size effects take place and, therefore, line tension should be taken into account.

Experiments indicate that intrusion pressure P_{int} decreases if the temperature of the system T increases for a wide range of pore radii r from 0.3 to 11.6 nm [8,9,16,17,19–21] and as far as we know, the opposite effect is rarely observed [22]. While extrusion pressure P_{ext} temperature dependence may be negative (documented for porous media with $r \sim 0.3$ nm [8,9]), as well as positive ($r \sim 1.3$ –11.6 nm [16,17,19–21,23]) for different materials. Qualitatively negative dependence on temperature for both intrusion and extrusion pressures is consistent with the capillary theory, taking into account negative temperature dependence of surface tension γ and contact angle θ [24–29]. The observed positive temperature dependence of extrusion pressure requires positive temperature dependence of contact angle, to be explained by means of the capillary theory [16,20], which is a rather rare case [25–29]. Another way to explain such behavior is to use the nucleation theory and assume that the limiting factor for liquid extrusion is the critical bubble nucleation [19,23].

In this paper we present an attempt to identify and explain the mechanisms responsible for intrusion/extrusion pressure temperature dependence for mesoporous matrices and water. For this purpose P_{int} and P_{ext} measurements have been performed within the 10–150 °C temperature range for {hydrophobized silica gel C8+water} system. As far as we know, such experiments have never been performed for 100–150 °C temperatures, although {hydrophobized silica gel C8+water} system became the object of intensive investigation in the field of unconventional mechanical energy dissipation [10–18]. The shock-absorber developed on the basis of this type of HLS has a number of interesting properties: typical value of dissipated energy is ~ 12 J/g (per gram of matrix) [14–17]; achieved power value reaches, but is not limited to 50 W/cm³ (twice as large as that for hydraulic shock-absorber) [14]; frequency bandwidth is 3–4 times higher (up to 22 Hz and more [14,17]) in comparison with classical analogs. Along this line devices have demonstrated high performance stability – up to 10 million of full compression–decompression cycles [15].

An unexpected temperature dependence of extrusion pressure, observed in the present paper, is interpreted in terms of the capillary and nucleation theories. The line tension effect and contact angle temperature dependence are taken into account.

2. Theoretical basis

The condition of the mechanical equilibrium for the three-phase “drop on a flat solid” system is usually described by the Young equation [30]:

$$\gamma_{\text{SL}} + \gamma \cos \theta^\infty = \gamma_{\text{SV}} \quad (1)$$

where γ , γ_{SL} , γ_{SV} are the interfacial tensions between the liquid and the vapor, the solid and the liquid, the solid and the vapor, respectively, θ^∞ is the equilibrium contact angle the drop makes with the solid.

If the drop size (radius r) is microscopic, the specific excess energy on the “solid–liquid–vapor” line, *i.e.* the line tension τ (J/m), must be taken into account. In the case of high curvature, the τ

value affects the contact angle magnitude, as it is reflected in the modified Young equation [31]:

$$\cos \theta = \cos \theta^\infty + \frac{\tau}{\gamma r} \quad (2)$$

where θ and θ^∞ are the contact angles of microscopic and macroscopic (in this case τ effect is negligible) drops, respectively.

It should be noted that the theory of the line tension is still under development, and there are ongoing discussions concerning the magnitude and even the sign of τ [32]. Several experiments and simulations give a typical absolute value for τ of the order $\sim 10^{-10}$ to 10^{-12} J/m [32–36]. Keeping in mind Eq. (2), Laplace–Washburn equation for intrusion, extrusion pressures may be written as [37]:

$$P_{\text{int,ext}}^C = -\frac{2\gamma \cos \theta_{A,R}}{r} \quad (3)$$

which applies for both the intrusion process (int) and the extrusion process (ext) with the respective corresponding advancing contact angle (A) and receding contact angle (R); the superscript (C) indicates that the intrusion/extrusion pressure is calculated according to the capillary theory.

Since most of the liquids exhibit negative temperature derivatives for the surface tension and the contact angle, $d\gamma/dT < 0$ and $d\theta/dT < 0$ respectively, the experimentally observed [8,9,16,17,19–21] negative temperature dependence of intrusion pressure, $dP_{\text{int}}/dT < 0$, may be explained by Eq. (3). As regards the observed positive temperature derivative of the extrusion pressure, $dP_{\text{ext}}/dT > 0$, Eq. (3) would stand only if the corresponding contact angle derivative is positive, $d\theta/dT > 0$, which is rarely the case [25–29]. This crucial point stimulated us to find other mechanisms, which determine such observed temperature dependence. Some authors [19,23] advance the idea that the limiting factor for intruded water to extrude from the pores is the critical bubble nucleation process. Using classical nucleation theory [38] the work of critical bubble formation in a cylindrical pore may be written as [19]:

$$\Delta \Omega_C \approx P_{\text{ext}}^N K_1 r^3 + \gamma K_2 r^2 + \tau K_3 r \Leftrightarrow P_{\text{ext}}^N \approx \frac{\Delta \Omega_C - \gamma K_2 r^2 - \tau K_3 r}{K_1 r^3} \quad (4)$$

where K_i are numerical polynomial coefficients which depend only on contact angle θ_R ; P_{ext}^N is considered as the extrusion pressure under which the critical bubble nucleation occurs. Later Charlaix and co-workers [23] provided the following K_i expressions as (applicable for $90^\circ \leq \theta \leq 135^\circ$)¹:

$$\begin{aligned} K_1 &= 4.1661 + 0.11242 \cdot \sin(0.11819 \cdot \theta_R + 0.16478); \\ K_2 &= 20.32 - 0.14879 \cdot \theta_R; \\ K_3 &= 3.355 + 0.14136 \cdot \theta_R - 0.00054762 \cdot \theta_R^2. \end{aligned} \quad (5)$$

Such approach allowed to explain [19,23] experimentally measured increase of the extrusion pressure with increasing temperature for a number of HLS's, using the assumption that work of critical bubble formation in a cylindrical pore $\Delta \Omega_C$ may be written as:

$$\Delta \Omega_C = A k_B T \quad (6)$$

where A is a constant, k_B is the Boltzmann constant. Eq. (6) follows from the usual theory of thermally activated nucleation, where the number of critical nucleus n created per unit time and unit volume

¹ Originally expressions in Eq. (5) were obtained using equilibrium contact angle [23].

writes as $n = (bt)^{-1} \cdot e^{-\Delta\Omega_c/k_B T}$, which is the classical Arrhenius law, where b is a microscopic length and t is a microscopic time. Assuming that the prefactor $(bt)^{-1}$ varies negligibly with temperature, one may write

$$\Delta\Omega_c = -k_B T \cdot \ln(nbt) \equiv A \cdot k_B T. \quad (7)$$

Eqs. (4)–(6) allow to predict the extrusion pressure P_{ext}^N within the nucleation theory (the coefficient A may be calculated using initial conditions) and to predict its positive temperature dependence. Although this model was successfully applied for the 25–80 °C temperature range [19,23], as this will be shown hereafter, further generalization may be required in the case of higher temperatures.

3. Materials and methods

The heterogeneous lyophobic system (HLS) used in this paper, consists of water and nanoporous grafted silica gel also known as SymmetryPrep C8, 7 μm supplied by the firm WATERS. The grafting was done with octylsilanes with density 2.1 groups/nm² according to the data provided by the firm. The pore size distribution is very narrow for this type of material, formed by the aggregation of elementary particles. The average pore radius of the material before grafting is 4.6 nm, but the effective calculated pore radius is 3.8 nm [20], taking into consideration grafting thickness [39,40]. Nitrogen sorption measurements on the grafted material at 77 K give a porous volume of 0.53 cm³/g and an average pore radius of 4.2 nm, obtained from the desorption branch using the classical BJH equation [20].

A modified ST-7M transiometer of the ST-7 model instrument (BGR-Tech) [41–44] was used to obtain PV-isotherms of the HLS along compression–decompression cycles. Detailed description of experimental setup is given elsewhere [9].

Sample preparation and experimental procedure are described below. A specific amount of silica gel was introduced into a metallic capsule, which is sealed by a metallic–ceramic porous cover. The approximate weight of the porous powder in the capsule was 0.5 g. The capsule with powder was thoroughly degassed to about 10^{−2} mbar for 2–4 h. After the degassing procedure, the capsule with powder was filled in situ with degassed distilled water through the porous cover. Filling of capsules with water was carried out under vacuum. This procedure guarantees efficient filling of interparticle spaces by water. Next, the capsule containing the HLS is positioned into the measuring vessel while an identical capsule just filled with degassed water is positioned into the reference vessel; both vessels were filled before with degassed water. The pressure–volume diagrams for the {silica gel C8+water} HLS were obtained for 15 temperatures, from 10 °C to 150 °C, while the chamber volumes (i.e. the associated volume changes measured by the bellow devices connected to the vessels) were recorded simultaneously during repeated cycling scans. At each temperature several compression and expansion cycles were realized at 1 MPa/min rate to make sure, of the good reproducibility of measurements. Previously it was verified that such compression rate does not bring any additional effects in comparison with lower (quasi-static) rates [20]. As a matter of fact, measurements under quasi reversible mode are prerequisite for transiometric runs. Measurements were performed by controlling precisely the three thermodynamic variables, namely: pressure within ± 0.15 MPa, volume within $\pm 3.3 \times 10^{-4}$ cm³ and a constant temperature within ± 0.01 K.

Typical compression–decompression cycles are presented in Fig. 1. Intrusion/extrusion pressure values indicated in Fig. 2 correspond to half of volume variation occurring during the system compression/decompression.

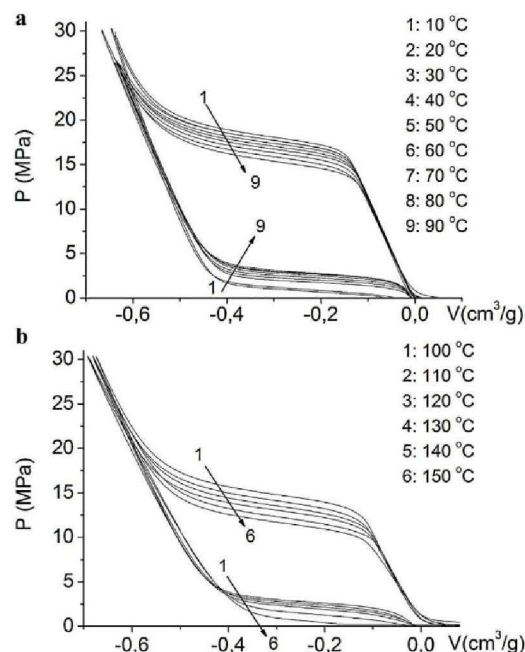


Fig. 1. PV-isotherms of {silica gel C8+water} heterogeneous lyophobic system under (a) 10–90 °C and (b) 100–150 °C.

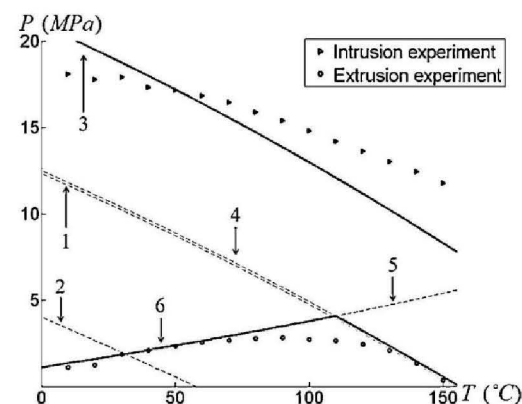


Fig. 2. Temperature dependence of intrusion P_{int} and extrusion P_{ext} pressures of {silica gel C8+water} system. Symbols, triangles and circles, are experimental points. Lines represent the model calculations: 1 and 2 – $P_{\text{int}}^{\text{C}\infty}$ and $P_{\text{ext}}^{\text{C}\infty}$ calculated according to Eq. (3); 3 and 4 – $P_{\text{int}}^{\text{C}}$ and $P_{\text{ext}}^{\text{C}}$ calculated according to Eq. (3), taking into account line tension effect, Eq. (2); 5 – extrusion pressure calculated according to nucleation theory, Eq. (4); 6 – P_{ext}^N extrusion pressure calculated according to capillary and nucleation approaches, Eq. (12).

4. Results and discussion

The PV-isotherms obtained for {silica gel C8+water} heterogeneous lyophobic system (HLS) are presented in Fig. 1a and b. Evolution of intrusion and extrusion with temperature is shown in Fig. 2. In the 10–90 °C range (Figs. 1a and 2) intrusion pressure decreases and extrusion pressure increases as temperature increases. Such results are consistent with previous experimental works: Lefevre et al. [19] reported it for two temperatures (25 and 50 °C) for {silica gel MCM-41+water} HLS; Coiffard and Eroshenko [20] and Suci et al. [16] observed such results for the same system investigated in this paper in 5–60 °C and 0–50 °C ranges, respectively;

Charlaix and coworkers [23] obtained it as well in the range 30–80 °C for some HLS's of the type {water+MCM-41, +HMS, and +SBA-15 silica gels}.

Remarkably in the 100–150 °C temperature range, in contrast to intrusion process, the extrusion pressure changes its trend and decreases with temperature increase (Figs. 1b and 2). Thus the overall temperature dependence of extrusion pressure is non-linear with a maximum around $T_{\text{extr}} = 100$ °C (Fig. 2). As far as we know, such behavior as well as experiment under 100–150 °C have not been reported before.

Obviously, any extreme (maximum) points, especially under high temperatures, may bring the question of structural changes of the matrix or phase transitions of the liquid. The argument in favor of the matrix stability is the absence of extreme points in the intrusion pressure curve and absolute cycle repeatability; not less than 3 cycles have been performed for every temperature with no visual changes in the PV-diagram. As for the liquid, it should be noted, that under the extrusion pressures experimented in this work, the boiling temperature of water is much higher than temperature under which intrusion–extrusion cycles were performed. The exception to both above arguments is with experiment at $T = 150$ °C, as under this temperature some of intruded water has not extruded from the matrix (Fig. 1b) and in fact under pressure of ~ 0.4 MPa, the boiling temperature of water is 144 °C [24]. Yet it should be kept in mind that reference data provided by NIST is obtained for bulk liquid. Effect of spatial confinement of water inside nanopores is not taken into account. And it is well established that such conditions may tremendously affect the properties of the liquid. For example, using molecular dynamic simulations it was shown for {hydrophobic carbon nanotubes + water} system that the boiling temperature of water increases considerably [50,51]. This effect depends on the pore radius. The fact that with the experiment at $T = 150$ °C not all the water extruded from the pores most probably means that only small pores of heteroporous matrix (deviation of intrusion pressure can be seen in Fig. 1) became empty. This means that we are dealing with pores with less than 4 nm radii. The hypothesis that spatial confinement of indicated pores may increase the boiling temperature of water by ~ 6 °C (e.g., due to effects described in [50,51]) seems reasonable. In addition, this point is not in contradiction with the general temperature trend of extrusion pressure (Fig. 2).

To identify the mechanisms responsible for observed behavior (Figs. 1 and 2) we next apply capillary and nucleation theories and compare them to experiment. To use classical capillary approach, i.e. Eq. (3), one must know the surface tension γ and contact angles $\theta_{A,R}$ temperature dependence. Water's γ is well documented and usually is considered as a linear function of temperature, but in the present rather wide temperature range it is preferable to use a more exact representation of experimental results [24] expressed using a second degree polynomial (Fig. 3):

$$\gamma = 0.0955 - (2.8116 \times 10^{-6}) \cdot T - (2.5497 \times 10^{-7}) \cdot T^2 \quad (8)$$

As for the contact angle temperature dependence, there is no unified theory to describe it and the lack of experimental data does not allow to formulate a more exact approximation. Recently it was suggested [29] to use the "Sharp kink" approximation approach [45,46] to predict the contact angle temperature dependence. Despite its simple expression, this method shows good agreement with experimental data [29]. Accordingly to this approach the following relation may be written:

$$\cos \theta^\infty = -1 + \frac{\Delta \rho}{\gamma} I, \quad (9)$$

where $\Delta \rho$ is the difference between the liquid and vapor densities (which are temperature dependent); negative Van der Waals integral $I = - \int_{z_{\min}}^{\infty} V(z) dz$, where $V(z)$ is a potential, responsible

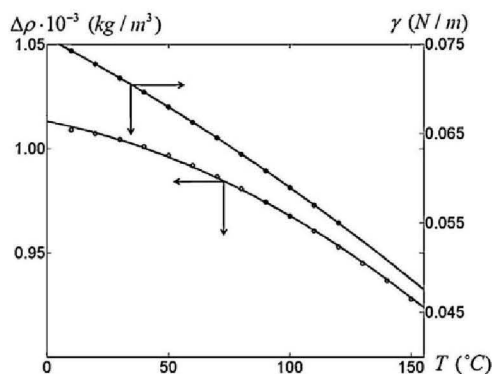


Fig. 3. Surface tension γ and density difference $\Delta \rho$ for water. Points are experimental data [24], lines are approximations with Eq. (9) for γ and Eq. (10) for $\Delta \rho$.

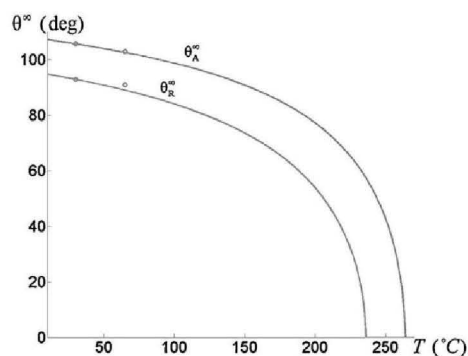


Fig. 4. Contact angles temperature dependence. Points are for experiments [28], lines represent model calculations.

for intermolecular interactions between the solid and the liquid phases, that is the potential energy of the adsorbate (liquid) to the substrate (solid), z being the interfacial distance.

The value of $V(z)$ has been determined for a number of solids and liquids (including water) [29] and a rather important conclusion is that with a certain approximation $V(z)$ may be considered as weekly temperature dependent, i.e. $I \approx \text{const}$ in Eq. (9), and consequently may be obtained using the initial condition, that is the value of contact angle at a given temperature. Advantageously, the values of advancing θ_A^∞ and receding θ_R^∞ contact angles of water on a flat surface which has been modified in the same way that our silica gel, have been measured by Fadeev and McCarthy [28]: $\theta_A^\infty = 106$, $\theta_R^\infty = 93$ °. Using the more exact approximation of $\Delta \rho$ according to experimental data [24] (Eq. (10), Fig. 3), we obtain $I_A = 3.5454 \times 10^{-5}$ (J · m/kg) and $I_R = 5.1363 \times 10^{-5}$ (J m/kg) for advancing and receding cases, respectively.

$$\Delta \rho = 910.3086 + 0.9833 \cdot T - 0.0022 \cdot T^2 \quad (10)$$

Next, we use Eqs. (8)–(10) and the calculated values of I_A and I_R to obtain the mathematical representation of the temperature dependence for the respective contact angles, as shown in (Fig. 4), and compare it to available experimental data [28].

Fig. 4 shows that the "Sharp kink" approximation gives quite satisfactory results in good agreement with available experimental measurements [28], yet of course, experimental data in a higher temperatures range is necessary for reliable verification/conformation of the model.

At this point since the temperature dependences of both contact angles and surface tension are explicitly established, we may

try to calculate the intrusion and extrusion pressures using the capillary theory. By introducing those dependences in Eq. (3) and using $r = 3.8$ nm [20], we see in Fig. 2 (curves 1 and 2) that the calculated curves are in poor agreement with experimental data: the intrusion pressure values are too low, while extrusion curve does not agree qualitatively with experiment. As the theoretical dependence for intrusion shows correct trend, it may be improved by taking into account the high curvature of the pore space, which affects the contact angle θ according to Eq. (2) through line tension τ [31].

Recently, by relating the line tension τ and retention force that acts on a drop on a tilted surface Tadmor pointed out [47] that in the case of axial symmetry and absolute isotropy, τ may be calculated using macroscopic values of advancing and receding contact angles as:

$$\tau = \gamma(\cos \theta_A^\infty - \cos \theta_R^\infty)r. \quad (11)$$

With respect that most of theoretical investigations of the line tension τ are made at the microscopic level, Eq. (11) is remarkably practical and simple, although in the case of capillary systems, such as the HLS's under investigation, we of course consider this approach more as approximate estimation of τ value, rather than its exact determination. Therefore, we should neglect the temperature dependence of τ , which (as well as the proper τ value) is still the subject of scientific debate [32].

By substituting $\gamma \approx 0.071$ (N/m) [24], $r = 3.8$ (nm) [20], $\theta_A^\infty = 106^\circ$, $\theta_R^\infty = 93^\circ$ [28] into Eq. (11) one obtains $\tau = -6.03 \times 10^{-11}$ (J/m). Such value of line tension is fully compatible with previous results [32–36]. Then, using the calculated τ value and Eq. (2) one may see the rather significant effect that the line tension has on the contact angles values – $\theta_A \approx 120^\circ$ and $\theta_R \approx 106^\circ$ – and on the intrusion and extrusion pressures curves, see Fig. 2 (curves 3 and 4), calculated using these values. Effectively, the theoretical intrusion pressure curve which incorporates such τ effect is much closer to experimental data. Obviously, the model calculations yield a temperature dependence more pronounced than experimental data, with a maximum deviation of about 30% around 150°C . Taking into account several assumptions, concerning contact angle and line tension temperature dependences and also the fact that none of experimental values of intrusion pressure were used, the achieved result (Fig. 2) may be considered as quite satisfactory. As for the extrusion curve, as expected its trend does not qualitatively corroborate the experimental dependence in the 10 – 90°C range, whereas it surprisingly agrees well with experiment in the 120 – 150°C range, with maximum deviation of less than $\sim 15\%$. Most likely, such agreement suggests that the extrusion pressure of investigated HLS is determined by capillary forces only under some conditions (such as high temperature). To verify this hypothesis the 10 – 90°C region must be examined.

To explain the experimentally observed [16,17,19–21,23] positive dependence of extrusion pressure, which in our case takes place at temperatures below 90°C , Lefevre et al. [19] suggested that the limiting factor for water to extrude from the pores is the nucleation of the critical bubble process. This phenomenon was successfully used to describe the observed extrusion pressure behavior for several hydrophobic silica gels in the 25 – 80°C range [19,23]. Applying this method (described in Section 2), i.e. Eqs. (4)–(6) and calculated contact angle value θ_R , we compare the theoretical curve to experiments in Fig. 2 (curve 5); for this the A constant was calculated using as initial condition – the experimental value of extrusion pressure at 30°C .

As observed in Fig. 2, the nucleation theory agrees well with experimental data for extrusion pressure in the 10 – 90°C range, with maximum deviation of only about 8%. For higher temperatures model and experiment are in qualitative disagreement.

From the above discussion and Fig. 2 the condition for liquid to extrude from the pores of the matrix may be suggested as follows: the pressure in the system must be lower than the pressure under which the critical bubble nucleation takes place and low enough for the capillary forces to overcome and expulse it (Eq. (3)). In other words, this condition may be written as:

$$P_{\text{ext}} = \min(P_{\text{ext}}^N, P_{\text{ext}}^C) \quad (12)$$

Keeping in mind that Eqs. (4)–(6) (used to calculate P_{ext}^N) were obtained under the condition of transition of pore from completely filled with liquid state to partially filled with vapor state [19,23], Eq. (12) basically means that if HLS pressure P drops below P_{ext}^N , the bubble will be formed in the pore, yet it does not guarantee that liquid will be extruded from the pore. The liquid extrusion takes place only if $P < P_{\text{ext}}^C$, i.e. the external force is lower than the capillary force able to expulse the liquid from energetically unfavorable pore environment.

Fig. 2 (curve 6) shows that the maximum deviation ($\sim 30\%$) between experiment and the theoretical representation according to Eq. (12) is observed in the 80 – 120°C range, near the expected maximum, and this is probably a consequence of the difference between linear theoretical and non-linear experimental temperature dependences of P_{ext}^N . Obviously, account of temperature dependence of τ in Eqs. (4)–(6), may directly affect (improve) the accuracy of calculation of the P_{ext}^N . However, it seems there is no solid approach to determine such dependence in the literature yet, which forces us to use the assumption $\tau = \text{const}$ for all the calculations.

Another source of error may be the contact angles temperature dependence, especially for intrusion process (advancing contact angle θ_A), for which the model curve is too temperature sensitive. Basically the theoretical curves should better fit the experiment, if according to the suggested model large contact angles (in our case θ_A) would be insignificantly temperature dependent, while small contact angles (in our case θ_R) on the contrary decreased significantly with temperature (close to the dependence expressed by Eq. (8)). Although the “Sharp-kink” approximation [29,45,46] does reconstitute such effect, it is not as strongly marked as, for example, with the Sullivan’s microscopic model [26]. However, the latter is rather cumbersome and its application is beyond the scope of this article.

Assumption of cylindrical symmetry may also bring additional inaccuracy to calculations in Eqs. (3)–(5), as C8 silica gel in fact has more complex topology [20]. And it should be noted that in general contact angles measured on flat surface (used from [28]) and on tilted surfaces (used to obtain Eq. (11) [47]) may have slightly different values [48].

In addition, mesoporous environment of silica gel C8 (pore diameter ~ 8 nm gives about 30 molecular diameters for water) may undoubtedly affect the properties of confined water, but it seems that such influence is rather weak if water thickness is greater than 2 – 3 nm (for example [49]).

In general, obtained theoretical and experimental results (Fig. 2) suggest that nucleation [19,23] and capillary [37] theories, including the line tension effect using the modified Young equation [31] and calculated using Tadmor’s approach [47,48], as well as account of contact angles temperature dependence, using the “Sharp-kink” approximation [29,45,46], may be used to identify and describe intrusion and extrusion pressures temperature dependence for mesoporous heterogeneous lyophobic systems, such as {silica gel C8 + water} system.

Further investigations will concern the study of HLS’s based on other matrices and liquids over a wide temperature range with the aim to improve the theoretical basis for the line tension and contact angles temperature dependence.

5. Conclusions

Experimental and theoretical investigation of intrusion and extrusion pressures temperature dependence for {Silica gel C8 + water} heterogeneous lyophobic system (HLS) has been realized over the temperature range 10–150 °C. As far as we know, experiments in the 100–150 °C temperature interval are performed for the first time for this system.

Previously unobserved negative temperature dependence of extrusion pressure is observed in the 100–150 °C range (Figs. 1b and 2). Within the 10–90 °C range the dependence is positive (Figs. 1a and 2), which is in agreement with previous works [16,17,19–21,23]. As expected, intrusion pressure decreased with temperature over the entire temperature range (Figs. 1 and 2).

It is suggested that the extrusion pressure of investigated HLS is determined by two phenomena (Eq. (12)): the bubble nucleation and capillary forces.

The “Sharp-kink” approximation [29,45,46] was used to account for the contact angles temperature dependence.

It is shown that advancing/receding contact angles measured on the flat surface may be used to calculate intrusion/extrusion pressures, but the line tension effect must be taken into account for mesoporous silica gel.

Satisfactory agreement between experimental data and model may serve as argument to validate the use of suggested approach to predict intrusion/extrusion pressures of mesoporous HLS.

Obtained results will be useful for a wide range of applications dealing with capillary phenomena, especially for the development and improvement of new high-efficiency shock-absorber based on HLS investigated in this paper [10–17].

Acknowledgements

One of us (O.V. I.) gratefully acknowledges the financial support from The Ministry of Education and Science, Youth and Sports of Ukraine for his six month stay at Institute of Chemistry of Clermont-Ferrand, where all experimental measurements have been carried out.

References

- [1] A.Y. Fadeev, V. Eroshenko, Study of penetration of water into hydrophobized porous silicas, *J. Colloid Interface Sci.* 187 (1997) 275.
- [2] J. Rouquerol, G. Baron, R. Denoyel, H. Giesche, J. Groen, P. Klobes, P. Levitz, A.V. Neimark, S. Rigby, R. Skudas, K. Sing, M. Thommes, K. Unger, Liquid intrusion and alternative methods for the characterization of macroporous materials (IUPAC technical report), *Pure Appl. Chem.* 84 (2012) 107–136.
- [3] A. Cavazzini, N. Marchetti, L. Pasti, R. Greco, F. Dondi, A. Laganà, A. Cioglia, F. Gasparrini, A new method to investigate the intrusion of water into porous hydrophobic structures under dynamic conditions, *Anal. Chem.* 85 (2013) 19–22.
- [4] V.A. Eroshenko, Soviet Patent No. 1,254,811, 1981, [priority of 24.07.1981, updated 02.09.1993 (date of free public access)].
- [5] V. Eroshenko, R.C. Regis, M. Souillard, J. Patarin, Energetics: a new field of applications for hydrophobic zeolites, *J. Am. Chem. Soc.* 123 (33) (2001) 8129–8130.
- [6] V. Eroshenko, R.C. Regis, M. Souillard, J. Patarin, The heterogeneous systems water–hydrophobic zeolites: new molecular springs, *C.R. Phys.* 3 (1) (2002) 111–119.
- [7] L. Tzanis, M. Trzpit, M. Souillard, J. Patarin, Energetic performances of channel and cage-type zeolites, *J. Phys. Chem. C* 116 (2012) 4802–4808.
- [8] Yu Qiao, V.K. Punyamurtula, A. Han, X. Kong, F.B. Surani, Temperature dependence of working pressure of a nanoporous liquid spring, *Appl. Phys. Lett.* 89 (2006) 251905.
- [9] O.V. Ievtushenko, V.A. Eroshenko, Y.G. Grosu, J.-M. Nedelec, J.-P.E. Grolier, Evolution of the energetic characteristics of {silicalite-1 + water} repulsive clathrates in a wide temperature range, *Phys. Chem. Chem. Phys.* 15 (12) (2013) 4451.
- [10] V.A. Eroshenko, Patent 94/14856, 1994, p. 1.
- [11] V.A. Eroshenko, Patent WO 01/55616 A1, 2001, p. 1.
- [12] C.V. Suci, T. Iwatsubo, S. Deki, Investigation of a colloidal damper, *J. Colloid Interface Sci.* 259 (2003) 62.
- [13] A.V. Erochenko, A new paradigm of mechanical energy dissipation; Part 1: theoretical aspects and practical solutions, *Proc. Inst. Mech. Eng., Part D, J. Automobile Eng.* 221 (2007) 285–300.
- [14] A.V. Erochenko, I. Piatiletov, L. Coiffard, V. Stoudenets, A new paradigm of mechanical energy dissipation. Part 2: experimental investigation and effectiveness of a novel car damper, *Proc. Inst. Mech. Eng., Part D, J. Automobile Eng.* 221 (2007) 301–312.
- [15] C.V. Suci, K. Yaguchi, Endurance tests on a colloidal damper destined to vehicle suspension, *Exp. Mech. Int. J.* 49 (2009) 383.
- [16] C.V. Suci, S. Tani, K. Miyoshi, Experimental study on the thermal characteristics of a colloidal damper, *J. Syst. Des. Dynamics* 4 (6) (2010) 899.
- [17] L. Guillemot, Institut National des Sciences Appliquées de Lyon (2010) (Ph.D. Thesis).
- [18] C.V. Suci, T. Iwatsubo, K. Yaguchi, M. Ikenaga, Novel and global approach of the complex and interconnected phenomena related to the contact line movement past a solid surface from hydrophobized silica gel, *J. Colloid Interface Sci.* 283 (1) (2005) 196–214.
- [19] B. Lefevre, A. Saugey, J.L. Barrat, L. Bocquet, E. Charlaix, P.F. Gobin, G. Vigier, Intrusion and extrusion of water in hydrophobic mesopores, *J. Chem. Phys.* 120 (2004) 10.
- [20] L. Coiffard, V. Eroshenko, Temperature effect on water intrusion/extrusion in grafted silica gels, *J. Colloid Interface Sci.* 300 (2006) 304–309.
- [21] L. Guillemot, A. Galarneau, G. Vigier, T. Abensur, É. Charlaix, New device to measure dynamic intrusion/extrusion cycles of lyophobic heterogeneous systems, *Rev. Sci. Instrum.* 83 (2012) 105105.
- [22] A. Han, W. Lu, T. Kim, V. Punyamurtula, Y. Qiao, The dependence of infiltration pressure and volume in zeolite Y on potassium chloride concentration, *Smart Mater. Struct.* 18 (2009) 024005.
- [23] L. Guillemot, T. Biben, A. Galarneau, G. Vigier, É. Charlaix, Activated drying in hydrophobic nanopores and the line tension of water, *Proc. Natl. Acad. Sci. U.S.A.* 109 (48) (2012) 19557–19562.
- [24] NIST Chemistry Web Book, <http://webbook.nist.gov/chemistry/>
- [25] A.W. Adamson, Potential distortion model for contact angle and spreading 2. Temperature dependent effects, *J. Colloid Interface Sci.* 44 (2) (1973) 273.
- [26] D.E. Sullivan, Surface tension and contact angle of a liquid–solid interface, *J. Chem. Phys.* 74 (4) (1981) 2604.
- [27] J.D. Bernardin, Issam Mudawar, C.B. Walsh, E.I. Franses, Contact angle temperature dependence for water droplets on practical aluminum surfaces, *Int. J. Heat Mass Transfer* 40 (5) (1997) 1017–1033.
- [28] A.Y. Fadeev, T.J. McCarthy, Trialkylsilane monolayers covalently attached to silicon surfaces: wettability studies indicating that molecular topography contributes to contact angle hysteresis, *Langmuir* 15 (1999) 3759–3766.
- [29] R. Garcia, K. Osborne, E. Subashi, Validity of the “Sharp-Kink approximation” for water and other fluids, *J. Phys. Chem. B* 112 (2008) 8114–8119.
- [30] T. Young, An essay on the cohesion of fluids, *Philos. Trans. R. Soc. Lond. Ser. A* 95 (1805) 65.
- [31] V.S. Vesselovsky, V.N. Pertzov, Adhesion of air bubbles to the solid surface, *Zh. Fiz. Khim.* 8 (1936) 245–259.
- [32] A. Amirfazli, A.W. Neumann, Status of the three-phase line tension, *Adv. Colloid Interface Sci.* 110 (2004) 121–141.
- [33] J. Drelich, J.L. Wilbur, J.D. Miller, G.M. Whitesides, Contact angles for liquid drops at a model heterogeneous surface consisting of alternating and parallel hydrophobic/hydrophilic strips, *Langmuir* 12 (7) (1996) 1913–1922.
- [34] A. Amirfazli, D.Y. Kwok, J. Gaydos, A.W. Neumann, Line tension measurements through drop size dependence of contact angle, *J. Colloid Interface Sci.* 205 (1) (1998) 1–11.
- [35] J.Y. Wang, S. Betelu, B.M. Law, Line tension effects near first-order wetting transitions, *Phys. Rev. Lett.* 83 (18) (1999) 3677–3680.
- [36] T. Pompe, S. Herminghaus, Three-phase contact line energetics from nanoscale liquid surface topographies, *Phys. Rev. Lett.* 85 (9) (2000) 1930–1933.
- [37] E.W. Washburn, The dynamics of capillary flow, *Phys. Rev.* 17 (3) (1921) 273.
- [38] J.S. Rowlinson, B. Widom, *Molecular Theory of Capillarity*, Oxford University, New York, 1989.
- [39] A. Fadeev, S.M. Yu, Staroverov, Geometric structural properties of bonded layers of chemically modified silicas, *J. Chromatogr. A* 447 (1988) 103–116.
- [40] V.A. Eroshenko, A. Fadeev, Intrusion and extrusion of water in hydrophobized porous silica, *Colloid J.* 57 (4) (1995) 446–449.
- [41] S.L. Randzio, J.-P.E. Grolier, J. Zaslona, J.R. Quint, French Patent No. 9109227, 1994, Polish Patent No. 295285, 1995.
- [42] S.L. Randzio, Scanning titrimetry, *Chem. Soc. Rev.* 25 (6) (1996) 383–392.
- [43] S.L. Randzio, J.-P.E. Grolier, Supercritical titrimetry of polymers, *Anal. Chem.* 70 (11) (1998) 2327–2330.
- [44] S.L. Randzio, C. Stachowiak, J. Grolier, Titrimetric determination of the three-phase curve in asymmetric binary systems, *J. Chem. Thermodyn.* 35 (4) (2003) 639–648.
- [45] S. Dietrich, M. Schick, Order of wetting transitions, *Phys. Rev. B* 33 (7) (1986) 4952.
- [46] E. Cheng, M.W. Cole, W.F. Saam, J. Treiner, Helium prewetting and nonwetting on weak-binding substrates, *Phys. Rev. Lett.* 67 (8) (1991) 1007–1010.

- [47] R. Tadmor, Line energy, line tension and drop size, *Surf. Sci.* 602 (14) (2008) 108–111.
- [48] R. Tadmor, P.S. Yadav, As-placed contact angles for sessile drops, *J. Colloid Interface Sci.* 317 (2008) 241–246.
- [49] U. Raviv, P. Laurat, J. Klein, Fluidity of water confined to subnanometre films, *Nature* 413 (2001) 51–54.
- [50] V.V. Chaban, V.P. Oleg, Water boiling inside carbon nanotubes: toward efficient drug release, *ACS Nano* 5 (7) (2011) 5647–5655.
- [51] V.V. Chaban, V.V. Prezhdo, O.V. Prezhdo, Confinement by carbon nanotubes drastically alters the boiling and critical behavior of water droplets, *ACS Nano* 6 (3) (2012) 2766–2773.



Corrigendum to “Water intrusion/extrusion in hydrophobized mesoporous silica gel in a wide temperature range: Capillarity, bubble nucleation and line tension effects”
[Colloids Surf. A: Physicochem. Eng. Aspects 441 (January) (2014) 549–555]

Ya. Grosu^a, O. Ievtushenko^{a,b,c}, V. Eroshenko^{a,*}, J.M. Nedelec^{b,c}, J.P.E. Grolier^{b,c,*}

^a National Technical University of Ukraine, Kyiv Polytechnic Institute, Laboratory of Thermomolecular Energetics, Prospect Peremogy 37, 03056 Kyiv, Ukraine

^b Clermont Université, ENSCCF, Institute of Chemistry of Clermont-Ferrand, BP 10448, 63000 Clermont-Ferrand, France

^c CNRS, UMR 6296, ICCF, 24 av. des Landais, 63171 Aubière, France

The Van der Waals integrals $I_A = 3.5454 \times 10^{-5}$ (J m/kg) and $I_R = 5.1363 \times 10^{-5}$ (J m/kg) quoted in the paper corresponds to microscopic advancing and receding contact angles respectively. While for calculation the temperature dependence of macroscopic advancing and receding contact angles in the Fig. 4 we naturally used Van der Waals integrals that corresponds to macroscopic case, which are $I_A^\infty = 5.1363 \times 10^{-5}$ (J m/kg) and $I_R^\infty = 6.7197 \times 10^{-5}$ (J m/kg), not the values of I_A and I_R , as it is indicated in the paper. Values of I_A^∞ and I_R^∞ can be directly obtained from Eq. (9) using macroscopic contact angles θ_A^∞ and θ_R^∞ , while values of I_A and I_R can be obtained from the same equation using microscopic contact angles θ_A and θ_R .

There are also few obvious typos in the paper. In the Fig. 3 $\Delta\rho$ axe should have 10^3 factor instead of 10^{-3} . On the page 550, in the right column, on the 12th line after Eq. (3), symbol “>” should be used instead of “<”, to be consistent with the description in the text. On the page 553, in the right column, in 7th line of 3rd paragraph symbol of line tension τ should be used instead of symbol of pressure P_{ext}^N .

The authors would like to apologise for any inconvenience caused.

DOI of original article: <http://dx.doi.org/10.1016/j.colsurfa.2013.10.022>.

* Corresponding author at: Clermont Université, ENSCCF, Institute of Chemistry of Clermont-Ferrand, BP 10448, 63000 Clermont-Ferrand, France.
E-mail addresses: eroshenko@kpi.ua, vae29@i.com.ua (V. Eroshenko), j-pierre.grolier@univ-bpclermont.fr (J.P.E. Grolier).

Similar analysis of intrusion and extrusion pressures was performed for the {Hypersil C18 + water} HLS. The experimental measurements are presented in Figures 3.6. and 3.7. Evolution of the mechanical energy stored and restored during intrusion-extrusion cycle of this HLS is presented in Table 3.1.

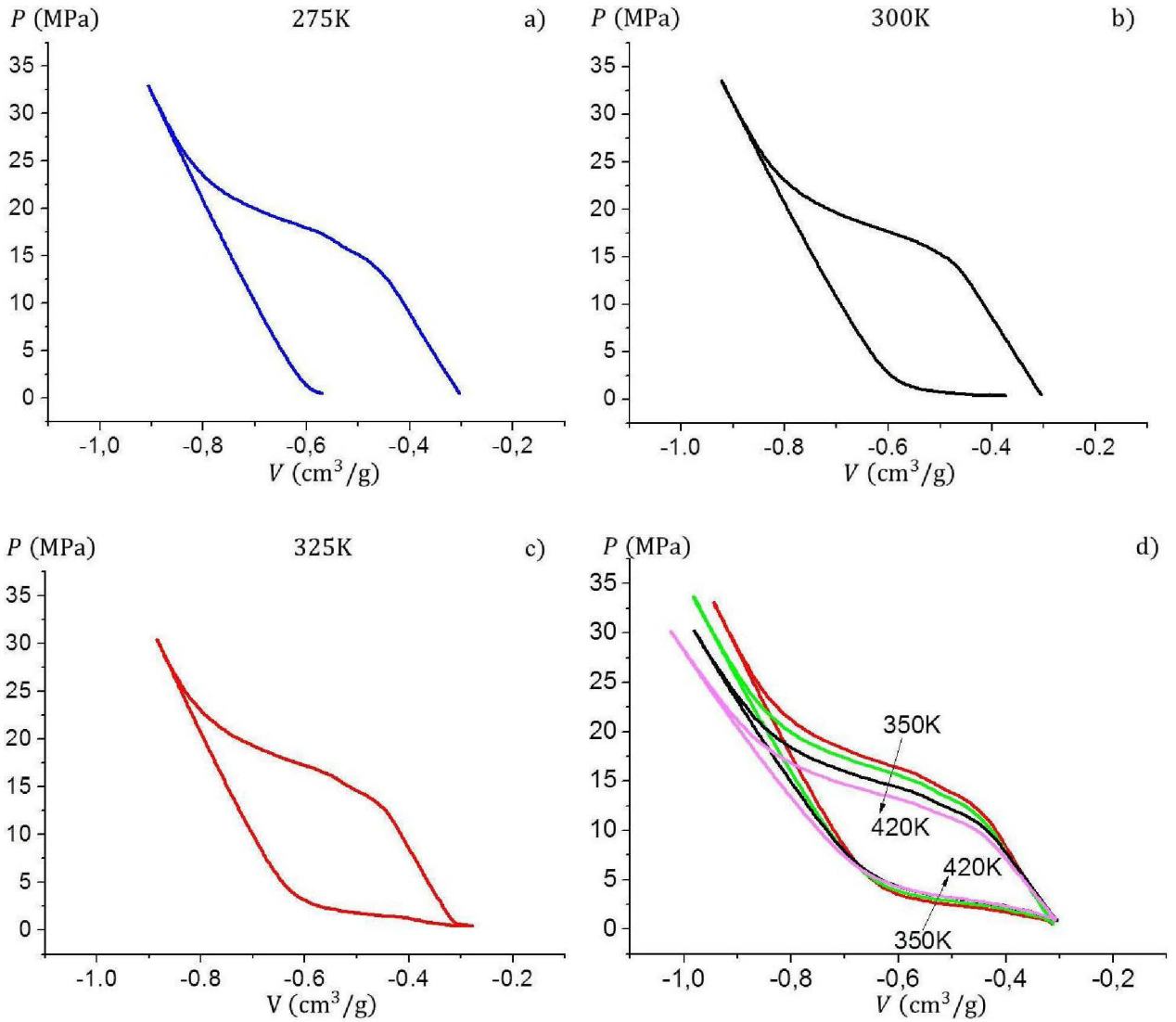


Fig. 3.6. PV-isotherms the {Hypersil C18 + water} HLS at different temperatures a) 275 K, b) 300 K, c) 325 K, d) 350 – 420 K.

Table 3.1.

Work of intrusion and extrusion for the {Hypersil C18 + water} HLS at different temperatures

T, K	275	300	325	350	370	400	420
$W_{int}, J/g$	7,3	7,1	6,9	6,6	6,4	5,9	5,5
$W_{ext}, J/g$	0	0,3	0,6	0,9	1,1	1,2	1,2

Interestingly for the {Hypersil C18 + water} HLS compression-decompression cycle becomes reversible (system returns to initial state when pressure returns to initial value after intrusion) only at temperatures higher than 325 K (Fig.3.6) and at lower temperatures liquid is not completely expelled from the pores. However if after such irreversible intrusion HLS is heated up to at least 325 K at atmospheric pressure the liquid extrudes from the pores and the HLS operates reversibly. *Such effect is shown for the first time. In fact in the literature this HLS was tested only at room temperature and since it was shown to be only partially reversible at these conditions (which is consistent with results presented here), it was considered as non-useful (Suciu et al. 2005). But it seems this HLS can operate quite well, but only at higher temperatures.*

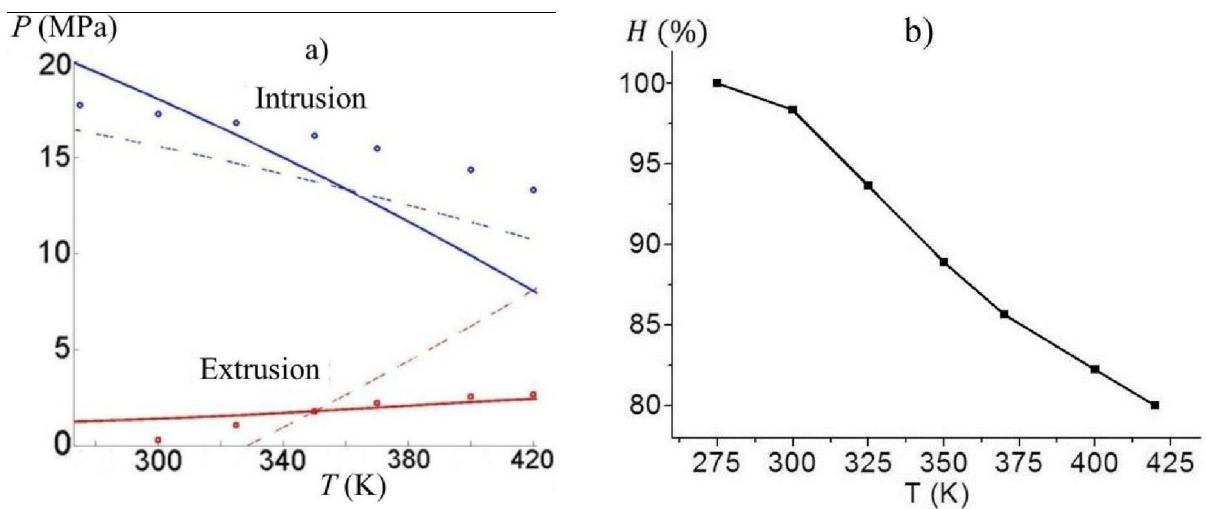


Fig. 3.7. Temperature dependence of a) intrusion and extrusion pressures: dots are experiment, solid lines are theoretical dependence calculated taking into account contact angles temperature dependences; dashes line are theoretical dependences calculated considering constant contact angles b) Hysteresis of intrusion and extrusion pressures of the {Hypersil C18 + water} HLS.

The evolution of intrusion and extrusion pressures (and the observed hysteresis) with temperature is presented in the Figure 3.7. The calculations made according to reference (Grosu et al. 2014c) allow to make the same conclusions as for {Waters C8 + water} HLS described in the previous reprint.

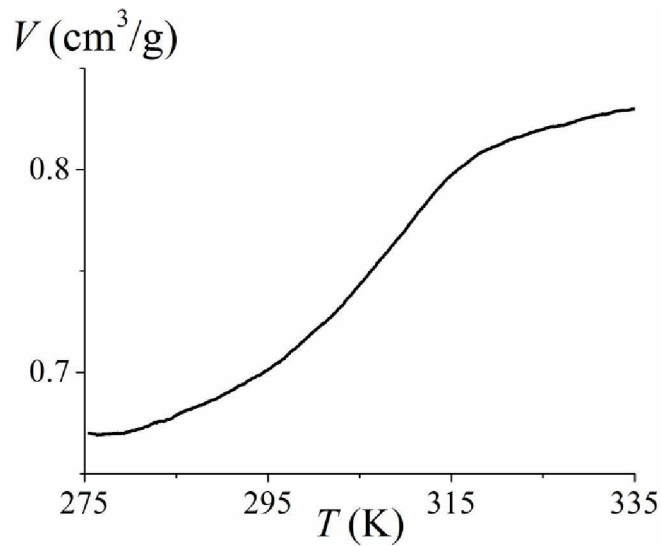


Fig.3.8. Temperature dependence of the volume of {Hypersil C18 + water} HLS at atmospheric pressure after one compression-decompression cycle at 275 K.

Transition from non-reversible (at lower temperatures) to reversible (at higher temperatures) behavior of the {Hypersil C18 + water} HLS allowed realizing new regime of HLS operation: that is extrusion of the liquid provoked by heating (Fig. 3.8). First system was compressed at 275 K temperature. After decompression no extrusion was observed (Fig. 3.6a). Next system was heated up to 335 K at controlled atmospheric pressure (Fig. 3.8), which leads to extrusion of the liquid and pronounced increase of the volume of HLS.

3.3. Stability of HLSs characteristics under operational conditions

Stability of the characteristics of HLSs is of paramount importance for practical applications. In the references (Ievtushenko 2013) and (Grosu et al. 2015b) some of the aspects of instability of HLSs characteristics which may be caused by the effect of high operational pressure or temperature (or by their simultaneous effect) are described. Since the stability of the characteristics of HLSs are investigated in a wide temperature range this publications have also information on temperature dependences of intrusion/extrusion pressures of investigated HLSs and their thermal effects. Reprints of indicated papers are presented hereafter.

Evolution of the energetic characteristics of {silicalite-1 + water} repulsive clathrates in a wide temperature range

Cite this: *Phys. Chem. Chem. Phys.*, 2013, 15, 4451

Oleksii V. Ievtushenko,^{abc} Valentin A. Eroshenko,^{*c} Yaroslav G. Grosu,^c Jean-Marie Nedelec^{ab} and Jean-Pierre E. Grolier^{*ab}

Recently {lyophobic porous powders + liquid} systems were proposed to be used for nontraditional energy storage and conversion purposes. This article reports the experimental study of the mechanical behavior, within the pressure–volume (PV) diagram, of the {hydrophobic silicalite-1 + water} system in the temperature range 10–80 °C. Repeated recordings of PV-isotherms and thermal effects of the repulsive clathrate during successive compression–decompression runs were performed using scanning transiometry. An unexpected steady decline in the intrusion–extrusion pressure and volume of embedded water was found during the forced (repeated) intrusion of water into the pores of silicalite-1 and its spontaneous extrusion at constant temperature. A discussion of possible reasons of unconventional behavior of these heterogeneous systems as well as a thermodynamic analysis is presented.

Received 18th December 2012,

Accepted 22nd January 2013

DOI: 10.1039/c3cp44587a

www.rsc.org/pccp

Introduction

Zeolites are porous materials with a pore radius of less than 1.5 nm that have a wide range of applications. Traditionally they are used as effective adsorbents, molecular sieves for gas and hydrocarbon cleaning, materials for membrane technology, for example.¹ Recently, the range of zeolite applications was extended to the field of alternative energy conversion. The highly advanced interface area between liquid and solid of lyophobic zeolites is used for energy accumulation and conversion in thermo-mechanical systems.^{2–4} The thermodynamic essence of this approach is based on forced intrusion of liquid into the pores of lyophobic porous media under high external pressure, which allows accumulation of surface Gibbs energy by means of the development of a high surface area between liquid and solid in the condensed system. During the external pressure reduction, the accumulated energy can be partially or completely released in the process of spontaneous extrusion of liquid clusters from the solid pore space (*i.e.*, spontaneous reduction of the interface area). The cycles of liquid intrusion–extrusion in the pore space

are close to reversibility for the heterogeneous systems based on hydrophobic zeolites (such as silicalite-1 (MFI structure type),^{5,6} ZSM-5 (MFI),⁷ SSZ-23 (STT),⁸ SSZ-24 (AFI), ferrierite (FER), silicalite-2 (MEL), ZSM-22 (TON), ZSM-12 (MTW), DD3R (DDR), and chabazite (CHA)⁹). Effective studies show that the value of hysteresis (*i.e.*, the difference between intrusion and extrusion pressures) for such systems is not more than about 5%. Together with the ability to accumulate a huge amount of mechanical energy (~5.5–15 J per gram of porous body), this makes such systems promising candidates to be used for creation of molecular springs.^{3,4} Such heterogeneous lyophobic systems (HLS) have been called “repulsive clathrates” (RC).¹⁰

This report presents the results of an experimental study of the mechanical and thermal characteristics of the {silicalite-1 + water} system during the repetitive compression–decompression cycles at different temperatures.

Experimental section

Materials

The silicalite-1 (prepared in fluoride medium) sample was bought from Aldrich. The same silica (but prepared in alkaline media) was used in ref. 11 as a commercial sample (see Discussion hereafter). The pore space of silicalite-1 has a simple topology having almost ideal cylindrical pores with radius $r \sim 0.3$ nm and high hydrophobicity.^{5,6,12}

^a Clermont University ENSCCF, Institute of Chemistry of Clermont-Ferrand, BP 10448, 63000 Clermont-Ferrand, France. E-mail: j-pierre.grolier@univ-bpclermont.fr

^b CNRS, UMR 6296, ICCF, 24 av. des Landais, 63171 Aubière, France

^c Laboratory of Thermomolecular Energetics, National Technical University of Ukraine, Kyiv Polytechnic Institute, Prospect Peremogy 37, 03056 Kyiv, Ukraine. E-mail: eroshenko@kpi.ua

Equipment and samples preparation procedure

A modified version (ST-7M) of the ST-7 instrument (BGR-Tech)¹³ was used to obtain *PV*-isotherms and thermal effects of RC along compression–decompression cycles. In contrast to the conventional ST-7,^{14–17} metal bellows connected to high-precision induction volumeters were added to the high-pressure transitionometric vessels (for pressure up to 200 MPa) of the ST-7M.

The experimental setup is shown in Fig. 1. As can be seen, the opened upper ends of bellows are rigidly fixed to the bottoms of the cylindrical part of the transitionometric vessels (the investigated sample is placed in the measuring vessel while a reference sample is placed in the reference vessel). The bottoms of bellows are connected through non-magnetic metal rods to the magnetic core of the induction sensors for the LVDT detection. The active parts of induction sensors are located in chambers made of non-magnetic material which are outside of the calorimeter detecting zone. Axial displacement of the bellow's bottoms (with a constant effective cross-section) represents the change in volume during the compression–decompression of RC. The displacement is detected by a linear variable differential transformer (LVDT) (also simply called a differential transformer).¹⁸ Reading of the LVDT signal, calibrated in terms of volume, can be performed both parallelly and differentially. The pressure in the measuring cell is generated by a high-pressure pump, driven by a stepping motor. In the ST-7 version, changes in volume during compression–decompression were detected by the number of steps. In the past, malfunctioning of the stepping motor and counting device led to serious errors in the determination of changes in volume during recording of *PV*-isotherms. In the improved version of the instrument (ST-7M), the unit “stepping motor + HP-pump” is still present, but plays a minor role. Changes in the system's volume are registered by the induction volumeters (LVDT), which noticeably improved the metrological characteristics of the instrument.

Recording of pressure in the hydraulic system was made *via* a pressure sensor (press.det.1) built in the hydraulic line connecting the pump to the transitionometric vessels (see Fig. 1).

The instrument can be operated in different modes^{13–17} *via* its complete control by Lab View programming. In the present study, changes in the volume of the investigated system, the pressure increase/decrease and the differential heat flow between the measuring and reference vessels during pressure scans were simultaneously recorded (by a computer) at a constant temperature (within ± 1 mW sensitivity). The rate of volumetric changes was approximately 10^{-4} cm³ s⁻¹. Low scanning speed was compulsory to ensure thermal equilibrium and to minimize thermal gradients during the scanning process. Measurements were performed by controlling precisely the three thermodynamic variables, namely: pressure within ± 0.15 MPa, volume within $\pm 3.3 \times 10^{-4}$ cm³ and a constant temperature within ± 0.01 K.

Fig. 1b shows the simplified scheme of sample preparation. A specific amount of silicalite-1 was introduced into the metallic capsule, which is sealed by a metallic–ceramic porous cover. The approximate weight of the porous powder in the capsule was 2.3 g. The capsule with powder was thoroughly degassed to about 10^{-2} mbar for 2–4 hours. After the degassing procedure, the capsule with powder was filled *in situ* with degassed distilled water through the porous cover. Filling of capsules with water was carried out under vacuum. This procedure guarantees efficient filling of interparticle spaces by water. As a result, the {silicalite-1 + water} system constitutes the repulsive clathrate (RC). The capsule containing the RC is positioned in the measuring vessel while an identical capsule just filled with degassed water is positioned in the reference vessel; both vessels were filled before with degassed water. During immersion of capsules, the water in excess is freely forced out from the cells through small outlets which block air from entering the cells. After this, outlets are tightly sealed by special

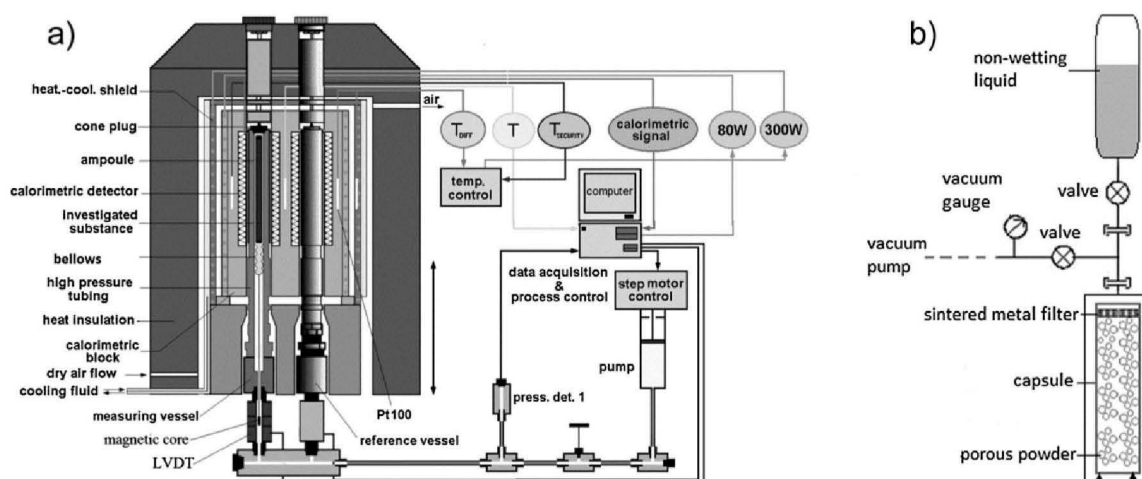


Fig. 1 (a) The experimental setup for determining the *PV*-diagram and associated heat effects. The measuring vessel on the left hand side shows the bellows connected to the high pressure line through the magnetic core device for the LVDT detection. (b) The setup used for degassing and filling the heterogeneous sample.

screw caps and the calorimeter with two receiving thermopiles is gently lowered over both vessels. Tight fit of the vessels in the calorimetric thermopiles of the calorimetric detector provides the efficient heat transfer between measuring and reference vessels with the corresponding thermopiles. This arrangement allows measuring the differential heat flux between the two vessels, yielding the thermal changes occurring in the RC while the differential volumeters yield the associated volume changes undergone by the RC during the pressure scans.

Results

Several cycles of isothermal compression–decompression were performed at temperatures of 10 °C, 30 °C, 50 °C, and 80 °C each for a new {silicalite-1 + water} repulsive clathrate. Fig. 2 shows the compression isotherms obtained for nine repeated successive compression–decompression cycles of the {silicalite-1 + water} system at a temperature of 30 °C.

The results of similar measurements at four different temperatures (*i.e.*, 10 °C, 30 °C, 50 °C and 80 °C) are shown in Fig. 3. The intrusion–extrusion pressures correspond to the maximum compressibility of the system: $(dV/dP)_{\text{int,ext}} \rightarrow \text{max}$, where V is the RC specific volume ($\text{cm}^3 \text{g}^{-1}$, gram of zeolite), P is the pressure (MPa). As shown, the cyclic loading of the RC leads to changes in its mechanical properties. For all temperatures, each successive compression–decompression cycle results in a slight decrease in intrusion–extrusion pressure (not more than 10%), but has almost no effect on the hysteresis, $H = P_{\text{int}} - P_{\text{ext}} \sim 3\%$. The tendency of pressure reduction with the number of cycles increases particularly at 50 °C. Fig. 4 shows the specific work of the intrusion and extrusion of water in the same porous powder (referred to as 1 g of powder), as well as, the tendency to reduce the amount of water filling the powder while the number of loading cycles increases. As shown in Fig. 2 and 4, the amount of water entering the porous material decreases with each cycle. This phenomenon is the most pronounced at 50 °C; at the fifth cycle, the decrease is about 54% compared to the first cycle. Naturally, the decline of the volume of embedded

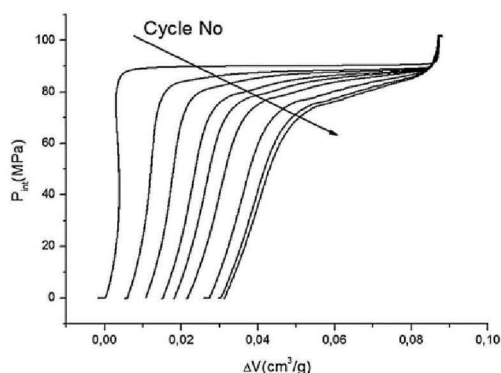


Fig. 2 {Silicalite-1 + water} system: PV -isotherms at 30 °C for the first compression of nine compression–decompression cycles.

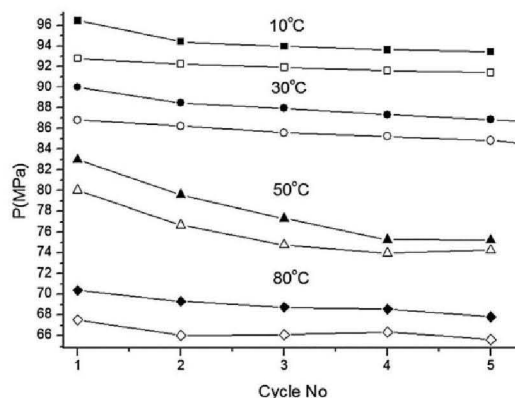


Fig. 3 Temperature dependence of the intrusion–extrusion pressure for the first five cycles during compression–decompression of the {silicalite-1 + water} system at different temperatures. Black symbols are for intrusion, open symbols are for extrusion.

water with the number of cycles reduces the value of the intrusion–extrusion work (Fig. 4).

The observed temperature dependency of the intrusion–extrusion pressure is approximately linear with a coefficient $dP/dT \approx -0.4 \text{ MPa } ^\circ\text{C}^{-1}$. Such a linear relationship between pressure and temperature was noted for the hydrophobic nanoporous zeolite {ZSM-5 + water} system,⁷ which demonstrated a slight effect of temperature on the volume of water intruded into the pore space. In our experiments (Fig. 4), the effect of temperature on the amount of intruded liquid was significantly larger. For instance, for the first cycle, an increase in temperature from 10 °C to 80 °C reduced the volume of intruded liquid by about 50%.

Discussion

The above-mentioned evolution of PV -isotherms of a repulsive clathrate was previously reported for RCs constituted by water and zeolites STT⁸ and ITQ-4.¹⁹ For these systems, Patarin and co-workers have shown that this phenomenon was caused by the formation of hydrophilic defects (silanol groups SiOH) in the structure of the studied porous matrices under mechanical stresses during the intrusion–extrusion process. Also, they have shown⁶ that for the hydrophobic {silicalite-1 + water} system changes in the shape of PV -isotherms occur only after the first cycle. In contrast to our results, significant changes of PV -isotherms in all subsequent compression–decompression cycles were not observed.

Using solid-state NMR spectroscopy, the same authors⁶ have shown that the repeated cycling of the hydrophobic system could also produce a small amount of hydrophilic defects (*i.e.*, increase in the number of silanol groups SiOH in the structure of the hydrophobic porous matrix). In an extensive and carefully performed work Trzpit *et al.*¹¹ have shown both experimentally and by using molecular dynamics methods that the presence of hydrophilic defects may cause spontaneous

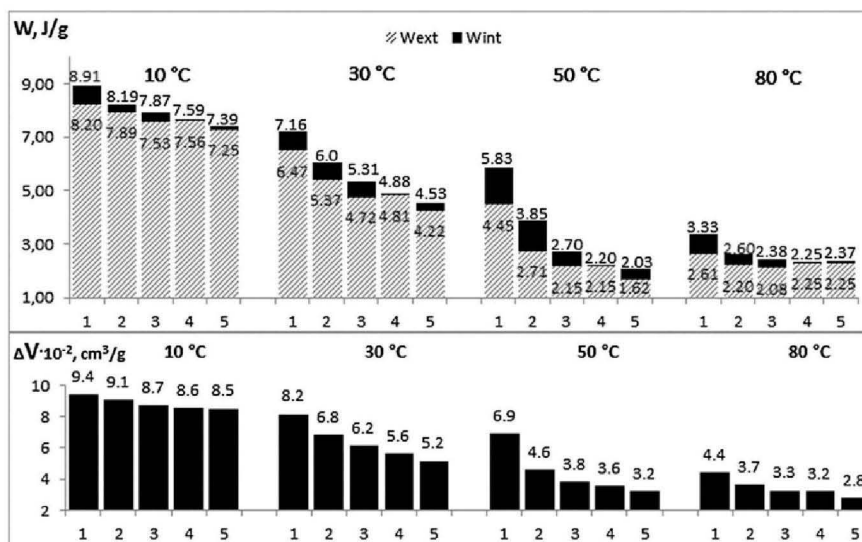


Fig. 4 The work of intrusion W_{int} and of extrusion W_{ext} in J g^{-1} (top). Amount of intruded liquid in $10^{-2} \text{ cm}^3 \text{ g}^{-1}$ (bottom).

adsorption of water molecules in these areas with, as a result, the decrease of volume of liquid embedded into the pore space and the simultaneous decrease of the intrusion pressure. We note that both these effects (decrease in the intrusion pressure and in the volume of embedded liquid) were observed in our experimental work (see Fig. 2–4).

Based on the results reported in ref. 6, 8, 11 and 19 it is logical to assume that the experimentally observed evolution of the PV -isotherms during cycling (see Fig. 2–4) is caused by the formation of silanol defects under each mechanical action on the system (especially during the forced water intrusion into the powder pore space). These defects could be generated through hydrolysis of the silicate backbone under pressure to create hydrophilic silanol sites most probably on the pore surface. Solid state NMR (^1H and ^{29}Si) would be very helpful to get more details and will be performed in future work. As our paper does not include any structural experiments, we may follow conclusions of Karbowski *et al.*⁶ that hydrophilic silanol defects (Si–OH) are formed as a result of breaking of siloxane bonds (Si–O–Si). Based on this assumption a simple qualitative explanation of the asymptotic cycling effect may be given: since the silanol group creation process is of statistical nature, obviously every successive intrusion–extrusion cycle will decrease the probability of further silanol defects creation due to the decrease in the number of available siloxane bonds. Intruded water volume decrease is another argument for this hypothesis. At the same time, the different behavior of the cycling on seemingly identical {silicalite-1 + water} systems remains unclear. In our experiments, a continuous decrease in the intrusion work after each cycle was observed, while in the other study,⁶ decrease in the intrusion work was observed only after the first cycle.

Conjectural explanation of these differences can be found in ref. 11, which shows that formally identical samples of

silicalite-1 but synthesized in different laboratories may have a different number of hydrophilic defects in their structure. Moreover, an amount of these defects could be high enough to produce significant differences (drop of the intrusion–extrusion pressure, increase of their dispersion, reduction of the volume of intruded liquid) even at the macroscopic level (on PV -isotherms of compression–decompression). Obviously, the use of RCs as molecular springs^{2–4} requires reduction of the risk of degradation of their energetic characteristics, which should be made through careful selection of non-defective superhydrophobic powders (MFI-F, MFI-OH, ZSM-5, STT, ITQ-4, *etc.*) produced in accordance to strict technological requirements.

Thermodynamic analysis and thermal effects of repulsive clathrates

Many features of {nanoporous solid + liquid} systems are the subject of recent theoretical investigations and are not fully understood. Especially if the liquid is water. As pointed out in a recent review by Bougeard and Smirnov²⁰ the role of water makes it a particularly difficult challenge for modeling work. Due to the propensity of water to form structures (*e.g.* aggregates) a pure modeling approach faces the double aspect of macroscopic behavior of structures and dynamic atomic/molecular organization. As reported by Caillez *et al.*²¹ the most important features of the intrusion–extrusion process should be understood in terms of equilibrium thermodynamic considerations.

Effectively, repulsive clathrates (RCs) are complex thermodynamic systems. In contrast to simple thermodynamic (gas/vapor) systems, where volume is the extensive parameter, for RCs the solid–liquid interface is the extensive parameter and the surface tension of the liquid is the intensive one.

RCs consist of condensed (almost incompressible) components – a lyophobic solid matrix and liquid – so primary volume change

under increasing pressure originates not from liquid and matrix compression (this effect is secondary), but results essentially from forced penetration of the liquid into the porous space of the matrix along the development of the solid–liquid interface Ω . This process takes place when the external pressure exceeds the Laplace capillary pressure (see eqn (5) and comments below). For every heterogeneous lyophobic system like these, there is a simple connection between volume and interface value ($dV = -kr d\Omega$), which is defined according to the pore radius r and the topology of the matrix ($0.33 < k < 0.50$). This connection allows quantifying the Ω value, which makes PV -isothermal measurements basic and nevertheless very useful tests for investigating RCs' energetic performances.

In compliance with thermodynamic phenomenology the state equation of the system can be proposed according to experimental data.²² For simple thermodynamic systems this state equation [expressed by the relationship $f(P, V, T) = 0$] represents the connection between such macroscopic parameters as pressure P , volume V and temperature T and, certainly, is required for fully valid thermodynamic description. Fig. 5 represents experimental compression–decompression curves of the repulsive clathrate under isothermal conditions (10 °C). Obviously, this relationship can be considered as the validation of the graphical interpretation of the state equation of the system, because it relates the RC's volume and the magnitude of the applied pressure. While at constant geometry and topology of the pore space of the matrix temperature determines the surface tension $\sigma = \sigma(T)$ and, consequently, the intrusion–extrusion pressure. The compressibility $\kappa_T = \left(\frac{\partial V}{\partial P}\right)_T$ that is the pressure dependence visualizes this relationship more clearly (see Fig. 5 inset): the peak corresponds to the intrusion–extrusion pressure. Taking into account clear similarity of κ_T pressure dependence and probability distribution functions, we consider the Cauchy distribution²³ as an appropriate approximation function for RC's compressibility

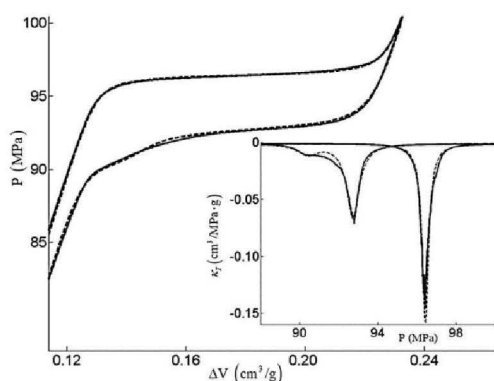


Fig. 5 Experimental (full line) and theoretical (dotted line) isothermal (10 °C) PV -curves and compressibility (inset) during a cycle for the {silicalite-1 + water} system. Parameters of theoretical PV -isotherms are given in Table 1.

Table 1 Parameters of theoretical PV -isotherm curves of Fig. 6

Peak number	Intrusion		Extrusion	
	1	1	1	2
$\max[\Delta V]$, $\text{cm}^3 \text{g}^{-1}$	0.10	0.08	0.018	
$P^{\text{int,ext}}$, MPa	96.44	92.73	90.4	
D , MPa	0.20	0.40	0.65	
$\kappa_T^{V_0} \times 10^{-2}$ $\text{cm}^3 \text{MPa}^{-1} \text{g}^{-1}$	1.4	1.4	1.4	

κ_T that is $f(x) = \frac{1}{\pi D_x \left(1 + \left(\frac{x - x_0}{D_x}\right)^2\right)}$, where x_0 is the mean

value of parameter x , which has standard deviation D_x . Considering the fact that RC's compressibility κ_T is determined by the interface Ω development/reduction (κ_T^Ω) and by the total volume V_0 of the system (*i.e.* matrix volume (V_M) + liquid volume (V_L)) and the elastic deformation ($\kappa_T^{V_0}$), the function (κ_T) can be written as follows:

$$\kappa_T = \kappa_T^\Omega + \kappa_T^{V_0} = -\frac{\max[\Delta V^{\text{int,ext}}]}{\pi D^{\text{int,ext}} \left(1 + \left(\frac{P - P^{\text{int,ext}}}{D^{\text{int,ext}}}\right)^2\right)} + \left(\frac{\partial V_0}{\partial P}\right)_T \quad (1)$$

where $\max[\Delta V]$ is the maximum volume variation due to intrusion–extrusion of water into pores; “int”/“ext” index corresponds to the intrusion–extrusion process; D is the standard deviation of intrusion–extrusion pressure $P^{\text{int,ext}}$. In general, the RC's compressibility curve may have more than one peak (Fig. 5 inset, extrusion), in that case it can be written as:

$$\kappa_T = \sum_i \kappa_{T(i)}^\Omega + \kappa_T^{V_0} \quad (2)$$

The number of terms in the sum $\sum_i \kappa_{T(i)}^\Omega$ is determined by the number of compressibility peaks.

Integrating eqn (1), the isothermal compression–decompression volume variation can be expressed as:

$$\begin{aligned} \Delta V^{\text{int,ext}} &= V_0 - V \\ &= \frac{\max[\Delta V^{\text{int,ext}}]}{\pi} \text{arctg}\left(\frac{P - P^{\text{int,ext}}}{D^{\text{int,ext}}}\right) + \kappa_T^{V_0} P + C \end{aligned} \quad (3)$$

The constant of integration C is determined from the initial conditions: $\Delta V^{\text{int,ext}}(P = P_0) = 0$, where P_0 and $V_0 = V_L + V_M$ are, respectively, initial pressure and volume of the system.

Fig. 5 represents both experimental (full line) and model (dotted line) curves of the first isothermal (at 10 °C) compression–decompression cycle for the RC {silicalite-1 + water}; compressibility is presented in the inset. Model curves are built according to eqn (1)–(3).

As can be seen from Fig. 5, the proposed equations appropriately describe the isothermal conditions. It should be noted that eqn (3) can be classified as an equation of state for a RC, if it is also suitable for describing the behavior of the system under other (adiabatic, isobaric, and isochoric) conditions. Such experiments are a topic for future research. However, eqn (1)–(3) can

already be useful for predicting the thermal effects that occur during isothermal compression–decompression of the RC.^{5,6} Using the general (Maxwell) thermodynamic relation $\left(\frac{\partial S}{\partial P}\right)_T = -\left(\frac{\partial V}{\partial T}\right)_P$, $\delta Q = TdS$ and eqn (1) the amount of heat generated due to pressure change, can be expressed as:

$$\begin{aligned}\Phi_T &\equiv \left(\frac{\partial Q}{\partial P}\right)_T^{\text{int,ext}} = T\kappa_T^0 \left(\frac{\partial P^{\text{int,ext}}}{\partial T}\right)_P + T\left(\frac{\partial V_0}{\partial T}\right)_P \\ &= \frac{T\max[\Delta V^{\text{int,ext}}]}{\pi D^{\text{int,ext}} \left(1 + \left(\frac{P - P^{\text{int,ext}}}{D^{\text{int,ext}}}\right)^2\right)} \left(\frac{\partial P^{\text{int,ext}}}{\partial T}\right)_P + T\left(\frac{\partial V_0}{\partial T}\right)_P\end{aligned}\quad (4)$$

Note, that only parameters of the PV -isothermal diagram were considered as known characteristics, intrusion–extrusion pressure temperature dependence $\left(\frac{\partial P^{\text{int,ext}}}{\partial T}\right)_P$ should be defined in eqn (4).

For RCs based on matrices with relatively large pore size (so intruded immobilized liquid can be considered as macroscopic media) the intrusion–extrusion pressure is determined according to the Laplace–Washburn equation (in our case for cylindrical pores):²⁴

$$P_{\text{macro}}^{\text{int,ext}} = \frac{2\sigma \cos\theta^{\text{int,ext}}}{r} \quad (5)$$

where r is the pore radius, and the contact angles hysteresis during intrusion θ^{int} and extrusion θ^{ext} are considered to explain pressure hysteresis during the cycle (Fig. 5). For lyophobic systems $\theta > 90^\circ$, so $\cos\theta < 0$. Obviously, eqn (5) cannot be used to predict the intrusion–extrusion pressure for systems which are discussed in this paper, since nanoscale changes the properties of capillary systems,²⁵ and the contact angle in the capillaries with the diameter that is comparable to the size of the liquid molecules has no physical meaning. However, the liquid surface tension σ is still temperature dependent and has an effect on the intrusion–extrusion pressure value for nanocapillary RCs. Hence, relying on the structure of eqn (5) it can be written: $P^{\text{int,ext}} = B^{\text{int,ext}}\sigma$, where $B^{\text{int,ext}}$ is a temperature independent coefficient. So the temperature derivative of the intrusion–extrusion pressure can be expressed as $\left(\frac{\partial P^{\text{int,ext}}}{\partial T}\right)_P = \frac{P^{\text{int,ext}}}{\sigma} \left(\frac{\partial \sigma}{\partial T}\right)_P$. Substituting this expression into eqn (4) and using values of $\sigma = 71.18 \text{ (mN m}^{-1}\text{)}$ and $\frac{d\sigma}{dT} = 0.158 \text{ (mN m}^{-1} \text{K}^{-1}\text{)}$,²⁶ allows us to plot the RC's compression–decompression heat effects and compare them with experimental data achieved at 10 °C (Fig. 6). For illustration purposes experimental and theoretical curves are normalized to the bulk ($d\Omega = 0$) phase heat effect $\left(\frac{\partial Q}{\partial P}\right)_{T,\Omega} \equiv \phi_{T,\Omega}$.

As shown in Fig. 6 the proposed model provides good agreement between theoretical and experimental curves, which proves that interface development/reduction effects are dominant

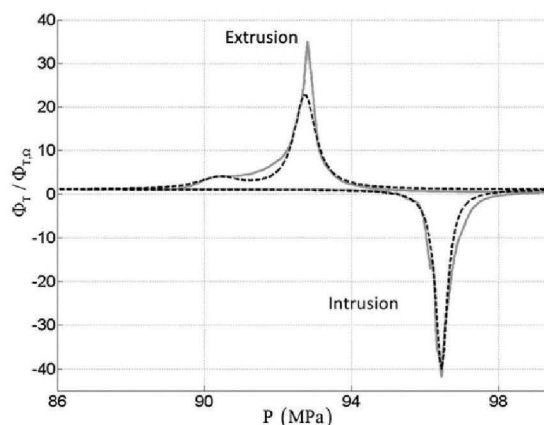


Fig. 6 Experimental (full line) and theoretical (dotted line) compression (intrusion)/decompression (extrusion) heat effects of the {silicalite-1 + water} system at 10 °C.

for the type of system under investigation. If the model assumption is failing, then comparing theoretical and experimental curves would be irrelevant, since it is a purely thermodynamic model. Hence, this approach allows identifying additional mechanisms, which can take place in RCs based on matrices with complex topology; for example, for bottle like pores forced intrusion will bring non-equilibrium effects even if compression is very slow. Thus, the thermodynamic analysis in conjunction with the calorimetric measurements can be useful for investigating RC's operations. Further in-depth understanding of these mechanisms (including silanol defects creation) and the development of recommendations for the production of stable superhydrophobic zeolites is the subject of future research and publications.

Conclusions

This paper demonstrates the energetic performances of {nanoporous silicalite-1 + water} repulsive clathrates (RC) in a wide temperature range (10 °C–80 °C). The effect of silanol defects present in the matrix and its influence on the RC's energetic performances during operation has been shown experimentally for the first time: the system still behaves as a molecular spring, but with declining capacity of accumulated mechanical energy during the cycling (water forced intrusion and spontaneous extrusion into/from matrix pores). In particular, for the {silicalite-1 + water} system compression–decompression work decreased by ~70% after 5 cycles in the whole temperature range. Specified energy performance degradation is caused by continuous intrusion–extrusion pressure (Fig. 2 and 3) and intruded water volume reduction (Fig. 4) after each cycle. The comparison of these results and experiments performed on STT-, ITQ-4-based RCs^{8,19} and more stable silicalite-1 systems^{6,11} allows assuming that cycling changes (intruded volume and intrusion–extrusion pressure reduction) are caused by the creation of silanol defects in the structure of the porous matrix.

Significant differences in the stability of the system during cycling and the results obtained in ref. 6 point out the importance of matrix technology production and its improvement in the way of reducing the risk of silanol defects creation during molecular spring exploitation. For maximum energy characteristics stability, the number of these defects should be minimal and the lyophobic system must be resistant to their formation under intensive mechanical stress. The proposed mathematical approach allows identifying the main mechanisms during RC's exploitation and may be useful for systems with complex topology.

Abbreviations

HLS	heterogeneous lyophobic system
RC	repulsive clathrate

Acknowledgements

The authors express their deepest appreciation and thanks to M. S. Chanchole, Director of XTechnologies, Ecole Polytechnique, Palaiseau, Paris, for the transfer of the Scanning Transitiometric setup to the Institute of Chemistry of Clermont-Ferrand (ICCF) where all experimental measurements have been carried out. The technical help as well as advices from Dr L. Coiffard to handle the transitiometric data are also highly appreciated. One of us (O.V.I.) gratefully acknowledges the financial support from The Ministry of Education and Science, Youth and Sports of Ukraine, for his six month stay at Clermont-Ferrand laboratory.

References

- 1 H. van Bekkum, A. Corma and F. Schuth, *Introduction to Zeolite Science and Practice*, Elsevier, Amsterdam, 2007.
- 2 V. A. Eroshenko, *Soviet Patent No. 1,254,811*, 1981, [priority of 24.07.1981, updated 02.09.1993 (date of free public access)].
- 3 V. Eroshenko, R. C. Regis, M. Soulard and J. Patarin, *J. Am. Chem. Soc.*, 2001, **123**(33), 8129–8130.
- 4 V. Eroshenko, R. C. Regis, M. Soulard and J. Patarin, *C. R. Phys.*, 2002, **3**(1), 111–119.
- 5 L. Coiffard, V. A. Eroshenko and J.-P. E. Grolier, *AIChE J.*, 2005, **51**(4), 1246–1257.
- 6 T. Karbowski, M.-A. Saada, S. Rigolet, A. Ballandras, G. Weber, I. Bezverkhy, M. Soulard, J. Patarin and J.-P. Bellat, *Phys. Chem. Chem. Phys.*, 2010, **12**, 11454–11466.
- 7 Y. Qiao, V. K. Punyamurtula, A. Han, X. Kong and F. B. Surani, *Appl. Phys. Lett.*, 2006, **89**, 251905.
- 8 L. Tzani, M. Trzpit, M. Soulard and J. Patarin, *J. Phys. Chem. C*, 2012, **116**, 4802–4808.
- 9 L. Tzani, M. Trzpit, M. Soulard and J. Patarin, *J. Phys. Chem. C*, 2012, **116**, 20389–20395.
- 10 V. Eroshenko, *Proceedings of Int. Post-SMIR Conf. «Seismic Isolation, passive Energy Dissipation and active Control of Seismic Vibrations of Structure»*, Taormina, Sicily, Italy, 1997, p. 783.
- 11 M. Trzpit, M. Soulard, J. Patarin, N. Desbiens, F. Cailliez, A. Boutin, I. Demachy and A. H. Fuchs, *Langmuir*, 2007, **23**(20), 10131–10139.
- 12 W. M. Meier, D. H. Olson and D. H. Baerlocher, *Ch. Atlas of Zeolite Structure Types*, Elsevier, London, 1996.
- 13 L. Coiffard and V. Eroshenko, *J. Colloid Interface Sci.*, 2006, **300**, 304–309.
- 14 S. L. Randzio, J.-P. E. Grolier, J. Zaslona and J. R. Quint, *French Patent No. 9109227*, 1994, *Polish Patent No. 295285*, 1995.
- 15 S. L. Randzio, *Chem. Soc. Rev.*, 1996, **25**, 383–392.
- 16 S. L. Randzio and J.-P. E. Grolier, *Anal. Chem.*, 1998, **70**, 2327–2330.
- 17 S. L. Randzio, Ch. Stachowiak and J.-P. E. Grolier, *J. Chem. Thermodyn.*, 2003, **35**, 639–648.
- 18 D. S. Nyce, *Linear Position Sensors: Theory and Application*, Wiley-Interscience, New Jersey, 2004.
- 19 M. A. Saada, S. Rigolet, J.-L. Paillaud, N. Bats, M. Soulard and J. Patarin, *J. Phys. Chem. C*, 2010, **114**(26), 11650–11658.
- 20 D. Bougeard and K. S. Smirnov, *Phys. Chem. Chem. Phys.*, 2007, **9**, 226–245.
- 21 F. Cailliez, M. Trzpit, M. Soulard, I. Demachy, A. Boutin, J. Patarin and A. H. Fuchs, *Phys. Chem. Chem. Phys.*, 2008, **10**, 4817–4826.
- 22 E. A. Guggenheim, *Thermodynamique*, Dunod, Paris, 1965.
- 23 N. L. Johnson, S. Kotz and N. Balakrishnan, *Continuous Univariate Distributions*, Wiley, New York, 1994.
- 24 E. W. Washburn, *Phys. Rev.*, 1921, **17**(3), 273–283.
- 25 J. W. van Honschoten, N. Brunets and N. R. Tas, *Chem. Soc. Rev.*, 2010, **39**, 1096–1114.
- 26 T. Reis, *Introduction à la chimie-physique des surfaces*, Dunod, Paris, 1952.



Cite this: DOI: 10.1039/c5nr01340b

Synergetic effect of temperature and pressure on energetic and structural characteristics of {ZIF-8 + water} molecular spring†

Ya. Grosu,^{a,b,c} G. Renaudin,^{a,b} V. Eroshenko,^{*c} J.-M. Nedelec^{a,b} and J.-P. E. Grolier^{a,b}

Metal-organic frameworks (MOFs) and particularly their subclass – Zeolite Imidazolate Frameworks (ZIFs) – are used for a variety of applications including particularly energy storage. Highly porous MOFs mixed with non-wetting liquids can be used to form molecular springs (MS) for efficient mechanical and thermal energy storage/transformation. In this paper by means of high-pressure calorimetry the energetic characteristics of {ZIF-8 + water} MS were investigated in wide temperature and pressure ranges. Unexpectedly XRD measurements show that the concomitant effects of temperature and pressure on {ZIF-8 + water} MS leads to an irreversible change of the ZIF-8 structure, transforming its symmetry from cubic to orthorhombic. Whereas, previous studies have demonstrated the stability of ZIF-8 under either high pressure or high temperature.

Received 28th February 2015,

Accepted 6th April 2015

DOI: 10.1039/c5nr01340b

www.rsc.org/nanoscale

Introduction

Metal organic frameworks (MOFs) have very attractive properties and characteristics in many fields of science and technology^{1,2} such as gas adsorption and separation,³ catalysis,⁴ drug delivery^{5,6} and energy.⁷ The Zeolite Imidazolate Frameworks – ZIFs (a subclass of MOFs) are particularly interesting due to their exceptional stability, which is essential for practical applications. Indeed, it has been shown both by experiments^{8–11} and by simulations^{12,13} that even for the most “fragile” ZIFs rather high values of pressure and temperature are required to provoke irreversible structural changes: for example for ZIF-8 the critical (hydrostatic and non-hydrostatic) pressure after which irreversible amorphisation takes place is ~0.34 GPa according to Chapman *et al.* or even 1.6 GPa according to Hu *et al.* (non-hydrostatic),⁸ while for ZIF-4 it is ~6.5 GPa.¹⁰ Naturally most of the studies on the stability of ZIFs characteristics were implemented to investigate separately the effects of pressure and temperature on the structure of the materials. To our knowledge there are no studies

devoted to the concomitant effects of pressure and temperature on the structure of ZIFs.

High pressure compression–decompression cycles over a wide temperature range are typical operational conditions for porous Heterogeneous Lyophobic Systems (HLSs) used for energy storage, transformation or dissipation (depending on the type of HLS).^{14–17} Recently the class of porous materials for HLS was extended to hydrophobic ZIF-8^{18–21} and ZIF-71²² metal organic frameworks. Such ZIFs demonstrated excellent characteristics when forming HLSs combined with water^{18,21,22} and aqueous electrolyte solutions.^{19,20,22} Yet the effect of temperature on their characteristics was not investigated. In this paper for the first time we present results of high-pressure calorimetric studies for the {ZIF-8 + water} system in the 275–360 K temperature range to determine its characteristics in terms of thermal and mechanical energy storage. In order to explore combined effects of pressure and temperature on the structure of ZIF-8 (and hence on the stability of the {ZIF-8 + water system}) additional X-Ray Diffraction (XRD), Fourier Transform Infra-Red (FTIR) spectroscopy and Scanning Electron Microscopy (SEM) characterization have been performed before and after compression–decompression cycles of the {ZIF-8 + water} system.

The operational principle of the {ZIF-8 + water} system is similar to the one for other HLSs formed by a lyophobic porous matrix and a non-wetting liquid^{14–17}: the non-wetting condition eliminates the spontaneous penetration of the liquid into the pores of the matrix. By increasing the pressure in the system to some critical value (intrusion pressure P_{in}) the liquid can be forced into the pores (similar to the mercury

^aClermont Université ENSCC, Institut de Chimie de Clermont-Ferrand, BP 10448, 63000 Clermont-Ferrand, France

^bCNRS, UMR 6296, ICCF, 24 av. des Landais, 63171 Aubière, France

^cLaboratory of Thermomolecular Energetics, National Technical University of Ukraine “Kyiv Polytechnic Institute”, Prospect Peremogy 37, 03056 Kyiv, Ukraine.

E-mail: eroshenko@kpi.ua

†Electronic supplementary information (ESI) available. See DOI: 10.1039/c5nr01340b

porosimetry technique); the mechanical energy necessary to break the intermolecular bonds of the liquid during intrusion is supplied to the system during the intrusion process. On the PV -diagram (on the macroscopic scale) this process is followed by a significant increase of compressibility of the system (Fig. 1): the corresponding plateau stands until the pores of the matrix are completely filled. As the breaking of intermolecular bonds of the liquid (during intrusion) is an endothermic process,^{16,17} the system stores not only mechanical, but also thermal energy during the intrusion. Since lyophobic pores constitute an energetically unfavorable environment for molecules of the non-wetting liquid, the decrease of the pressure in the system down to some critical value (extrusion pressure P_{ext}) leads to the extrusion of the liquid from the pores of the matrix, which is followed by the release of mechanical (large

expansion of the system, see Fig. 1) and thermal energy (renewal of intermolecular bonds of the liquid with an exothermic effect). Hence, such a system acts as the Molecular Spring (MS) and can be used for energy storage.

The high specific energy which the system stores/restores during the intrusion/extrusion process can be obtained by using porous materials with a large specific surface area ($400\text{--}2000\text{ m}^2\text{ g}^{-1}$) possessing a large specific volume change (mechanical energy) and large specific number of broken/renewed intermolecular bonds (generating thermal energy) during intrusion/extrusion process. In this work we investigated the {ZIF-8 + water} system in a wide temperature and pressure range. The structure of ZIF-8 consists of cage-like pores of $\sim 11.6\text{ \AA}$ diameter connected by 6-ring windows of only $\sim 3.4\text{ \AA}$ and is characterized by a huge specific surface area of *ca.* $1800\text{ m}^2\text{ g}^{-1}$ (ref. 11) that is very favorable for molecular spring applications.

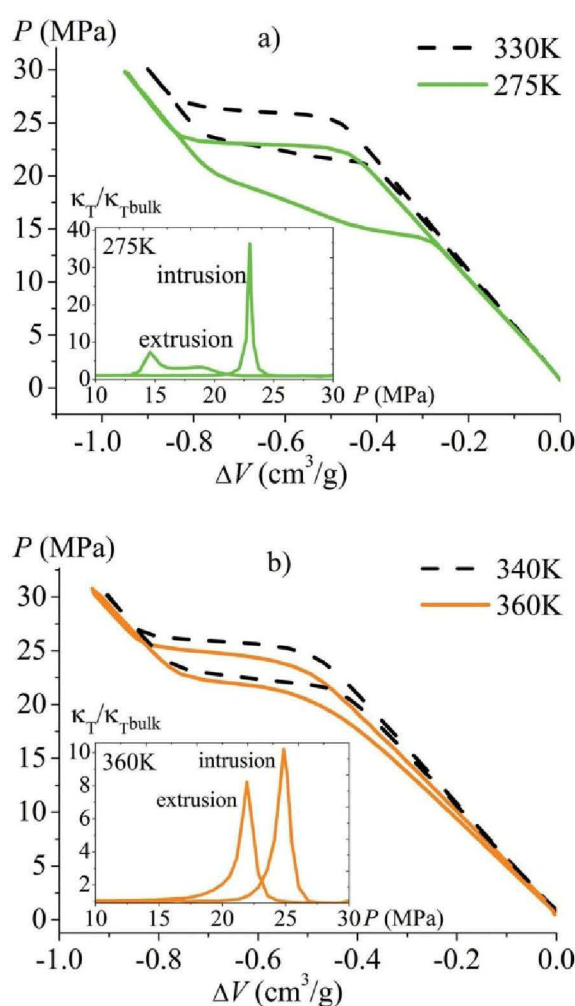


Fig. 1 PV -isotherms at (a) 275 K and 330 K, (b) 340 K and 360 K for the {ZIF-8 + water} molecular spring. Insert: normalized compressibility at (a) 275 K, (b) 360 K.

Experimental section

Materials

Microporous ZIF-8 was purchased from Sigma Aldrich as Basolite Z1200. Distilled water was used as non-wetting liquid.

Experimental technique

High-pressure calorimetry. A modified ST-7M transitiometer of the ST-7 model instrument (BGR-Tech)^{23–25} was used to obtain simultaneously the PV -isotherms of the {ZIF-8 + water} MS and the corresponding thermal effects along compression–decompression cycles. A detailed description of the experimental setup is given elsewhere.²⁶ The scheme of calorimeter setup is given in the ESI†

The sample preparation and the experimental procedure are described here below. A specific amount of ZIF-8 was introduced into a metallic capsule, which was sealed by a metallic–ceramic porous cover. The approximate weight of the porous powder in the capsule was 0.5 g. The capsule with the powder was thoroughly degassed to about 10^{-2} mbar for 2–4 hours. After the degassing procedure, the capsule with the powder was filled *in situ* with degassed distilled water through the porous cover. An ultrasound degassing bath FB 15051 (Fisher Scientific) was used to degas water for 2 hours at a temperature of 60 °C. The concentration of ZIF-8 in water in the measuring cell was 2.5 wt%.

The filling of the capsule with water was carried out under vacuum. This procedure guarantees efficient filling of interparticle spaces with water. Next, the capsule containing the HLS was positioned into the measuring vessel while an identical capsule just filled with degassed water was positioned into the reference vessel; both vessels were filled earlier with degassed water. The pressure–volume diagrams and corresponding thermal effects for the {ZIF-8 + water} system were obtained for 8 temperatures, from 275 to 360 K. At each temperature 3 compression–decompression cycles were realized at a low rate of 1 MPa min^{-1} to assure the good reproducibility of

measurements. It has been verified previously that such a compression rate does not bring any additional effect in comparison with lower (quasi-static) rates.²⁷ In general, of course the compression–decompression rate may have an influence on the energetic characteristics of the HLS.¹⁵ Particularly for the investigated system it was verified that the compression speed of 1 MPa min^{−1} is low enough to consider the process as quasi-static and its further decrease does not bring any changes to the *PV*-isotherms or calorimetric measurements. Measurements were performed by controlling precisely the three thermodynamic variables, namely: pressure within ±0.15 MPa, volume within ±3.3 × 10^{−4} cm³ and a constant temperature within ±0.01 K.

XRD patterns of pristine ZIF-8 and of ZIF-8 modified after intrusion/extrusion cycle were recorded on an X'Pert Pro PANalytical diffractometer θ - θ geometry, using Cu K α radiation ($\lambda = 1.54184$ Å). XRD patterns were recorded at room temperature in the interval of $3^\circ < 2\theta < 120^\circ$, with a step size of $\Delta 2\theta = 0.0167^\circ$ and a counting time of 119 s for each data value. A total counting time of about 200 min was used for each sample.

FTIR spectra were recorded in transmission mode using the KBr pellet technique with a Nicolet 5700 spectrometer from Thermo Scientific.

SEM micrographs were recorded on a Zeiss supra 55-VP microscope.

Results and discussion

Energetic characteristics of {ZIF-8 + water} molecular spring

The obtained isothermal compression–decompression curves of the {ZIF-8 + water} molecular spring are presented in Fig. 1. It can be observed that the intrusion of the liquid into the pores of ZIF-8 is followed by a pronounced one-step plateau on the *PV*-isotherm with a weak temperature dependence of the intrusion pressure around 25 MPa (Fig. 2). Interestingly at lower temperatures the extrusion process is two-stepwise (Fig. 1a), which is clearly seen from the pressure dependence of the compressibility of the system (Fig. 1a, insert) and it becomes one-stepwise at higher temperatures (Fig. 1b and 1b inserts).

In inserts of Fig. 1 $\kappa_T = \frac{1}{V} \left(\frac{\partial V}{\partial P} \right)_T$ is the compressibility of HLS and $\kappa_{T,\text{bulk}} = \frac{1}{V} \left(\frac{\partial V_0}{\partial P} \right)_{T,\Omega}$ is the compressibility of bulk components of HLS (matrix and liquid) excluding intrusion/extrusion effects (interface area $\Omega = \text{const}$). The obtained results are consistent with the room temperature experiment reported by Patarin and coworkers¹⁸ and with our previously published data at two temperatures for the {ZIF-8 + water} MS.²¹ They are also consistent with the experiments performed with ZIF-8 associated with different aqueous electrolyte solutions at room temperature showing similar two-step extrusion and one step intrusion (two-peak κ_T for decompression and one-peak κ_T compression)¹⁹ and with the experiment performed at 343 K showing a one-step intrusion and extrusion

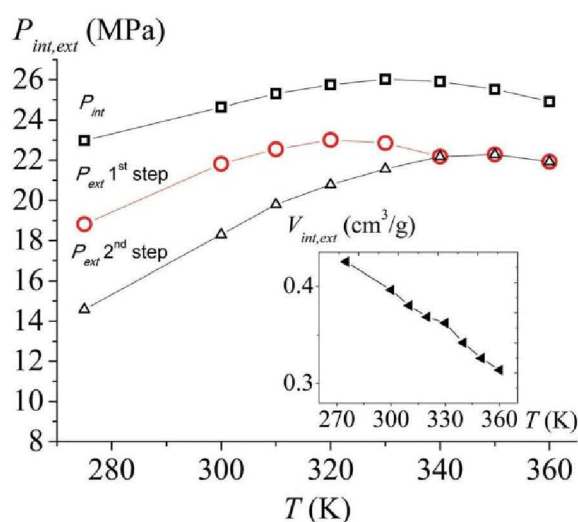


Fig. 2 Temperature dependences of the intrusion pressure and of the extrusion pressures (two steps) of {ZIF-8 + water} molecular spring. Insert: temperature dependence of the intrusion/extrusion volume of the water.

(one-peak κ_T for compression and decompression).²⁰ Two-step N₂ adsorption isotherms have previously been observed for ZIF-8²⁸ and were associated with a reversible phase transition of the structure of ZIF-8 resulting from a swing effect of the imidazolate linker, which leads to an increase in the pore volume. It seems that the two-step extrusion corroborates the presence of such phase transitions. Even though the high-pressure *PV*-diagrams were obtained under quasistatic conditions, at some temperatures (275 K, 330 K – Fig. 1a) a two-step extrusion is observed following a one-step intrusion. This would suggest that during the intrusion the above phase transition may occur simultaneously with the filling of the initial pore volume and hence is not visible on the *PV*-diagram.

According to the available data it appears that the temperature is a key factor for different extrusion behavior of HLS based on ZIF-8. It is logical to assume that the dynamics (*i.e.* the velocity) of the compression–decompression cycles should be reflected by the observed characteristic properties. In any case it seems that such structural phase transition of ZIF-8 is reversible and does not affect the stability of energetic characteristics of {ZIF-8 + water} MS, which is the main topic of this paper.

Fig. 2 represents the temperature dependence of the intrusion pressure P_{int} and of the extrusion pressures of first P_{ext1} and second P_{ext2} steps: both intrusion and extrusion pressures have non-linear temperature dependence in the 320–360 K range. The intrusion/extrusion pressure values indicated in Fig. 2 correspond to peaks of compressibility (see the inserts of the Fig. 1). To our knowledge such dependence has not been previously observed for water based HLSs. We believe that such dependence is a result of two factors which defines intru-

sion/extrusion pressure and have mutually opposite temperature dependences, that is: (1) Firstly a temperature dependent compressibility of ZIF-8, which under higher temperatures leads to smaller orifices of the pores before the intrusion step; this effect is dominant in the 275–330 K range (Fig. 1a and 2). (2) Second a well-known negative temperature dependence of surface tension σ of water, which according to the Laplace equation leads to the negative temperature dependence of intrusion/extrusion pressure ($P_{\text{inf,ext}} \sim \frac{2\sigma \cos \theta}{r}$). Taking into account the extreme confinement of ZIF-8 pores this equation should be used only qualitatively. The second factor is quite obvious and seems to be responsible for the negative temperature dependence of intrusion for both microporous and mesoporous HLSs.^{26,27,29,30} The first factor supports the decrease with the temperature of the volume of intruded/extruded water (*i.e.* the effective volume of pore space before intrusion), which is shown in the insert of Fig. 2. Although it seems that compression–decompression cycles of {ZIF-8 + water} system at higher temperatures induce irreversible changes in the ZIF-8 structure, this is discussed in detail here after.

The corresponding temperature dependence of the mechanical energy which the system stores/restores during intrusion/extrusion (excluding the elastic effects of ZIF-8 and water) is presented in Table 1S and in Fig. 1S of ESI† specified to one gram of ZIF-8. The hysteresis of stored/restored mechanical energy decreases with the temperature increase (Table 1S and insert of Fig. 1S of ESI†).

The thermal effects of intrusion and extrusion are presented in Fig. 3. For HLSs^{16,17,26} the intrusion is typically followed by an endothermic effect, while the extrusion is exothermic (Fig. 3 insert). This means that during the intrusion/extrusion (compression/decompression) HLS stores/restores not only mechanical energy, but also thermal energy.

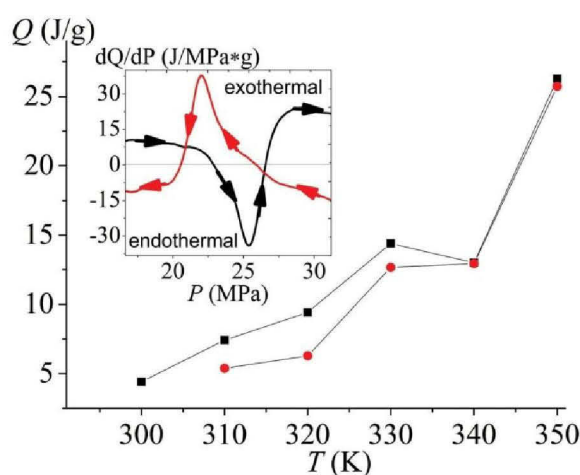


Fig. 3 Temperature dependence of the absolute values of the thermal effects of intrusion (■) and extrusion (●) for the {ZIF-8 + water} system. Insert: differential heats of intrusion and extrusion at 350 K.

Vice versa thermal effects (exothermal intrusion and endothermal extrusion) are rare. The difference seems to depend on the pore geometry and size.^{16,31,32} It is interesting to compare obtained endothermal/exothermal effects for intrusion/extrusion to known exothermal/endothermal adsorption/desorption effects for hydrophilic materials. The difference of the sign of thermal effects for hydrophobic and hydrophilic materials is expected from the thermodynamic point of view. From the well-known equation expressing the heat of development/reduction of the interface Ω , $\delta Q = T \frac{\partial(\sigma \cos \theta)}{\partial T} d\Omega$, we see that the sign of $\cos \theta$ directly influences the sign of the thermal effects: the hydrophobic condition is $\theta > 90^\circ$ then $\cos \theta < 0$ and the hydrophilic condition is $\theta < 90^\circ$ then $\cos \theta > 0$.

Absolute values of the heat supplied to/taken from the system during the isothermal intrusion/extrusion process in the 275–350 K temperature range are presented in Fig. 3 and Table 1S† (the thermal effects at 275 K are too small with regard to the sensitivity of the experimental equipment used). As it can be seen the temperature dependence is positive as expected according to the above equation for the heat of development/reduction of the interface Ω (again due to the extreme confinement of the ZIF-8 pores this equation should be used only qualitatively).

The maximum value of mechanical energy stored due to water intrusion into ZIF-8 is about 10 J g^{-1} in the investigated temperature range, while the thermal energy reaches about 25 J g^{-1} at 350 K and can be almost reversibly restored. Considering the huge specific surface area of ZIF-8 and relatively low operational pressures (of intrusion/extrusion), the prevailing role of the thermal effects in the overall energy capacity of the {ZIF-8 + water} MS is expected. The obtained thermal effects at temperatures close to ambient are of the same order of magnitude as those reported for the {silicalite-1 + water}^{16,17} and {chabazite + water} molecular springs,³¹ whereas the temperature increase leads to much higher values, which is expected from a thermodynamic point of view. As far as we know there are no data for thermal effects of intrusion/extrusion in HLS at high temperatures available in the literature for comparison. The mechanical energy capacity of the investigated system may be considered close to the average value of that of a wide range of available HLSs,^{14–17,22,26,27,31,33,34} but it should be noted that in most of these cases higher values of the stored mechanical energy is reached through an increase of the operational (intrusion) pressure, which is not always suitable for practical applications. The low temperature sensitivity of the mechanical performances (Table 1S and Fig. 1S†) of the investigated system is another advantage.

Irreversible structural changes of ZIF-8

From Fig. 1 it can be seen that the PV -isotherms for the {ZIF-8 + water} MS at higher temperatures (Fig. 1b) have less pronounced intrusion/extrusion steps in comparison with the ones at lower temperatures (Fig. 1a). In addition it can be observed that after intrusion–extrusion cycles at temperatures close to 360 K a slight irreversible decrease of intrusion–extru-

sion volume of water takes place, while experiments at lower temperatures (both before and after cycles at 360 K) are stable and do not affect the *PV*-diagram of HLS. Such changes of characteristics are typical for zeolites based HLSs if the degradation of the structure takes place during high-pressure operations.^{26,35} In order to understand the stability of the energetic characteristics of the {ZIF-8 + water} MS and the stability of the structure of ZIF-8 after an operation cycle at high temperatures FTIR, XRD and SEM analyses have been made on a reference ZIF-8 and compared to the analyses made on the samples which have been subjected to the previously described compression–decompression cycles in the 275–360 K temperature range (that is, overall 25 cycles: 3 cycles for each temperature + 1 first cycle at room temperature).

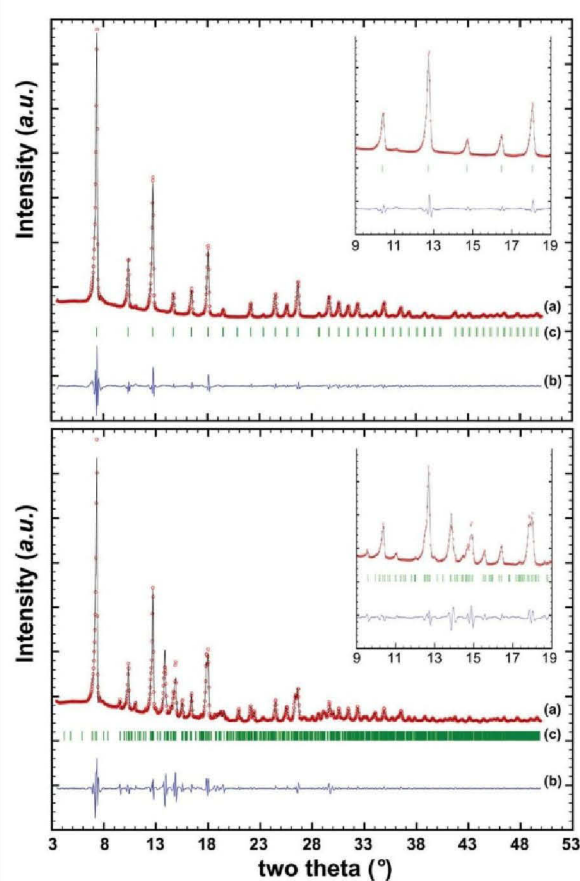


Fig. 4 Refinement plots from 3° to 50° two theta (insets showing details between 9° and 19° two theta) for ZIF-8 sample as received (top: Rietveld plot with the known cubic structure, $a = 17.040$ (1) Å, $V = 4947.8$ Å³ (6) Å³) and after treatment (bottom: Le Bail plot with the new orthorhombic symmetry, $a = 36.927$ (2) Å, $b = 25.653$ (2) Å and $c = 8.4741$ (5) Å, $V = 8027.3$ (8) Å³). Refinements have been performed on diffractograms recorded between 3° and 120° two theta with $\lambda = 1.5418$ Å: (a) measured (red dots) and calculated (black lines), (b) differences curves, and (c) Bragg peaks.

FTIR spectra do not show any significant difference between the reference and used ZIF-8 (Fig. 2S of ESI†) indicating the preservation of molecular groups in the structure of ZIF-8.

On the other hand, XRD data (Fig. 4) show strong discrepancies before and after intrusion/extrusion cycles and an irreversible structural modification. This modification is surprising as available investigations on structural stability of ZIF-8 show that much higher pressure^{8,9,12} or temperature¹¹ values are required to irreversibly modify the structure of ZIF-8. It seems that this structural change is a result of simultaneous effect of pressure and temperature during intrusion–extrusion experiments.

The as-received ZIF-8 sample corresponds to the described cubic structure (space group $I\bar{4}3m$ with $Z = 12$ formula units of composition $\text{Zn}(\text{C}_8\text{H}_{12}\text{N}_4)^{36}$ as represented at the top of Fig. 4. After compression–decompression cycles at 275–360 K the material presents a structural modification. The main features of the diffractogram are still present with the intense peak at about 7.3°, and Bragg peaks position related to the regular cubic unit cell (with the previously refined parameter $a = 17.040$ (1) Å). It indicates that ZIF-8 has been modified but not destroyed. Additional peaks are evidenced (bottom of Fig. 4, inset shows new diffraction peaks at about 9.5°, 13.8° or 15.5°) together with splitting (around 14.7° or 17.9°) in agreement with a superstructure due to the loss of symmetry operators. Attempts to find the new unit cell, by considering a loss of symmetry, were realized with the DICVOL04 program³⁷ and a solution was obtained with an orthorhombic symmetry. The refined lattice parameters, by the Le Bail method using the FULLPROF.2k program,³⁸ are: $a = 36.927$ (2) Å, $b = 25.653$ (2) Å, $c = 8.4741$ (5) Å. The three orthorhombic parameters are directly correlated with the parent cubic ones as follows: $a_{\text{orth.}} \sim 2 a_{\text{cub.}}$, $b_{\text{orth.}} \sim 1.5 a_{\text{cub.}}$ and $c_{\text{orth.}} \sim 0.5 a_{\text{cub.}}$ (the exact coefficients are 2.17, 1.51 and 0.50). Such results evidence the irreversible structural transition from cubic ZIF-8 to orthorhombic {ZIF-8 + water} after intrusion/extrusion cycles, accompanied with an increase in the unit volume of 8.16%. The introduction of water molecules inside the cages of the ZIF-8 structure should certainly explain such an important increase of the unit volume. X-ray powder diffraction data did not allow us to solve the orthorhombic structure of the modified ZIF-8 compound. The determined orthorhombic unit cell contains 18 Zn atoms, or 18 $\text{Zn}(\text{C}_8\text{H}_{12}\text{N}_4)$ motifs, which necessitates very high quality powder (synchrotron) diffraction patterns or single crystal data.

SEM images (Fig. 5) demonstrate a decrease in the sharpness of crystals of ZIF-8 after operational compression–decompression cycles. Also some oblong formations, not observed for reference sample, are observed for the used ZIF-8. On a larger scale it can be seen that micron-size conglomerates are formed in ZIF-8 powder after compression–decompression cycles, which in principle may also lead to intrusion/extrusion step delay (sharpness decrease) during pressure increase/decrease, due to impeded access of water molecule to/from the openings of the pores.

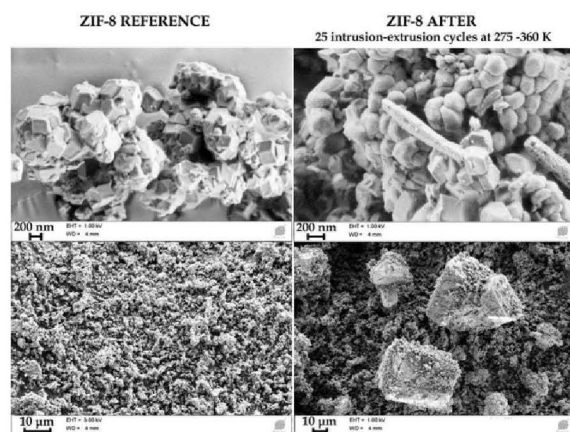


Fig. 5 SEM images of ZIF-8 before (left) and after (right) 25 cycles of intrusion–extrusion in the 275–360 K temperature range.

In order to confirm our hypothesis on the combined effects of pressure and temperature on the structure of ZIF-8 (and hence on the stability of energetic characteristics of the {ZIF-8 + water} system) four additional experiments were performed.

- To show that there is no separate effect of pressure on the characteristics of the {ZIF-8 + water} system, 30 successive compression–decompression cycles were performed over the pressure range 0.1–30 MPa at 300 K. They show excellent reproducibility. All the cycles are shown in Fig. 3S of the ESI;† no modifications of the *PV*-diagram are observed.

- To show that there is no separate effect of temperature on the characteristics of the {ZIF-8 + water} system, its temperature was brought up to 360 K under 0.1 MPa for 24 h. After cooling no effects appeared on the *PV*-diagrams at 300 K. Compression–decompression cycles before and after the heating are presented in the same Fig. 3S.†

By means of molecular dynamic simulations Qiao and co-workers have demonstrated that the diffusion of gas molecules into the liquid intruded into the pores of HLS may lead to its irreversible compression–decompression cycle (absence of liquid expulsion).³⁴ The authors indirectly confirmed this effect by keeping the HLS compressed for 12 h, after which unlike for fast compression–decompression, no extrusion occurred.³⁴

- To exclude the possibility of such effect on *PV*-diagrams of {ZIF-8 + water} system a third additional experiment was performed. The {ZIF-8 + water} system was compressed up to 30 MPa at 300 K (so that intrusion could take place) and maintained at such conditions for 24 h. After the pressure decrease extrusion took place and no modifications of *PV*-diagram were observed. The 32nd cycle with 24 h pause and the 33rd cycle at regular compression/decompression velocity are also shown in Fig. 3S.†

- To show the combined effects of pressure and temperature on the characteristics of the {ZIF-8 + water} system, the fourth experiment consisted of performing 25 compression–

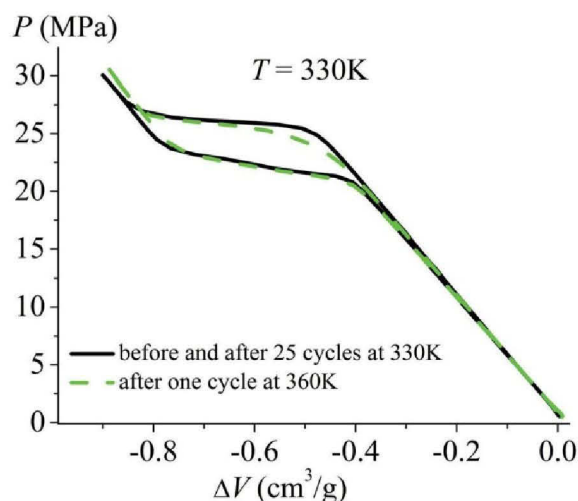


Fig. 6 *PV*-diagrams for the {ZIF-8 + water} molecular spring at 330 K: 2nd and 25th cycles (solid line) and 27th cycle (dashed line) after one cycle at 360 K.

decompression cycles at 330 K. They show excellent repeatability. The next 26th cycle was performed at 360 K. Then the system was cooled down to 330 K and the 27th cycle was conducted. Comparison of the 2nd cycle at 330 K (which is no different from the 3rd–25th cycles) with the 27th cycle at the same temperature is shown in Fig. 6: the effect of the single cycle at 360 K is evident, that is decrease in the sharpness of the intrusion–extrusion steps and slight decrease of the intruded volume of water.

From additional experiments performed it is logical to assume that intrusion–extrusion cycles at higher temperatures (say 360 K) lead to irreversible modification of the ZIF-8 structure, which was not previously observed at these values of either temperature or pressure, with a resulting degradation of {ZIF-8 + water} system's characteristics. However operation of this system at lower temperatures seems to be not affected. Such results obviously allow one to recommend the optimal operational temperature range for this system. But on the other hand they show that modifying of the structure of ZIF-8 may be obtained by easily achieved physical conditions.

Conclusions

In this work thermal and mechanical energetic characteristics of {ZIF-8 + water} porous Heterogeneous Lyophobic System (HLS), which acts as a molecular spring are reported in the 275–360 K temperature range for the first time. A non-linear temperature dependence of intrusion and extrusion pressures, never observed for water based HLSs, was recorded. Such dependence is most likely explained by contradictory temperature dependences of the ZIF-8 compressibility and of the surface tension of water. The stability of the indicated

characteristics of {ZIF-8 + water} molecular spring (determined by stability of ZIF-8) were investigated by means of XRD, SEM, FTIR and additional high pressure experiments under various conditions. It is demonstrated that the {ZIF-8 + water} system features stable operations at temperatures below *ca.* 340–350 K, while operational cycles at higher temperatures lead to structural modifications of ZIF-8 and degradation of characteristics of the {ZIF-8 + water} system. Such structural modifications are irreversible unlike the widely explored reversible structural transition caused by a swing effect of the imidazolate linker in ZIF-8 (see for example ref. 28 and 39) and correspond to the irreversible structure transition from cubic to orthorhombic symmetry, accompanied by an increase of the unit volume, which is probably due to the synergetic effect of temperature and pressure during intrusion of water molecules inside the cages of the ZIF-8 structure.

To our knowledge it is shown for the first time that irreversible structural changes of ZIF-8 may be achieved under rather low temperature (360 K) and pressure (30 MPa) by means of water intrusion–extrusion. This information is of importance for the rapidly growing field of MOFs applications as regards the stability of their characteristics.

Acknowledgements

One of us (G. Ya.) gratefully acknowledges the financial support from the French Ministry of Foreign Affairs (Embassy of France in Ukraine) for his stay at the Institute of Chemistry of Clermont-Ferrand, where all experimental measurements have been carried out. Useful advice and technical support on the transitionometry technique from Prof. Randzio S.L. are highly appreciated.

References

- U. Mueller, M. Schubert, F. Teich, H. Puetter, K. Schierle-Arndt and J. Pastre, *J. Mater. Chem.*, 2006, **16**, 626.
- J. Canivet, A. Fateeva, Y. Guo, B. Coasne and D. Farrusseng, *Chem. Soc. Rev.*, 2014, **43**, 5594.
- J. R. Li, R. J. Kuppler and H. C. Zhou, *Chem. Soc. Rev.*, 2009, **38**, 1477.
- D. Farrusseng, *Metal–organic frameworks: applications from catalysis to gas storage*, Wiley, 2011.
- P. Horcajada, C. Serre, G. Maurin, N. A. Ramsahye, F. Balas, M. Vallet-Regí, M. Sebban, F. Taulelle and G. Férey, *J. Am. Chem. Soc.*, 2008, **130**, 6774.
- P. Horcajada, *et al.*, *Nat. Mater.*, 2010, **9**, 172.
- J. Rodriguez, I. Beurroies, T. Loiseau, R. Denoyel and P. L. Llewellyn, *Angew. Chem., Int. Ed.*, 2015, **54**, 4626.
- K. W. Chapman, G. J. Halder and P. J. Chupas, *J. Am. Chem. Soc.*, 2009, **131**, 17546; Y. Hu, H. Kazemian, S. Rohani, Y. Huang and Y. Song, *Chem. Commun.*, 2011, **47**, 12694.
- S. A. Moggach, T. D. Bennett and A. K. Cheetham, *Angew. Chem., Int. Ed.*, 2009, **121**, 7221.
- T. D. Bennett, P. Simoncic, S. A. Moggach, F. Gozzo, P. Macchi, D. A. Keen, J.-C. Tan and A. K. Cheetham, *Chem. Commun.*, 2011, **47**, 7983.
- K. S. Park, Z. Ni, A. P. Côté, J. Y. Choi, R. Huang, F. J. Uribe-Romo, H. K. Chae, M. O’Keeffe and O. M. Yaghi, *Proc. Natl. Acad. Sci. U. S. A.*, 2006, **103**, 10186.
- Z. Hu, L. Zhang and J. Jiang, *J. Chem. Phys.*, 2012, **136**, 244703.
- A. U. Ortiz, A. Boutin, A. H. Fuchs and F. X. Coudert, *J. Phys. Chem. Lett.*, 2013, **4**, 1861.
- V. Eroshenko, R. C. Regis, M. Soulard and J. Patarin, *J. Am. Chem. Soc.*, 2001, **123**, 8129.
- V. A. Eroshenko, I. Piatiletov, L. Coiffard and V. Stoudenets, *Proc. Inst. Mech. Eng., Part D*, 2007, **221**, 301.
- L. Coiffard, V. A. Eroshenko and J. P. E. Grolier, *AICChE J.*, 2005, **51**, 1246.
- T. Karbowiak, *et al.*, *Phys. Chem. Chem. Phys.*, 2010, **12**, 11454.
- G. Ortiz, H. Nouali, C. Marichal, G. Chaplais and J. Patarin, *Phys. Chem. Chem. Phys.*, 2013, **15**, 4888.
- G. Ortiz, H. Nouali, C. Marichal, G. Chaplais and J. Patarin, *J. Phys. Chem. C*, 2014, **118**, 5397.
- M. Michelin-Jamois, C. Picard, E. Charlaix and G. Vigier, arXiv preprint arXiv:1404.5318., 2014.
- Y. Grosu, V. Eroshenko, J.-M. Nedelec and J.-P. E. Grolier, *Phys. Chem. Chem. Phys.*, 2015, **17**, 1572.
- G. Ortiz, H. Nouali, C. Marichal, G. Chaplais and J. Patarin, *J. Phys. Chem. C*, 2014, **118**, 7321.
- S. L. Randzio, J. P. E. Grolier, J. Zaslona and J. R. Quint, *French patent* 9109227, 1994.
- S. L. Randzio, J. P. E. Grolier, J. Zaslona and J. R. Quint, *Polish Patent* 295285, 1995.
- S. L. Randzio, *Chem. Soc. Rev.*, 1996, **25**, 383.
- O. V. Ievtushenko, V. A. Eroshenko, Y. G. Grosu, J. M. Nedelec and J. P. E. Grolier, *Phys. Chem. Chem. Phys.*, 2013, **15**, 4451.
- L. Coiffard and V. Eroshenko, *J. Colloid Interface Sci.*, 2006, **300**, 304.
- D. Fairen-Jimenez, S. A. Moggach, M. T. Wharmby, P. A. Wright, S. Parsons and T. Duren, *J. Am. Chem. Soc.*, 2011, **133**, 8900.
- Y. Qiao, V. K. Punyamurtula, A. Han, X. Kong and F. Surani, *Appl. Phys. Lett.*, 2006, **89**, 251905.
- C. V. Suci, S. Tani and K. Miyoshi, *J. Syst. Des. Dyn.*, 2010, **4**, 899.
- T. Karbowiak, G. Weber and J. P. Bellat, *Langmuir*, 2013, **30**, 213.
- F. Cailliez, M. Trzpit, M. Soulard, I. Demachy, A. Boutin, J. Patarin and A. H. Fuchs, *Phys. Chem. Chem. Phys.*, 2008, **10**, 4817.
- L. Tzani, M. Trzpit, M. Soulard and J. Patarin, *J. Phys. Chem. C*, 2012, **116**, 20389.
- Y. Qiao, G. Cao and X. Chen, *J. Am. Chem. Soc.*, 2007, **129**, 2355.

- 35 M. Trzpit, *et al.*, *Langmuir*, 2007, **23**, 10131.
- 36 H. Wu, W. Zhou and T. Yildirim, *J. Am. Chem. Soc.*, 2007, **129**, 5314.
- 37 A. Boulitif and D. Louër, *J. Appl. Crystallogr.*, 2004, **37**, 724.
- 38 J. Rodriguez-Carvajal, *PROGRAM FullProf.2k - version 3.20*, Laboratoire Léon Brillouin (CEA-CNRS), Saclay, 2005, Full-prof.2k manual available at <http://www.ill.eu/sites/fullprof/>.
- 39 H. Tanaka, S. Ohsaki, S. Hiraide, D. Yamamoto, S. Watanabe and M. T. Miyahara, *J. Phys. Chem. C*, 2014, **118**, 8445.

Synergetic effect of temperature and pressure on energetic and structural characteristics of {ZIF-8 + water} molecular spring

Ya. Grosu ^{a,b,c}, G. Renaudin ^{a,b}, V. Eroshenko ^c, J.-M. Nedelec ^{a,b}, J.-P.E. Grolier ^{a,b}

^a Clermont University ENSCCF, Institute of Chemistry of Clermont-Ferrand, BP 10448, 63000 Clermont-Ferrand, France.

^b CNRS, UMR 6296, ICCF, 24 av. des Landais, 63171 Aubière, France.

^c Laboratory of Thermomolecular Energetics, National Technical University of Ukraine “Kyiv Polytechnic Institute”, Prospect Peremogy 37, 03056 Kyiv, Ukraine.

Corresponding Author: eroshenko@kpi.ua

Supplementary information

Scheme 1S. The calorimeter setup.

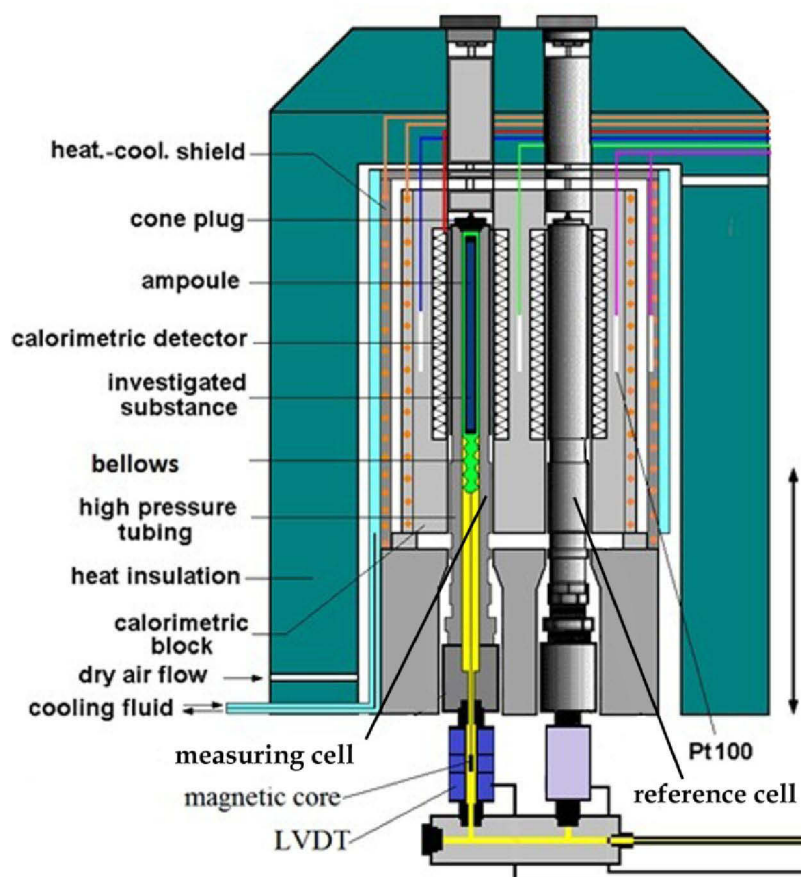


Table 1S. Energetic characteristics of the {ZIF-8 + water} molecular spring

T,K	275	300	310	320	330	340	350	360
W_{int} [J g ⁻¹]	8.8	9.6	9.8	9.9	9.9	9.9	9.8	9.5
W_{ext} [J g ⁻¹]	5.7	7.0	7.5	7.9	8.2	8.4	8.4	8.3
Q_{int} [J g ⁻¹]		4.4	7.4	9.4	14.4	13	26.3	
Q_{ext} [J g ⁻¹]			5.4	6.3	12.7	12.9	25.7	
P_{int} [MPa]	23.0	24.6	25.3	25.8	26.0	25.9	25.5	24.9
P_{ext} (1 st peak) [MPa]	18.8	21.8	22.5	23.0	22.9	22.2	22.3	21.9
P_{ext2} (2 nd peak) [MPa]	14.6	18.3	19.8	20.8	21.6			
$V_{int,ext}$ [cm ³ g ⁻¹]	0.43	0.40	0.38	0.37	0.36	0.34	0.33	0.31

Figure 1S represents the work of intrusion and extrusion of {ZIF-8 + water} molecular spring at different temperatures and the hysteresis of their values, calculated as follows:

$$H_W = \frac{W_{int} - W_{ext}}{W_{int}} \cdot 100\%$$

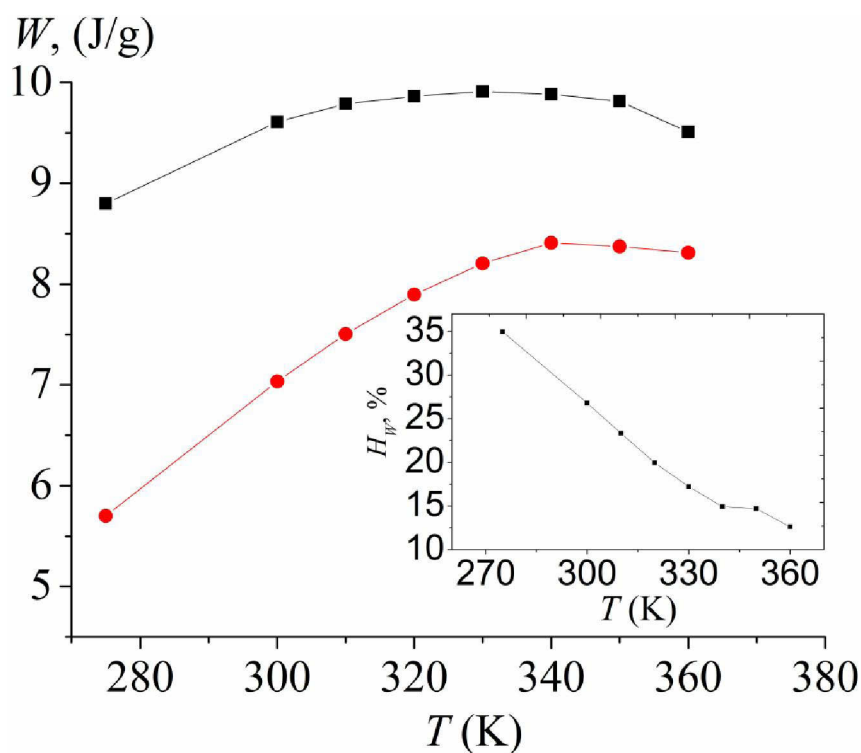


Figure 1S. Temperature dependence of intrusion (a) and extrusion (b) work for the {ZIF-8 + water} molecular spring. Insert: hysteresis of work for intrusion-extrusion cycle.

Figure 2S represents the FTIR spectra of ZIF-8 before and after 25 cycles of intrusion-extrusion at temperatures in the range of 275 – 360K.

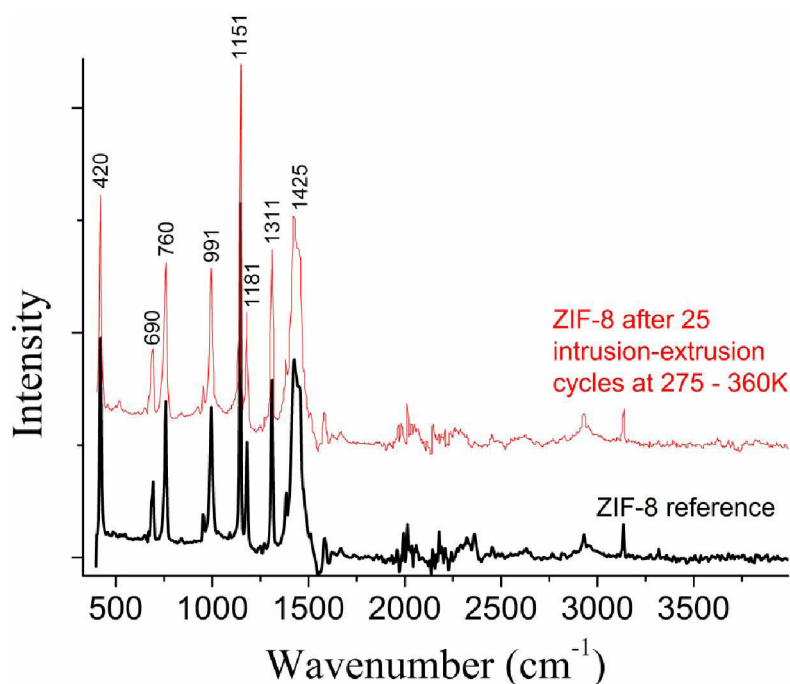


Figure2S. FTIR spectra of ZIF-8 before (bottom) and after (top) 25 cycles of intrusion-extrusion in the 275 – 360K temperature range

Figure 3S represents the absence of visual effect of compression-decompression cycles on PV-diagrams of {ZIF-8 + water} molecular spring under different conditions.

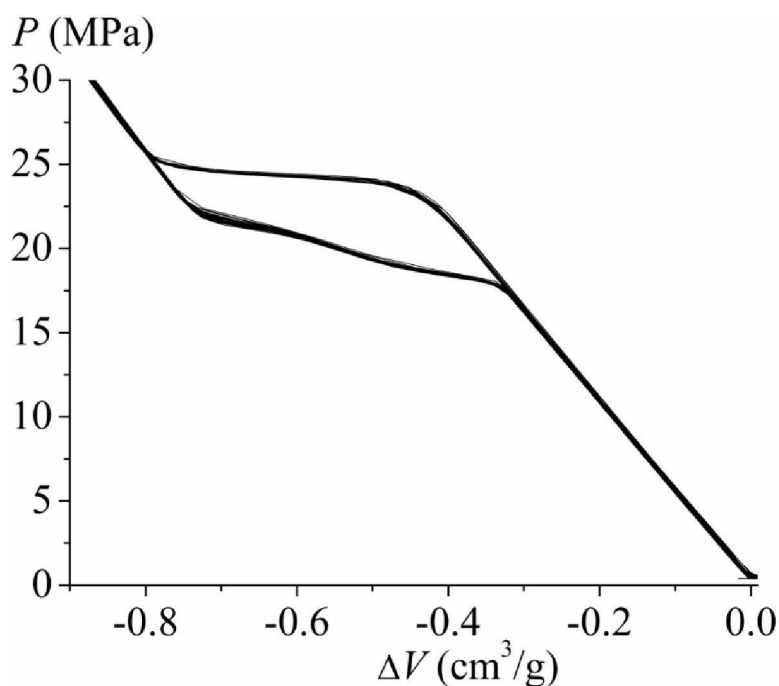


Figure3S. 33 compression-decompression cycles of the {ZIF-8 + water} system: 2nd – 30th cycles are at 300K; 31st cycle is after keeping system at 360K and 0.1MPa during 24h; 32nd cycle is with a 24h pause at 30 MPa; 33rd cycle is at 300K after all mentioned above cycles.

CONCLUSIONS

CONCLUSIONS

The main results of this work are focusing on a deeper understanding of the operating mechanisms of porous Heterogeneous Lyophobic Systems (HLS) in energy applications. Also important part of this work is dedicated to determination of optimal conditions and regimes of HLSs operation, realized by recording their thermomechanical characteristics in extended temperature and pressure ranges.

Some striking results are highlighted:

1. An equation of state for an HLS, which takes into account pore size distribution as well as compressibility and thermal expansion of the liquid and the matrix, was proposed. Using this equation, it was shown that pressure and temperature dependences of the thermal (thermomechanical) coefficients, the thermal effects of compression/decompression, and the heat capacities of HLS may be tuned using porous materials with different pore size distribution functions.

2. Using a rigorous thermodynamic analysis it was demonstrated that the temperature dependence of intrusion and extrusion pressures of an HLS plays a dominant role in the applicability of their energetic characteristics. It was shown that an intrusion/extrusion process for an HLS is a second order phase transition process. For example the change of isobaric heat capacity caused by intrusion/extrusion during heating/cooling of an HLS can be described by Erenfest equation.

3. For a mesoporous HLS a system of equations was proposed, which allows to calculate the intrusion/extrusion temperature dependences using the capillarity and bubble nucleation approach, where the size effects are taken into account with the concept of line tension, while the temperature dependences of advancing and receding contact angles are obtained by means of the “sharp-kink” approximation.

4. The energetic characteristics of four distinct HLSs were collected in a wide temperature range. It was shown that the capacity to storing/restoring thermal energy for investigated systems increase with temperature. As regards the capacity to storing/restoring mechanical energy, a more complex (non-linear) temperature dependence was observed, mainly due to a more complex temperature dependence of the intrusion/extrusion pressure.

5. Investigation of performance stability of HLS demonstrated that the main reason for the degradation of the energetic characteristics under high pressure and/or temperature is irreversible changes in the structure of the porous matrix. For the {Silicalite-1 + water} HLS such irreversible changes are associated with silanol defects formation, while for the {ZIF-8 + water} HLS with the change of the symmetry of the structure: from cubic to orthorhombic. Such change of the structure of ZIF-8 was shown for the first time.

6. It was shown both experimentally and by means of the thermodynamic analysis that an HLS can be used to obtain an effect of Negative Thermal Expansion (NTE) within a controlled temperature window, with NTE-coefficient orders of magnitude higher compared to best known materials.

7. Some new operation regimes of HLSs were investigated under controlled isobaric conditions: intrusion of the liquid by cooling a {ZIF-8 + water} HLS; extrusion of the liquid by heating a {HC18 + water} HLS. Such effects are associated with huge changes of the isobaric heat capacity of the HLSs.

REFERENCES

REFERENCES

1. **Borman V. D., Belogorlov A. A., Byrkin V. A., Lisichkin G. V., Tronin V. N. & Troyan, V. I. (2011).** The infiltration of nonwetting liquid into nanoporous media and the thermal effect. In *Journal of Physics: Conference Series* (Vol. 291, No. 1, p. 012044). IOP Publishing.
2. **Borman V. D., Belogorlov A. A., Byrkin V. A., Tronin V. N. & Troyan V. I. (2012).** Observation of a dispersion transition and the stability of a liquid in a nanoporous medium. *JETP letters*, 95(10), 511-514.
3. **Borman V. D., Belogorlov A. A., Grekhov A. M., Lisichkin G. V., Tronin V. N. & Troyan V. I. (2005).** The percolation transition in filling a nanoporous body by a nonwetting liquid. *Journal of Experimental and Theoretical Physics*, 100(2), 385-397.
4. **Borman V. D., Belogorlov A. A., Grekhov A. M., Lisichkin G. V., Tronin V. N. & Troyan V. I. (2004).** The mechanism of mechanical energy accumulation in a nonwetting liquid-nanoporous solid system. *Technical physics letters*, 30(12), 973-975.
5. **Borman V. D., Belogorlov A. A., Grekhov A. M., Tronin V. N. & Troyan V. I. (2001).** Observation of dynamic effects in the percolation transition in a “nonwetting liquid-nanoporous body” system. *Journal of Experimental and Theoretical Physics Letters*, 74(5), 258-261.
6. **Borman V. D., Belogorlov A. A., Lisichkin G. V., Tronin V. N. & Troyan V. I. (2009).** Investigation of the dynamics of a percolation transition under rapid compression of a nanoporous body-nonwetting liquid system. *Journal of Experimental and Theoretical Physics*, 108(3), 389-410.
7. **Borman V. D., Grekhov A. M. & Troyan V. I. (2000).** Investigation of the percolation transition in a nonwetting liquid-nanoporous medium system. *Journal of Experimental and Theoretical Physics*, 91(1), 170-181.
8. **Bushuev Y. G. & Sastre G. (2010).** Feasibility of pure silica zeolites. *The Journal of Physical Chemistry C*, 114(45), 19157-19168.
9. **Bushuev Y. G. & Sastre G. (2011).** Atomistic Simulation of Water Intrusion–Extrusion in ITQ-4 (IFR) and ZSM-22 (TON): The Role of Silanol Defects. *The Journal of Physical Chemistry C*, 115(44), 21942-21953.
10. **Bushuev Y. G., Sastre G., de Julian-Ortiz J. V. & Gálvez J. (2012).** Water–Hydrophobic

- Zeolite Systems. *The Journal of Physical Chemistry C*, 116(47), 24916-24929.
11. **Cailliez F., Trzpit M., Soulard M., Demachy I., Boutin A., Patarin J., & Fuchs A. H. (2008).** Thermodynamics of water intrusion in nanoporous hydrophobic solids. *Physical Chemistry Chemical Physics*, 10(32), 4817-4826.
 12. **Cao G., Qiao Y., Zhou Q. & Chen X. (2008a).** Water infiltration behaviours in carbon nanotubes under quasi-static and dynamic loading conditions. *Molecular Simulation*, 34(10-15), 1267-1274.
 13. **Cao G., Qiao Y., Zhou Q. & Chen X. (2008b).** Infiltration behaviour of water in a carbon nanotube under external pressure. *Philosophical Magazine Letters*, 88(5), 371-378.
 14. **Chen X., Cao G., Han A., Punyamurtula V. K., Liu L., Culligan P. J., ... & Qiao Y. (2008).** Nanoscale fluid transport: size and rate effects. *Nano letters*, 8(9), 2988-2992.
 15. **Chen X., Surani F. B., Kong X., Punyamurtula V. K. & Qiao Y. (2006).** Energy absorption performance of steel tubes enhanced by a nanoporous material functionalized liquid. *Applied physics letters*, 89(24), 241918.
 16. **Coiffard L. and Eroshenko V. (2006).** Temperature effect on water intrusion/expulsion in grafted silica gels. *Journal of colloid and interface science*, 300(1), 304-309.
 17. **Coiffard L., Eroshenko V. A. & Grolier J. P. E. (2005).** Thermomechanics of the variation of interfaces in heterogeneous lyophobic systems. *AIChE journal*, 51(4), 1246-1257.
 18. **Eroshenko (1981).** Patent No. 1,254,811 USSR (1981-classified) — Russia (1993), F 03 G 7/00. Heterogeneous thermodynamic system, Eroshenko method of converting thermal energy into mechanical energy and device for its implementation.
 19. **Eroshenko V. (2003).** U.S. Patent No. 6,615,959. Washington, DC: U.S. Patent and Trademark Office.
 20. **Eroshenko V. A. (1981).** “Heterogeneous Thermodynamical System, Eroshenko Cycle of Transformation of Thermal Energy into Mechanical Energy and Devices to Achieve It,” in Russian, Soviet Patent No. 1,254,811 (1981) [priority of 24.07.1981], updated 02.09.1993 (date of free public access).
 21. **Eroshenko V. A. (1987b).** Effect of Heat Exchange on Filling of Lyophobic Pores and Capillaries with Liquid. *Kolloidn. Zh.*, 49, 875.
 22. **Eroshenko V. A. (1990).** Les proprietes Non-Ordinaires d'un Systeme Thermodynamique Complexe. *C. R. Acad. Sci. Ukraine, Ser. A*, 10, 79.
 23. **Eroshenko V. A. (1996).** Non-Compressibilite et Non-Dilatabilite Adiabatiques d'un Systeme Thermodynamique Complexe. *Entropie*. 196, 17.
 24. **Eroshenko V. A. (1997).** Dimensionnalite de l'Espace Comme Potentiel Thermodynamique

d'un Systeme. Entropie. 202, 110.

25. **Eroshenko V. A. (2000)**. Amortisseur a Haut Pouvoir Dissipatif. French Patent No. FR 2 804 188 A1.
26. **Eroshenko V. A. (2007)**. A new paradigm of mechanical energy dissipation. Part 1: theoretical aspects and practical solutions. Proceedings of the Institution of Mechanical Engineers, Part D: Journal of Automobile Engineering. No. 3., P. 285 – 300.
27. **Eroshenko V. A. and A. Y. Fadeev (1995)**. Intrusion and Extrusion of Water in Hydrophobized Porous Silica. Colloid J. 57, 4, 446.
28. **Eroshenko V. A. and Lazarev Y. F. (2012)**. Rheology and dynamics of repulsive clathrates. Journal of Applied Mechanics and Technical Physics, 53(1), 98-112.
29. **Eroshenko V. A. and Stoudenets V. P. (2002)**. The influence of developed interfaces upon the heterogeneous nanosystem thermal capacity. Composites Part A: Applied Science and Manufacturing, 33(10), 1349-1353.
30. **Eroshenko V. A.** Russian-Soviet Patents No. 943,444 (**1980**); 1,382,078 (**1982**), 1,380,357 (**1983**), 1,333,870 (**1985a**), 1,434,881 (**1985b**), 1,452,262 (**1986**), 1,508,665 (**1987a**).
31. **Eroshenko V. A., and Fadeev A. (1995)**. Intrusion and extrusion of water in hydrophobized porous silica. Colloid journal. 57(4), P. 446-449.
32. **Eroshenko V. and Grosu Y. (2014a)**. Importance Of Synthesis Of Lyophobic Porous Materials And Corresponding Liquids For Development Of Thermomolecular Energy Devices Of New Generation. Proceedings of MMT-2014 conference. Ariel, Israel, 29 July – 01 August 2014.
33. **Eroshenko V. A., Grosu Y. G. (2013a)**. Maxwell's relations and thermal coefficients for repulsive clathrates. Journal of Technical Physics. V. 58., No. 8., P. 1087 – 1093.
34. **Eroshenko V. A., Grosu Y. G. (2013c)**. Thermomechanical and thermophysical properties of repulsive clathrates. Journal of Applied Mechanics and Technical Physics. 54(5), P. 798 – 808.
35. **Eroshenko V. A., Grosu, Y. G. (2013b)**. Thermodynamic and Operational Properties of Heterogeneous Lyophobic Systems. International Journal of Thermodynamics. 16(1), P. 1 – 9.
36. **Eroshenko V., Grosu Ya., Tsyryn N.N., Stoudenets V.P., Nedelec J-M., Grolier J-P.E. (2015)**. Exceptionally large and controlled effect of negative thermal expansion in porous heterogeneous lyophobic systems. Under submission.
37. **Eroshenko V. A., Piatiletov I., Coiffard L., Stoudenets V. (2007)**. A new paradigm of mechanical energy dissipation. Part 2: experimental investigation and effectiveness of a novel car damper. Proceedings of the Institution of Mechanical Engineers, Part D: Journal of

- Automobile Engineering, 221(3), 301-312.
38. **Eroshenko V. A., Regis R.-C., Soulard M., and Patarin J. (2001).** Energetics: A New Field of Applications for Hydrophobic Zeolites. *J. Am. Chem. Soc.*, 123, 8129.
 39. **Eroshenko V. A., Regis R.-C., Soulard M., and Patarin J. (2002).** Les Systemes Heterogenes Eau-Zeolithe Hydrophobe: De Nouveaux Ressorts Moleculaires. *C. R. Acad. Sci., Ser. B*, 3, 111.
 40. **Fadeev A. Y. and Eroshenko V. A. (1997).** Study of Penetration of Water into Hydrophobized Porous Silica. *J. Colloid Interface Sci.*, 187, 275.
 41. **Fadeev A. Yu. and Staroverov S. M. (1988).** Geometric structural properties of bonded layers of chemically modified silicas. *Journal of Chromatography A.*, V. 447, P. 103-116.
 42. **Grosu Y., Eroshenko V., Ievtushenko O., Nedelec J. M., Grolier J. P. E. (2014b).** Anomalous negative thermal expansion in a condensed heterogeneous lyophobic system. *Ukr. J. Phys.*, V. 59, No. 1, pp. 69-78.
 43. **Grosu Y., Eroshenko V., Nedelec J. M., Grolier J. P. E. (2015a).** A new working mode for molecular springs: water intrusion induced by cooling and associated isobaric heat capacity change of a {ZIF-8+ water} system. *Physical Chemistry Chemical Physics*. 17(3), P. 1572 – 1574.
 44. **Grosu Y., Ievtushenko, O., Eroshenko V., Nedelec J. M., Grolier J. P. E. (2014c)** Water intrusion/extrusion in hydrophobized mesoporous silica gel in a wide temperature range: Capillarity, bubble nucleation and line tension effects. *Colloids Surf., A*. 441, 549-555.
 45. **Grosu Ya., Renaudin G., Eroshenko V., Nedelec J.-M., Grolier J.-P.E. (2015b).** Synergetic effect of temperature and pressure on energetic and structural characteristics of {ZIF-8 + water} molecular spring. *RSC Nanoscale*. DOI: 10.1039/C5NR01340B.
 46. **Guan W., Tong J., Chen S. P., Liu Q. S. & Gao S. L. (2010).** Density and surface tension of amino acid ionic liquid 1-alkyl-3-methylimidazolium glutamate. *Journal of Chemical & Engineering Data*, 55(9), 4075-4079.
 47. **Guillemot L. (2010).** Systèmes Hétérogènes Lyophobes: Influence de la température et de la vitesse sur les cycles d'intrusion/extrusion forcées de liquides non mouillants dans des matériaux mésoporeux (Doctoral dissertation, INSA de Lyon).
 48. **Guillemot L., Biben T., Galarneau A., Vigier G. & Charlaix É. (2012b).** Activated drying in hydrophobic nanopores and the line tension of water. *Proceedings of the National Academy of Sciences*, 109(48), 19557-19562.
 49. **Guillemot L., Galarneau A., Vigier G., Abensur T. & Charlaix É. (2012a).** New device to measure dynamic intrusion/extrusion cycles of lyophobic heterogeneous systems. *Review of Scientific Instruments*, 83(10), 105105.

50. **Han A. & Qiao Y. (2006).** Pressure-induced infiltration of aqueous solutions of multiple promoters in a nanoporous silica. *Journal of the American Chemical Society*, 128(32), 10348-10349.
51. **Han A. & Qiao Y. (2007a).** Controlling infiltration pressure of a nanoporous silica gel via surface treatment. *Chemistry Letters*, 36(7), 882-883.
52. **Han A. & Qiao Y. (2007b).** Infiltration pressure of a nanoporous liquid spring modified by an electrolyte. *Journal of materials research*, 22(03), 644-648.
53. **Han A. & Qiao Y. (2007c).** A volume-memory liquid. *Applied Physics Letters*, 91(17), 173123
54. **Han A., & Qiao Y. (2007d).** Infiltration of liquid water in an acid-leached zeolite. *Journal of Materials Research*, 22(12), 3538-3541.
55. **Han A., Chen X., & Qiao Y. (2008a).** Effects of the addition of electrolyte on liquid infiltration in a hydrophobic nanoporous silica gel. *Langmuir*, 24(14), 7044-7047.
56. **Han A., Kong X. & Qiao Y. (2006).** Pressure induced liquid infiltration in nanopores. *Journal of applied physics*, 100(1), 014308.
57. **Han A., Lu W., Kim T., Chen X., & Qiao Y. (2008b).** Influence of anions on liquid infiltration and defiltration in a zeolite Y. *Physical Review E*, 78(3), 031408.
58. **Han A., Lu W., Kim T., Punyamurtula V. K., & Qiao Y. (2009b).** The dependence of infiltration pressure and volume in zeolite Y on potassium chloride concentration. *Smart Materials and Structures*, 18(2), 024005.
59. **Han A., Lu W., Punyamurtula V. K., Chen X., Surani F. B. Kim T., & Qiao Y. (2008c).** Effective viscosity of glycerin in a nanoporous silica gel. *Journal of Applied Physics*, 104(12), 124908.
60. **Han A., Lu W., Punyamurtula V. K., Kim T., & Qiao Y. (2009a).** Temperature variation in liquid infiltration and defiltration in a MCM41. *Journal of Applied Physics*, 105(2), 024309.
61. **Han A., Punyamurtula V. K., & Qiao Y. (2008d).** Effects of decomposition-treatment temperature on infiltration pressure of a surface modified nanoporous silica gel. *Chemical Engineering Journal*, 139(2), 426-429.
62. **Han A., Punyamurtula V. K., & Qiao Y. (2008e).** Effects of cation size on infiltration and defiltration pressures of a MCM-41. *Applied Physics Letters*, 92(15), 153117.
63. **Ievtushenko O. V., Eroshenko V. A., Grosu Y. G., Nedelec J. M., Grolier J. P. E. (2013).** Evolution of the energetic characteristics of {silicalite-1+ water} repulsive clathrates in a wide temperature range. *Physical Chemistry Chemical Physics*. 15(12), P. 4451 – 4457.
64. **Iwatsubo T., Suci C. V., Ikenagao M. & Yaguchio K. (2007).** Dynamic characteristics of

a new damping element based on surface extension principle in nanopore. *Journal of Sound and Vibration*, 308(3), 579-590.

65. **Karbowiak T., Paulin C. & Bellat J. P. (2010b)**. Determination of water intrusion heat in hydrophobic microporous materials by high pressure calorimetry. *Microporous and Mesoporous Materials*, 134(1), 8-15.
66. **Karbowiak T., Paulin C., Ballandras A., Weber G. & Bellat J. P. (2009)**. Thermal Effects of Water Intrusion in Hydrophobic Nanoporous Materials. *Journal of the American Chemical Society*, 131(29), 9898-9899.
67. **Karbowiak T., Weber G. & Bellat J. P. (2013)**. Confinement of water in hydrophobic nanopores: effect of the geometry on the energy of intrusion. *Langmuir*, 30(1), 213-219.
68. **Karbowiak, T., Saada, M. A., Rigolet, S., Ballandras, A., Weber, G., Bezverkhyy, I., ... & Bellat, J. P. (2010a)**. New insights in the formation of silanol defects in silicalite-1 by water intrusion under high pressure. *Physical Chemistry Chemical Physics*. 12(37), P. 11454 – 11466.
69. **Khay I., Daou T. J., Nouali H., Ryzhikov A., Rigolet S., & Patarin J. (2014)**. High Pressure Intrusion–Extrusion of LiCl Aqueous Solutions in Silicalite-1 Zeolite: Influence on Energetic Performances. *The Journal of Physical Chemistry C*, 118(8), 3935-3941.
70. **Khay I., Tzanis L., Daou T. J., Nouali H., Ryzhikov A., & Patarin J. (2013)**. Energetic behavior of the pure silica ITQ-12 (ITW) zeolite under high pressure water intrusion. *Physical Chemistry Chemical Physics*, 15(46), 20320-20325.
71. **Kong X. & Qiao Y. (2005a)**. Thermal effects on pressure-induced infiltration of a nanoporous system. *Philosophical magazine letters*, 85(7), 331-337.
72. **Kong X. & Qiao Y. (2005b)**. Improvement of recoverability of a nanoporous energy absorption system by using chemical admixture. *Applied Physics Letters*, 86(15), 151919.
73. **Kong X., Surani F. B. & Qiao Y. (2005)**. Effects of addition of ethanol on the infiltration pressure of a mesoporous silica. *Journal of materials research*, 20(04), 1042-1045.
74. **Laouir A., Luo L., Tondeur D., Cachot T., Le Goff P. (2003)**. Thermal machines based on surface energy of wetting: Thermodynamic analysis *AIChE journal*. No. 3. pp. 764-781.
75. **Lefevre B., Saugey A., Barrat J. L., Bocquet L., Charlaix E., Gobin P. F. & Vigier G. (2004a)**. Intrusion and extrusion of water in hydrophobic mesopores. *The Journal of chemical physics*, 120(10), 4927-4938.
76. **Lefevre B., Saugey A., Barrat J. L., Bocquet L., Charlaix E., Gobin P. F. & Vigier G. (2004b)**. Intrusion and extrusion of water in highly hydrophobic mesoporous materials: effect of the pore texture. *Colloids and Surfaces A: Physicochemical and Engineering Aspects*, 241(1), 265-272.

77. **Liu L., Chen X., Lu W., Han A. & Qiao Y. (2009a).** Infiltration of electrolytes in molecular-sized nanopores. *Physical review letters*, 102(18), 184501.
78. **Liu L., Qiao Y. & Chen X. (2008).** Pressure-driven water infiltration into carbon nanotube: The effect of applied charges. *Applied Physics Letters*, 92(10), 101927.
79. **Liu L., Zhao J., Culligan P. J., Qiao Y., & Chen X. (2009b).** Thermally Responsive Fluid Behaviors in Hydrophobic Nanopores. *Langmuir*, 25(19), 11862-11868.
80. **Michelin-Jamois M., Guillemot L., Abensur T., Charlaix E., Vigier G. (2013).** On the use of lyophobic heterogeneous systems (LHS) in payload comfort. Proceedings of 5th European conference for aeronautics and space sciences. Munich, Germany, 1-5 July 2013.
81. **Michelin-Jamois M., Picard C., Charlaix E. & Vigier G. (2014).** Osmotic pressure effects upon intrusion of liquid electrolytes inside hydrophobic MOF's. arXiv preprint arXiv:1404.5318.
82. **Ortiz G., Nouali H., Marichal C., Chaplais G., & Patarin J. (2013).** Energetic performances of the metal–organic framework ZIF-8 obtained using high pressure water intrusion–extrusion experiments. *Physical Chemistry Chemical Physics*, 15(14), 4888-4891.
83. **Ortiz G., Nouali H., Marichal C., Chaplais G., & Patarin J. (2014a).** Energetic performances of “ZIF-71–aqueous solution” systems: A perfect shock-absorber with water. *The Journal of Physical Chemistry C*, 118(37), 21316-21322.
84. **Ortiz G., Nouali H., Marichal C., Chaplais G., & Patarin J. (2014b).** Versatile Energetic Behavior of ZIF-8 upon High Pressure Intrusion–Extrusion of Aqueous Electrolyte Solutions. *The Journal of Physical Chemistry C*, 118(14), 7321-7328.
85. **Qiao Y. & Han A. (2007).** Thermal effects on infiltration of a solubility-sensitive volume-memory liquid. *Philosophical magazine letters*, 87(1), 25-31.
86. **Qiao Y., Cao G. & Chen X. (2007).** Effects of gas molecules on nanofluidic behaviors. *Journal of the American Chemical Society*, 129(8), 2355-2359.
87. **Qiao Y., Punyamurtula V. K., Han A., Kong X. & Surani F. B. (2006).** Temperature dependence of working pressure of a nanoporous liquid spring. *Applied physics letters*, 89(25), 251905.
88. **Randzio S. L. (1996).** Scanning titrimetry. *Chem. Soc. Rev.* No. 6. P. 383 – 392.
89. **Randzio S. L., Grolier J. P. E. (1998).** Supercritical titrimetry of polymers. *Analytical chemistry*. No. 11. P. 2327 – 2330.
90. **Randzio S. L., Grolier J. P. E., Zaslona J., Quint J. R. (1994).** French patent №9109227.
91. **Randzio S. L., Grolier J. P. E., Zaslona J., Quint J. R. (1995).** Polish Patent No. 295285.
92. **Randzio S. L., Stachowiak C., Grolier J. (2003).** Titrimetric determination of the three-phase curve in asymmetric binary systems. *The Journal of Chemical Thermodynamics*.

No. 4. P. 639 – 648.

93. **Saada M. A., Rigolet S., Paillaud J. L., Bats N., Soulard M., & Patarin J. (2010a).** Investigation of the energetic performance of pure silica itq-4 (ifr) zeolite under high pressure water intrusion. *The Journal of Physical Chemistry C*, 114(26), 11650-11658.
94. **Saada M. A., Soulard M., Marler B., Gies H., & Patarin J. (2010b).** High-pressure water intrusion investigation of pure silica RUB-41 and S-SOD Zeolite Materials. *The Journal of Physical Chemistry C*, 115(2), 425-430.
95. **Suciu C. V., & Buma S. (2013).** On the structural simplification, compact and light design of a vehicle suspension, achieved by using a colloidal cylinder with a dual function of absorber and compression-spring. In *Proceedings of the FISITA 2012 World Automotive Congress* (pp. 21-32). Springer Berlin Heidelberg.
96. **Suciu C. V., & Kimura Y. (2012).** Experimental study on the forced heating and natural cooling of a colloidal damper. *Journal of System Design and Dynamics*, 6(5), 538-554.
97. **Suciu C. V., & Tobiishi T. (2012).** Comfortableness Evaluation of an Autovehicle Equipped with Colloidal Suspensions. *Journal of System Design and Dynamics*, 6(5), 555-567.
98. **Suciu C. V., & Yaguchi K. (2009).** Endurance tests on a colloidal damper destined to vehicle suspension. *Experimental mechanics*, 49(3), 383-393.
99. **Suciu C. V., Bonneau O., Brun-Picard D., Fre J., & Pascovici M. D. (2000).** Study of a novel squeeze film damper and vibration generator. *Journal of tribology*, 122(1), 211-218.
100. **Suciu C. V., Iwatsubo T., & Deki S. (2003).** Investigation of a colloidal damper. *Journal of colloid and interface science*, 259(1), 62-80.
101. **Suciu C. V., Iwatsubo T., & Deki S. (2004).** Novel Principle of Mechanical Energy Dissipation (Part 1-Static Performances of Colloidal Damper). *JSME International Journal Series C*, 47(1), 180-188.
102. **Suciu C. V., Iwatsubo T., Deki S. (2003).** Investigation of a colloidal damper *Journal of colloid and interface science*. No. 1., P. 62 – 80.
103. **Suciu C. V., Iwatsubo T., Yaguchi K., & Ikenaga M. (2005).** Novel and global approach of the complex and interconnected phenomena related to the contact line movement past a solid surface from hydrophobized silica gel. *Journal of colloid and interface science*, 283(1), 196-214.
104. **Suciu C. V., Kimura Y., & Tani S. (2010a).** On the Generated Heat at Advancing/Receding of Water on Surface Engineered Nanoporous Silica. *Advanced Materials Research*, 123, 1003-1006.
105. **Suciu C. V., Tani S., & Miyoshi K. (2010c).** Experimental study on the thermal

- characteristics of a colloidal damper. *Journal of System Design and Dynamics*, 4(6), 899-913.
106. **Suciu C. V., Tani S., & Yaguchi K. (2010b)**. On the fatigue fracture at adsorption/desorption of water in/from liquid-repellent nanoporous silica. *Acta mechanica*, 214(1-2), 195-203.
 107. **Suciu C. V., Yaguchi K. (2009)**. Endurance tests on a colloidal damper destined to vehicle suspension. *Experimental mechanics*. No. 3., P. 383 –393.
 108. **Suciu, C. V. (2008)**. U.S. Patent Application 12/452,039.
 109. **Suciu, C. V. (2010)**. Ride-comfort of an automobile equipped with colloidal dampers at its frontal suspension. In *Proc. Int. Conf. on Noise and Vibration Eng* (pp. 4233-4245).
 110. **Surani F. B. & Qiao Y. (2006a)**. Infiltration and defiltration of an electrolyte solution in nanopores. *Journal of applied physics*, 100(3), 034311.
 111. **Surani F. B., & Qiao Y. (2006b)**. Pressure-induced infiltration of an epsomite–silica system. *Philosophical magazine letters*, 86(04), 253-260.
 112. **Surani F. B., & Qiao Y. (2006c)**. Pressure induced liquid infiltration in a functionalized poly (acrylic acid-co acrylamide) potassium salt gel matrix material. *Materials Research Innovations*, 10(1), 129-137.
 113. **Surani F. B., Han A., & Qiao Y. (2006)**. Experimental investigation on pressurized liquid in confining nanoenvironment. *Applied physics letters*, 89(9), 093108.
 114. **Surani F. B., Kong X., Panchal D. B. & Qiao Y. (2005)**. Energy absorption of a nanoporous system subjected to dynamic loadings. *Applied Physics Letters*, 87(16), 163111.
 115. **Trzpit M., Rigolet S., Paillaud J. L., Marichal C., Soulard M., & Patarin J. (2008)**. Pure Silica Chabazite Molecular Spring: A Structural Study on Water Intrusion– Extrusion Processes. *The Journal of Physical Chemistry B*, 112(24), 7257-7266.
 116. **Trzpit M., Soulard M., & Patarin J. (2007b)**. The pure silica chabazite: a high volume molecular spring at low pressure for energy storage. *Chemistry Letters*, 36(8), 980-981.
 117. **Trzpit M., Soulard M., & Patarin J. (2009a)**. Water intrusion in mesoporous silicalite-1: An increase of the stored energy. *Microporous and Mesoporous Materials*, 117(3), 627-634.
 118. **Trzpit M., Soulard M., & Patarin J. (2009b)**. Water intrusion-extrusion in silicalite-1 with tunable mesoporosity prepared in fluoride medium. *Journal of materials science*, 44(24), 6525-6530.
 119. **Trzpit M., Soulard M., Patarin J., Desbiens N., Cailliez F., Boutin A., ... & Fuchs A. H. (2007a)**. The effect of local defects on water adsorption in silicalite-1 zeolite: A joint experimental and molecular simulation study. *Langmuir*, 23(20), 10131-10139.

120. **Tzaniş L., Nouali H., Daou T. J., Soulard M., & Patarin J. (2014).** Influence of the aqueous medium on the energetic performances of Silicalite-1. *Materials Letters*, 115, 229-232.
121. **Tzaniş L., Trzpit M., Soulard M., & Patarin J. (2011).** High pressure water intrusion investigation of pure silica 1D channel AFI, MTW and TON-type zeolites. *Microporous and Mesoporous Materials*, 146(1), 119-126.
122. **Tzaniş L., Trzpit M., Soulard M., & Patarin J. (2012a).** Energetic performances of channel and cage-type zeosils. *The Journal of Physical Chemistry C*, 116(38), 20389-20395.
123. **Tzaniş L., Trzpit M., Soulard M., & Patarin J. (2012b).** Energetic Performances of STT-Type Zeosil: Influence of the Nature of the Mineralizing Agent Used for the Synthesis. *The Journal of Physical Chemistry C*, 116(7), 4802-4808.
124. **Xu B., Qiao Y., Park T., Tak M., Zhou Q., & Chen X. (2011b).** A conceptual thermal actuation system driven by interface tension of nanofluids. *Energy & Environmental Science*, 4(9), 3632-3639.
125. **Xu B., Qiao Y., Zhou Q., & Chen X. (2011a).** Effect of electric field on liquid infiltration into hydrophobic nanopores. *Langmuir*, 27(10), 6349-6357.

APPENDIXES

APPENDIXES

Appendix A

Maxwell relations for HLS

The internal energy of HLS may be written as follows:

$$dU = TdS - PdV_0 - \sigma \cos\theta d\Omega$$

Next we consider three possible conditions, which are $V_0 = \text{const}$, $\Omega = \text{const}$, $S = \text{const}$.

1) $V_0 = \text{const} \Rightarrow dU = TdS - \sigma \cos\theta d\Omega$. Then:

$$\left(\frac{\partial U}{\partial S}\right)_{\Omega, V_0} = T, \quad \Rightarrow \frac{\partial^2 U}{\partial S \partial \Omega} = \left(\frac{\partial T}{\partial \Omega}\right)_{S, V_0},$$

$$\left(\frac{\partial U}{\partial \Omega}\right)_{S, V_0} = -\sigma \cos\theta, \quad \Rightarrow \frac{\partial^2 U}{\partial \Omega \partial S} = -\left(\frac{\partial \sigma \cos\theta}{\partial S}\right)_{\Omega, V_0}.$$

Next using following relation $\frac{\partial^2 U}{\partial S \partial \Omega} = \frac{\partial^2 U}{\partial \Omega \partial S}$ one obtains Maxwell relation:

$$\left(\frac{\partial T}{\partial \Omega}\right)_{S, V_0} = -\left(\frac{\partial \sigma \cos\theta}{\partial S}\right)_{\Omega, V_0}$$

For other two cases the procedure is similar.

2) $\Omega = \text{const} \Rightarrow dU = TdS - PdV_0$.

$$\left\{ \begin{array}{l} \left(\frac{\partial U}{\partial S}\right)_{V_0, \Omega} = T, \Rightarrow \frac{\partial^2 U}{\partial V_0 \partial S} = \left(\frac{\partial T}{\partial V_0}\right)_{S, \Omega} \\ \left(\frac{\partial U}{\partial V_0}\right)_{S, \Omega} = -P, \Rightarrow \frac{\partial^2 U}{\partial S \partial V_0} = -\left(\frac{\partial P}{\partial S}\right)_{V_0, \Omega} \end{array} \right. \Rightarrow$$

$$\left(\frac{\partial T}{\partial V_0}\right)_{S, \Omega} = -\left(\frac{\partial P}{\partial S}\right)_{V_0, \Omega}$$

3) $S = \text{const} \Rightarrow dU = -PdV_0 - \sigma \cos\theta d\Omega$.

$$\left\{ \begin{array}{l} \left(\frac{\partial U}{\partial V_0} \right)_{\Omega, S} = -P, \Rightarrow \frac{\partial^2 U}{\partial \Omega \partial V_0} = - \left(\frac{\partial P}{\partial \Omega} \right)_{V_0, S} \\ \left(\frac{\partial U}{\partial \Omega} \right)_{V_0, S} = -\sigma \cos \theta, \Rightarrow \frac{\partial^2 U}{\partial V_0 \partial \Omega} = - \left(\frac{\partial \sigma \cos \theta}{\partial V_0} \right)_{\Omega, S} \end{array} \right. \Rightarrow \left(\frac{\partial P}{\partial \Omega} \right)_{V_0, S} = \left(\frac{\partial \sigma \cos \theta}{\partial V_0} \right)_{\Omega, S}$$

Such relation does not have physical sense. Since we consider quasi-static regime of an HLS operation, the interface development ($d\Omega \neq 0$) is impossible without considering variation of the volume of the bulk phase V_0 , which makes left-hand-side derivative null. While the surface tension as well as the contact angle do not depend on the volume of the bulk phase V_0 .

Let us repeat this algorithm for all thermodynamic characterization functions.

Enthalpy of an HLS: $dH = TdS + (V_0 - kr\Omega)dP$.

$$\left\{ \begin{array}{l} \left(\frac{\partial H}{\partial S} \right)_P = T, \Rightarrow \frac{\partial^2 H}{\partial P \partial S} = \left(\frac{\partial T}{\partial P} \right)_S \\ \left(\frac{\partial H}{\partial P} \right)_S = V_0 - kr\Omega, \Rightarrow \frac{\partial^2 H}{\partial S \partial P} = \left(\frac{\partial V_0}{\partial S} \right)_P - kr \left(\frac{\partial \Omega}{\partial S} \right)_P \end{array} \right. \Rightarrow$$

$$\left(\frac{\partial T}{\partial P} \right)_S = \left(\frac{\partial V_0}{\partial S} \right)_P - kr \left(\frac{\partial \Omega}{\partial S} \right)_P$$

Free Helmholtz energy $dF = -PdV_0 + \sigma \cos \theta d\Omega - SdT$.

1) $V_0 = const \Rightarrow dF = \sigma \cos \theta d\Omega - SdT$

$$\left\{ \begin{array}{l} \left(\frac{\partial F}{\partial \Omega} \right)_{T, V_0} = \sigma \cos \theta, \Rightarrow \frac{\partial^2 F}{\partial T \partial \Omega} = \left(\frac{\partial \sigma \cos \theta}{\partial T} \right)_{\Omega, V_0} \\ \left(\frac{\partial F}{\partial T} \right)_{\Omega, V_0} = -S, \Rightarrow \frac{\partial^2 F}{\partial \Omega \partial T} = - \left(\frac{\partial S}{\partial \Omega} \right)_{T, V_0} \end{array} \right. \Rightarrow$$

$$\left(\frac{\partial \sigma \cos \theta}{\partial T} \right)_{\Omega, V_0} = - \left(\frac{\partial S}{\partial \Omega} \right)_{T, V_0}$$

2) $\Omega = const \Rightarrow dF = -PdV_0 - SdT$

$$\left\{ \begin{array}{l} \left(\frac{\partial F}{\partial V_0} \right)_{T, \Omega} = -P, \Rightarrow \frac{\partial^2 F}{\partial T \partial V_0} = - \left(\frac{\partial P}{\partial T} \right)_{V_0, \Omega} \\ \left(\frac{\partial F}{\partial T} \right)_{V_0, \Omega} = -S, \Rightarrow \frac{\partial^2 F}{\partial V_0 \partial T} = - \left(\frac{\partial S}{\partial V_0} \right)_{T, \Omega} \end{array} \right. \Rightarrow$$

$$\left(\frac{\partial P}{\partial T} \right)_{V_0, \Omega} = \left(\frac{\partial S}{\partial V_0} \right)_{T, \Omega}$$

3) $T = const \Rightarrow dF = -PdV_0 + \sigma \cos \theta d\Omega$

$$\left\{ \begin{array}{l} \left(\frac{\partial F}{\partial V_0} \right)_{\Omega, T} = -P, \Rightarrow \frac{\partial^2 F}{\partial \Omega \partial V_0} = - \left(\frac{\partial P}{\partial T} \right)_{V_0, \Omega} \\ \left(\frac{\partial F}{\partial \Omega} \right)_{V_0, T} = \sigma \cos \theta, \Rightarrow \frac{\partial^2 F}{\partial V_0 \partial \Omega} = - \left(\frac{\partial \sigma \cos \theta}{\partial V_0} \right)_{T, \Omega} \end{array} \right. \Rightarrow \left(\frac{\partial P}{\partial \Omega} \right)_{V_0, T} = - \left(\frac{\partial \sigma \cos \theta}{\partial V_0} \right)_{T, \Omega}$$

Again we take into consideration here that $\left(\frac{\partial \sigma \cos \theta}{\partial V_0} \right)_{\Omega, T} \approx 0$.

Gibbs potential: $dG = (V_0 - kr\Omega)dP - SdT$.

$$\left\{ \begin{array}{l} \left(\frac{\partial G}{\partial P} \right)_T = V_0 - kr\Omega, \Rightarrow \frac{\partial^2 G}{\partial T \partial P} = \left(\frac{\partial V_0}{\partial T} \right)_P - kr \left(\frac{\partial \Omega}{\partial T} \right)_P \\ \left(\frac{\partial G}{\partial T} \right)_P = -S, \Rightarrow \frac{\partial^2 G}{\partial P \partial T} = - \left(\frac{\partial S}{\partial P} \right)_T \end{array} \right. \Rightarrow$$

$$- \left(\frac{\partial S}{\partial P} \right)_T = \left(\frac{\partial V_0}{\partial T} \right)_P - kr \left(\frac{\partial \Omega}{\partial T} \right)_P$$

Appendix B

Thermal coefficients

Adiabatic coefficient of compressibility of HLS may be written using its definition and equation (3.4):

$$\mu_S^{int,ext} = -\frac{1}{V_0^0} \left(\frac{\partial V}{\partial P} \right)_S = -\frac{1}{V_0^0} \left(\frac{\partial V_\Omega}{\partial P} \right)_S - \frac{1}{V_0^0} \left(\frac{\partial V_0}{\partial P} \right)_S = -\frac{1}{V_0^0} \left(\frac{\partial f_{int,ext}}{\partial P} \right)_S + \mu_S^0 \quad (\text{B.1})$$

Next we using function f in the form of Cauchy distribution function one may write:

$$\left(\frac{\partial f_{int,ext}}{\partial P} \right)_S = -\frac{V_{pore}}{\pi D_{int,ext}} \cdot \frac{1}{\left(\frac{P - P_{int,ext}(T)}{D_{int,ext}} \right)^2 + 1} \left(1 - \left(\frac{\partial P_{int,ext}}{\partial P} \right)_S \right) \quad (\text{B.2})$$

Next $P_{int,ext}$ is considered as a function of only temperature: $\left(\frac{\partial P_{int,ext}}{\partial T} \right)_S = \frac{dP_{int,ext}}{dT}$.

Compression/decompression of the HLS under adiabatic condition would provoke temperature change and hence the change of intrusion/extrusion pressure: $\left(\frac{\partial P_{int,ext}}{\partial P} \right)_S = \left(\frac{\partial P_{int,ext}}{\partial T} \right)_S \left(\frac{\partial T}{\partial P} \right)_S = \frac{dP_{int,ext}}{dT} \left(\frac{\partial T}{\partial P} \right)_S$. To find $\left(\frac{\partial T}{\partial P} \right)_S$ derivative let use equation (3.15) considering under adiabatic conditions $dS = 0$ and differentiate it by P :

$$\left(\frac{\partial T}{\partial P} \right)_S = \frac{T}{C_V^0} \left(-\left(\frac{\partial P}{\partial T} \right)_{V_0,\Omega} \left(\frac{\partial V_0}{\partial P} \right)_S - \frac{dP_{int,ext}}{dT} \left(\frac{\partial f_{int,ext}}{\partial P} \right)_S \right) \quad (\text{B.3})$$

then from the system of equations (B.2) and (B.3) to find $\left(\frac{\partial f_{int,ext}}{\partial P} \right)_S$ and $\left(\frac{\partial T}{\partial P} \right)_S$ and then use eq. (B.1) to finally obtain:

$$\mu_S^{int,ext} = -\frac{1 - P_0 \frac{dP_{int,ext}}{dT} \frac{T}{C_V^0} \beta^0 \mu_S^0}{\frac{V_0^0}{f'_{int,ext}} - \left(\frac{dP_{int,ext}}{dT} \right)^2 \frac{T}{C_V^0}} + \mu_S^0$$

Temperature variation under adiabatic conditions due to pressure change is an important characteristic. From mathematical manipulations described above it may be written:

$$\left(\frac{\partial T}{\partial P}\right)_S = \frac{\frac{T}{C_V} \left(\left(\frac{\partial P}{\partial T}\right)_{V_0, \Omega} \left(\frac{\partial V_0}{\partial P}\right)_S + \frac{dP_{int,ext}}{dT} \frac{V_{pore}}{\pi D_{int,ext}} \frac{1}{\left(\frac{P - P_{int,ext}}{D_{int,ext}}\right)^2 + 1} \right)}{\left(\frac{T}{C_V} \left(\frac{dP_{int,ext}}{dT}\right)^2 \frac{V_{pore}}{\pi D_{int,ext}} \frac{1}{\left(\frac{P - P_{int,ext}}{D_{int,ext}}\right)^2 + 1} - 1 \right)}$$

Next, considering that under adiabatic conditions the temperature variation may be achieved only by pressure variation we write: $\left(\frac{\partial T}{\partial P}\right)_S = \frac{dT}{dP} = \frac{dT}{dP_{int,ext}} \frac{dP_{int,ext}}{dP}$. By indicating $P - P_{int,ext} = x$ we may write:

$$\left(1 + \frac{dx}{dT} \frac{dT}{dP_{int,ext}}\right) \frac{dP_{int,ext}}{dT} = \frac{\frac{T}{C_V} \left(\left(\frac{\partial P}{\partial T}\right)_{V_0, \Omega} \left(\frac{\partial V_0}{\partial P}\right)_S + \frac{dP_{int,ext}}{dT} \frac{V_{pore}}{\pi D_{int,ext}} \frac{1}{\left(\frac{x}{D_{int,ext}}\right)^2 + 1} \right)}{\left(\frac{T}{C_V} \left(\frac{dP_{int,ext}}{dT}\right)^2 \frac{V_{pore}}{\pi D_{int,ext}} \frac{1}{\left(\frac{x}{D_{int,ext}}\right)^2 + 1} - 1 \right)}$$

In this differential equation separation of variables is possible, which allows to integrate it:

$$\begin{aligned} P_0 V_0 \beta^0 \mu^0 (P - P_{int,ext}) + \frac{dP_{int,ext}}{dT} \frac{V_{pore}}{\pi} \arctan\left(\frac{P - P_{int,ext}}{D_{int,ext}}\right) \\ = -C_V \ln\left(\frac{T}{T_0}\right) - (T - T_0) \frac{dP_{int,ext}}{dT} P_0 V_0 \beta^0 \mu^0 + C_2 \end{aligned}$$

Where constant C_2 may be found from initial conditions $T(P = P_0) = T_0$.

In order to determine Isochoric Coefficient of Pressure (ICP) of HLS let us write the full differential of pressure as function of T, V_0, Ω as follows:

$$dP(T, V_0, \Omega) = \left(\frac{\partial P}{\partial T}\right)_{V_0, \Omega} dT + \left(\frac{\partial P}{\partial V_0}\right)_{T, \Omega} dV_0 + \left(\frac{\partial P}{\partial \Omega}\right)_{T, V_0} d\Omega \quad (\text{B.4})$$

We may write $\left(\frac{\partial P}{\partial \Omega}\right)_{T, V_0} = 0$ because the variation of the interface area Ω is not possible without the variation of V_0 under isothermal conditions for a quasi-static process. Then equation (B.4) can be written:

$$\left(\frac{\partial P}{\partial T}\right)_V = \left(\frac{\partial P}{\partial T}\right)_{V_0,\Omega} + \left(\frac{\partial P}{\partial V_0}\right)_{T,\Omega} \left(\frac{\partial V_0}{\partial T}\right)_V = P_0\beta^0 - \frac{1}{V_0\mu_T^0} \left(\frac{\partial V_0}{\partial T}\right)_V \quad (\text{B.5})$$

Derivative $\left(\frac{\partial V_0}{\partial T}\right)_V$ can be found from equation (3.4) which is $dV = dV_0 - kr d\Omega$:

$$\begin{aligned} \left(\frac{\partial V_0}{\partial T}\right)_V &= -\left(\frac{\partial f_{int,ext}}{\partial T}\right)_V = \left(\left(\frac{\partial P}{\partial T}\right)_V - \frac{dP_{int,ext}}{dT}\right) \frac{V_{pore}}{\pi D_{int,ext}} \frac{1}{\left(\frac{P - P_{int,ext}}{D_{int,ext}}\right)^2 + 1} \\ &\equiv -\left(\left(\frac{\partial P}{\partial T}\right)_V - \frac{dP_{int,ext}}{dT}\right) f'_{int,ext} \end{aligned} \quad (\text{B.6})$$

By solving system of equations (B.5) and (B.6) one obtains:

$$\beta^{int,ext} = \frac{1}{P_0} \left(\frac{\partial P}{\partial T}\right)_V = \frac{\beta^0 - \frac{dP_{int,ext}}{dT} \frac{f'_{int,ext}}{P_0 V_0 \mu_T^0}}{1 - \frac{f'_{int,ext}}{V_0 \mu_T^0}}$$

$$\left(\frac{\partial P}{\partial T}\right)_V = P_0\beta^0 + \frac{1}{V_0\mu_T^0} \left(\left(\frac{\partial P}{\partial T}\right)_V - \frac{dP_{int,ext}}{dT}\right) \frac{V_{pore}}{\pi D_{int,ext}} \frac{1}{\left(\frac{P - P_{int,ext}}{D_{int,ext}}\right)^2 + 1} \quad (\text{B.7})$$

Appendix C

Thermal effects of compression-decompression

In order to obtain the pressure derivative of the heat of compression/decompression of HLS at isothermal conditions we use equation (3.15) and (3.3):

$$\begin{aligned} \left(\frac{\partial Q_{int,ext}}{\partial P}\right)_T &= T \left(\frac{\partial S}{\partial P}\right)_T = -TP_0V_0\mu_T^0\beta^0 - T \frac{d(\sigma \cos\theta_{A,R})}{dT} \frac{f'_{int,ext}}{kr} \\ &= -TP_0V_0\mu_T^0\beta^0 + T \left(\frac{d\sigma}{dT} \cos\theta_{A,R} + \sigma \frac{d\cos\theta_{A,R}}{dT}\right) \frac{f'_{int,ext}}{kr} \end{aligned} \quad (C.1)$$

The temperature coefficient of surface tension $\frac{d\sigma}{dT}$ normally is a known characteristic of the liquid, the derivative $\frac{d\cos\theta}{dT}$ may be rewritten using the generalized Young equation:

$$\frac{d\cos\theta_{A,R}}{dT} = \frac{d\cos\theta_{A,R}^\infty}{dT} - \frac{\tau}{r \cdot \sigma^2} \frac{d\sigma}{dT} \quad (C.2)$$

Derivative $\frac{d\cos\theta_{A,R}^\infty}{dT}$ may be found by means of ‘‘Sharp-kink’’ approximation as described in reference (Grosu et al. 2014c):

$$\frac{d\cos\theta_{A,R}^\infty}{dT} = \left(\frac{d\Delta\rho}{dT} \frac{1}{\sigma} - \Delta\rho \frac{1}{\sigma^2} \frac{d\sigma}{dT}\right) I_{int,ext} \quad (C.3)$$

Next substituting (C.3) into (C.2) we obtain for microscopic advancing and receding contact angles:

$$\frac{d\cos\theta_{A,R}}{dT} = \frac{d\Delta\rho}{dT} \frac{I_{int,ext}}{\sigma} - \frac{1}{\sigma^2} \frac{d\sigma}{dT} \left(\frac{\tau}{r} + \Delta\rho \cdot I_{int,ext}\right) \quad (C.4)$$

Substituting (C.4) into (C1) and taking into account generalized Young equation and equation (C.3), we finally obtain:

$$\left(\frac{\partial Q_{int,ext}}{\partial P}\right)_T = -TP_0V_0\mu_T^0\beta^0 - T \left(\frac{d\sigma}{dT} - \frac{d\Delta\rho}{dT} I_{int,ext}\right) \frac{f'_{int,ext}}{kr}$$

Appendix D

Isochoric and isothermal heat capacity

In order to obtain the equations for heat capacity at constant volume and constant pressure we use the classical definition and equation (3.15):

$$\begin{aligned} C_V^{int,ext} &= \left(\frac{\partial Q^{int,ext}}{\partial T} \right)_V = T \left(\frac{\partial S^{int,ext}}{\partial T} \right)_V \\ &= C_V^0 + T \left(\frac{\partial P}{\partial T} \right)_{\Omega, V_{LM}} \left(\frac{\partial V_0}{\partial T} \right)_V + T \frac{d(\sigma \cos \theta_{A,R})}{dT} \left(\frac{\partial \Omega}{\partial T} \right)_V \end{aligned} \quad (D.1)$$

From the condition of constant volume $dV = dV_0 - kr d\Omega = 0$ one obtains $\left(\frac{\partial V_0}{\partial T} \right)_V = kr \left(\frac{\partial \Omega}{\partial T} \right)_V$. Using $\frac{dP^{int,ext}}{dT} = -\frac{1}{kr} \frac{d(\sigma \cos \theta_{A,R})}{dT}$, we rewrite (D.1):

$$C_V^{int,ext} = C_V^0 + T \left(\left(\frac{\partial P}{\partial T} \right)_{\Omega, V_{LM}} - \frac{dP^{int,ext}}{dT} \right) \left(\frac{\partial V_0}{\partial T} \right)_V$$

Next using equation (B.6) we write:

$$C_V^{int,ext} = C_V^0 - T \left(\left(\frac{\partial P}{\partial T} \right)_{\Omega, V_{LM}} - \frac{dP^{int,ext}}{dT} \right)^2 f'_{int,ext}$$

Using the same algorithm we obtain for the isobaric heat capacity:

$$C_P^{int,ext} = C_V^0 + TP_0 V_0 \beta^0 \alpha^0 - T \left(\frac{dP^{int,ext}}{dT} \right)^2 f'_{int,ext}$$

Next, using well known relation $C_P^0 = C_V^0 + TP_0 V_0 \beta^0 \alpha^0$ one can write:

$$C_P^{int,ext} = C_P^0 - T \left(\frac{dP^{int,ext}}{dT} \right)^2 f'_{int,ext}$$

Appendix E.

Energetic characteristics of HLS

In what follows energetic characteristics of investigated heterogeneous lyophobic systems are presented. Abbreviations are the following: T is temperature, W_{int} and W_{ext} are work of intrusion and extrusion respectively, $H_W = \frac{W_{int}-W_{ext}}{W_{int}} \cdot 100\%$ is the hysteresis of intrusion-extrusion work, Q_{int} and Q_{ext} are the heats of intrusion and extrusion respectively, $H_Q = \frac{Q_{int}-Q_{ext}}{Q_{int}} \cdot 100\%$ is hysteresis of intrusion-extrusion heat.

Table E.1.

Energetic characteristics of {ZIF-8 + water} HLS

{ZIF-8 + water}						
T, K	$W_{int}, J/g$	$W_{ext}, J/g$	$H_W, \%$	$Q_{int}, J/g$	$Q_{ext}, J/g$	$H_Q, \%$
280	9,0	5,9	35,0			
300	9,6	7,0	26,8	4,4		
310	9,8	7,5	23,3	7,4	5,4	27,5
320	9,9	7,9	19,9	9,4	6,3	33,3
330	9,9	8,2	17,2	14,4	12,7	12,0
340	9,9	8,4	14,9	13,0	12,9	0,4
350	9,8	8,4	14,7	26,3	25,7	2,0
360	9,5	8,3	12,6			

Table E.2.

Energetic characteristics of {Hypersil C18 + water} HLS

{Hypersil C18 + water}						
T, K	$W_{int}, J/g$	$W_{ext}, J/g$	$H_W, \%$	$Q_{int}, J/g$	$Q_{ext}, J/g$	$H_Q, \%$
275	7,3	0,0	100			
300	7,1	0,3	96	3,3	0,0	100
325	6,9	0,6	91	17,4	3,5	80
350	6,6	0,9	86	25,0	9,8	61
370	6,4	1,1	83	27,8	16,5	41
400	5,9	1,2	80	29,8	2,3	92
420	5,5	1,2	77	40,7	10,8	74

Table E.3.

Energetic characteristics of {Waters C8 + water} HLS

{Waters C8 + water}								
T, K	283	303	323	343	363	383	403	423
$W_{int}, J/g$	9,23	9,05	8,71	8,35	7,86	7,24	6,64	6,00
$W_{ext}, J/g$	0,57	0,96	1,21	1,38	1,52	1,37	1,07	0,19
$H_W, \%$	94	89	86	83	81	81	84	97

**THERMODYNAMICS AND OPERATIONAL PROPERTIES OF
NANOPOROUS HETEROGENEOUS LYOPHOBIC SYSTEMS
FOR MECHANICAL AND THERMAL ENERGY
STORAGE/DISSIPATION**

**THERMODYNAMIQUE ET PROPRIETES
OPÉRATIONNELLES DE SYSTÈMES NANOPOREUX
HETEROGENES LYOPHOBES POUR LE STOCKAGE / LA
DISSIPATION D'ENERGIE MECANIQUE ET THERMIQUE**

RESUME

The thesis is devoted to the theoretical and experimental investigations of thermodynamic and operational properties of nanoporous Heterogeneous Lyophobic Systems (HLS) and their temperature dependences in order to determine optimal conditions and increase efficiency of HLS-based energetical devices.

The thesis reflects results obtained in three main directions of research: 1. Thermodynamic analysis; 2. Characteristics of HLS in a wide temperature range; 3. Stability of HLS under different operational conditions. Maximum temperature range investigated is to 2 - 150 ° C. Pressure range is 0.1 - 120 MPa. Particularly, results include proposed equation of state for real HLS, which takes into account pore size distribution function; the energetic characteristics of four (two mesoporous and two microporous) HLSs collected in a wide temperature range; some new operation regimes of HLSs were investigated under controlled isobaric conditions; proposed concept of usage of HLS as a system with pronounced negative thermal expansion.

Keywords: storage, conversion, dissipation of energy; interface, porous body, complex thermodynamic system.

RESUME

La thèse est consacrée à l'étude théorique et expérimentale des propriétés thermodynamiques et d'usage de Systèmes Hétérogènes de Lyophobes nanoporeux (SHL) et leurs dépendances en fonction de la température afin de déterminer les conditions optimales et accroître l'efficacité des dispositifs énergétiques à base de SHL.

La thèse présente les résultats obtenus dans trois directions principales de recherche: 1. Analyse thermodynamique; 2. Caractéristiques des SHL dans une large plage de température; 3. Stabilité de SHL dans différentes conditions opérationnelles. La gamme maximale de température étudiée est à 2 - 150 °C et 0.1 - 120 MPa pour la pression. En particulier, les résultats comprennent une équation d'état pour décrire des SHL réels qui prend en compte la distribution de taille des pores; les caractéristiques énergétiques de quatre (deux mésoporeux et deux microporeux) SHLs mesurées dans une large plage de température; certains nouveaux régimes de fonctionnement de SHLs ont été étudiés dans des conditions isobares contrôlées; enfin le concept d'utilisation de SHL comme système avec dilatation thermique négative prononcée est proposé.

Mots clés: stockage, conversion, dissipation de l'énergie; interface, matériaux poreux, système thermodynamique complexe.

